DIFFERENTIATION CONTROLS IN SUBSILICEOUS
GABBROS

by

GEORGE HALSEY BEALL
B.Sc., McGill University
(1956)
M.Sc., McGill University
(1958)

SUBMITTED IN PARTIAL FULFILLMENT
OF THE REQUIREMENTS FOR THE
DEGREE OF DOCTOR OF
PHILOSOPHY
at the
MASSACHUSETTS INSTITUTE OF
TECHNOLOGY
August, 1962

Signature of Author ....
        Department of Geology and Geophysics, August 20, 1962

Certified by ....
                                        Thesis Supervisor

Accepted by ....
                Chairman, Departmental Committee
                        on Graduate Students

DIFFERENTIATION CONTROLS IN SUBSILICEOUS GABBROS

by George H. Beall

Submitted to the Department of Geology and Geophysics
on August 20, 1962, in partial fulfillment of the require-
ments for the degree of Doctor of Philosophy.

Abstract.

Subsiliceous gabbros fall into two classes, a magnesian
group, the olivine tholeiites, composed largely of normative
components olivine, hypersthene, diopside, and plagioclase, and
a more calcic group, the basanites, composed largely of
normative components diopside, olivine, anorthite, and some
nepheline.

The position of the olivine-orthopyroxene liquidus
boundary exerts a dominant influence on the course of differen-
tiation of the olivine tholeiites. Increasing pressure shifts
this boundary away from silica; the effect of dissolved
volatiles is to shift it towards silica. Fractional crystal-
lization taking place in a 'wet' environment will therefore
result in the precipitation of more olivine than would occur in
a 'dry' environment. Consequently, the residual magmas of deep
crystallization are likely to be more enriched in silica than
those which form close to the surface.

While experiments have shown that the addition of
plagioclase to the system diopside-enstatite shifts the
pyroxene liquidus minimum from about Di 80 En 20 to about Di 65
En 35, field evidence dictates a frequent shift to over 50 per-
cent enstatite. Such a shift is expected on theoretical
grounds if abundant steam is dissolved in the melt.

The Chukotat Sills of Ungava, Quebec, differentiated
olivine tholeiites, were intruded at considerable depth and
under conditions of considerable volatile content in the melt.
The largest sills are of the settled differentiated type, char-
acterized by an ultrabasic base and a gabbro cap. Field,
microscopic, and chemical evidence all suggest that they were
injected as a mixture of gabbroic magma and olivine crystals.
The latter sank forming a homogeneous layer, and the overlying
gabbro then differentiated. The major effects predicted for
basaltic crystallization under high water pressure are in
evidence, namely, excess olivine accumulation and the
hypersthene shift in the pyroxene liquidus trough.

Aluminum substitution in clinopyroxenes is, along with
quantity of dissolved volatiles, a critical factor in deter-
mining the course of differentiation of the calcic subsiliceous,

or basanite, magmas. From a zone of residual uncertainty,
falling close to the normative composition clinopyroxene-
olivine-plagioclase, magmas may differentiate towards criti-
cally undersaturated residua or towards saturated and over-
saturated residua. Plagioclase saturation at the time of
pyroxene separation plus 'wet' conditions favour more siliceous
residua, high aluminum substitution in early pyroxenes, and the
development of silica-poor hydrous phases.

The Monteregian Hills of the Montreal area are basanite
stocks of the high temperature and 'dry' type. Differentiation
towards critically undersaturated residua was generally
favoured. The sodic nature of these residua, dominantly
nepheline syenites, is due to the initial separation of highly
anorthitic plagioclase from the parent magma; the albite compo-
nent was severely restricted by the subsiliceous nature of this
melt.

The parent magmas of the Chukotat Sills and Monteregian
Hills intrusives, representing the two classes of subsiliceous
basalts, are believed related in depth of origin. Simple or
repetitive partial fusion of a mantle of peridotite composition
at depths over 100 kilometers would yield silica-poor melts,
largely due to expansion of the pyroxene and garnet liquidus
fields with increasing pressure. The magnesium to calcium
ratio in the melt would depend directly upon the degree of
fusion.

Thesis Supervisor: Harry Hughes
Title: Assistant Professor of Geophysics

TABLE OF CONTENTS

LIST OF FIGURES

LIST OF TABLES

LIST OF PLATES

INTRODUCTION AND ACKNOWLEDGEMENTS

It is well known that basaltic magmas with only slight differences in composition can produce through differentiation melts which show great chemical contrast. For example, a melt consisting largely of normative components plagioclase, diopside, and olivine, with a little nepheline, may differentiate to a strongly alkaline nepheline syenite, while a similar melt with a slight amount of normative hypersthene instead of nepheline may differentiate to a syenite or, in some cases, even a granite.

Yoder and Tilley have recently introduced a useful simple basalt system, nepheline-forsterite-diopside-silica, which can be generalized to nepheline-olivine-clinopyroxene-silica with enstatite becoming 'orthopyroxene' and albite 'plagioclase'. Within this generalized system, which can be represented by a tetrahedron, they define three groups of basalts: tholeiite, composed of normative clinopyroxene, orthopyroxene, plagioclase, and silica; olivine tholeiite, composed of olivine, clino-pyroxene, orthopyroxene, and plagioclase; and basanite, composed of normative olivine, plagioclase, clinopyroxene, and nepheline. These three groups are separated by two normative 'planes'; basanite and olivine tholeiite are separated by the 'plane of critical undersaturation' olivine-clinopyroxene-plagioclase, olivine tholeiite and tholeiite are separated by the 'plane of oversaturation' clinopyroxene-orthopyroxene-plagioclase. The

plane of critical undersaturation is a thermal barrier whose exact chemical position in basaltic systems is poorly defined. In general, basalts falling on the nepheline side of this plane differentiate towards alkaline residua, while basalts falling on the orthopyroxene side differentiate towards calc-alkaline residua.

The plane of oversaturation, on the other hand, is not a thermal barrier, and whether or not it is crossed during differentiation depends upon several factors, among them, the composition of the original magma, the degree of fractional crystallization, and the conditions of pressure and quantity of volatiles present during crystallization.

Subsiliceous gabbros or basalts, as defined in this thesis, contain less than 47 percent of silica. They can be subdivided into two main classes: the magnesian subsiliceous gabbros, whose norm is composed largely of olivine and hypersthene, with some plagioclase and diopside, and the calcic subsiliceous gabbros, whose norm is composed largely of diopside, olivine, and plagioclase, with nepheline and sometimes negative silica. The magnesian group falls into the olivine tholeiite class and the calcic group into the basanite class.

It is the major purpose of this thesis to study a differentiated intrusive complex representative of each of these two classes of subsiliceous gabbros, with particular emphasis upon the trend of differentiation as it was influenced by the physical conditions of crystallization. The Chukotat Sills of

the Ungava region of northern Quebec are differentiated olivine tholeiites, while the mafic phases of the Monteregian Hills intrusives of the Montreal area are basanitic gabbros. While the former crystallized at considerable depth with abundant volatiles dissolved in the melt, the latter crystallized under low pressures near the surface of the earth.

Chapter I presents a thermodynamic and phase equilibrium analysis of simple chemical systems of major importance in basalt differentiation. Although the experimental data and theoretical results will be referred to in the later portions of the thesis, the reader unfamiliar with physico-chemical petrology may find it desirable to omit this chapter. Chapters III and IV, respectively, present the detailed petrology of the mafic phases of the Chukotat Sills and Monteregian Hills, respectively. These two sections can be considered entirely independent of one another, but they are linked together by Chapter II, which discusses the general similarities and critical differences in the mineralogy of the two complexes, and by Chapter V, which presents an hypothesis of origin of subsiliceous gabbro magmas, both olivine tholeiites and basanites.

The writer takes pleasure in acknowledging the guidance and help given by his thesis director, Professor Harry Hughes. In particular, he is grateful for the amount of time Professor Hughes spent with him in discussions of all phases of the thesis,

and for valuable criticisms and suggestions offered, particularly with regard to the more theoretical portions of the text. He would also like to thank Professor J. B. Thompson, Jr. of Harvard University for a discussion of some of the problems involved in pyroxene crystallization, and also for originally stimulating his interest in the field of igneous petrology.

The writer is grateful to the Quebec Department of Mines for financial aid in the form of a scholarship held during the academic year 1958-1959.

Finally, he would like to thank all those graduate students and postdoctoral fellows in the Department of Geology and Geophysics at the Massachusetts Institute of Technology with whom he held frequent discussions concerning various problems involved in this thesis. He specifically acknowledges the help of Mr. John A. Philpotts, who discussed with him some of the field relations and thin section analyses, Dr. Charles Schnetzler, who aided him with the chemical analyses, and Dr. Gunter Faure, who provided interesting ideas concerning Sr 87/Sr 86 evidence bearing on the origin of basalts.

Chapter I: PHASE EQUILIBRIA AND THERMODYNAMIC ANALYSES OF BASALTIC SYSTEMS

1. Two Phases in Equilibrium in a Binary System

For two phases, α and β, in equilibrium in a binary system of components i and j, the chemical potential of j in phase α is equal to that in phase β, or

$$\mu_{i\alpha}(P,T) = \mu_{i\beta}(P,T), \quad \mu_{j\alpha}(P,T) = \mu_{j\beta}(P,T) \quad (1)$$

By definition,

$$\mu_{i\alpha}(P,T) = \left(\frac{\partial G_\alpha}{\partial n_{i\alpha}}\right)_{P,T,n_{j\alpha}}, \quad \mu_{i\beta}(P,T) = \left(\frac{\partial G_\beta}{\partial n_{i\beta}}\right)_{P,T,n_{j\beta}}$$

$$\mu_{j\alpha}(P,T) = \left(\frac{\partial G_\alpha}{\partial n_{j\alpha}}\right)_{P,T,n_{i\alpha}}, \quad \mu_{j\beta}(P,T) = \left(\frac{\partial G_\beta}{\partial n_{j\beta}}\right)_{P,T,n_{i\beta}}$$

where G_α and G_β are the Gibbs free energy of phases α and β, and $n_{i\alpha}$, $n_{j\alpha}$, $n_{i\beta}$, $n_{j\beta}$, are the number of moles of i and j in phases α and β, respectively.

These equations can be rewritten in the following form:

$$\mu_{j\alpha}(P,T) = \left[\frac{\partial(n_{i\alpha}+n_{j\alpha})\bar{G}_\alpha}{\partial n_{j\alpha}}\right]_{P,T,n_{i\alpha}} = (n_{i\alpha}+n_{j\alpha})\left(\frac{\partial \bar{G}_\alpha}{\partial n_{j\alpha}}\right)_{P,T,n_{i\alpha}} + \bar{G}_\alpha(T,P,n_{i\alpha},n_{j\alpha}) \quad (2)$$

where $\overline{G}_\alpha$ is the mean molar free energy of phase α.

Now, the mole fraction of component j in phase α, $X_{j\alpha}$, is defined by

$$X_{j\alpha} = \frac{n_{j\alpha}}{n_{i\alpha} + n_{j\alpha}} \qquad , \qquad \therefore \qquad \left(\frac{\partial X_{j\alpha}}{\partial n_{j\alpha}}\right)_{n_{i\alpha}} = \frac{n_{i\alpha}}{\left(n_{i\alpha} + n_{j\alpha}\right)^2} \qquad (3)$$

Combining (3) and (2),

$$\mathcal{M}_{j\alpha}(P,T) = \frac{1}{(n_{i\alpha} + n_{j\alpha})} \left(\frac{\partial \overline{G}_\alpha}{\partial X_{j\alpha}}\right)_{P,T} n_{i\alpha} + \overline{G}_\alpha(P,T,X_{j\alpha})$$

$$\mathcal{M}_{j\alpha}(P,T) = X_{i\alpha} \left(\frac{\partial \overline{G}_\alpha}{\partial X_{j\alpha}}\right)_{P,T} + \overline{G}_\alpha(P,T,X_{j\alpha}) \qquad (4)$$

Similarly

$$\mathcal{M}_{i\alpha}(P,T) = X_{j\alpha} \left(\frac{\partial \overline{G}_\alpha}{\partial X_{i\alpha}}\right)_{P,T} + \overline{G}_\alpha(P,T,X_{j\alpha}) \qquad (5)$$

Subtracting (5) from (4), we obtain

$$\mathcal{M}_{j\alpha}(P,T) - \mathcal{M}_{i\alpha}(P,T) = \left(X_{i\alpha} + X_{j\alpha}\right)\left(\frac{\partial \overline{G}_\alpha}{\partial X_{j\alpha}}\right)_{P,T}$$

or

$$\left(\frac{\partial \overline{G}_\alpha}{\partial X_{j\alpha}}\right)_{P,T} = \mathcal{M}_{j\alpha}(P,T) - \mathcal{M}_{i\alpha}(P,T) \qquad (6)$$

Similarly
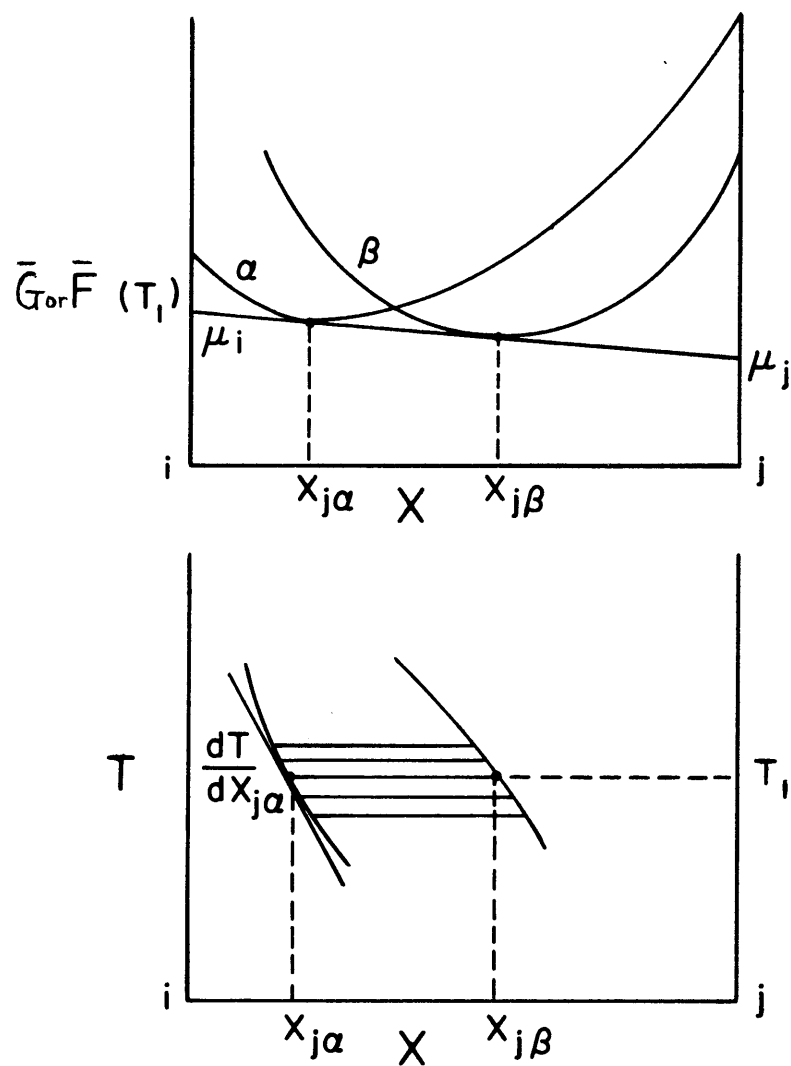
FIG. 1   FREE ENERGY-COMPOSITION AND TEMPERATURE -
        COMPOSITION DIAGRAMS SHOWING TWO PHASES α AND β
        IN EQUILIBRIUM AT CONSTANT PRESSURE.

$$\left(\frac{\delta \bar{G}_\beta}{\delta X_{j\beta}}\right)_{P,T} = \mathcal{M}_{j\beta}\left(P,T\right) - \mathcal{M}_{i\beta}\left(P,T\right) \tag{7}$$

and from (1) we now obtain, for two phases in equilibrium

$$\left(\frac{\delta \bar{G}_\alpha}{\delta X_{j\alpha}}\right)_{P,T} = \left(\frac{\delta \bar{G}_\beta}{\delta X_{j\beta}}\right)_{P,T} \tag{8}$$

Also, from equation (4) and an analogous equation for phase β

$$\mathcal{M}_{j\alpha}\left(P,T\right) - \mathcal{M}_{j\beta}\left(P,T\right) = X_{i\alpha}\left(\frac{\delta \bar{G}_\alpha}{\delta X_{j\alpha}}\right)_{P,T} - X_{i\beta}\left(\frac{\delta \bar{G}_\beta}{\delta X_{j\beta}}\right)_{P,T} + \bar{G}_\alpha\left(P,T,X_{j\alpha}\right) - \bar{G}_\beta\left(P,T,X_{j\beta}\right)$$

From (1) and (8) this simplifies to, for two phases in equilibrium

$$\bar{G}_\alpha\left(P,T,X_{j\alpha}\right) - \bar{G}_\beta\left(P,T,X_{j\beta}\right) = \left(X_{j\alpha} - X_{j\beta}\right)\left(\frac{\delta \bar{G}_\alpha}{\delta X_{j\alpha}}\right)_{P,T} \tag{9}$$

Multiplying equation (4) by $X_{j\alpha}$ and equation (5) by $X_{j\alpha}$ and adding, noting that $X_{j\alpha} + X_{i\alpha} = 1$, and $dX_{j\alpha} = -dX_{i\alpha}$, we obtain

$$\bar{G}_\alpha\left(P,T,X_{j\alpha}\right) = X_{i\alpha}\mathcal{M}_{i\alpha} + X_{j\alpha}\mathcal{M}_{j\alpha} \tag{10}$$

which can be seen in graphical representation, Fig. 1.

Now, at constant pressure

$$d\mu_{j\alpha}(P,T) = \left(\frac{\partial\mu_{j\alpha}}{\partial T}\right)_{X_{j\alpha},P} dT + \left(\frac{\partial\mu_{j\alpha}}{\partial X_{j\alpha}}\right)_{T,P} dX_{j\alpha}$$

$$d\mu_{j\beta}(P,T) = \left(\frac{\partial\mu_{j\beta}}{\partial T}\right)_{X_{j\beta},P} dT + \left(\frac{\partial\mu_{j\beta}}{\partial X_{j\beta}}\right)_{T,P} dX_{j\beta}$$

Therefore, from (1)

$$0 = \left[\left(\frac{\partial\mu_{j\alpha}}{\partial T}\right)_{P,X_{j\alpha}} - \left(\frac{\partial\mu_{j\beta}}{\partial T}\right)_{P,X_{j\beta}}\right] dT + \left(\frac{\partial\mu_{j\alpha}}{\partial X_{j\alpha}}\right)_{T,P} dX_{j\alpha} - \left(\frac{\partial\mu_{j\beta}}{\partial X_{j\beta}}\right)_{T,P} dX_{j\beta} \tag{11}$$

and the analogous equation with component i

$$0 = \left[\left(\frac{\partial\mu_{i\alpha}}{\partial T}\right)_{X_{i\alpha},P} - \left(\frac{\partial\mu_{i\beta}}{\partial T}\right)_{P,X_{i\beta}}\right] dT + \left(\frac{\partial\mu_{i\alpha}}{\partial X_{i\alpha}}\right)_{T,P} dX_{i\alpha} - \left(\frac{\partial\mu_{i\beta}}{\partial X_{i\beta}}\right)_{P,T} dX_{i\beta} \tag{12}$$

Differentiating (4) and (5), we obtain

$$\left(\frac{\partial\mu_{j\alpha}}{\partial X_{j\alpha}}\right)_{P,T} = X_{i\alpha}\left(\frac{\partial^2\bar{G}_\alpha}{\partial X_{j\alpha}^2}\right)_{P,T} \tag{13}$$

$$\left(\frac{\partial\mu_{i\alpha}}{\partial X_{i\alpha}}\right)_{P,T} = X_{j\alpha}\left(\frac{\partial^2\bar{G}_\alpha}{\partial X_{i\alpha}^2}\right)_{P,T} \tag{14}$$

Using these relations and similar equations for the phase β

$$\left[\left(\frac{\partial \mu_{i\alpha}}{\partial T}\right)_{P,X_{j\alpha}} - \left(\frac{\partial \mu_{i\beta}}{\partial T}\right)_{P,X_{j\alpha}}\right] dT + X_{j\alpha}\left(\frac{\partial^2 \bar{G}_\alpha}{\partial X_{j\alpha}^2}\right)_{P,T} dX_{i\alpha} - X_{j\beta}\left(\frac{\partial^2 \bar{G}_\beta}{\partial X_{i\beta}^2}\right)_{P,T} dX_{i\beta} = 0 \tag{15}$$

$$\left[\left(\frac{\partial \mu_{j\alpha}}{\partial T}\right)_{P,X_{j\alpha}} - \left(\frac{\partial \mu_{j\beta}}{\partial T}\right)_{P,X_{j\alpha}}\right] dT + X_{i\alpha}\left(\frac{\partial^2 \bar{G}_\alpha}{\partial X_{i\alpha}^2}\right)_{P,T} dX_{j\alpha} - X_{i\beta}\left(\frac{\partial^2 \bar{G}_\beta}{\partial X_{j\beta}^2}\right)_{P,T} dX_{j\beta} = 0 \tag{16}$$

Multiply (15) by $X_{i\beta}$, (16) by $X_{j\beta}$, substitute $dX_{i\beta} = -dX_{j\beta}$, $dX_{i\alpha} = -dX_{j\alpha}$, and add:

$$X_{j\beta}\left[\left(\frac{\partial \mu_{j\alpha}}{\partial T}\right)_{P,X_{j\alpha}} - \left(\frac{\partial \mu_{j\beta}}{\partial T}\right)_{P,X_{j\beta}}\right] dT + X_{i\beta}\left[\left(\frac{\partial \mu_{i\alpha}}{\partial T}\right)_{P,X_{i\alpha}} - \left(\frac{\partial \mu_{i\beta}}{\partial T}\right)_{P,X_{j\beta}}\right] dT - \left(X_{i\beta}X_{j\alpha} - X_{i\alpha}X_{j\beta}\right)\left(\frac{\partial^2 \bar{G}_\alpha}{\partial X_{j\alpha}^2}\right) dX_{j\alpha} = 0 \tag{17}$$

Differentiating (4) and (5), we obtain :

$$\left(\frac{\partial \mu_{j\alpha}}{\partial T}\right)_{P,X_{j\alpha}} = X_{i\alpha}\left(\frac{\partial^2 \bar{G}_\alpha}{\partial X_{j\alpha}\partial T}\right)_{P} + \left(\frac{\partial \bar{G}_\alpha}{\partial T}\right)_{P,X_{j\alpha}} \tag{18}$$

$$\left(\frac{\partial \mu_{i\alpha}}{\partial T}\right)_{P,X_{j\alpha}} = X_{j\alpha}\left(\frac{\partial^2 \bar{G}_\alpha}{\partial X_{i\alpha}\partial T}\right)_{P} + \left(\frac{\partial \bar{G}_\alpha}{\partial T}\right)_{P,X_{j\alpha}} \tag{19}$$

Substituting equations (18) and (19) and analogous equations corresponding to the phase β into (17) we obtain

$$\left[X_{j\beta} \left\{ X_{i\alpha} \left(\frac{\partial^2 \bar{G}_\alpha}{\partial X_{j\alpha} \partial T} \right)_P + \left(\frac{\partial \bar{G}_\alpha}{\partial T} \right)_{P, X_{j\alpha}} - X_{i\beta} \left(\frac{\partial^2 \bar{G}_\beta}{\partial X_{j\beta} \partial T} \right)_P - \left(\frac{\partial \bar{G}_\beta}{\partial T} \right)_{P, X_{j\beta}} \right\} \right.$$

$$\left. + X_{i\beta} \left\{ X_{j\alpha} \left(\frac{\partial^2 \bar{G}_\alpha}{\partial X_{i\alpha} \partial T} \right)_P + \left(\frac{\partial \bar{G}_\alpha}{\partial T} \right)_{P, X_{j\alpha}} - X_{j\beta} \left(\frac{\partial^2 \bar{G}_\beta}{\partial X_{i\beta} \partial T} \right)_P - \left(\frac{\partial \bar{G}_\beta}{\partial T} \right)_{P, X_{j\beta}} \right\} \right] dT$$

$$- \left(X_{i\beta} X_{j\alpha} - X_{i\alpha} X_{j\beta} \right) \left(\frac{\partial^2 \bar{G}_\alpha}{\partial X_{j\alpha}^2} \right)_{P, T} dX_{j\alpha} \quad = 0$$

$$\left[\left(X_{j\beta} X_{i\alpha} - X_{i\beta} X_{j\alpha} \right) \left(\frac{\partial^2 \bar{G}_\alpha}{\partial X_{j\alpha} \partial T} \right)_P + \left(X_{j\beta} + X_{i\beta} \right) \left(\frac{\partial \bar{G}_\alpha}{\partial T} \right)_{P, X_{j\alpha}} - \left(X_{j\alpha} X_{i\beta} - X_{i\beta} X_{j\beta} \right) \left(\frac{\partial^2 \bar{G}_\beta}{\partial X_{j\beta} \partial T} \right)_P \right.$$

$$\left. - \left(X_{j\beta} + X_{i\beta} \right) \left(\frac{\partial \bar{G}_\beta}{\partial T} \right)_{P, X_{j\beta}} \right] dT + \left(X_{i\beta} X_{j\alpha} - X_{i\alpha} X_{j\beta} \right) \left(\frac{\partial^2 \bar{G}_\alpha}{\partial X_{j\alpha}^2} \right)_{P, T} dX_{j\alpha} = 0$$

substituting for X_i using $X_i + X_j = 1$, we obtain

$$\left[\left(\frac{\partial \bar{G}_\alpha}{\partial T} \right)_{P, X_{j\alpha}} - \left(\frac{\partial \bar{G}_\beta}{\partial T} \right)_{P, X_{j\beta}} + \left(X_{j\beta} - X_{j\alpha} \right) \left(\frac{\partial^2 \bar{G}_\alpha}{\partial X_{j\alpha} \partial T} \right)_P \right] dT - \left(X_{j\alpha} - X_{j\beta} \right) \left(\frac{\partial^2 \bar{G}_\alpha}{\partial X_{j\alpha}^2} \right) dX_{j\alpha}$$

or

$$= 0$$

$$\left(\frac{dT}{dX_{j\alpha}}\right)_P = \frac{\left(X_{j\alpha} - X_{j\beta}\right)\left(\frac{\partial^2 \bar{G}_\alpha}{\partial X_{j\alpha}^2}\right)_{P,T}}{\left(X_{j\beta} - X_{j\alpha}\right)\left(\frac{\partial^2 \bar{G}_\alpha}{\partial X_{j\alpha} \partial T}\right)_P + \left(\frac{\partial \bar{G}_\alpha}{\partial T}\right)_{P,X_{j\alpha}} - \left(\frac{\partial \bar{G}_\beta}{\partial T}\right)_{P,X_{j\beta}}} \quad (20)$$

Equations (8), (9), and (20) will be found useful in defining the free energy functions of pairs of phases in terms of their experimentally determined compositions and temperatures at equilibrium.

2. System Mg_2SiO_4-Fe_2SiO_4

The melting relations in the binary system Mg_2SiO_4-Fe_2SiO_4, or forsterite-fayalite, were investigated by Bowen and Schairer (1935). The determined liquidus and solidus curves are compatible with the assumptions of ideality in both liquid and solid solutions providing the molar heat of melting of both forsterite and fayalite is about 28,000 calories. Bowen and Schairer gave a value of only half this figure, 14,000 calories, for they failed to recognize that in a mole of olivine the iron and magnesium ions can be permuted over 2N rather than N lattice sites.

The formulae defining liquidus and solidus curves for an ideal binary system involving double substitution are

$$\frac{1-X_{jl}}{1-X_{js}} = \exp\left\{\frac{\Delta\bar{S}_i\,(T-T_{mi})}{2RT}\right\} \tag{21}$$

$$\frac{X_{jl}}{X_{js}} = \exp\left\{\frac{\Delta\bar{S}_j\,(T-T_{mj})}{2RT}\right\} \tag{22}$$

where l and s refer to liquid and solid phases, $\Delta\bar{S}_i$ and $\Delta\bar{S}_j$ are the molar entropies of melting of pure components i and j, and T_{mi} and T_{mj} are the temperatures of melting of the pure components.

The results of Bowen and Schairer do not themselves prove
that the olivine system is ideal, even though it is possible to
fit ideal curves to the liquidus and solidus data. If the
entropies of melting of forsterite and fayalite are appreciably
different from those necessary for the assumptions of ideality
[Equations (21) and (22)] , the experimentally determined
liquidus and solidus conditions can still be satisfied by the
addition of an appropriate heat of mixing term applied to
either the solid or liquid solution. Such non-ideal behavior
seems unlikely, however, since Sahama and Torgeson (1949) have
found no deviation from linearity in the experimentally deter-
mined molar heats of solution of forsteritic, intermediate,
and fayalitic olivine. If no appreciable nonideality occurs
in the olivine solid solution, it is unlikely that appreciable
nonideality exists in the liquid solution.

It is interesting to note one effect of the entropy of
melting of fayalite, 19.0 cal/^{o}mole, being considerably
greater than that of forsterite, 12.9 cal/^{o}mole. The differ-
ence in the crystallization temperature of these two minerals
will become less as the olivine liquidus temperatures are
lowered by the addition of other silicate components or
volatiles. Hence, under low temperatures of crystallization,
olivines will precipitate with an iron to magnesium ratio more
similar to that of the host liquid than would be the case at
higher temperatures. This means that high temperature of
crystallization of olivines favours iron-magnesium

differentiation, whereas lower temperature crystallization, such as would be expected under conditions of considerable dissolved volatiles in the melt, does not.

3. Entropies of Melting of Enstatite and Diopside

Before it is possible to thermodynamically analyze binary systems involving pyroxenes, it is necessary to estimate the entropy of melting of enstatite and diopside.

The heat of melting of diopside has been determined by several methods, and the results have been tabulated by Yoder (1952) and are listed in Table 1. The entropy of melting calculated from the average heat of melting value, 102 cal/gm, is 13.3 ± 1.0 cal/$^{\circ}$C mole.

As Yoder noted, it is not possible to derive this result from the pressure-temperature melting curve for diopside according to the Clausius-Clapeyron equation

$$\frac{dP}{dT} = \frac{\Delta S}{\Delta V} \tag{23}$$

This is possibly because the change in volume at the melting point is considerably less than the total volume change in the temperature region in the vicinity of the melting point. Presumably, however, the entropies of melting of diopside and enstatite can be compared by examination of the average slopes of the melting curves over 30 kilobars pressure of these two minerals. These curves have been determined by Boyd and England (1961), and while the enstatite curve is linear, the diopside curve shows appreciable curvature. The theoretical reason for this curvature is not known. The average slopes of

both curves are about 9.0°/kilobar, any difference being within the limit of precision of the curves. Moreover, the total volume change in the temperature vicinity of melting as measured by density determinations on crystal and glass are 10.0 ccs/mole for both 2-enstatite and diopside (Birch, 1942).

Since there is no significant difference between molar volume changes in the temperature vicinity of melting for diopside and 2-enstatite, and since their melting curve slopes are similar at low pressures, the entropy of melting of 2-enstatite cannot be very different from that of diopside, i.e. 13.3 cal/$^\circ$C (2 moles enstatite or 1 mole diopside).

By the freezing point lowering method used in the determination of the olivine entropies of melting (equations (21) and (22), p. 24), the entropy of melting of enstatite can be estimated independently from the pyroxene liquidus and solidus in the pseudobinary system $FeSiO_3$-$MgSiO_3$ (Bowen and Schairer, 1935). The heat of melting of enstatite determined by this method is 24,000 cals/2 mole, and the entropy of melting is 13.1 cal/$^\circ$C 2 mole, very similar to the accepted value for 1 mole of diopside.

Reference	ΔH (cal/gm)	Method
Tammann	93	Heat of Solution
Vogt	102	Heating curve
White	106	"
Bowen	108	Freezing Point Lowering
Bowen & Schairer	97	"
Kracek	102	Heat of Solution

Table 1: Heat of Melting of Diopside
(after Yoder, 1952)

4. System MgO-SiO$_2$

4.1 Determination of the Form of the Free Energy Function in the Vicinity of the Forsterite-Enstatite Peritectic

There are no solid solution phases along the binary system MgO-SiO$_2$, the stoichiometric solid phases being periclase, MgO, forsterite, Mg$_2$SiO$_4$, enstatite, MgSiO$_3$, and silica, SiO$_2$.

Although the type of ionic substitution in the liquid phase across this binary system is unknown, we may represent as a first approximation the free energy curve for the liquid by the equation:

$$\bar{G}_L\left(X_{jL}, T, P\right) = X_{jL}\,\bar{G}_L\left(1, T, P\right) + \left(1 - X_{jL}\right)\bar{G}_L\left(0, T, P\right)$$
$$+ RT\left\{X_{jL}\ln X_{jL} + \left(1 - X_{jL}\right)\ln\left(1 - X_{jL}\right)\right\} \quad (24)$$
$$+ a\,X_{jL}\left(1 - X_{jL}\right)$$

where the first two terms represent the contribution of the free energy of the end members, the third term the contribution of the entropy of mixing assuming unit substitution of MgO for SiO$_2$, probably a crude approximation, and the last term a parabolic heat of mixing term.

Differentiating (24) with respect to X_{jL}, the mole fraction of SiO$_2$ in the liquid, we obtain

$$\left(\frac{\partial \bar{G}_L}{\partial X_{jL}}\right)_{P,T} = \bar{G}_L(1,T,P) - \bar{G}_L(0,T,P) + RT\ln\left(\frac{X_{jL}}{1-X_{jL}}\right) + a\left(1-2X_{jL}\right) \quad (25)$$

For two phase equilibrium of any solid and liquid in a binary system, we have, from equation (9)

$$\bar{G}_L(X_{jL},T,P) - \bar{G}_S(X_{jS},T,P) = \left(\frac{\partial \bar{G}_L}{\partial X_{jL}}\right)_{P,T}\left(X_{jL}-X_{jS}\right) \quad (26)$$

and

$$\bar{G}_S(X_{jS},T,P) = \bar{G}_L^{\circ}\left(\overset{X_{jL}=}{X_{jS}},T,P\right) + \left(T-T_m\right)\Delta\bar{S} \quad (27)$$

where $\Delta\bar{S}$ is the entropy of melting and T_m the congruent melting point of the solid.

Combining equations (24) to (27), we obtain

$$\Delta\bar{S}\left(T-T_m\right) = RT\left[X_{jL}\ln X_{jL} + \left(1-X_{jL}\right)\ln\left(1-X_{jL}\right)\right.$$
$$\left. + X_{jS}\ln X_{jS} + \left(1-X_{jS}\right)\ln\left(1-X_{jS}\right)\right] \quad (28)$$
$$+ a\left[X_{jL}\left(1-X_{jL}\right) - X_{jS}\left(1-X_{jS}\right)\right]$$
$$- \left(X_{jL}-X_{jS}\right)\left[RT\ln\left(\frac{X_{jL}}{1-X_{jL}}\right) + a\left(1-2X_{jL}\right)\right]$$

For the region between forsterite and enstatite at temperatures where forsterite is in equilibrium with a liquid, values of the parabolic heat of mixing coefficient, a, can be

determined using equation (28). Table 2 lists the values
obtained for various temperatures. It is noted that the
entropy of melting of forsterite, taken as 12.9 cal/$^{\circ}$C mole,
must be multiplied by 1/3 since only 1/3 mole of forsterite
can be made from 2/3 mole MgO and 1/3 mole SiO_2.

Fig. 2 shows an approximate free energy-composition
diagram drawn for a temperature of 1557°C the incongruent
melting point of enstatite as atmospheric pressure. The
parabolic heat of mixing coefficient, a, is assumed to be
-42,000 calories, the average of the results listed in Table 2.
The silica portion of the diagram is modified to allow for the
observed liquid immiscibility in this region (Bowen, 1914).

T $^{\circ}$C	$\overline{G}_{fo} - \overline{G}_L (X_{jL} = 0.33) / X_{jS}$ calories	X_{jL}	a calories
1800	-387	0.415	-46,000
1700	-818	0.463	-41,000
1600	-1250	0.497	-39,000
1557	-1432	0.510	-44,000

Table 2: Determination of the Parabolic Heat of
Mixing Coefficient in the Equilibrium
Region Forsterite-Liquid, System MgO-SiO_2,
at Atmospheric Pressure
(equilibrium data taken from Bowen, 1914)
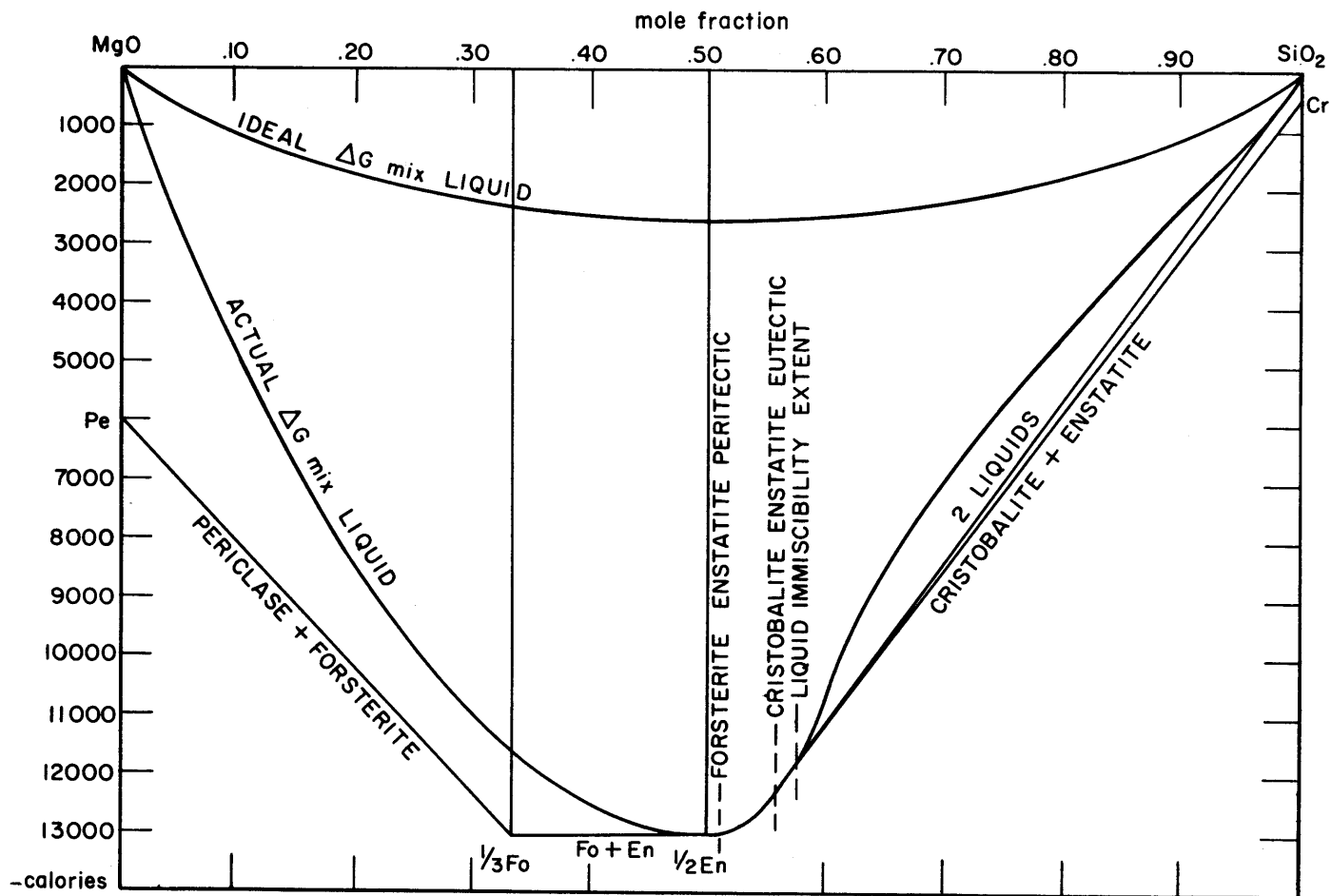
FIG. 2   APPROXIMATE FREE ENERGY DIAGRAM FOR BINARY
SYSTEM MgO-SiO$_2$ AT 1557°C AND 1 ATM.

(ΔS, Tm for periclase taken as 2800°; 3.0 cal/°).   Liquid
free energy curves assuming no heat of mixing and assum-
ing heat of mixing as calculated from MgO-SiO$_2$ liquidus
diagram can be compared.

4.2 Shift of the Forsterite-Enstatite Field Boundary with Total Pressure

Boyd and England (1961) have recently reported from high pressure studies on the melting of enstatite that while this mineral melts incongruently to forsterite plus liquid at atmospheric pressure, it melts congruently at higher pressures. The transition point has not been determined accurately but certainly lies within 5 and 15 kilobars pressure, and probably between 5 and 10 kilobars.

This discovery is of great importance in petrogenesis, since the behavior of olivine-pyroxene-liquid equilibria with total pressure and pressure of volatile saturation is almost certain to have a great effect upon both fractional crystallization and fractional fusion of mafic rocks.

The pressure at which the melting of enstatite changes from incongruent to congruent can be determined roughly from thermodynamic relations, providing the melting curve for enstatite, and the relative entropies of melting and volumes of melting of enstatite and forsterite are known.

From the Clausius Clapeyron equation and the slope of the determined enstatite congruent melting curve (Boyd and England, 1961) we have

$$\left(\frac{dP}{dT}\right)_{m \; En} = \frac{\Delta \overline{S}_{en}}{\Delta \overline{V}_{en}} = \frac{1 \; kb}{9.0°C} \tag{29}$$

Now the variation of chemical potential of Mg_2SiO_4, forsterite, in a melt of enstatite composition is given by

$$d\mu_{fo} (X_j = 0.5) = \tilde{V}_{L\,fo} (X_j = 0.5) \, dP - \tilde{S}_{L\,fo} (X = 0.5) \, dT \qquad (30)$$

where $\tilde{V}_{L\,fo} (X = 0.5)$ and $\bar{S}_{L\,fo} (X = 0.5)$ are the partial molar volume and entropy of forsterite in the melt of enstatite composition.

For solid forsterite, we have

$$d\mu_{fo} = d\bar{G}_{fo} = \bar{V}_{fo} \, dP - \bar{S}_{fo} \, dT \qquad (31)$$

Hence, for forsterite in equilibrium with a liquid of composition $MgSiO_3$, we obtain the relation

$$\left(\frac{dP}{dT}\right)_{fo,\ X_{jL} = 0.5} = \frac{\tilde{S}_{L\,f} - \tilde{S}_{s\,fo}}{\tilde{V}_{L\,fo} - \tilde{V}_{s\,fo}} \doteq \frac{\Delta \bar{S}_{fo}}{\Delta \bar{V}_{fo}} \qquad (32)$$

where X_{jL} refers to mole fraction of SiO_2 in the liquid. The approximation is used because the small differences between the partial molar entropy of Mg_2SiO_4 in $MgSiO_3$ liquid and the mean molar entropy of $MgSiO_4$ liquid and between the partial molar volume of Mg_2SiO_4 in $MgSiO_3$ liquid and the mean molar volume of $MgSiO_4$ liquid, are not significant in the light of the general uncertainties in the entropies and volumes of melting.

Dividing (29) by (32), we obtain

$$\left(\frac{dP}{dT}\right)_{m\ en} \Bigg/ \left(\frac{dP}{dT}\right)_{fo,\ X_\mu = 0.5} = \frac{\Delta\bar{S}_{en} \cdot \Delta\bar{V}_{fo}}{\Delta\bar{V}_{en}\ \Delta\bar{S}_{fo}} \quad (33)$$

As we have seen (p. 27), the volume changes on melting determined by glass and crystal specific gravity measurements do not satisfy the Clausius Clapeyron equation in the cases of the experimental enstatite and diopside melting curves. In the case of equation (33), however, it is the ratio of the entropies and volumes of melting of forsterite and enstatite which are important in comparing the pressure temperature slopes of enstatite melting congruently and forsterite saturation in enstatite liquid. Therefore, using the values of the entropies of melting: $\Delta\bar{S}_{fo} = 12.9$ cal/°, $\Delta\bar{S}_{en} = 6.6$ cal/°, and volumes of melting: $\Delta\bar{V}_{fo} = 8.5$ cm^3, $\Delta\bar{V}_{en} = 5.0$ cm^3 (Birch, 1942), we will obtain a good value for equation (33) as long as the volume of melting ratio determined from glass-crystal data is similar to that which satisfies the Clausius Clapeyron equation, a reasonable assumption.

Substituting these values, we obtain

$$\left(\frac{dP}{dT}\right)_{m\ en} \Bigg/ \left(\frac{dP}{dT}\right)_{fo,\ X_\mu = 0.5} = 0.87, \quad (34)$$

and from (33) and (29)

$$\left(\frac{dP}{dT}\right)_{fo,\ X_{\mu}=0.5} = \frac{1\ kb}{7.8°C} \tag{35}$$

Comparing (29) and (35), it is seen that the congruent melting of enstatite increases in temperature with a given pressure rise more than the liquidus temperature of olivine at the enstatite composition. The metastable congruent melting point of enstatite at atmospheric pressure is about 1558°C, and the olivine liquidus point at the enstatite composition is 1577°C, a difference of about 19 degrees (Boyd and England, 1961). The total pressure necessary to bring these points together (invariant equilibrium enstatite-forsterite-enstatite liquid) is roughly given by

$$\Delta P = \frac{19°\ bars}{1.2°} = 16\ kbars$$

and the temperature by

$$\Delta T_{m\ en} = 16 \times 9.0 = 144,\ T_{invariant} = 1702°C$$

It should be noted that this result is sensitive to the value of $\left(dP/dT\right)_{m\ en} / \left(dP/dT\right)_{fo,\ X_{\mu}=0.5}$ in equation (34). For example, if 0.75 instead of 0.87 is used as the value of this ratio, the value of ΔP would be reduced to 8 kilobars.

The theoretical result of 16 kilobars can be compared with

the experimental result, $15 \, kb > \Delta P > 5 \, kb$, with the most likely
value being 6 kilobars (Boyd and England, 1961). This corre-
sponds to an invariant point temperature of $1617^\circ C$. Although
the experimental determination of this invariant point is not
precise, the theoretical determination, with present entropy
and volume of melting data, is probably less reliable.

4.3 Effect of Addition of Alien Components on the Forsterite-Enstatite Peritectic

To assess the geological importance of the forsterite-
enstatite peritectic in the crystallization of basalts, it is
necessary to consider the effects on this cosaturation point of
certain common components of basaltic magmas not involved in
the system $MgO-SiO_2$, namely: anorthite, albite, fayalite,
ferrosilite, and dissolved volatiles.

Andersen (1915) studied the effects of the addition of
anorthite to the system $Mg_2SiO_4-SiO_2$, and more recently,
Schairer and Yoder (1959) have completed the system albite-
forsterite-silica (Fig. 3). In both cases it was determined
that the addition of plagioclase shifts the forsterite-
enstatite peritectic towards silica as it lowers the tempera-
ture of cosaturation. This shift amounts to 6 and 8 weight
percent per 100 degrees lowering of temperature in the case of
addition of anorthite and albite respectively, measured on the
binary section $Mg_2SiO_4-SiO_2$ projected through plagioclase (Fig. 3).
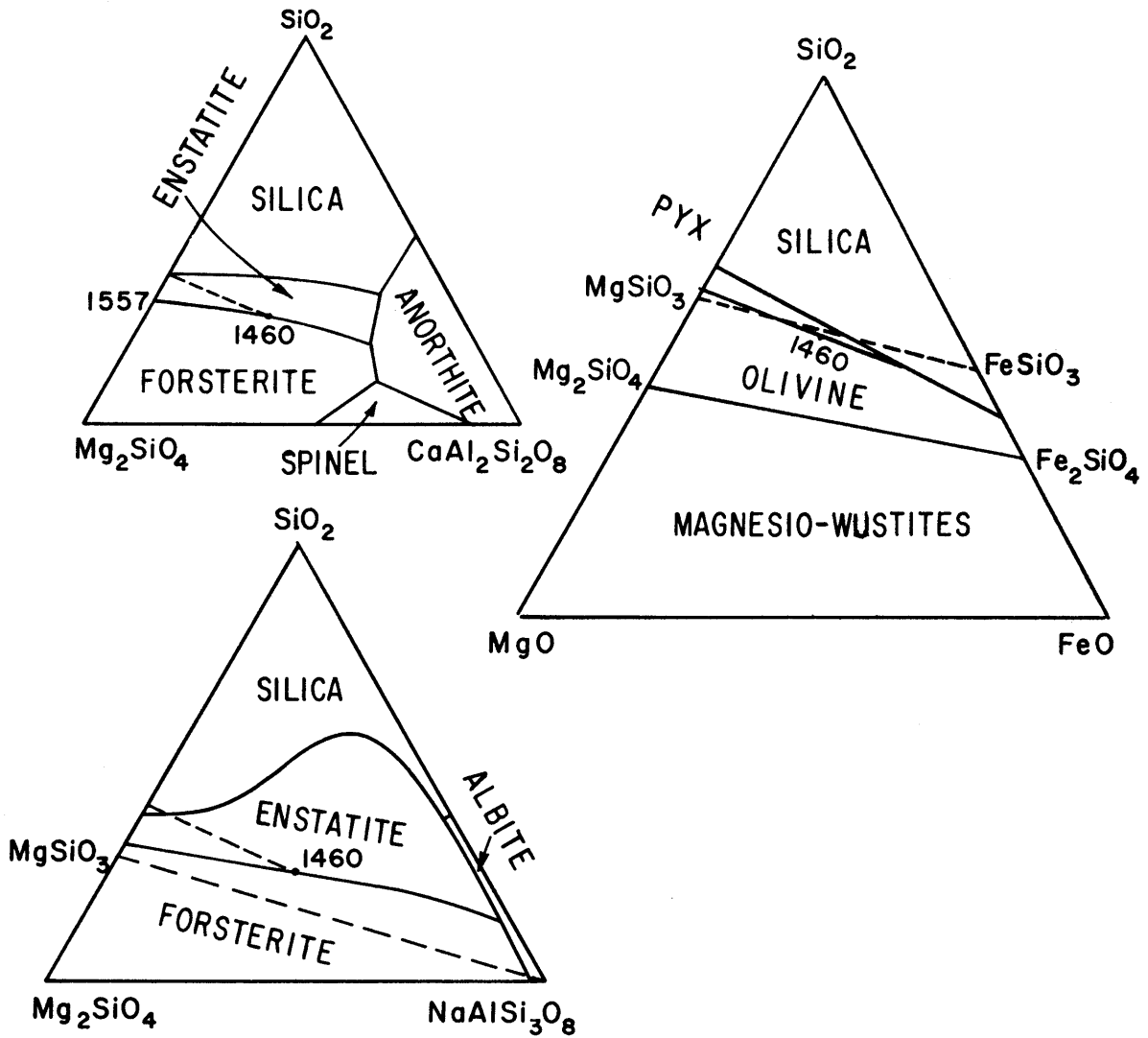
FIG. 3   SYSTEMS Mg_2SiO_4-SiO_2-$CaAl_2Si_2O_8$, Mg_2SiO_4-SiO_2-$NaAlSi_3O_8$,
MgO-FeO-SiO_2 SHOWING SHIFT OF OLIVINE-PYROXENE
COSATURATION COMPOSITION WITH ADDITION OF ANORTHITE,
ALBITE, AND FeO COMPONENTS TO A MAGNESIAN MELT.

(After Andesen, 1915, Schairer and Yoder, 1960, and Bowen
and Schairer, 1935).

The addition of iron oxide to the system $MgO-SiO_2$ has an opposite effect on the olivine-pyroxene cosaturation composition (Bowen and Schairer, 1935). At liquid compositions of equal weight percents of iron and magnesium oxides, the temperature of the field boundary is about 100 degrees lower than the pure magnesian peritectic, and the field boundary has changed to an even cotectic condition through a shift of 4.5 weight percent away from silica, measured with reference to the ternary system forsterite-fayalite-silica (Fig. 3).

It is now useful to estimate the effect of dissolved volatiles on the composition of the forsterite-enstatite peritectic. Assuming initially that the free energy of mixing in the liquid solution $MgO-SiO_2$ is not changed in the enstatite region with the addition of dissolved volatiles, the ratio of the depression of the enstatite liquidus to that of forsterite will be equal to the ratio of the entropy of melting of 1/3 mole forsterite to that of 1/2 mole enstatite, or 4.3/3.3, or 1.3. A depression of the melting point of forsterite of 200 degrees would then result in a depression of the enstatite saturation curve of roughly 260 degrees, for a relative depression of the enstatite over the forsterite liquidus of 60 degrees.

Now it is readily seen from the $MgO-SiO_2$ liquidus diagram (Bowen, 1914) that a relative depression of the forsterite over the enstatite liquidus of 19 degrees causes a shift of 1 mole percent away from silica. Therefore, a relative

depression of the enstatite to forsterite saturation curves of 60 degrees would cause a shift in the peritectic of about 3 mole percent towards silica. This corresponds to a 5 percent shift in weight percent in the binary system Mg_2SiO_4-SiO_2 per 200 degrees lowering of the forsterite liquidus.

However, adding H_2O to the melt will change the free energy of mixing between MgO and SiO_2. Substitution of one cation for another in silicate melts frequently does not require any energy where silicon is not involved in the substitution, i.e. the substitution is observed to be ideal. If the addition of H_2O to an MgO-SiO_2 melt is ideal in this sense, the chemical potential of MgO is unchanged, except for the slight effect of dilution, but that of SiO_2 is rapidly reduced with increasing cation content, particularly for melts near enstatite in composition (Fig. 2, p.33). Because there is more SiO_2 in 1/2 gfw. enstatite than in 1/3 gfw. forsterite, the reduction of mixing free energy of the former is the greater, and so the lowering of the enstatite liquidus relative the forsterite liquidus is enhanced. Quantitative estimates suggest that the relative lowering due to this mixing effect of H_2O alone is of similar magnitude to that calculated above assuming no mixing effect.

Thus, the shift of the forsterite-enstatite peritectic towards silica in the forsterite-silica binary is likely about 10 percent under conditions of dissolved steam sufficient to lower the olivine liquidus by 200 degrees. Perhaps it is not

A. atmospheric pressure   B. high pressure   C. volatiles dissolved in melt (high water pressure)
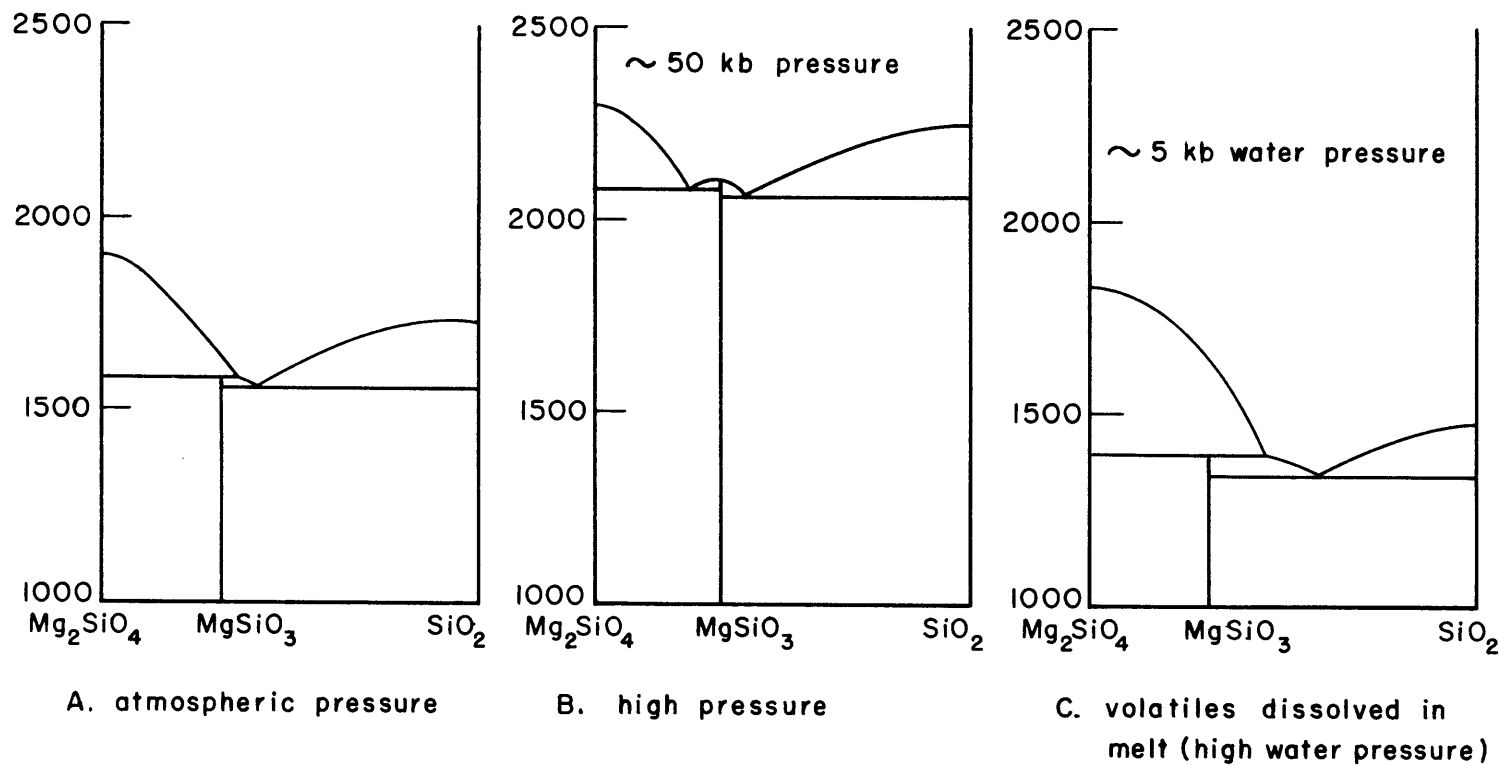
FIG. 4   SCHEMATIC REPRESENTATION OF SYSTEM Mg_2SiO_4-SiO_2
MELTING RELATIONS AT ATMOSPHERIC PRESSURE,
HIGH PRESSURES, AND UNDER CONDITIONS OF VOLATILES
PRESENT UNDER MODEST PRESSURE SHOWING SHIFT IN
OLIVINE PYROXENE COSATURATION POINT.

merely coincidence that this is the same shift per 200 degrees liquidus lowering determined experimentally by Andersen (1915) for the case of the addition of dissolved anorthite.

Fig. 4 illustrates this behavior of dissolved volatiles on the forsterite-enstatite cosaturation point in comparison to the opposite effect of total pressure.

5. System $CaMgSi_2O_6 - MgSiO_3$

The melting relations in the system diopside-enstatite
have been investigated by Bowen (1914) and are shown in
Fig. 7 (p. 53). Forsterite appears on the liquidus over all
but the diopside end of the system, but the effect of this
early olivine crystallization upon the composition of the
liquid is slight. The maximum deviation of the liquid from the
binary section is about one percent silica.

Two univariant points occur in the system, a minimum
congruent melting point at about Di 82 En 18, and a peritectic
three phase equilibrium Di 45 En 55 - Di 60 En 40 - liquid at
about $1390^{\circ}C$. The latter univariant point occurs as a result
of the intersection of the pyroxene solvus and the solidus,
which has been confirmed by Boyd and Schairer (1957).

5.1 Derivation of an Empirical Free Energy Function for the Solid Solution at Constant Pressure

The form of the diopside-clinoenstatite miscibility gap
as determined by Boyd and Schairer is shown in Fig. 5. The
critical point at atmospheric pressure is metastable, but
extrapolation of the gap above the solidus indicates its
position at approximately Di 54 En 46 and $1406^{\circ}C$.

An empirical equation for the free energy of this solid
solution can be written involving three groups of terms, one
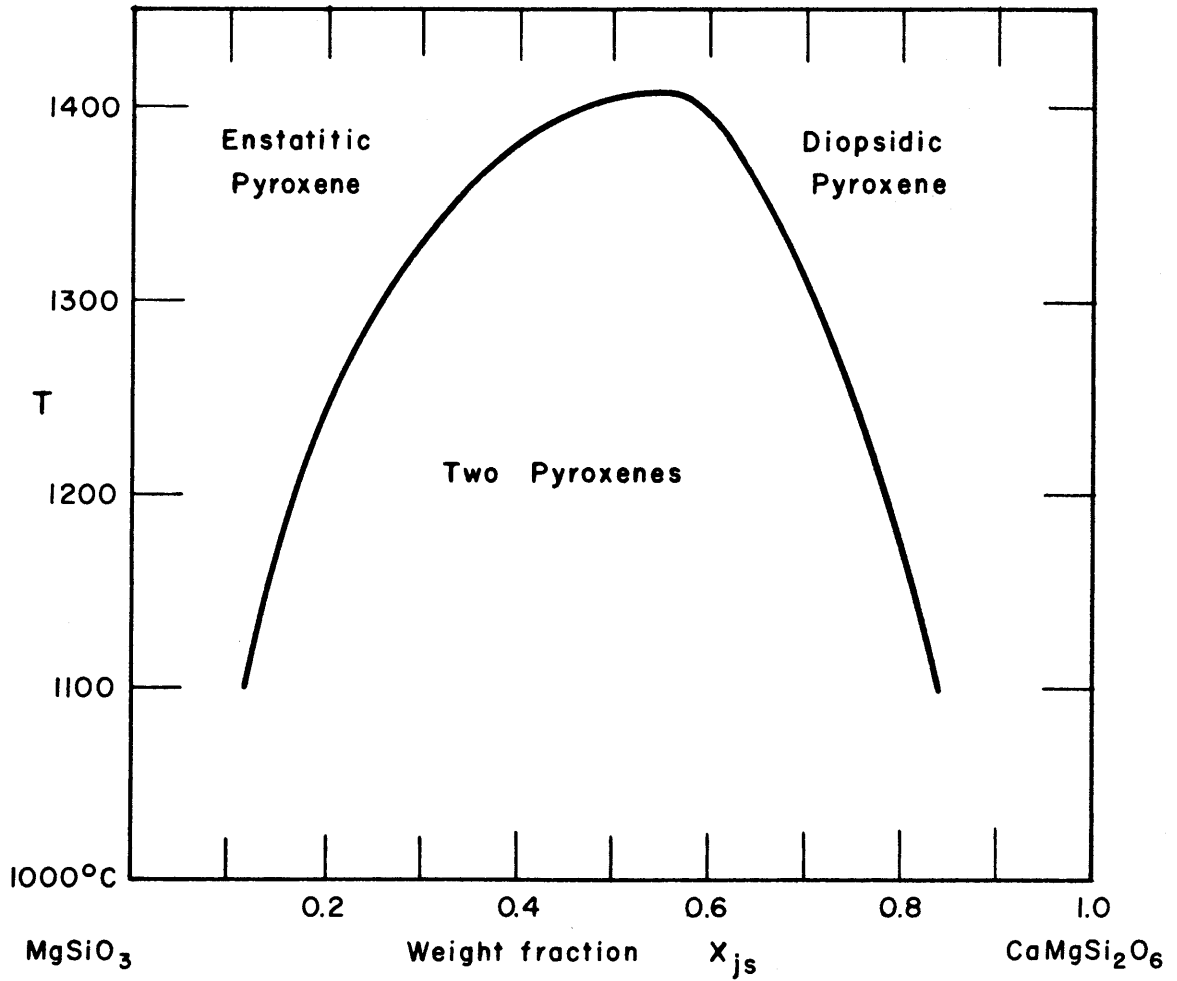
FIG. 5   MISCIBILITY GAP IN THE SYSTEM $CaMgSi_2O_6$-$MgSiO_3$.
(After Boyd and Schairer, 1957).

the free energy contribution of the end members, one a
temperature dependent series corresponding largely to an
entropy of mixing contribution, and one a temperature inde-
pendent series corresponding largely to an enthalpy of mixing
contribution.

$$
\begin{aligned}
\overline{G}_s(X_{js}, T) = & (1-X_{js})\overline{G}_s(0,T) + X_{js}\overline{G}_s(1,T) \\
& + \left[1+k(T-T_c) + \ell(T-T_c)^2\right]\left[a+b(X_{js}-X_{jc})\right. \\
& \left. + c(X_{js}-X_{jc})^2 + d(X_{js}-X_{jc})^3 + e(X_{js}-X_{jc})^4\right] \\
& + f + g(X_{js}-X_{jc}) + h(X_{js}-X_{jc})^2
\end{aligned} \tag{36}
$$

where X_{js} is the mole fraction of diopside, $\overline{G}_s(0,T)$ and $\overline{G}_s(1,T)$
are the molar free energies of pure enstatite and diopside,
and X_c and T_c are the composition and temperature of the
critical point.

Differentiating (36) we obtain

$$
\begin{aligned}
\left(\frac{\partial \overline{G}_s}{\partial X_{js}}\right)_T = & -\overline{G}_s(0,T) + \overline{G}_s(1,T) \\
& + \left[1+k(T-T_c)+\ell(T-T_c)^2\right]\left[b+2c(X_{js}-X_{jc})\right. \\
& \left. + 3d(X_{js}-X_{jc})^2 + 4e(X_{js}-X_{jc})^3\right] \\
& + g + 2h(X_{js}-X_{jc})
\end{aligned} \tag{37}
$$

and

$$
\left(\frac{\partial^2 \overline{G}_s}{\partial X_{js}^2}\right)_T = \left(1+k(T-T_c)+\ell(T-T_c)^2\right)\left[2c+6d(X_{js}-X_c)+12e(X_{js}-X_{jc})^2\right] \\
+ 2h \tag{38}
$$

At the critical point, $X_{js} = X_{jc}$, $T = T_c$, $\left(\dfrac{\partial^2 \bar{G}}{\partial X_{js}^2}\right)_T = 0$, hence

$$c = -h \tag{39}$$

Furthermore, we have boundary conditions. When $X_{js} = 0$, we have for all temperatures

$$\bar{G}_s\left(X_{js}, T\right) = \bar{G}_s\left(0, T\right)$$

Hence,

$$a - b X_{jc} + c X_{jc}^2 - d X_{jc}^3 + e X_{jc}^4 = 0 \tag{40}$$

$$f - g X_{jc} + h X_{jc}^2 = 0 \tag{41}$$

Similarly, when $X_{jc} = 1$

$$a + b\left(1 - X_{jc}\right) + c\left(1 - X_{jc}\right)^2 + d\left(1 - X_{jc}\right)^3 + e\left(1 - X_{jc}\right)^4 = 0 \tag{42}$$

$$f + g\left(1 - X_{jc}\right) + h\left(1 - X_{jc}\right)^2 = 0 \tag{43}$$

We also have from (8) and (9) for the two phase immiscibility region:

$$\left(\frac{\partial \bar{G}_\alpha}{\partial X_{js\alpha}}\right)_T = \left(\frac{\partial \bar{G}_\beta}{\partial X_{js\beta}}\right)_T \tag{44}$$

and

$$\bar{G}_\alpha\left(X_{js\alpha}, T\right) - \bar{G}_\beta\left(X_{js\beta}, T\right) = \left(X_{js\alpha} - X_{js\beta}\right)\left(\frac{\partial \bar{G}_\alpha}{\partial X_{js\alpha}}\right)_T \tag{45}$$

From (36) we may define the free energy of mixing by

$$\bar{G}_{s\,mix}(X_{js},T) = \left[1 + k(T-T_c) + \ell(T-T_c)^2 \right]\left[a + b(X_{js}-X_{jk}) \right.$$
$$\left. + c(X_{js}-X_{jk})^2 + d(X_{js}-X_{jk})^3 + e(X_{js}-X_{jk})^4 \right] \quad (46)$$
$$+ f + g(X_{js}-X_{jk}) + h(X_{js}-X_{jk})^2$$

Differentiating, we obtain

$$\left(\frac{\partial \bar{G}_{s\,mix}}{\partial T} \right)_{X_{js}} = -\bar{S}_{mix}(X_{js},T) = \left[k + 2\ell(T-T_c) \right]\left[a + b(X_{js}-X_{jk}) + \dots \right] \quad (47)$$

and

$$\left(\frac{\partial^2 \bar{G}_{s\,mix}}{\partial T^2} \right)_{X_{js}} = -\left(\frac{\partial \bar{S}_{mix}}{\partial T} \right)_{X_{js}} = 2\ell\left[a + b(X_{js}-X_{jk}) + \dots \right] \quad (48)$$

The variation of the molar entropy of mixing, $\bar{S}_{mix}$, with temperature theoretically should be very small, since heat capacities are characteristically very small and Cp mix/T is certainly minute, less than 10^{-4} cal/^{o}mole. Allowing a to be about 2000 calories, l is likely about $10^{-8}/^o$, almost negligable.

At various temperatures, the compositions of the two pyroxenes in equilibrium can be read from Fig. 5. The weight percent readings can be considered equivalent to mole percent if one 'mole' of diopside and 2-enstatite is taken to be 208 grams, permissible in a completely empirical analysis such as this. The conventional mole or gram formula weight is 216 grams for diopside and 200 grams for 2-enstatite, not very

different from 208 grams.

Substituting (37) into (44) for the following tempera-
tures and corresponding pyroxene compositions: $T = 1200^\circ C$,
$X'_{js\alpha} = 0.169, X_{js\beta} = 0.782$; $T = 1300^\circ C, X_{js\alpha} = 0.260, X_{js\beta} = 0.705$;
$T = 1350^\circ C, X_{js\alpha} = 0.332, X_{js\beta} = 0.657$, we obtain by reducing the
number of independent variables by equations (39) to (43),

$$
\begin{aligned}
f(-56)\left[-.650\,c + .0880\,d - .0424\,e\right] + .650\,c &= 0 \\
f(-106)\left[-.890\,c + .1536\,d - .1056\,e\right] + .890\,c &= 0 \\
f(-206)\left[-1.226\,c + .2373\,d - .2680\,e\right] + 1.226\,c &= 0
\end{aligned}
\right\} \quad (49)
$$

where $f(T - T_c) = 1 + k(T - T_c) + 1(T - T_c)^2$.

In addition, substituting (36) and (37) into (45) we
obtain at $1300^\circ C$,

$$
f(-106)\left[-.1980\,c + .0783\,d - .0337\,e\right] + .1980\,e = 0 \quad (50)
$$

· For 1 to be minimized, these equations (49 and 50) are
solved approximately by $e/c = 0.550$, $d/c = 0.1269$, $k = 4.15$ x
$10^{-4}/^\circ$, $1 = 6.5$ x $10^{-8}/^{\circ 2}$. These values for k and l only
approximately satisfy the immiscibility data in the range
$-100 < T - T_c < 0$, the largest error in temperature for a given
pyroxene immiscibility spread as T approaches T_c being 12
degrees. This discrepancy can be erased through the use of
smaller k values in the range of small negative values of
$T - T_c$. For example if 1 is set equal to zero, corrected
values of k to fit the immiscibility data exactly at
$T - T_c = -106^\circ$, -56°, and -16° are 3.92 x $10^{-4}/^\circ$, 3.28 x $10^{-4}/^\circ$,

and $1.34 \times 10^{-4}/^{o}$, respectively. Using the values of k and l determined according to the above equations, $k = 4.15 \times 10^{-4}/^{o}$, $l = 6.5 \times 10^{-8}/^{o2}$, the critical point would occur at $1394^{o}C$ instead of $1406^{o}C$. It is doubtful if the critical temperature is known to better than about 10°, and so this empirical correction at the top of the solvus is not important.

From equations (39) through (44), we can now list all the empirical coefficients of equation (36) in terms of one of the coefficients, say a. Although the value of a cannot be determined from the diopside-enstatite phase diagram, it should not be very different from the theoretical value of the entropy of mixing contribution to the free energy in a binary solution with single substitution at $T = T_c$, $X = X_c$, roughly -2500 calories/mole. This figure, -2500/208 grams, will be used for a in equation (36).throughout the analysis of the pyroxene solid and liquid free energy relations. If the actual value is quite different, the conclusions of the next section, which are based upon the relations between liquid and solid free energy functions, will not be affected. A numerical value of a is only convenient in the graphical representation of the free energy functions, and -2500 cal/208 grams is a reasonable magnitude for the constant a. The other constants of equations (36) are according to this value of a: b = 630 cal/208 g, c = 8930 cal/208 g, d = 1130 cal/208 g, e = 4910 cal/208 g, f = 2220 cal/208 g, g = -710 cal/208 g, h = -8930 cal/208 g, $k = 4.15 \times 10^{-4}/^{o}C$, $l = 6.5 \times 10^{-8}/^{o}C^{2}$.
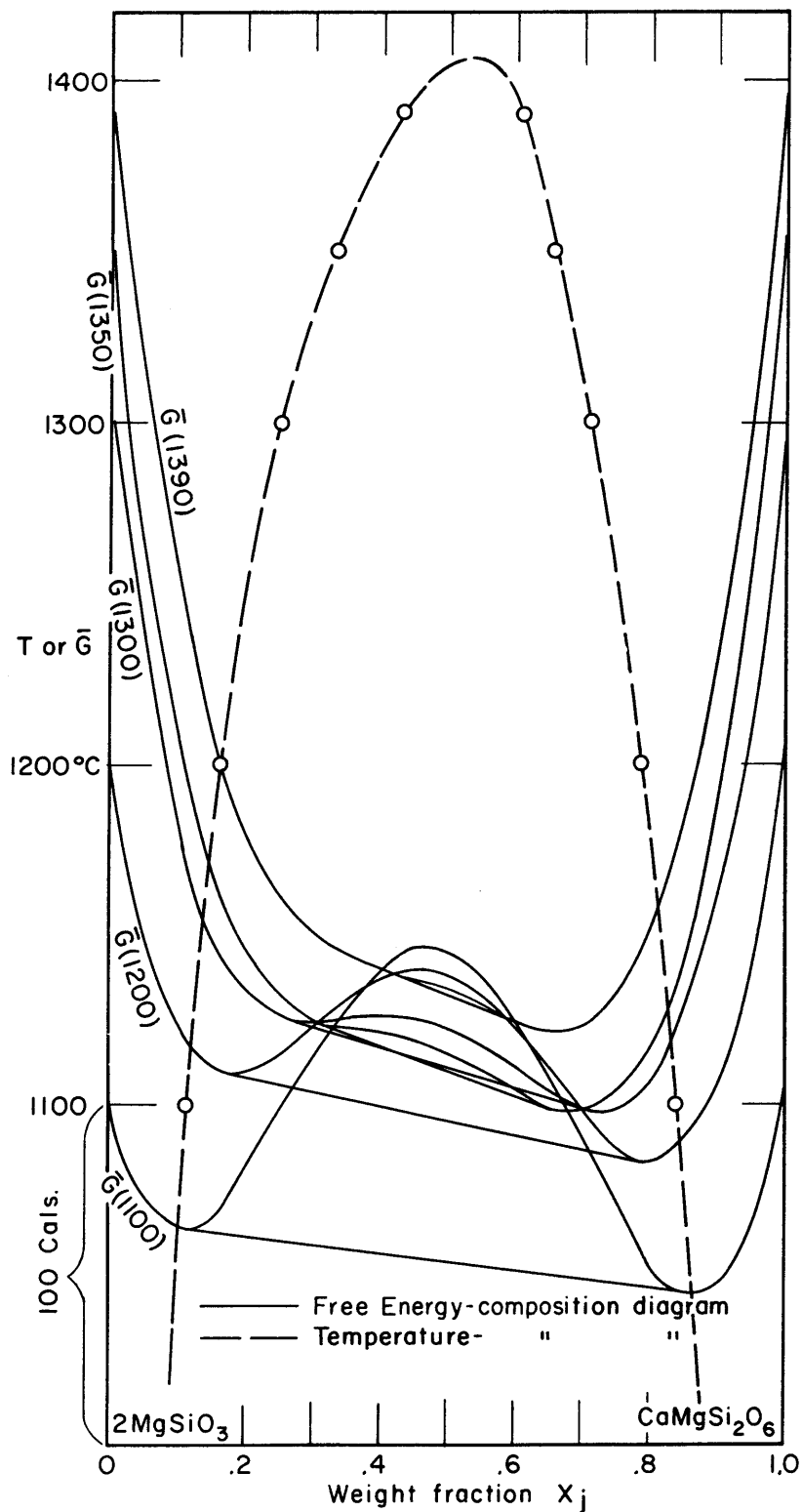
FIG. 6   FREE ENERGIES OF MIXING OF SOLID SOLUTION $CaMgSi_2O_6$-$2MgSiO_3$.

(Plotted at various temperatures - also shown is the miscibility gap.)

Fig. 6 shows the behavior of the free energy of mixing function [Equation (46)] at temperatures of 1100°C, 1200°C, 1300°C, and 1390°C. The values of k and l used at 1300°C and 1390°C are 3.28 x 10^{-4}, 0, and 1.34 x 10^{-4}, 0, respectively. Failure to apply this correction, as we have noted, would result in a 12 degrees flattening of the miscibility gap.

5.2 Derivation of an Empirical Free Energy Function for the Liquid Solution at Constant Pressure

The melting relations in the pseudobinary system $CaMgSi_2O_6 - 2MgSiO_3$ are shown in Fig. 7. The compositions of all liquids in this system lie either on or very close (within one percent of silica) to the binary composition line $CaMgSi_2O_6 - 2MgSiO_3$, and hence the appearance of forsterite on the liquidus can be ignored in an analysis of pyroxene-liquid equilibria.

An empirical equation for the free energy of the liquid solution can be written as follows:

$$\overline{G}_L\left(X_{jL}, T\right) = \left(1 - X_{jL}\right)\overline{G}_L\left(0, T\right) + X_{jL}\overline{G}_L\left(1, T\right)$$
$$+ \left[1 + m\left(T - T_c\right)\right]\left[p + q\left(X_{jL} - X_{jc}\right) + n\left(X_{jL} - X_{jc}\right)^2\right.$$
$$\left. + s\left(X_{jL} - X_{jc}\right)^3 + t\left(X_{jL} - X_{jc}\right)^4 + u\left(X_{jL} - X_{jc}\right)^5\right] \quad (51)$$

where X_{jL} is the mole fraction* of diopside component in the liquid, $\overline{G}_L(0,T)$ and $\overline{G}_L(1,T)$ are the molar* free energies of pure enstatite and diopside liquids, and X_{jc} and T_c are the

---

* based upon 208 g.
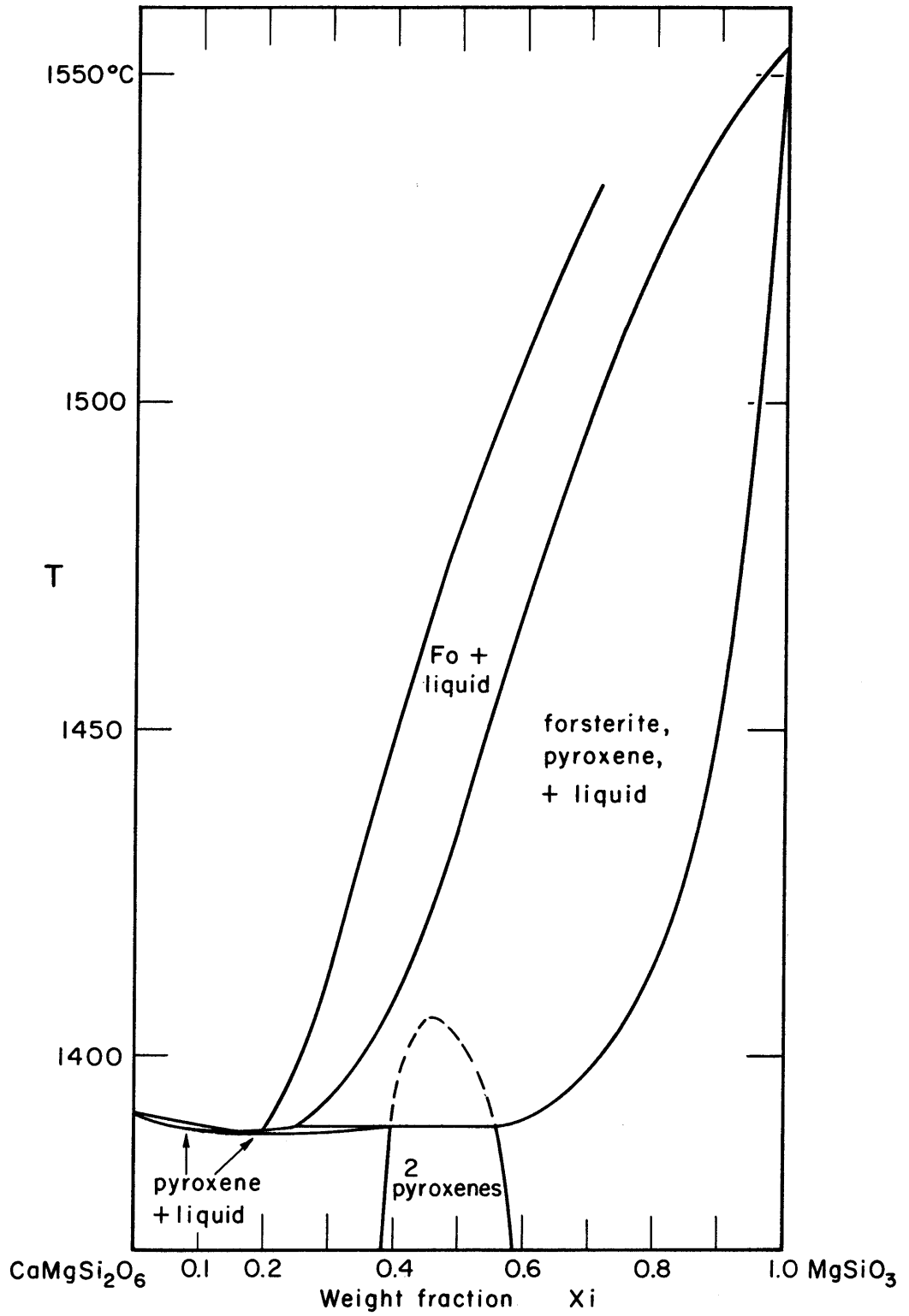
FIG. 7 MELTING RELATIONS IN THE PSEUDOBINARY SYSTEM $CaMgSi_2O_6$-$MgSiO_3$.

(After Bowen, 1914; Boyd and Schairer, 1957).

composition and temperature of the critical point in the solid solution, 0.540 and 1406°C.

Differentiating (51) we obtain

$$\left(\frac{\partial \bar{G}_L}{\partial X_{j_L}}\right)_T = \begin{array}{l} -\bar{G}_L(0,T) + \bar{G}_L(1,T) \\ + \left[1 + m(T-T_c)\right]\left[q + 2r(X_{j_L}-X_{j_c})\right. \\ \left. + 3s(X_{j_L}-X_{j_c})^2 + 4t(X_{j_L}-X_{j_c})^3 + 5u(X_{j_L}-X_{j_c})^4\right] \end{array} \quad (52)$$

In addition, we have from (51) at all temperatures the following boundary conditions:

$$p - qX_{j_c} + rX_{j_c}^2 - sX_{j_c}^3 + tX_{j_c}^4 - uX_{j_c}^5 = 0$$
$$p + q(1-X_{j_c}) + r(1-X_{j_c})^2 + s(1-X_{j_c})^3 + t(1-X_{j_c})^4 + u(1-X_{j_c})^5 = 0 \quad (53)$$

We also have from (8) and (9) for the two phase liquid-solid region:

$$\left(\frac{\partial \bar{G}_L}{\partial X_{j_L}}\right)_T = \left(\frac{\partial \bar{G}_S}{\partial X_{j_S}}\right)_T \quad (54)$$

and

$$\bar{G}_L(X_{j_L}, T) - \bar{G}_S(X_{j_S}, T) = (X_{j_L} - X_{j_S})\left(\frac{\partial \bar{G}_S}{\partial X_{j_S}}\right)_T \quad (55)$$

In the pyroxene immiscibility analysis, both coexisting phases were part of the same binary series and had identical end members, solid diopside and clinoenstatite. In an analysis of the two phase region pyroxene-liquid, however, we are dealing with two solutions, solid and liquid, each with different end

members. Hence the relative free energies of the end members
of the two phases is of great importance.

The free energies of pure liquid enstatite and diopside
can be given approximately in terms of those of solid clino-
enstatite and diopside:

$$\begin{aligned}
\overline{G}_L\left(0,T\right) &= \overline{G}_s\left(0,T_{mo}\right) + \left(T_{mo}-T\right)\Delta\overline{S}_0 \\
\overline{G}_L\left(1,T\right) &= \overline{G}_s\left(1,T_{mi}\right) + \left(T_{mi}-T\right)\Delta\overline{S}_1
\end{aligned} \right\} \tag{56}$$

where T_{mo} and T_{mi} are the melting points of enstatite and
diopside, 1557°C and 1391°C, respectively. $\Delta\overline{S}_0$, the entropy of
melting of enstatite, is taken as 13.2 e.u./200 g or 13.7 e.u./
208 g. $\Delta\overline{S}_1$, the entropy of melting of diopside is given an
identical value, 13.7 e.u./208 g. The entropies of melting of
these two pyroxenes, although not known precisely, are likely
very similar, as we have seen (p. 27), and they are therefore
taken equal for the empirical 208 gram 'moles' used in this
analysis.

Substituting (37) and (52) into the slope equality relation
(54) using the values of the coefficients determined in the
miscibility gap analysis, we obtain three equations using the
following liquid-solid equilibrium data from Fig. 7: at 1390°C,
$X_{js} = 0.400$, $X_{jL} = 0.750$; at 1410°C, $X_{js} = 0.218$, $X_{jL} = 0.592$; at
1500°C, $X_{js} = 0.040$, $X_{jL} = 0.787$. The equations obtained after
the unknowns have been reduced through the boundary conditions
of equations (53) are:

$$\left(1-16m\right)\left(.500n - .1225s + .0772t - .0568u\right) = 2207$$
$$\left(1+4m\right)\left(.1840n - .2467s + .0408t - .0665u\right) = 1875$$
$$\left(1+94m\right)\left(-.426n - .0628s - .0246t - .0460u\right) = 197 \tag{57}$$

Similarly, substituting equations (36), (37) and (51) into the chemical potential equality relation, equation (55), we obtain the following relation:

$$\left(1+4m\right)\left(-.2415n + .0069s - .0612t + .0065u\right) = -1065 \tag{58}$$

It was found impossible to determine m, the temperature coefficient, from the liquid-solid equilibria. This coefficient is far too small to have much effect upon either the free energy slopes or the chemical potentials of the liquid solid equilibria. This was not the case with the solid immiscibility equilibria which are wholly controlled by changes in the free energy of mixing and are independent of end member free energies. In the liquid-solid equilibria, changes in the free energy of mixing of the solutions are insignificant in comparison to end member variations. The value of m, however, can be estimated as $6 \times 10^{-4}/^{\circ}$, approximately that of an ideal binary solution.

Solving (57) and (58) using $m = 6 \times 10^{-4}/^{\circ}$, we arrive at the following values for the coefficients of (51), which as we can see from (57) and (58) are only very slightly dependent upon m: p = -1160 cal/208 g, q = 1830 cal/208 g, r = 370 cal/ 208 g, s = -1090 cal/208 g, u = -14300 cal/208 g, t = 14230 cal/ 208 g.

Fig. 8 shows the form of this liquid molar free energy of mixing function at 1410°C. It is interesting to compare this function with the ideal free energy of mixing function for a liquid in the system $2CaSiO_3 - 2MgSiO_3$. The free energy of mixing of such a liquid would be given by:

$$\overline{G}_{L \text{ mix ideal}} = 2RT\left[X_{CaSiO_3}\ln X_{CaSiO_3} + \left(1-X_{CaSiO_3}\right)\ln\left(1-X_{CaSiO_3}\right)\right] \quad (59)$$

where X_{CaSiO_3} is the mole fraction of $CaSiO_3$ in the liquid. All the empirical coefficients derived for the solid and liquid free energy functions are based upon the assigned value of -2500 cal/208 g for the temperature dependent portion of the free energy of mixing for the solid solution at the critical temperature and composition. This assigned value is roughly similar in magnitude to the entropy of mixing contribution to the free energy at this temperature and composition in a binary solution with single substitution.

2-enstatite-diopside is such a system if it is considered that the magnesium in the Y position of the clinopyroxene formula XYZ_2O_6 is fixed with single calcium and magnesium substitution allowed in the X position. If the temperature dependent free energy of mixing here is -2500 cal/208 g at $T = 1406^\circ$ and $X_{js} = 0.540$, the analogous ideal free energy of mixing in equation (59) at $T = 1406^\circ$C, $X_{CaSiO_3} = 0.520$ should equal 5000 cal/mole. Setting $\overline{G}_{L \text{ mix ideal}}$ in this manner defines an ideal curve for the liquid $CaSiO_3 - MgSiO_3$ which can be directly compared with the empirical liquid free energy
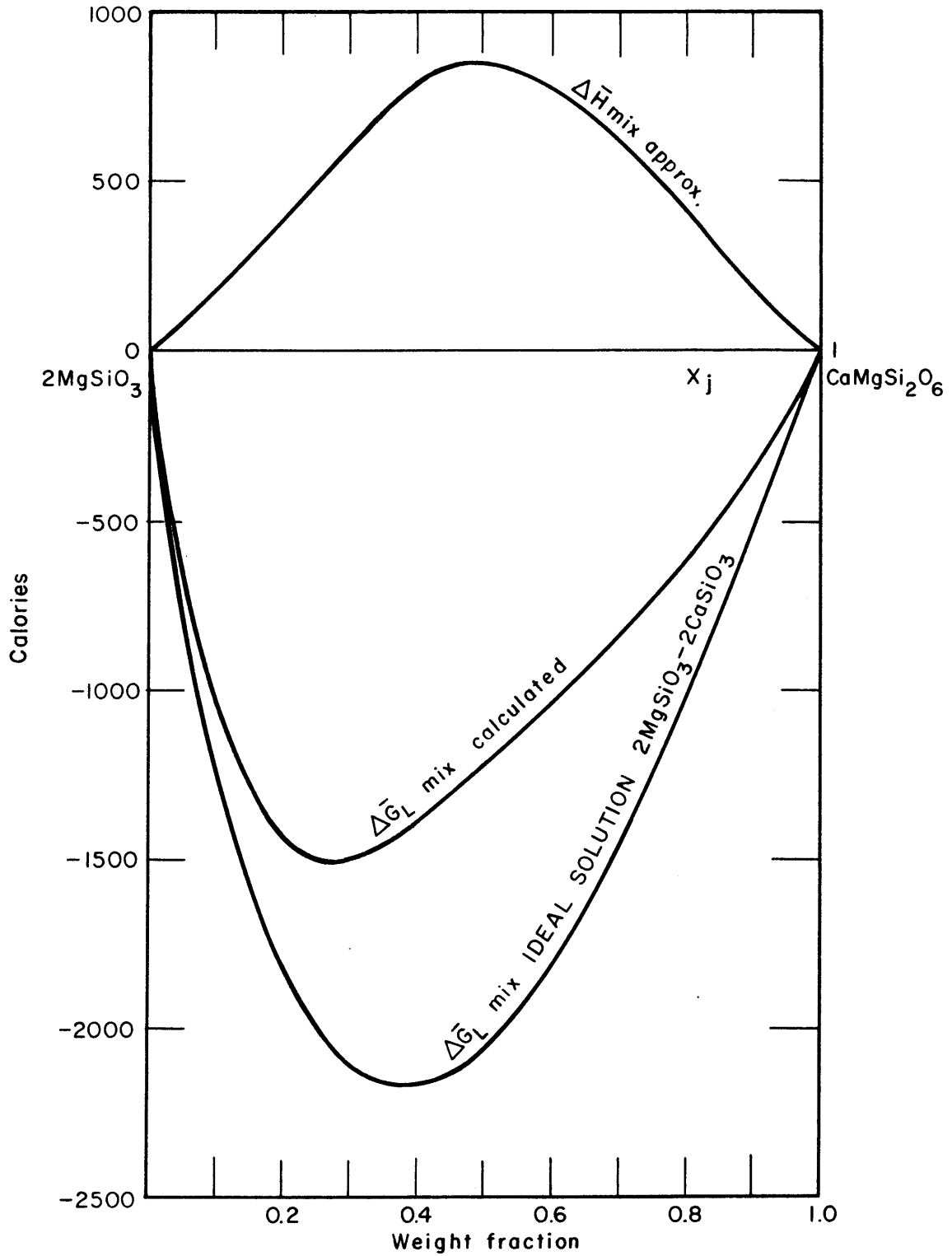
FIG. 8   CALCULATED FREE ENERGY OF MIXING OF LIQUID

SOLUTION $CaMgSi_2O_6$-$2MgSiO_3$ COMPARED WITH IDEAL

CURVE FOR SOLUTION $2CaSiO_3$-$2MgSiO_3$ AT $1410^\circ C$.

curve, which is also pegged to the value -2500 cal/208 g for the solid free energy of mixing at the critical temperature and composition.

In Fig. 8, the mixing between $CaMgSi_2O_6$ and $2MgSiO_3$ according to equation (59) with a value of -5000 cal/gfw. at $T = 1406$, $X_{CaSiO_3} = 0.052$, is shown. The composition scale is adjusted to X_{jl}, mole percent with equal weighted end members, or simply weight percent, and the free energy at the diopside and enstatite composition is set at zero.

Subtracting the empirical curve from this ideal curve, an approximate heat of mixing function for the liquid $CaMgSi_2O_6$-$2MgSiO_3$ is obtained. It is interesting to note that this curve has a maximum at about $X_{jl} = 0.5$, even though the maximum free energy of mixing for the liquid is close to $X_{jl} = 0.3$. It is likely that this heat of mixing represents a modification of the heat of mixing associated with the solid solution, suggesting the existence of some structure in the liquid analogous to that in the solid. Perhaps this is due to incipient grouping of pyroxene type silica chains in the liquid. The maximum value of this liquid heat of mixing, 850 cal/208 grams, can be compared with the empirically determined temperature independent contribution to the solid free energy of mixing, 2250 cal/208 grams, which roughly represents the heat of mixing in the solid. These numerical values are of course in proportion to the value of -2500 calories/208 g for the temperature dependent contribution to the free energy of mixing.
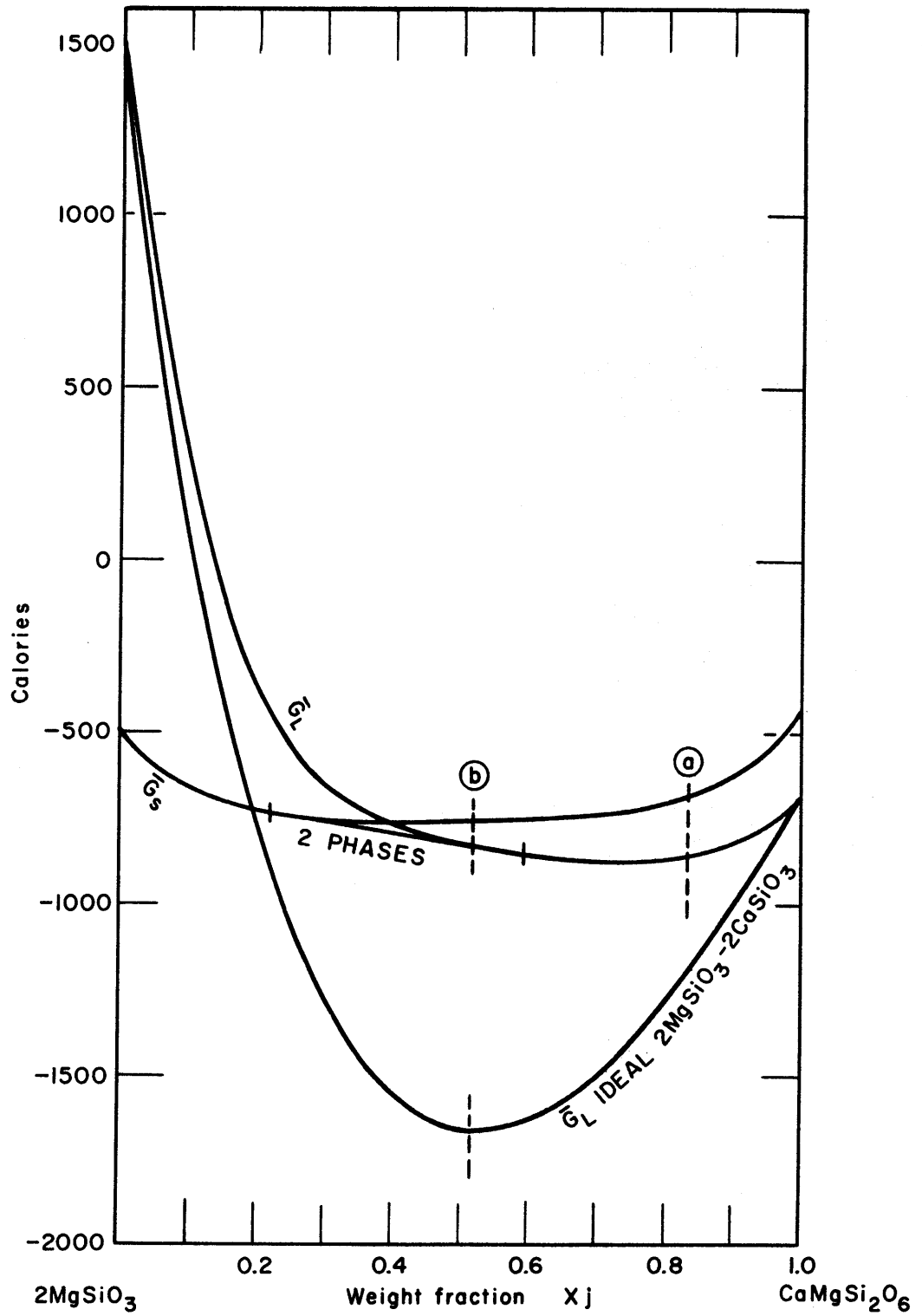
FIG. 9   FREE ENERGY-COMPOSITION DIAGRAM AT $1410^{\circ}C$ FOR

SYSTEM $CaMgSi_2O_6$-$2MgSiO_3$.

(Dotted lines show position of solidus minimum (a) with and

(b) without consideration of liquid heat of mixing.)

Fig. 9 shows a free energy composition diagram for the temperature $1410^\circ C$. If the temperature is lowered, the liquid free energy curve will move upward with respect to the solid curve and the liquid will disappear at $X_j = 0.83$. Since the entropies of melting of diopside and enstatite are similar, no relative tilting of the two curves occurs.

It can be noted that if the liquid solution were ideal, the liquid would disappear at $X_j = 0.52$, with a eutectic valley of about 50 degrees occurring.

5.3 Form of the Liquid Heat of Mixing Function Inferred from the Slope of the Enstatite Liquidus

The slope of the enstatite liquidus curve in Fig. 7 can be used to obtain further information on the heat of mixing in the liquid solution $CaMgSi_2O_6 - 2MgSiO_3$.

We can write the free energy of mixing of solid and liquid solutions $CaMgSi_2O_6 - 2MgSiO_3$ assuming single substitution in the solid from $CaMgSi_2O_6$ (di) to $2MgSiO_3$ (en), and double substitution in the liquid from $2CaSiO_3$ (wo) to $2MgSiO_3$ (en) as follows:

$$\overline{G}_s \text{ mix} = \left(1 - X_s\, di\right)\overline{G}_s\left(0,T\right) + X_s\, di\, \overline{G}_s\left(1,T\right) \\ + RT\left[X_s\, di\, \ln X_s di + \left(1 - X_s di\right)\ln\left(1 - X_s\, di\right)\right] \\ + \overline{H}_s \text{ mix} \tag{60}$$

$$\bar{G}_{L \; mix} = (1 - X_L di) \bar{G}_L (0,T) + X_L di \, \bar{G}_L (1,T)$$
$$+ 2RT \left[X_{L wo} \ln X_{L wo} + (1 - X_{L wo}) \ln (1 - X_{L wo}) + 0.693 X_L di \right] + \bar{H}_L \; mix \quad (61)$$

where 0 and 1 refer to en and di, X's are gram formula weight or 'mole' fractions.

Differentiating (60) and (61), we obtain, noting that $dX_{wo} = 2 dX_{di}$:

$$\left(\frac{\partial^2 \bar{G}_L}{\partial X_L di^2} \right)_T = \frac{RT}{4 X_{di L} (1 - X_{di L})} + \frac{d^2 \bar{H}_{L \; mix}}{d X_{di L}^2} \quad (62)$$

$$\left(\frac{\partial \bar{G}_L}{\partial T} \right)_X = -(1 - X_L di) \bar{S}_L (0) - X_L di \, \bar{S}_L (1)$$
$$+ 2R \left[\frac{X_L di}{2} \ln X_L di + \frac{(1 - X_L di)}{2} \ln (1 - X_L di) + 0.693 X_L di \right] \quad (63)$$

$$\left(\frac{\partial \bar{G}_S}{\partial T} \right)_X = -(1 - X_S di) \bar{S}_S (0) - X_S di \, \bar{S}_S (1)$$
$$+ R \left[X_S di \ln X_S di + (1 - X_S di) \ln (1 - X_S di) \right] \quad (64)$$

$$\left(\frac{\partial^2 \bar{G}_L}{\partial X_L di \, \partial T} \right) = \bar{S}_L (0) - \bar{S}_L (1) + R \ln \left(\frac{X_L di}{1 - X_L di} \right) + 1.386 \, R \quad (65)$$

Now, from (20) we have for the two phase equilibrium enstatitic pyroxene—liquid in the system $CaMgSi_2O_6 - 2MgSiO_3$:

$$\left(\frac{dT}{dX_{dil}}\right) = \frac{\left(X_{dil}-X_{dis}\right)\left(\frac{\partial^2 \bar{G}_L}{\partial X_{dil}^2}\right)_T}{\left(X_{dis}-X_{dil}\right)\left(\frac{\partial^2 \bar{G}_L}{\partial X_{dil}\partial T}\right) + \left(\frac{\partial \bar{G}_L}{\partial T}\right)_{X_{dil}} - \left(\frac{\partial \bar{G}_S}{\partial T}\right)_{X_{dis}}} \quad (66)$$

Substituting from equations (60) to (65) at $1410°C$, where from Fig. 7, $X_{dil} = 0.573$, $X_{wol} = 0.287$, $X_{dis} = 0.205$, and $\Delta \bar{S}(o) = \Delta \bar{S}(i) = 13.5$, we obtain:

$$\left(\frac{dT}{dX_{dil}}\right) = \frac{0.900 RT + 0.368 \left(\frac{d^2 \bar{H}_{L\,mix}}{dX_{dil}^2}\right)}{-0.072 R - 13.5_{e.u.}}$$

At $1410°$, from Fig. 7, $dT/dX_{dil} = -200°$; hence

$$\frac{d^2 \bar{H}_{L\,mix}}{dX_{dil}^2} = \frac{-310}{0.368} = -840 \text{ cals.}$$

From the slope of the enstatite liquidus at $1410°$, then, a liquid heat of mixing function convex upwards at $X_{dil} = 0.573$, or $X_{d_L} = 0.592$ is suggested. This agrees in sign with the empirical data of Fig. 8, but the curvature of the endothermic heat of mixing function derived empirically is greater by almost an order of magnitude, about -7500 calories. The empirical determination of this second derivative is not reliable, however, but the determination from the slope of the enstatite

liquidus cannot be too erroneous. The slope of this liquidus can be read fairly accurately from Fig. 7, and the major contribution to the denominator of equation (66) is $-\Delta \bar{S}(c) +$ $X_{di.s} \left\{ \Delta \bar{S}(c) - \Delta \bar{S}(l) \right\}$, which is not likely in error by more than 10 percent. This indicates the second derivative of the heat of mixing with respect to composition lies between 0 and -1500 calories, a very slight curvature. This suggests that the heat of mixing in the liquid between $2MgSiO_3$ and $CaMgSi_2O_6$ can be represented roughly by two fairly linear functions increasing from 0 at $2MgSiO_3$ and $CaMgSi_2O_6$ to a maximum around 800 calories at about 1 $MgSiO_3$, 1/2 $CaMgSi_2O_6$.

5.4 Effect of Dissolved Steam on the Phase Relations

It is well known that the effect of water dissolved in silicate magmas is to lower the melting point of the solids. For the first pyroxene to crystallize from an Hawaiian tholeiitic basalt, this lowering amounted to some $100^{\circ}C$ with a pressure of steam saturation of 5 kilobars (Yoder and Tilley, 1956), a similar value to the lowering of the melting point of pure diopside at this pressure (Yoder, 1955).

It is interesting to consider the probable effects of dissolved volatiles such as water upon the liquid free energy function and upon the form of the pyroxene liquidus in the system $2MgSiO_3 - CaMgSi_2O_6$. No shift in the minimum melting composition, approximately at Di 17 En 83 at atmospheric

pressure, could occur if a given melt volatile content
lowered the free energy of both liquid end members identically,
without affecting the free energy of mixing. This is because
the entropies of melting of diopside and 2-enstatite are
similar. There is the possibility that volatiles would depress
the free energy of diopside and enstatite liquids unequally,
but a difference of about 500 calories in the lowering of the
free energy for 208 grams is necessary to cause appreciable
shift in the minimum (see Fig. 9). This seems unlikely, since
under 5 kilobars water pressure, the total lowering of the free
energy of diopside liquid corresponding to a melting point
lowering of 100 degrees is only about 1350 calories/208 grams,
and enstatite liquid, the melt of a similar compound, would not
be expected to behave radically different.

The probable effect of dissolved H_2O upon the free energy
of mixing of liquid diopside and enstatite is important,
however. Wasserburg (1957) considers a silicate melt as
essentially a rigid structure composed of a tetrahedral segment
as the fundamental unit. These tetrahedra are linked in three
dimensions to one another through silicon-oxygen-silicon
bridges, or they have oxygens bonded to other cations unshared
by other SiO_4 tetrahedra. In either case, Wasserburg believes
water may break down the oxygen linkage as follows:

$$-\overset{\displaystyle |}{\underset{\displaystyle |}{Si}} - O - \overset{\displaystyle |}{\underset{\displaystyle |}{Si}} - \longrightarrow -\overset{\displaystyle |}{\underset{\displaystyle |}{Si}} - OH \quad HO - \overset{\displaystyle |}{\underset{\displaystyle |}{Si}} -$$

or
$$-\underset{|}{\overset{|}{Si}} - O \cdot R \longrightarrow -\underset{|}{\overset{|}{Si}} - OH \quad HO \cdot R,$$
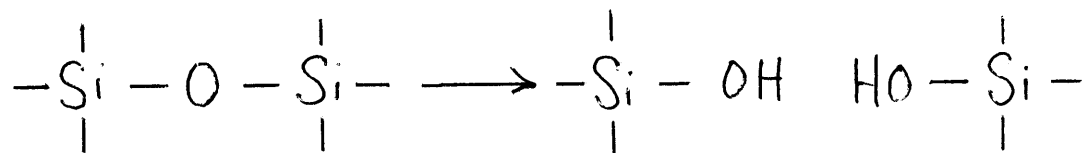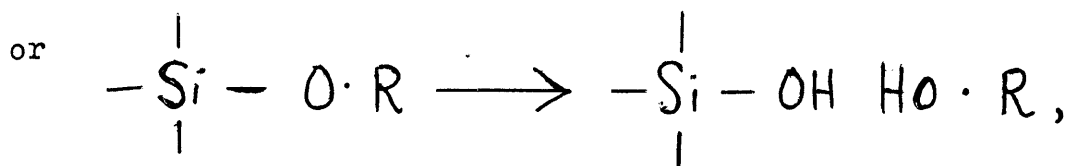
where R is a cation not in the silicon position.

The net result of the hydration of a silicate melt would then be the breakdown of the tetrahedral arrangement and the destruction of any remnant structure in the liquid related to a more ordered structure in the corresponding solid. Thus, in the case of the diopside — 2-enstatite system, where we have immiscibility in the solid and a considerable endothermic heat of mixing in the liquid, both presumably due to the favouring of the diopside and enstatite calcium to magnesium proportions, we might expect a breakdown in the liquid of this pseudo-pyroxene behavior. Such a breakdown of incipient liquid structure would be equivalent thermodynamically to the disappearance of the heat of mixing in the liquid. Thus the form of the free energy of mixing between diopside and 2-enstatite would, as water is added to the system, be expected to approach the ideal free energy of mixing curve of Fig. 9. Therefore, the effect of dissolved volatiles on the system diopside—enstatite can be expected to be twofold: i) to shift the minimum melting point from a shallow minimum near diopside (Di 17 En 83) towards a eutectic trough about 50 degrees deep near Di 50 En 50, and ii) to lower the melting point of the end members. This eutectic condition, as we shall see, is also inferred from field evidence.
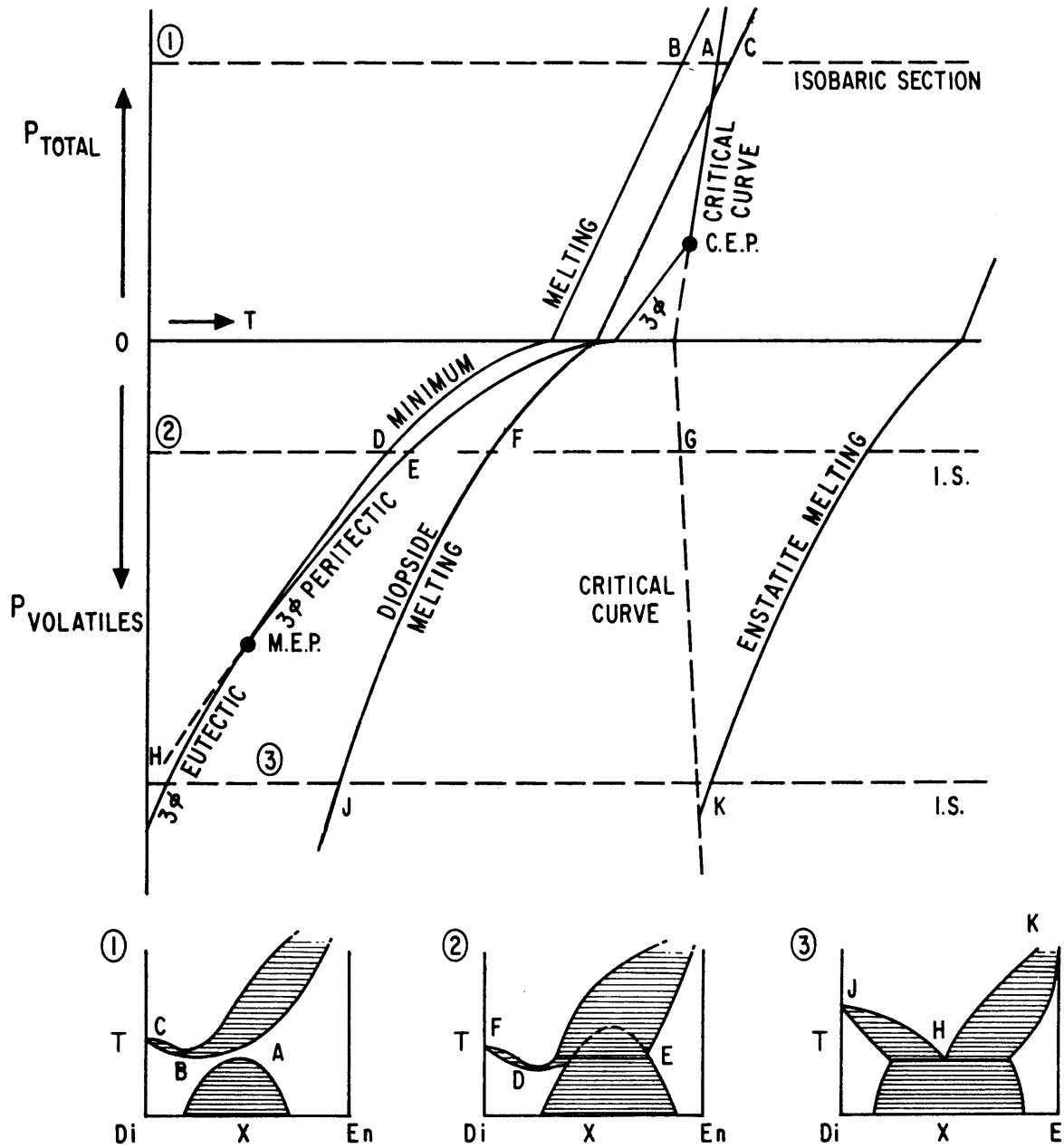
FIG. 10 SCHEMATIC PRESSURE-TEMPERATURE DIAGRAM FOR
THE PYROXENE RELATIONS IN THE PSEUDOBINARY
SYSTEM $CaMgSi_2O_6$-$MgSiO_3$.

(C. E. P. , M. E. P. , refer to invariant critical and minimum
end points; ϕ refers to phase.)

Fig. 10 shows these pyroxene melting relations in the form
of a schematic pressure-temperature diagram. The upper portion
involves increasing total pressure, the lower portion increas-
ing pressure of steam saturation. The temperature of all the
univariant melting relations increases with total pressure and
decreases with water pressure, except the critical curve for
the solid, which increases in temperature under any pressure
because the volume of mixing in the pyroxene solid solution is
positive. It is likely that water pressures of about 5 kilo-
bars will lower the melting points of enstatite and diopside
about $100^{\circ}C$ and reduce the liquid heat of mixing sufficiently
to produce the eutectic condition at temperatures below the
minimum end point.

5.5 Effect of Plagioclase on the Phase Relations

The effect of plagioclase upon the melting relation of
the lime-magnesian pyroxenes has been investigated by Andersen
(forsterite-anorthite-silica, 1915), by Osborn and Tait
(diopside-anorthite-silica, 1952), and more recently by
Schairer and Morimoto (enstatite-diopside-albite, 1959), and
by Hytonen and Schairer (enstatite-diopside-anorthite, 1961).
Since all basalts contain a considerable proportion of
plagioclase, the effect of albite and anorthite components
upon the form of the pyroxene saturation and liquidus surfaces
must be considered in any discussion of the crystallization of

natural pyroxenes.

Fig. 11 shows the pyroxene and plagioclase saturation surfaces on the planes enstatite-diopside-anorthite and enstatite-diopside-albite. These surfaces are the actual liquidus surfaces only where forsterite does not appear on the liquidus. It can be seen that the addition of plagioclase to the diopside-enstatite composition line not only causes a reduction in the temperature of precipitation of the first pyroxene, but also increases the range of liquid compositions where the first pyroxene to crystallize is diopsidic and decreases the range where it is enstatitic.

In the case of natural basalts, we are concerned with the portions of the systems up to about 60 percent plagioclase. In this range, the point of four fold saturation, forsterite-anorthite-enstatitic pyroxene-diopsidic pyroxene, at 1260°C (Point Q, Fig. 11), represents the most magnesian composition (ignoring the plagioclase component) in either of the two diagrams of Fig. 11, where diopside is the first pyroxene to crystallize. This point represents the maximum shift of the minimum melting point between diopside and enstatite towards enstatite that is possible through the addition of anorthite, and probably also represents the maximum shift due to plagioclase we might expect in a natural basalt.

Projecting through anorthite on the base enstatite-diopside, this composition can be seen as Di 39 En 61. This point (Point P, Fig. 11), however, does not represent the
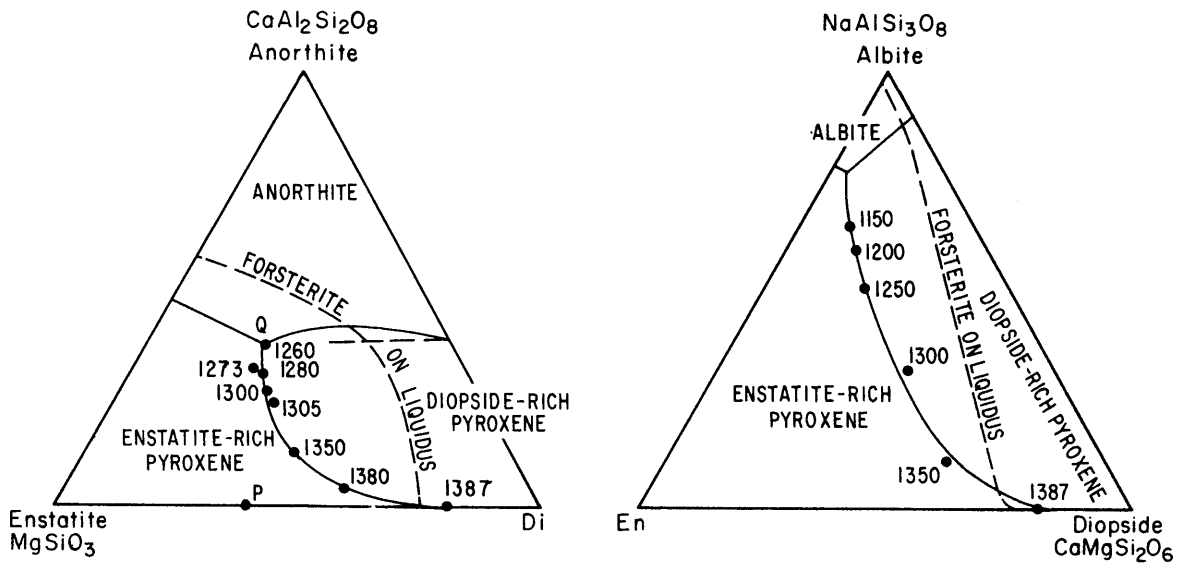
FIG. 11   MELTING RELATIONS ON THE PLANES $MgSiO_3$-$CaAl_2Si_2O_8$-$CaMgSi_2O_6$ AND $MgSiO_3$-$NaAlSi_3O_8$-$CaMgSi_2O_6$.

The extent of the forsterite liquidus is shown by the dotted lines. The intersection of the saturation surfaces of diopsidic and enstatitic pyroxene and anorthite or albite can be seen below the forsterite liquidus. Temperatures along these intersections are also shown. (Data taken from isothermal sections given by Hytonen and Schairer, 1961; Schairer and Morimoto, 1959.)

composition of the eutectic mixture of pyroxenes which first precipitates from a liquid at Q, because considerable forsterite separates before the pyroxenes, and the liquid has a much higher Di/(En + Di) ratio at pyroxene saturation than 0.39. Hence to get an idea of the actual shift of the pyroxene minimum due to plagioclase, we must consider the amount of forsterite which precipitates prior to pyroxene separation.

Fig. 12 represents the liquidus relations in the system forsterite-diopside-silica-anorthite, saturated with and projected through anorthite onto the triangle forsterite-diopside-silica. The shift of the forsterite-enstatite and forsterite-diopside field boundaries towards silica and forsterite, respectively, with anorthite saturation has been determined by Andersen (1915) and Osborn and Tait (1952), and the position of the complete forsterite-pyroxene field boundary saturated with anorthite inferred from these data is drawn.

The point A on the line diopside-enstatite at Di 39 En 61 (Fig. 12), is equivalent to points P and Q of Fig. 11, and represents the liquid composition from which diopsidic and enstatitic pyroxenes will precipitate simultaneously after forsterite. The liquid composition when the pyroxenes first crystallize is shown at B, and the pyroxene cotectic is therefore drawn towards silica from this point B. The proportion of diopside and enstatite crystallizing along this cotectic is given by the point F, which represents a mixture of 28 percent of enstatite of composition E and 72 percent of
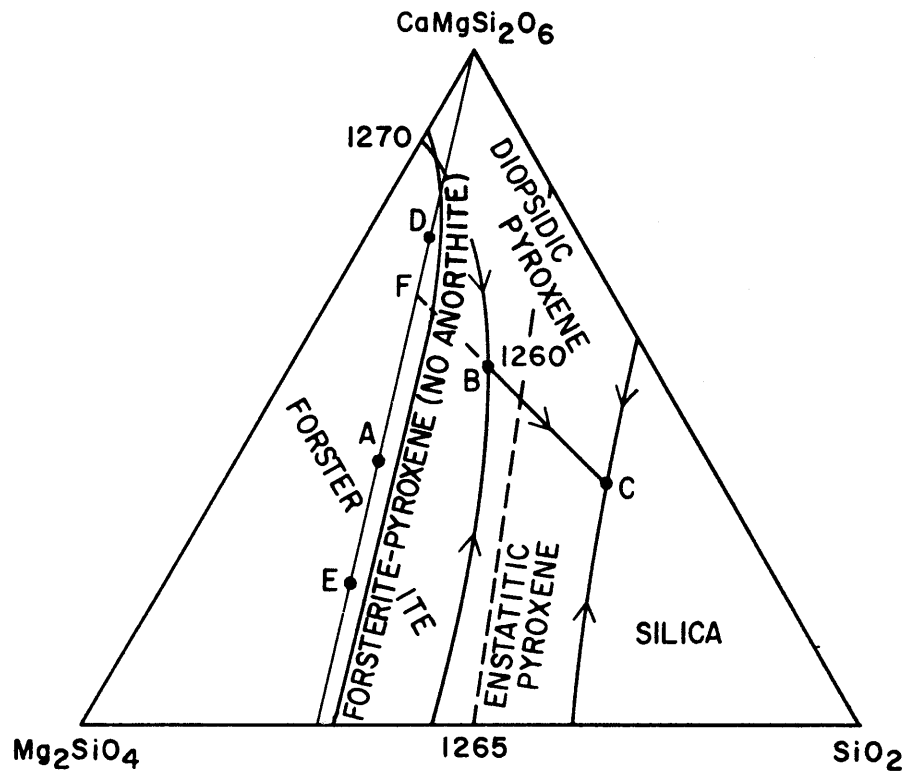
FIG. 12   SYSTEM $CaMgSi_2O_6$-Mg_2SiO_4-$CaAl_2Si_2O_8$-SiO_2:   LIQUIDUS
RELATIONS SATURATED WITH ANORTHITE AND PROJECTED
THROUGH ANORTHITE ON THE PLANE DIOPSIDE-FORSTERITE-
SILICA.

(Relations to the right of the dotted line are schematic.)

(Data after Andersen, 1915; Osborn and Tait, 1952;

Hytonen and Schairer, 1961.)

diopside of composition D. Of course, both these pyroxenes will contain some Al_2O_3 because of the anorthite content of the melt, but Al_2O_3 dissolved in both pyroxenes should not affect the conclusions drawn here drastically.

We can conclude that although the addition of plagioclase to a lime-magnesian pyroxene liquid can change the form of dual pyroxene crystallization from a peritectic-type relation with enstatite reacting with liquid to give diopside to a eutectic type of coprecipitation, it cannot account, even under conditions of anorthite saturation, for a shift in the pyroxene minimum of more than from Di 18 to Di 35. It therefore does not appear able to explain the coprecipitation of equal quantities of enstatite and diopside observed coexisting in the absence of olivine in layered basaltic intrusives (Hess, 1941, 1960). As we have seen, however, dissolved volatiles, even without plagioclase, are likely able to shift this minimum to about Di 50.

Chapter II: MINERALOGICAL SIMILARITY OF THE MAFIC PHASES OF

THE CHUKOTAT SILLS AND THE MONTEREGIAN HILLS -

EXAMPLES OF THE TWO CLASSES OF SUBSILICEOUS GABBROS

Yoder and Tilley (1960) have recently classified basaltic
rocks and magmas according to their principal normative miner-
als, namely: anorthite, albite, diopside, forsterite, enstatite,
nepheline, and quartz. Generalizing their simple basalt tetra-
hedron, forsterite-diopside-nepheline-quartz, which contains
all of the above components but anorthite, they include members
commonly in solid solution with the tetrahedral components and
arrived at the graphical basalt classification reproduced in
Fig. 13.

It can be seen from this figure that basalts can be clas-
sified into three groups: those whose normative composition
falls within the tetrahedron clinopyroxene-orthopyroxene-
plagioclase-quartz, the tholeiites, those which fall within the
tetrahedron olivine-clinopyroxene-orthopyroxene-plagioclase,
the olivine tholeiites, and those which fall within the tetra-
hedron olivine-clinopyroxene-plagioclase-nepheline, the
basanites. For the purpose of this thesis, basaltic rocks
which contain less than 47 percent of silica are referred to
as subsiliceous (average gabbro contains 48 percent silica,
average basalt, 49 percent - Daly (Barth, 1951, p. 70). Sub-
siliceous gabbros may, therefore, according to the classifica-
tion of Yoder and Tilley, be either olivine tholeiites or
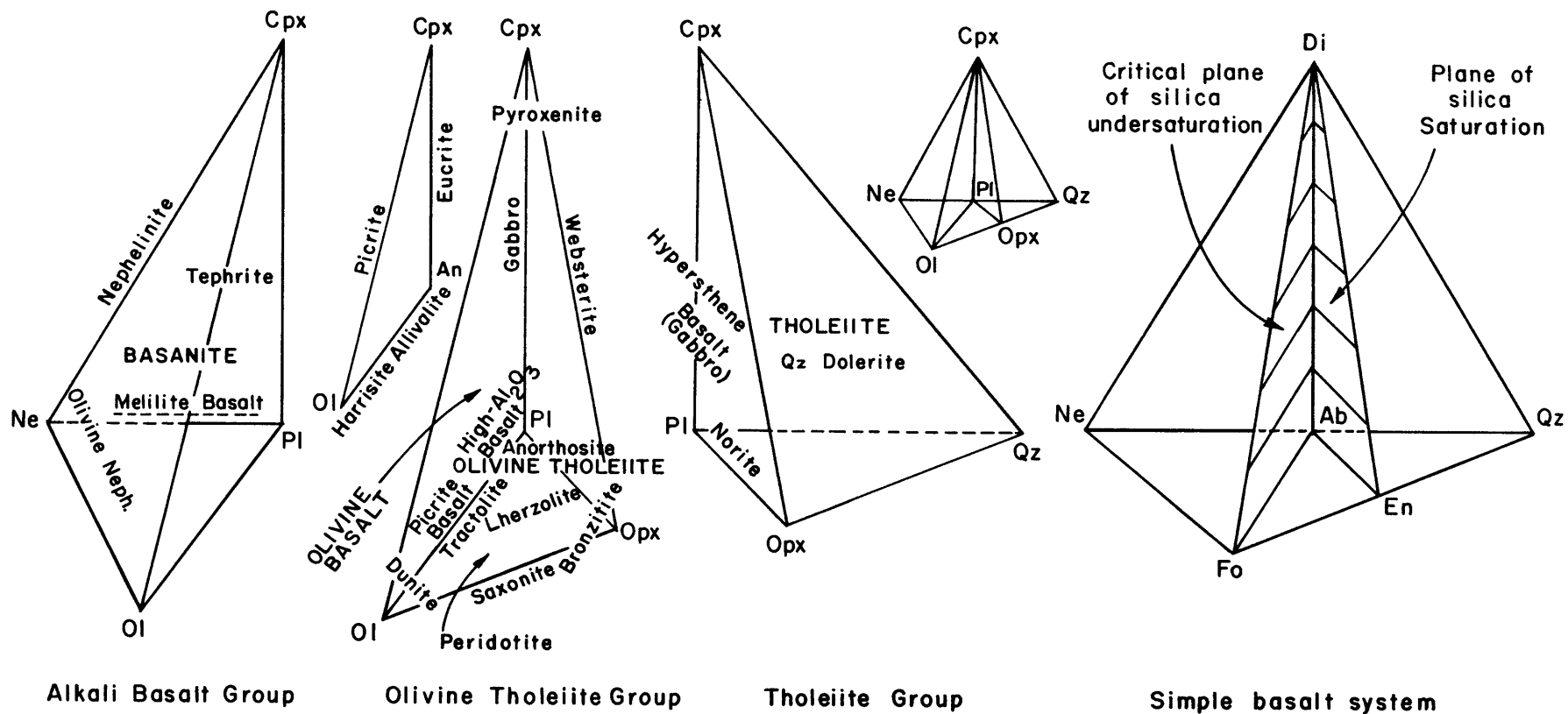
FIG. 13 SIMPLE BASALT TETRAHEDRON Mg_2SiO_4-$CaMgSi_2O_6$-
SiO_2-$NaAlSiO_4$ AND RESULTING GENERAL BASALT
CLASSIFICATION.

(after Yoder and Tilley, 1960)

basanites, as long as they are not unusually rich in iron, in which case they could conceivably be tholeiites.

It is of great petrological interest to attempt to determine the principal liquid courses of differentiation for the olivine tholeiite and basanite types of subsiliceous gabbros. While it is generally true that basalts falling into the olivine tholeiite class may differentiate towards oversaturated residua which will crystallize free quartz while those falling into the basanite class may differentiate towards critically undersaturated residua which crystallize feldspathoids or melilites, subtle features affecting the crystallization may modify or negate this generalization. For example, while the composition "plane" clinopyroxene-olivine-plagioclase in Fig. 13 has been recognized by Yoder and Tilley (1957, 1960) as a general thermal barrier and has been referred by these authors as the "critical plane of undersaturation", the position of this thermal barrier with respect to normative olivine, nepheline, clinopyroxene, and orthopyroxene will be shown to vary depending upon the quantity of volatiles and feldspar dissolved in the melt in a generally predictable fashion. In some cases therefore a melt of given normative proportions of olivine, clinopyroxene, and nepheline will differentiate towards silica while in other cases it may differentiate away from silica. The crystallization of amphiboles and aluminous pyroxenes are two of the complicating factors. Similarly, it will be shown that an olivine tholeiite may differentiate to

an oversaturated or merely a saturated magma depending upon physical factors of crystallization, particularly the quantity of dissolved volatiles in the melt during olivine separation.

Two suites of differentiated rocks, one whose gabbro phases are representative of the olivine tholeiite group, the Chukotat Sills of the Cape Smith-Wakeham Bay belt of New Quebec, and the other, a representative of the basanite group, the Monteregian Hill intrusives of the Montreal Area have been studied by the author. The mafic phases of these two groups are very similar in mineralogy, but normative analyses necessitate their division into the olivine tholeiite and basanite classes.

The Chukotat Sills are differentiated plutons, varying in composition from peridotite or serpentinite to quartz diorite. The peridotites, where unaltered, are composed almost entirely of chrysolite and endiopside, with minor serpentine and magnetite. Pyroxenites are composed almost entirely of augite, with some actinolite and altered plagioclase, while the gabbros contain augite, actinolite, and saussuritized plagioclase, and are often altered to an actinolite-albite-zoisite epidiorite.

The mafic phases of the Monteregian Hills, which make up some 60 percent of the outcrop area, are, contrary to popular notion, not generally alkaline, in fact, they contain less alkalis than the average gabbro. They are, however, subsiliceous, which results in the appearance of nepheline in their norms. The majority of the dark colored rocks are

peridotites, pyroxenites, and gabbros. Minor essexite and
nepheline syenodiorite occur as transition stages between the
mafic rocks and the associated strongly alkaline syenites.

The Monteregian peridotites are composed of endiopside
and chrysolite, with some oxyhornblende, calcic plagioclase,
and iron ore. The pyroxenites are almost entirely augite, with
some oxyhornblende, calcic plagioclase, and olivine, while the
gabbros contain augite, oxyhornblende, calcic plagioclase, and
minor olivine, iron ore, and occasionally biotite. Where the
plagioclase becomes intermediate in composition, either as
sodic labradorite or andesine, soda orthoclase, nepheline, and
sodalite may enter the assemblage, producing essexites and
syenodiorites. These alkali gabbros and diorites comprise a
small fraction of the Monteregian mafic rocks.

It can therefore be seen that in both the Chukotat Sills
and Monteregian Hills, the essential primary minerals in the
peridotites are chrysolite and endiopside, in the pyroxenites,
augite, and in the gabbros, augite and plagioclase. Both
suites are characterized by the consistent occurrence of a
single pyroxene instead of the common coexistence of two
pyroxenes. Both suites have originated from a liquid abnor-
mally low in silica as is inferred from the fact that the
initial pyroxenes to crystallize are close in composition to
diopside. This lack of silica is displayed in chemical
analyses. The average silica content of six basic phases of
the Monteregian Hills is 42 percent, that of the two of these

which are gabbros is also 42 percent. The average silica
content across a typical Chukotat sill is about 45 percent.
These values are considerably lower than those given by Daly
for the average gabbro, 48 percent, and for the average basalt,
49 percent.

Mineralogical differences in the Chukotat and Monteregian
mafics are two-fold. The Monteregian gabbros contain
titaniferous oxyhornblende as an essential mineral; the
Chukotat rocks do not. The Chukotat suite has undergone hydro-
thermal alteration, in which the formation of serpentine,
actinolite, and zoisite have in most exposures changed radi-
cally the original mineralogy. Textural evidence suggests that
most of the serpentinization and some of the actinolite develop-
ment are autometasomatic, i.e. part of the igneous process, but
the formation of much of the actinolite and zoisite is believed
due to regional metamorphism. Except for minor serpentine
development, no hydrothermal activity is indicated in the
Monteregian rocks.

These differences are certainly small compared to the
great chemical differences in the differentiation products of
the Monteregian and Chukotat suites. The Chukotat Sills
differentiate upward to an altered quartz-diorite, and there
is no evidence of increasing alkalinity. The Monteregian Hills,
on the other hand, become strongly sodic and the differen-
tiation proceeds from the gabbros to essexite, syenodiorite,
and syenite.

The Monteregian Hills are known to have crystallized at very shallow depths, whereas the Chukotat Sills were intruded into a thick lava sequence at considerable depths. These differing physical conditions played an equally important role to the bulk compositions in determining the course of differentiation of the two magmas.

Chapter III: PETROLOGY OF THE CHUKOTAT SILLS

1. Introduction

The Chukotat Sills are differentiated mafic sills varying
in thickness from less than 10 to about 2000 feet. They are
intruded into a series of predominantly volcanic rocks of
Precambrian age. This series, named the Chukotat Series by
Bergeron (1957), is the upper of two folded groups of sedimen-
tary and volcanic rocks which together comprise the east-west
trending Cape Smith - Wakeham Bay Belt of New Quebec.

According to recent radioactive age measurements (Beall
et al, 1962), the Chukotat Series was deposited between 1450
and 1600 my. The underlying Povungnituk Series, separated
from the Chukotat Series by an angular unconformity, is com-
posed largely of metamorphosed sedimentary and volcanic rocks.
These rocks, in turn, overlie granite and granitic gneisses of
the Superior Province of the Canadian Shield.

The Quebec Department of Natural Resources has, since the
summer of 1957, been systematically mapping portions of the
Cape Smith belt. The author, in the summers of 1958 and 1959,
mapped the Cross Lake and Laflamme Lake areas, adjoining
regions comprising about 600 square miles in the east central
portion of the belt (see maps in pocket). It is in these
areas that the best exposures of the Chukotat Sills and asso-
ciated nickel-copper prospects are found, and it is in these

areas that the sills and surrounding rocks have been studied
(Shepherd, 1959; Beall, 1959, 1960).

2. Geological Environment of the Chukotat Sills

2.1 General Petrology of the Chukotat Series

The Chukotat Series is composed largely of basaltic flows with minor interbedded slate, quartzite, greywacke, tuff, and dolomite. The basalt can be divided into two main types: olivine basalt, which predominates, and leucobasalt, which is locally important, particularly in the central portion of the Cross Lake area (see map in pocket). The term metabasalt is used to refer to lavas of both types which have undergone complete alteration to secondary minerals.

The lava generally occurs in large, resistant, cliff-forming outcrops displaying a most characteristic feature of the Chukotat basalts, well developed pillow structure (Plate 1). East of Cross Lake, where exposures are excellent, distinct flows averaging 15 to 20 feet in thickness with tops displaying breadcrust patterns are common. Ropy structure was also observed.

Mineralogically, the olivine basalt, originally composed of augite, plagioclase, and olivine, all of which are frequently visible in thin section, is now largely altered to actinolite-clinozoisite-serpentine-chlorite rock. Serpentine or chlorite pseudomorphs after olivine, plumose clinozoisite-albite aggregates after plagioclase, and actinolite alteration of augite generally occur with devitrified glass, giving the

Plate 1: Pillowed basalt of the Chukotat Series
(2 miles east of Cross Lake, New Quebec)

rock a green to dark green, fine grained appearance.

The leucobasalt, of similar mineralogy, but pale green to whitish in hand specimen, differs from the olivine basalt in that the quantity of pale actinolite is greater, and that of the darker chlorite and serpentine less. The percentage of original augite was greater, and that of olivine, presumably less.

Both these basalts must be classified generally as olivine basalts as opposed to normal tholeiitic basalts. A chemical analysis of a sample of typical leucobasalt from Cross Lake is compared to an average of 34 olivine basalts and an average of 36 tholeiitic basalts from the literature (Turner and Verhoogan, 1951, p. 180).in Table 3. It is seen to approach the olivine basalt composition much more closely than the tholeiitic composition. In fact, the leucobasalt appears richer in iron and magnesium than the olivine basalt average. Allowing for the fact that the average darker coloured basalt from the Cross Lake and Lac Laflamme areas contains more chlorite and serpentine and less actinolite and clinozoisite than the leucobasalt, it can be seen that the Chukotat volcanics are both undersaturated and very strongly mafic. They are not, however, alkaline olivine basalts. In fact, according to the classification of Yoder and Tilley (1960, see also Fig. 13, p. 75), these basalts, because of their normative composition, (Table 3), which shows considerable hypersthene, should be termed olivine tholeiites.

Table 3:   Chemical Composition of Chukotat Sill Rocks and
           Related Extrusives
           Compared to Typical Basalts and Gabbros

	Tholeiite[a]	Tholeiite-Kennedy[b]	Olivine Basalt[c]	Olivine Basalt-Kennedy[d]	Average Gabbro[e]
SiO_2	50.51	50	49.79	45	48.24
TiO_2	1.59				0.97
Al_2O_3	14.00	13	14.10	15	17.88
FeO	9.41	13*	11.7*	13*	5.95
Fe_2O_3	3.40				3.16
MnO	0.17				0.13
MgO	5.73	5	8.40	8	7.51
CaO	9.21	10	9.60	9	10.99
Na_2O	2.81	2.8	2.6	2.5	2.55
K_2O	0.80	1.2	0.9	0.5	0.89
H_2O	2.34				1.45
P_2O_5	0.34				0.28

* total Fe as FeO

a average of 36

b Kennedy magma type

c average of 34

d Kennedy magma type

e Daly average

(after Turner and Verhoogan, 1951, p. 180)

Table 3: Chemical Composition of Chukotat Sill Rocks and
Related Extrusives
Compared to Typical Basalts and Gabbros (cont.)

	Serpentinite[f] Cross Lake	Serpentinite[g] Esker Lake	Leucobasalt[k] Cross Lake	Chukotat Sill[h] "Parent Magma"
SiO_2	40.24	39.50	49.59	45
TiO_2				
Al_2O_3	5.45	5.45	11.70	8.5
FeO	10.04	10.05	10.4	11.0
Fe_2O_3	3.06	3.43	3.7	2.5
MgO	26.67	27.11	10.67	20
CaO	5.09	3.92	7.75	6
Na_2O	0.25	0.25	3.00	1.7
H_2O	7.45	8.73	3.08	
Ab			27.5	15.4
An			18.8	16.0
Mt.			3.9	3.0
Di			16.4	11.6
Hy			23.4	18.0
Ol			9.8	36.0

f average of 5 serpentinite samples, Cross Lake (Shepherd, 1959)

g Quebec Department Mines Chemical Laboratory

k Quebec Department Mines Chemical Laboratory

h estimated Chukotat Sill "parent magma" - see text.

The pyroxenes of the Chukotat lavas are typical of olivine basalts in general, that is, a single calcium rich pyroxene occurs, in this case augite. Nowhere have the co-existing augite-hypersthene or augite-pigeonite pairs so typical of tholeiitic basalts been observed, perhaps because of selective hydrothermal alteration of orthopyroxene.

The sedimentary rocks of the Chukotat Series consist of siliceous and graphitic slates, fine tuff, some sandstone, and occasionally interbedded with the lavas, thin lenses of dolomite. At the base of the series, a conglomerate composed of fragments of the underlying Povungnituk rocks and ancient Superior granite has been observed in the northern part of the Cross Lake area along the thrust fault just south of Wrong Lake. To the south in the Laflamme Lake area, the base of the Chukotat Series is either marked by a thin chert bed, or, more frequently, a lava flow or a sill injected along the unconformity.

2.2 Major Structure of the Chukotat Series

The major portion of the Cross Lake area is underlain by the rocks of the Chukotat Series. A thickness of about 20,000 feet is visible between two large thrust faults in the northern part of the area, but the total thickness is probably considerably greater than this.

The most outstanding structural feature in the Cross Lake

area is a large open syncline which plunges eastward from
Cross Lake and continues to the eastern border of the area.
The adjoining anticline to the north is dislocated by a large
east-west fault just north of Cross Lake, but is quite apparent
six miles east of the lake where the fault dies out. North of
this anticlinal axis, a northward dipping group of pillow
lavas and sills stretches for three miles, where it is cut by
a large thrust fault which is traceable across the area.
South of Wrong Lake this fault brings the conglomerate at the
base of the Chukotat Series on the hanging wall into contact
with footwall rocks which are underlain by over 10,000 feet
of Chukotat lavas to the south. Hence the displacement is
likely of the order of several miles.

North of this thrust fault, another pillow lava series
dips north at an average of about 50 degrees. More than
20,000 feet of Chukotat volcanics are exposed here. This
group is terminated on the north by a large northeasterly
trending thrust fault even more conspicuous than the first.
This fault, which brings soft sedimentary rocks of the
Povungnituk Series on the north into contact with cliff-
forming lavas to the south, was seen to dip about 40 degrees
north. The fault-line scarp is traceable from a point about
20 miles northeast of the Cross Lake area westward to Hudson
Bay, a distance of some 150 miles. Its exact displacement is
unknown, but it is probably several miles.

South of the Cross Lake syncline is a series of tight

east-west isoclinal folds, overturned to the south. One mile
south of Cross Lake, laminated tuffs striking north and dipping
60 degrees east display vertical flow cleavage striking east.
Such relations suggest an anticline plunging east, and the nose
of this anticline may be seen one half mile west of Long Lake,
where a gabbro sill is sharply bent through 180 degrees.
Farther south, overturned folds are indicated by the attitudes
of pillows. Shearing is particularly apparent along the axes
of these folds.

Minor cross folds were observed in the Cross Lake area.
An example is the north-trending anticline at Cross Lake. This
fold separates the eastward plunging Cross Lake syncline from
a westward plunging synclinal complex along the western border
of the area. This axis of cross folding, plus irregular minor
folds within the main east-trending synclinal area, undoubtedly
created an area of unusually complex stress conditions, the
results of which are manifest in several faults.

In the Laflamme Lake area, the Chukotat Series is well
exposed in the north central part of the area from Mequillon
Lake to Gog and Forcier Lakes. The Chukotat rocks lie in a
long refolded synclinorium which strikes east-northeast across
the area. The synclinorium is composed of a series of pre-
dominantly east-trending folds commonly overturned to the
south and generally quasi-isoclinal. This sequence of folds
has been gently refolded along northwest trending axes, this
open refolding being most obvious in aerial photographs of

Plate 2: Aerial photograph of complex refolding in
the Vaillant Lake region, New Quebec

(The lower Vaillant Lake sill can be seen
where it dips to the west on the east side
of Vaillant Lake)

- scale: ½ mile = 1 inch

the area (Plate 2). Particularly striking are the large
anticline east of Vaillant Lake, the Vaillant Lake syncline,
the anticline east of Carre Lake, and the Carre Lake syncline.

The east-trending folds represent the first and main
period of folding of the Chukotat Series, but because of their
isoclinal nature are not so obvious as the superimposed north-
west trending folds. For example, in the Vaillant Lake area,
five synclinal and four anticlinal axes trend eastward along
the southern flank of the Vaillant Lake syncline. These are
difficult to outline from aerial photographs alone.

An arcuate overturned anticlinal dome, a typical feature
of refolding, is well displayed just west of the north end of
Carre Lake. Basin outliers of Chukotat rocks lying on folded
Povungnituk rocks are found in the northwestern section of the
Laflamme Lake area and the southernmost portion of the Cross
Lake area. These are particularly large along the western edge
of the Laflamme Lake area, where the folding was less intense
than in the rest of the area.

The thickness of exposed Chukotat strata in the Vaillant
Lake - Carre Lake vicinity, where the best exposures of the
Chukotat Sills are found, is about 4000 feet. The sequence is
as follows:

        8. Upper gabbro

        7. Upper peridotite (serpentinite)

        6. Slates

        5. Lower gabbro

4. Lower peridotite

3. Slates

2. Basal gabbro

1. Pillow basalt

Units 4 and 5, which are the least altered of all the twin peridotite-gabbro sills in the Cross Lake and Laflamme Lake areas, are roughly 900 and 500 feet in thickness, respectively. They were systematically sampled by the writer where they out-crop in almost continuous exposure immediately east of Vaillant Lake (Plate 2).

3. <u>Form and Distribution: Field Evidence of Mode of Sill</u>

   <u>Formation</u>

The Chukotat Sills can be divided into three distinct
types: (1) ultrabasic, (2) gabbro, and (3) settled differen-
tiated. The latter type is, in effect, a combination of the
first two types.

3.1 <u>The Ultrabasic Sills</u>

The ultrabasic sills, generally serpentinite, but occasion-
ally mainly peridotite, range in thickness from less than ten
to over 1000 feet in thickness. They are found in the western
section of the Laflamme Lake area (see map in pocket) and are
quite numerous in the central portion of the Cross Lake area.
They are easily distinguished from the grey weathering lavas
and gabbros by their rusty weathered surface. Fairly persistent
along strike, one sill 6 miles northeast of Cross Lake, is
about 150 feet in thickness, but can be traced for over four
miles. Another, averaging about 500 feet in thickness, can be
traced between the Povungnituk and Little Povungnituk Rivers in
the western part of the Laflamme Lake area for a distance of
over ten miles.

These ultrabasic sills generally show only minor variation
in composition and texture. The main portions range from
serpentinite to porphyritic pyroxene serpentinite, or where

less altered, from peridotite to dunitic peridotite. Veinlets
of magnetite and brittle chrysotile are common.

Sheet jointing parallel to the bedding of associated rocks
is characteristic of the ultrabasic sills, and it affords a
valuable criterion for attitude determination. Columnar joint-
ing is well developed in several sills three miles northwest of
Wrong Lake in the Cross Lake area (Plate 3). Since columnar
jointing is indicative of shallow crystallization, these sills
probably lie fairly close to the top of the Chukotat Series.
Over 7000 feet of strata are observed above the jointed sills,
however, before a thrust fault causes stratigraphic repetition.

Where seen in contact with slates, the ultrabasic boundary
is characteristically sharp, with some contact metamorphic and
metasomatic effects visible in the slates. Moreover, a chill
or reaction zone, sometimes tens of feet in thickness, composed
of amphibole, is generally produced in the ultrabasic contact
area. Tremolite, or pale magnesian hornblende, and occasionally
grossularite, zoisite, muscovite, and sphene are produced in
the slates, which generally contain only quartz, calcite,
graphite, and fine micaceous material.

Where in contact with lava, on the other hand, the bound-
ary is gradational through a zone of several feet, with no un-
usual mineralogy developed in either lava or ultrabasic.

In the vicinity of the large gorge, about six miles north-
east of Cross Lake, a group of unusually small serpentinite
'sills' are found. Apparently ductless, these lenses, many of

Plate 3: Columnar jointing in serpentinite sill near the
top of the Chukotat Series
(2 miles northwest of Wrong Lake, New Quebec)

them less than ten feet in thickness and less than 100 feet in outcrop length, may be the result of extrusion of clots of ultrabasic crystalline material, mainly olivine, with the basaltic lavas which enclose them. Shepherd (1959) recognized the necessity of an extrusive origin for these minute lenses but proposed the extrusion of an ultramafic liquid. Aside from the well known difficulties of producing such liquids at basaltic temperatures (Bowen and Tuttle, 1949), it is difficult to imagine simultaneous outpourings of basalt and ultramafic liquid without mixing, and it seems certain that the ultramafic bodies are too small to represent independent extrusions.

3.2 Gabbro Sills

The grey weathering gabbro sills, ubiquitous in the Chukotat Series wherever it is exposed, range in thickness from less than 50 feet to more than 1000 feet. Like the ultrabasic sills, they are easily traceable for long distances along strike; individual sills can occasionally be followed for over ten miles, as in the case of the 500 feet thick sill seven miles from Cross Lake along the gorge draining northwest from the lake.

The thicker gabbro sills usually show the effects of fractional crystallization and gravitational differentiation. They commonly grade from pyroxenite at the base through gabbro and diorite to quartz diorite at the top. The average

composition of a sill, while usually typically gabbroic, may range from olivine gabbro to feldspathic gabbro.

3.3 Settled Differentiated Sills: Field Evidence of Mode of Sill Injection

In examining the gabbro and ultrabasic sills of the Cross Lake and Laflamme Lake area, one is impressed by the intimate association of these two sill types in many exposures. In fact, the great majority of the larger ultramafic sills form, in contact with gabbro, what appear to be composite sills, that is twin sills formed by two separate magmatic injections, one of ultrabasic magma and one of gabbroic magma. Shepherd (1959) invoked this two-magma hypothesis for the origin of the twin sills. He proposed an initial ultramafic liquid injection, followed by a gabbroic liquid injection. Lenticular inclusions of ultrabasic material in gabbro found one mile southeast of Cross Lake near a serpentinite-gabbro contact were cited as evidence for this age relationship. One major difficulty, pointed out by Shepherd, was the unlikely existence of an ultramafic liquid at temperatures low enough to have produced only lower amphibolite facies metamorphism in surrounding sediments.

In addition to this problem, there are three other facts which belie the two magma theory, and suggest that the twin gabbro-ultrabasic sills are not composite, but differentiated,

their twin nature resulting from magmatic differentiation and
gravitational settling.

Firstly, these twin sills invariably contain their ultra-
mafic portion at or very near the sill base and their main
gabbroic portion at the sill top. This was observed by
Shepherd (1959) but not explained. There are no exceptions to
this rule in the Cross Lake and Laflamme Lake areas, at least
as far as is known from exposures where the facing can be defi-
nitely determined.

Secondly, there is no evidence of differentiation by
fractional crystallization within the thick ultrabasic zones
whereas such evidence is obvious in both hand specimen and thin
section within the overlying gabbro masses. This would indi-
cate that the ultramafic crystals did not crystallize from a
liquid after injection, as is implied in the two-magma theory.

Thirdly, the contacts between gabbro and ultrabasic rock
display unusual features. Though usually sharp and easily
defined, these contacts occasionally display a fine interlayer-
ing of ultrabasic rock, usually serpentinite, and pyroxenite,
a common basal phase of the gabbro. This banding was observed
one mile south of Gog Lake in the Laflamme Lake area, and also
three miles due northeast of Cross Lake in a large exposure of
the main Cross Lake sill. One mile southeast of Cross Lake,
very close to the serpentinite inclusions in gabbro described
by Shepherd (1959), a tongue-like mass of serpentinite some
10 feet long was seen protruding into overlying gabbro. In

another contact exposure in the same region, an irregular gabbro-serpentinite contact displays a wavy nature, such as might result if an accumulation of crystals were disturbed by currents in an overlying magmatic mass.

These observations are all compatible with the following hypothesis of sill formation:

The igneous material upon intrusion consisted of gabbroic liquid in equilibrium with and saturated with a mass of ultrabasic crystals, mainly olivine. After intrusion, the crystals settled to the base in a uniform mass. The gabbro then proceeded to crystallize with consequent gravitational differentiation, the underlying ultramafic crystal mush not yet having consolidated. Minor convection produced irregular contact effects such as clot inclusions of ultramafic swirls, and convectional interlayering of settled olivine crystals and lighter newly formed pyroxenes crystallizing from the gabbro.

If the injected material was largely ultrabasic and crystalline with only minor interstitial aqueous or gabbroic fluid, a simple ultrabasic sill resulted. If it was largely gabbroic liquid with few or no crystals, a simple gabbro sill resulted. If, however, the injected material was a mixture of crystals and liquid, a settled differentiated sill of ultrabasic material capped by gabbro developed.

It should be noted that an hypothesis of simple post-injection differentiation from a single magma is precluded by the existence of all proportions of peridotite and gabbro in

a single twin sill, such as the lower twin sill in the
Laflamme Lake area. This sill varies from pure gabbro, as
seen in the overturned anticline just north of Forcier Lake,
and also in a similar anticline one half mile north northwest
of Vaillant Lake, to pure serpentinized peridotite, as seen in
the western section of the area between Povungnituk and Little
Povungnituk rivers.

Most of the largest of the ultrabasic sills in the Cross
Lake and Laflamme Lake areas are capped by gabbro, and hence
are of the settled differentiated type. The large twin sill
just east of Cross Lake arcs around the Cross Lake syncline
reaching thicknesses of over 2000 feet three miles northeast of
the lake. Tracing this sill southward to Cross Lake across the
faulted anticline north of the lake, a conspicuous band of lava
about 500 feet thick can be seen one mile west of the south end
of the lake. This unusual slab of lava is apparently trapped
between the ultrabasic base and gabbro cap of the Cross Lake
Sill. This is the only case in the areas studied where part of
the ultrabasic and gabbro sections of a twin sill are separated
by another rock type. The slab is some four miles long and
seems to have resulted from large scale magmatic stoping. A
large fracture in the lava 500 feet above the sill probably
caused separation and sinking of the lava slab into the under-
lying still molten gabbro, the slab finally coming to rest at
the top of the ultramafic mush layer, which presumably sep-
arated gravitationally just after injection. Xenoliths, not

common elsewhere in the ultrabasic sills, have been reported
(Shepherd, 1959) along the upper contact of the serpentinite
in this zone. Blocks of lava, separated from the sinking slab,
and covered by a mass of agitated crystals strewn up from the
crystal mush layer below, could be expected to form such
xenoliths. This stoping hypothesis is supported by the fact
that the upper contact of the gabbro sill above the lava zone
is higher stratigraphically in the syncline in this area than
elsewhere.

Aside from the main Cross Lake sill, which outcrops around
the Cross Lake syncline and also to the north, west, and south
of the lake where it is repeated by folding and faulting,
several other settled differentiated sills are found in the
dipping lava series west of Wrong Lake.

In the Laflamme Lake area, two settled differentiated
sills are observed in the stratigraphic section in the Vaillant
Lake region. The lower sill, some 1400 feet in thickness, is
best exposed east of Vaillant Lake, and the upper sill (see
map and Plate 2) just west of the central part of Vaillant
Lake. The extent of the upper sill is not known, it being too
high in the stratigraphic column to outcrop consistently in
this region. The lower sill can be traced along strike from
east to west across the entire area, a distance of some 25
miles, although the gabbro capping disappears in the western
part of the area four miles west of Forcier Lake.

While the gabbro portion of this sill is restricted in

extent towards the western end of the area, the ultramafic portion, while traceable across the entire area along strike from Vaillant Lake, is nevertheless absent on the flanks of several of the east trending overturned folds where the gabbro is present. Examples of such folds are the overturned syncline two miles due north of Gog Lake, the overturned anticline one mile northeast of the northern tip of Carre Lake, and the overturned anticline one half mile northwest of the northern tip of Vaillant Lake.

It thus appears that in the Laflamme Lake area, the ultrabasic crystalline material of the lower settled differentiated sill was injected in a sheet more continuous in the east west than the north south direction, while the gabbro host liquid, except for the westernmost part of the area, was intruded as a continuous sheet.

Two factors indicate that all the sills in the Cross Lake and Laflamme Lake areas were intruded prior to the initiation of folding. Firstly, there is a general lack of any relation between sill thickness and fold geometry. Secondly, the attitudes of stratification banding in the gabbro sills and along gabbro-ultrabasic contacts are invariably parallel or sub-parallel to the attitudes of the surrounding lava flows or sedimentary horizons. This indicates the Chukotat Series was approximately horizontal when the sills were injected.

4. Sill Mineralogy at Vaillant Lake

The lower settled differentiated sill in the Laflamme Lake area is best exposed along the east side of Vaillant Lake where continuous outcrop bares a basal peridotite member 900 feet in thickness and an upper gabbro member 500 feet in thickness. The sill has been intruded into slates which are exposed along both sill contacts.

Thirty specimens were collected at regular intervals across this sill, 17 thin sections have been studied, 10 pyroxene concentrates have been partially analyzed by the rapid silicate methods (Brannock and Shapiro, 1956), and the compositions of three olivine concentrates have been determined by optical powder techniques (see Appendix for analytical details).

4.1 Peridotite Member

The peridotite member of the Vaillant Lake sill, 900 feet in thickness, can be divided roughly into three zones, a basal contact amphibolite zone about 20 feet in thickness, a lower serpentinite zone about 50 feet in thickness, and the main portion, composed of peridotite, over 800 feet in thickness.

The contact phase is a light green medium grained rock composed almost entirely of two amphiboles: actinolite and hornblende. Zircon is an important accessory. This basal amphibolite is a common phase of the Chukotat ultrabasic sills

(Shepherd, 1959), frequently reaching a thickness of over 50 feet. It probably represents a chill zone, its only moderately basic composition resulting from early crystallization from the gabbroic melt subsequent to the settling of the olivine rich ultrabasic portion.

The lower serpentinized zone, unlike the amphibolite zone, is not a typical feature of the Chukotat ultrabasics. Rather than occurring only near the sill base, such serpentinite may make up the greater part of a sill, and may be found at any horizon in regular bands or irregular masses. It is generally composed of medium grained antigorite pseudomorphs poikilitically enclosed in either coarse endiopside crystals or in a fine antigorite groundmass. A few of the endiopside crystals are partially altered to a fine grained aggregate of actinolite and bastite serpentine. Chlorite, of the anomalously birefringent type, penninite, is generally present as part of the serpentine groundmass. Veins of chrysotile and magnetite, the latter also occurring as a widespread accessory mineral, are found scattered throughout the ultrabasic member, but are extremely common in the serpentinite zones.

The main peridotite zone at Vaillant Lake is amazingly simple and undeviating in its mineralogy. Chrysolite, endiopside, and antigorite are the only important major minerals, iron ore, penninite, and actinolite, the only important accessory minerals. The major minerals tend to occur in the following rough proportions: olivine, 60 to 70 percent,

pyroxene, 15 to 20 percent, serpentine, 15 to 20 percent. The olivine may be present as subhedral or anhedral grains, generally less than a millimeter, but occasionally several millimeters in length, enclosed poikilitically in large endiopside crystals averaging from five millimeters to one centimeter in width. It also may be present without pyroxene as closely knitted grains enmeshed in a fine serpentine groundmass.

There is strong evidence of resorption of olivine during the crystallization of pyroxene. The chrysolite grains in contact with endiopside, show the typical fuzzy borders of magmatic resorption (Plate 4). Shepherd (1959) recognized such corroded grains in ultrabasic zones of the Cross Lake sill, where, although no fresh olivine could be seen, serpentine pseudomorphs retained the corroded shapes of the original crystals.

Moreover, in the Vaillant Lake peridotite, individual olivine crystals have been partially dissolved into two or more small grains, their original relationship being revealed by optical continuity. The poikilitic nature of the large endiopside plates also suggests that pyroxene may have crystallized after olivine as the product of an olivine-liquid reaction. Poikilitic enclosure of olivine by enstatite is common in many peridotites, and the separation of enstatite from a melt in the presence of olivine is known to involve resorption of olivine (Bowen, 1914).

Table 4 presents the results of chemical determinations of oxides of magnesium, iron, and calcium, and in two cases, titanium and sodium for eight pyroxenes from various levels of the peridotite (see Appendix for individual analyses). The compositions of coexisting olivines in terms of mole percentages of forsterite and fayalite are also listed. It is noted that there is no significant variation in the compositions of either the pyroxenes or the olivines. The slight scatter in the pyroxene compositions may be partially due to the difficulties in obtaining a pure mineral separate (see Appendix).

These data support the theory of rapid gravitational settling of the ultramafic portion of the sill immediately after injection. Olivine crystals in equilibrium with gabbroic liquid at the time of injection would not be expected to show any chemical variation. After sinking, these crystals would react with the small quantities of interstitial liquid forming large poikilic crystals of endiopside which, throughout the sill, would maintain a constant composition. The interstitial gabbroic liquid would not be expected to precipitate significant quantities of feldspar if it maintained diffusional contact with the main mass of overlying gabbro magma, because this main gabbro magma would not be saturated with respect to feldspar. This is indicated by the first crystal accumulate at the gabbro base, which is augite, not plagioclase. Hess (1960, pp. 111, 146-148) has used this principle of diffusional contact between interstitial 'mush liquid' and overlying magma
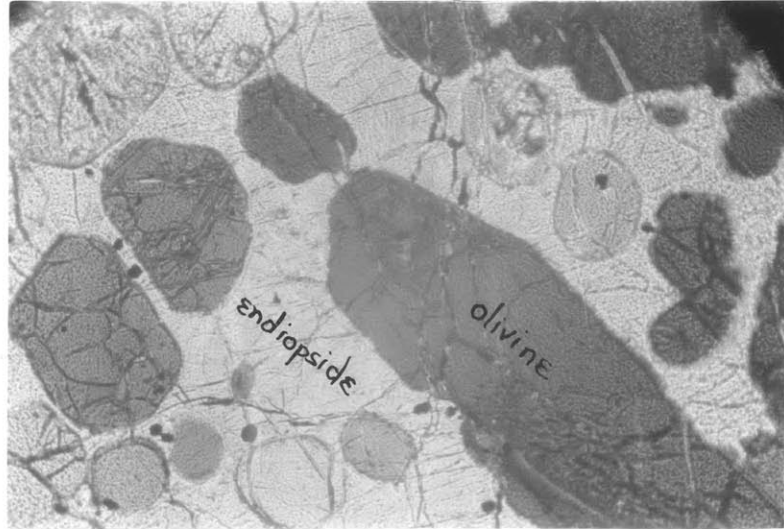
Plate 4: Corroded olivine crystals enclosed in
poikilitic endiopside

(peridotite member of lower Vaillant Lake
sill)

cross nicols, photo length = 5mm.
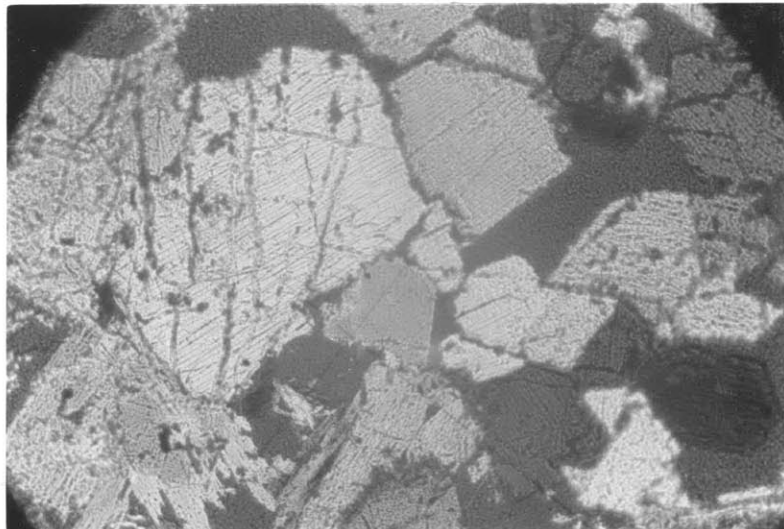
Plate 5: Fragmental augite crystals in serpentine
groundmass, a result of gravitational settling

(serpentine pyroxenite zone, gabbro member,
lower Vaillant Lake sill)

cross nicols, photo length = 5mm.

Table 4: <u>Chemical Composition of Pyroxenes, Olivine, and Plagioclase</u>
<u>from the Chukotat Sills, Vaillant Lake, New Quebec</u>

Level	110'	230'	270'	350'	410'	620'	800'	860'	920'	990'
				Ultrabasic					Gabbro	
Pyroxene										
SiO_2									51.52	52.41
TiO_2			0.24				0.26		0.33	0.45
Al_2O_3									6.18	5.55
CeO	19.35	19.47	19.94	19.37	19.26	19.83	19.71	19.48	18.53	16.85
MgO	16.17	16.65	15.71	16.88	15.44	15.65	16.38	16.69	17.41	17.67
FeO	4.57*	3.89*	3.19	3.44	3.49	4.17*	3.56	3.59	5.30	6.63
Fe_2O_3			0.65	0.46	0.46		0.61	0.68	0.87	0.21
Na_2O			0.31				0.76		0.41	0.59
K_2O			0.07				0.10		0.10	0.09
Total									100.65	100.45

Olivine										
Fo		83.0		83.0		83.0				
Fa		17.0		17.0		17.0				

		1180'	1270'	1360'
Plagioclase				
Ab		67	71	73
An		33	29	27

* Total Fe as FeO

in explaining the lack of pyroxene in anorthosite bands over-
lain by pyroxene gabbro in the Stillwater Complex, Montana.
Perhaps, in the Chukotat ultrabasic layer, equilibrium was not
always attained between the interstitial peridotite 'mush
liquid' and the overlying gabbro magma, and very small quan-
tities of plagioclase were formed. Such plagioclase may have
been subsequently altered with some olivine to form minor
actinolite and penninite, which have been observed with
antigorite in the peridotite groundmass.

4.2
Gabbro Member

The gabbro member of the lower sill at Vaillant Lake is
roughly 500 feet thick, and can be divided into a basal
pyroxenite zone about 75 feet thick, a gabbro-diorite zone
about 350 feet thick, and a quartz diorite zone about 75 feet
thick.

The pyroxenite zone varies from a serpentine pyroxenite
along the gabbro-ultrabasic contact to a hornblende pyroxenite
at higher levels. The serpentine pyroxenite is a medium
grained close knitted aggregate of equigranular subhedral
augite. Fine antigorite laths form the interstitial material.
The augite grains, which generally make up from 80 to 95 per-
cent of the rock, generally form a crude interlocking mesh,
such as would be expected if they had settled through gravita-
tional differentiation (Plate 5).

The hornblende pyroxenite contains actinolitic hornblende as an essential mineral, forming up to 25 percent of the rock. It occurs both as uralite rims on augite and as separate laths. Since it increases upwards in the sill, first as a pyroxene reaction product and then as separate laths not pseudomorphic after pyroxene, it is likely a primary mineral which crystallized first as a liquid-pyroxene reaction product and then as a coprecipitant with plagioclase.

The main gabbro zone, typically a medium to coarse grained rock, is composed largely of actinolitic hornblende, the major amphibole in the gabbros of the Chukotat Series, and altered plagioclase, generally in about equal proportions. The pale actinolitic hornblende is occasionally rimmed by green hornblende. The altered plagioclase occurs as euhedral or subhedral laths partially composed of fresh andesine, but mainly altered to aggregates of fine material, largely anomalously birefringent clinozoisite, with some chlorite and quartz.

The diorite is similar to the gabbro, but the unaltered plagioclase is usually oligoclase. The quartz diorite, which forms the upper 75 feet of the sill, is composed of quartz, about 25 percent, unaltered oligoclase, about 30 percent, actinolite, about 30 percent, epidote, about 15 percent, and minor sphene and rutile. The quartz and oligoclase frequently occur as myrmekitic intergrowths. Unlike the clinozoisite aggregates, which form pseudomorphs after plagioclase, the epidote in this rock occurs as large plates in association with

hornblende.

Complete chemical analyses of two augite concentrates, one from the serpentine pyroxenite at the gabbro base, and one from the hornblende pyroxenite just below the main feldspathic zone, are given in Table 4. The trend of pyroxene crystallization in the Vaillant Lake Sill can be seen in Fig. 14, where mole proportions of MgO, FeO, and CaO are plotted for these two gabbro pyroxenes as well as those from the underlying ultrabasic member.

It is interesting to note that with decreasing temperature the crystallizing pyroxenes not only became richer in FeO but also in proportion of MgO to CaO. This would be expected if the crystallization took place according to the projected section across the pyroxene liquidus drawn below (Fig. 15). This figure was proposed by Hess (1941) to explain common pyroxene field relations, and as we have seen (pp. 64-73), it is likely valid in cases of crystallization from a melt containing considerable dissolved volatile material, that is, a normal volatile bearing melt under high pressure. This diagram indicates the following simple crystallization trend. A melt of composition A^O initially precipitates a pyroxene of composition C'. The melt then moves towards B while the pyroxenes crystallizing move towards D. The final result of fractional crystallization is coprecipitation of two pyroxenes of compositions D

^{O} The actual melt composition is not part of the system $CaSiO_3$-$MgSiO_3$-$FeSiO_3$, since it contains considerable plagioclase.

' Pyroxenes actually contain considerable Al_2O_3, about 10 percent of Tschermak's molecule (Ca, Mg)Al_2SiO_6 in the two analyzed.
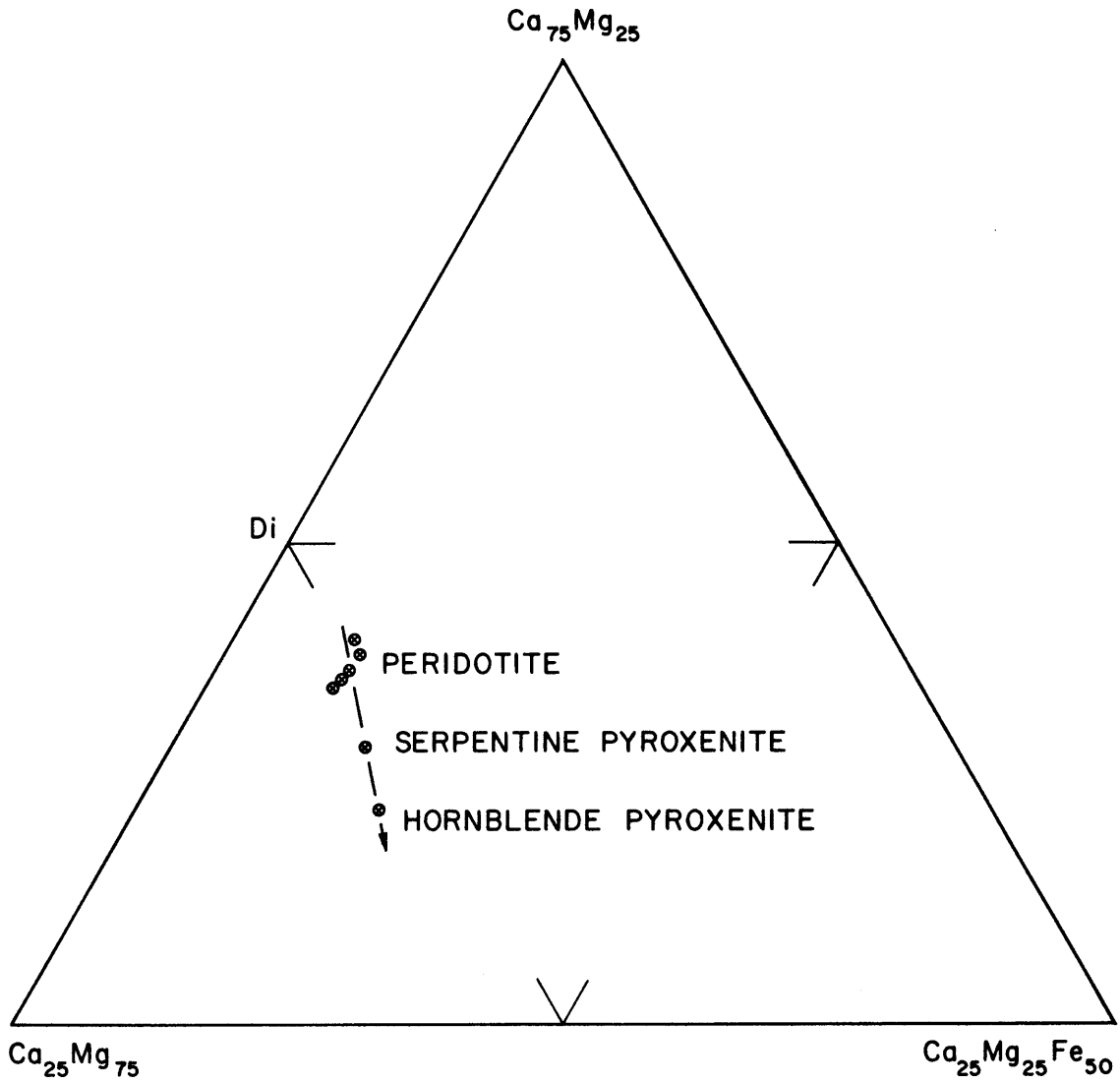
FIG. 14 TREND OF DIFFERENTIATION OF CLINOPYROXENES IN
CHUKOTAT SILL AT VAILLANT LAKE, P.Q.
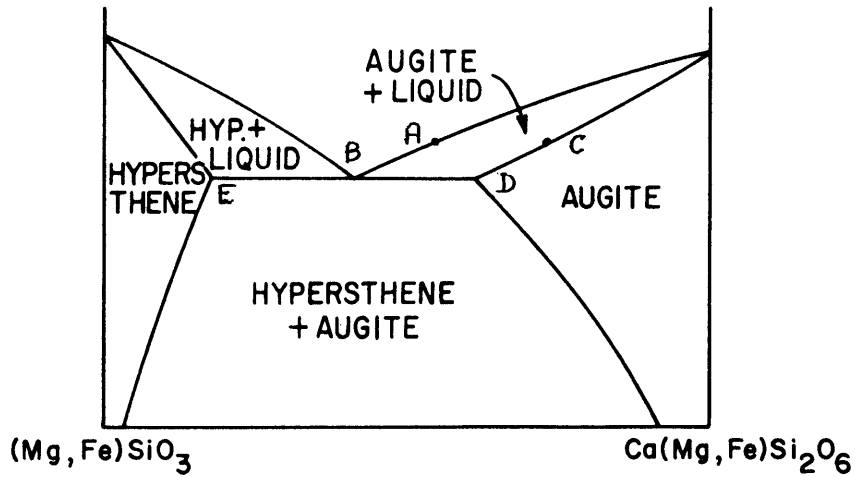
FIG. 15   SCHEMATIC SECTION ACROSS PYROXENE LIQUIDUS SHOWING
TREND TOWARDS COTECTIC PRECIPITATION OF AUGITE
AND HYPERSTHENE.

(Similar to diagram by Hess, 1941)

and E.

Unfortunately, pyroxenes are not present above the lowest 100 feet in the 500 foot gabbro member at Vaillant Lake. It is typical of the Chukotat gabbros that actinolitic hornblende replaces pyroxene as the main mafic mineral at the base of the feldspathic zone. As has been noted, this amphibole seems to be a primary mineral of the gabbro, but one can speculate on the pyroxenes which would have crystallized had favourable conditions for amphibole formation not occurred. The solid solution limit of hypersthene in augite would have been reached (Pt. D, Fig. 15), and two pyroxenes would have formed. The introduction of actinolitic hornblende, $Ca_2(Mg,Fe,Al)_5(Si,Al)_8 O_{22}(OH)_2$, acts similarly to cotectic pyroxene crystallization, the $CaO/MgO + FeO$ ratio being very close to 2:5 for both actinolitic hornblende and typical cotectic pyroxene mixtures (Hess, 1941, 1960, p. 76).

It might be argued that the actinolitic amphibole of the main gabbro zone is completely secondary, the result of hydrothermal alteration of an augite-hypersthene mixture. If this is so, it would be very unusual that no remnants of orthopyroxene or actinolite pseudomorphs after pyroxene are now visible. Moreover, altered plagioclase laths and large plates of amphibole are generally arranged in an interlocking granitic texture suggestive of cotectic crystallization (Plate 6).

If the actinolitic hornblende is indeed primary, as textural evidence suggests, its initial precipitation appears
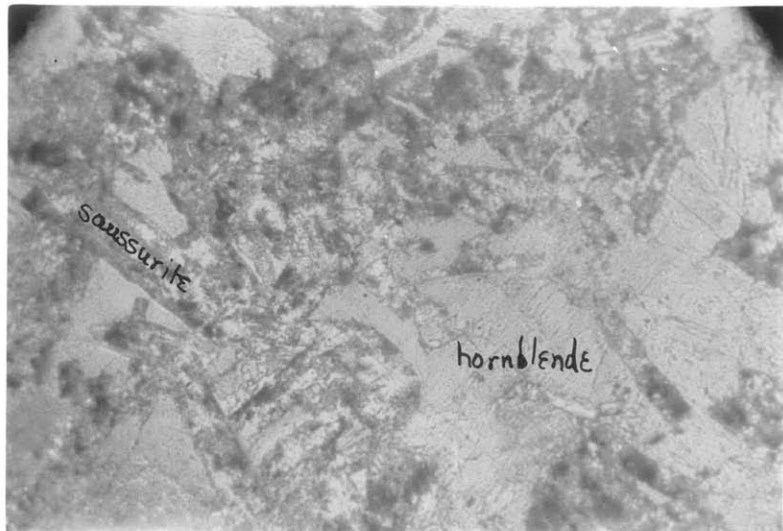
Plate 6: Primary hornblende and plagioclase displaying
intersertal texture

(gabbro member, lower Vaillant Lake sill;
plagioclase largely altered to clinozoisite)

photo length = 8 mm.
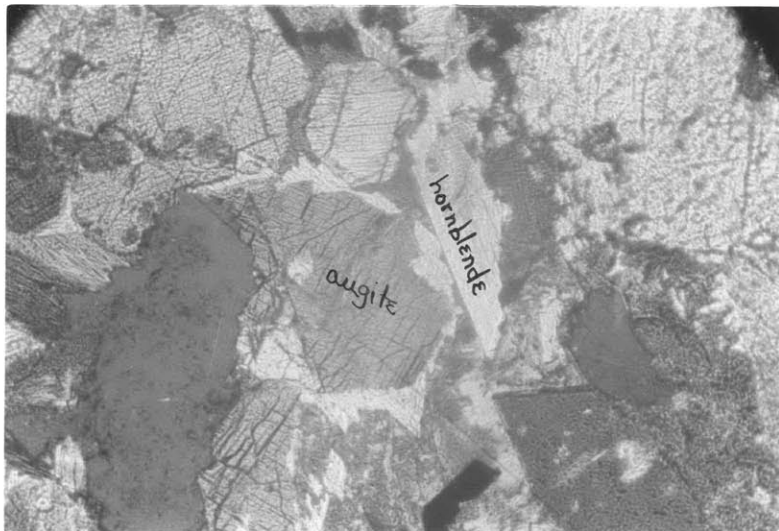
Plate 7: Actinolitic hornblende formed at the expense
of augite

(hornblende pyroxenite zone, gabbro member,
lower Vaillant Lake sill)

cross nicols, photo length = 5 mm.

to be another example of odd crystallization, with resorption this time of augite (Plate 7). Such resorption is only of minor importance in affecting the sill chemistry, however, since most of the augite had apparently settled to a fairly compact pyroxene layer before actinolite began to form.

The composition of three of the plagioclases of the gabbro member have been determined by conventional optical methods (Appendix, p. 264), and are listed in Table 4. The two from the main gabbro zone have been determined from grains which have been largely altered to clinozoisite and other saussurite minerals, and are likely too sodic. The clinozoisite nuclei leached calcium from all sections of the plagioclase grains, as can be seen by the fact that there is never any variation in extinction from saussuritic patches to unaltered zones.

The main saussurite reaction can be approximated by the following:

36 anorthite + 6 actinolite + 22 H_2O

$\longrightarrow$ 24 clinozoisite + 5 chlorite + 28 quartz

36 $CaAl_2Si_2O_8$ + 6 $Ca_2(Mg,Fe)_5Si_8O_{22}(OH)_2$ + 22 H_2O

$\longrightarrow$ 24 $Ca_2Al_3Si_3O_{12}(OH)$ + 5 $Mg_6Si_4O_{10}(OH)_8$ + 28 SiO_2
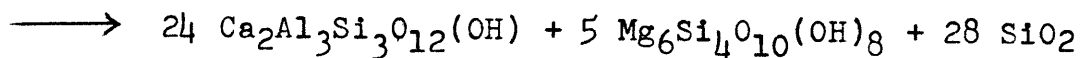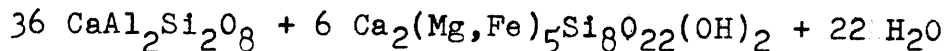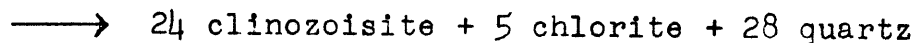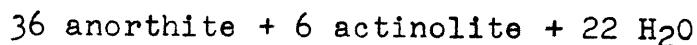
Small relict crystals of actinolite, as well as the existence of chlorite in the saussurite aggregates, indicate that amphibole played a role in the feldspar alteration.

Because the zones composed mainly of saussurite seem to predominate over those composed mainly of unaltered plagioclase, it is certain that the original anorthite content of the

plagioclase was appreciably greater than can now be determined
optically from the unaltered portions. Thus, the andesine,
An 33, of specimen A-25 at the 1180-foot level, and the
oligoclase, An 28, of specimen A-27 at the 1360-foot level, were
originally more calcic, probably labradorite or calcic andesine.
The oligoclase composition of the unaltered plagioclase in the
uppermost quartz diorite zone (Table 4) indicates the trend of
upward differentiation from calcic to sodic plagioclase.

5. Chemical Differentiation of the Chukotat Sill Magma

5.1 Composition of the Parent Magma

It is interesting to attempt to estimate the initial chemical composition of the parent magma of the Chukotat Sills, that is, the composition of the magma prior to both intrusion and initial olivine crystallization. Taking its average composition to approximate the bulk composition of a typical settled differentiated sill, one half untrabasic and one half gabbro, which is the preponderant sill type in the Chukotat Series, the silica content of the original magma is estimated to be about 45 percent.

The ultrabasic section at Vaillant Lake, of rough mineralogical composition: chrysolite, 70 percent, endiopside, 15 percent, and antigorite, 15 percent, has a silica content of about 40 percent. The average silica content of the serpentinites at Cross Lake (Table 3, p. 87) is 40.2 percent, and can be compared to a similar analysis of a serpentinite from Esker Lake, 6 miles west of Cross Lake, which gives a result of 39.5 percent. As expected, serpentinization has little effect on the silica percentage in these rocks, since antigorite and chrysolite have similar silica contents, roughly 39 percent.

The silica content of the average Chukotat gabbro as inferred from a mineral assemblage: 50 percent actinolite, 30 percent clinozoisite, and 20 percent andesine, is about

52 percent. Allowing for the amphibole being actinolitic hornblende and not pure actinolite, thus containing about five percent of Al_2O_3, this estimate should be reduced to about 50 percent. The Chukotat leucobasalts are very similar in mineralogy to the gabbros, composed largely of an alteration mass of actinolite and clinozoisite in roughly equal proportions. They contain about 50 percent of silica. It would seem that the typical gabbros almost certainly contain between 49 and 51 percent of silica, based on these considerations.

One must, however, consider the basal pyroxenite zones, with a silica content of about 52 percent (Table 4), and the upper quartz diorite zone, which, with a typical assemblage of 30 percent actinolite, 30 percent oligoclase, 25 percent quartz, and 15 percent epidote, contains about 65 percent of silica. Allowing for a thickness of about 75 feet of each of these zones as opposed to about 350 feet of normal gabbro, as is the case at Vaillant Lake, the average silica content of a typical gabbro member is about 53 percent of silica, with possible deviations of at least two percent.

The settled differentiated sills of the Cross Lake and Laflamme Lake areas contain roughly similar thicknesses of gabbro and ultrabasic rock, but the latter seems to generally predominate. At Vaillant Lake, for example, the peridotite is 900 feet in thickness, the gabbro capping only 500 feet. The proportion of these two members, as we have seen is very variable, both members occurring separately, and hence the

silica content of the original melt is difficult to estimate.
Taking a 6:4 ratio of ultrabasic material to gabbro as about
the most common ratio in the settled sills, a silica content of
45 percent is obtained for the parent magma, but values from
43 to 47 percent would seem possible.

Similar estimates of the percentage of other major elements
from mineralogical proportions and by comparison of ultrabasic
and leucobasalt bulk analyses are listed in Table 3. Compared
to typical gabbros and basalts, there can be no doubt that the
Chukotat Sill parent magma is very low in aluminum, low in
calcium and silica, and very high in magnesium. Normative
mineral percentages place the parent magma in the olivine
tholeite class of Yoder and Tilley (Table 3). This class of
magmas falls between the critical planes of undersaturation
and oversaturation in the simple basalt system Mg_2SiO_4-
$CaMgSi_2O_6$-$NaAlSiO_4$-SiO_2 of the same authors (Fig. 13). As we
have seen (p. 85), the olivine basalts of the Chukotat Series
fall in the same class.

5.2: Olivine-Pyroxene Crystallization Relationships

Two points in the chemical course of crystallization of
the Chukotat Sill magma are notable. Firstly, although the
normative olivine content of the parent magma is only 36 per-
cent, the quantity of modal olivine is about 50 percent, con-
siderably higher. A ratio of 6:4 for the ultrabasic to gabbro

proportion is assumed in both normative and modal values, but
the normative to modal ratio would not vary appreciably if this
ratio was changed.

Secondly, although normative hypersthene outweighs norma-
tive diopside, diopside is the first to crystallize. This is
particularly unusual since all experimental systems so far
investigated show large enstatite and small diopside liquidus
fields with diopside-enstatite-liquid equilibria odd with re-
spect to enstatite, or just slightly even with diopside the
main precipitant (Figs. 11 and 12, pp. **70, 72**). Under these
conditions, hypersthene or enstatite must be the first pyroxene
to crystallize from a magma which contains more normative
orthopyroxene than clinopyroxene. Also, hypersthene or
enstatite must build up in quantities very close to their
normative concentration prior to diopside saturation.

Both of these phenomena, the excess precipitation of
olivine, and the existence of diopside as the initial pyroxene,
can be easily explained if the crystallization of the Chukotat
Sills, at least in the Vaillant Lake vicinity, followed paths
similar to those predicted for mafic magmas under conditions of
considerable melt volatile content (pp. **42, 67**).

Three liquidus diagrams are presented below (Fig. 16):
(1) the system Mg_2SiO_4-$CaMgSi_2O_6$-SiO_2, dry, (ii) the system
Mg_2SiO_4-$CaMgSi_2O_6$-SiO_2-$CaAl_2Si_2O_8$ with liquids projected through
the anorthite composition on the triangle Mg_2SiO_4-$CaMgSi_2O_6$-
SiO_2, and (iii) diagram for the system (ii) with considerable

melt content of dissolved H_2O, i.e. saturated with steam under
about 5 kilobars pressure. Figs. 16 (i) and (ii) have been
determined from experimental data (Bowen, 1914; Andersen, 1915;
Boyd and Schairer, 1957; Hytonen and Schairer, 1960), Fig. 16
(iii) is derived from the theoretical considerations discussed
on pp. **40 - 70.** These diagrams represent crystallization paths
of iron free olivines and pyroxenes under the following condi-
tions: (i) bulk composition of magma can be represented by the
components forsterite, diopside, and silica, (ii) feldspar is
present in melt in considerable quantities, and (iii) feldspar
and steam are present in melt in considerable quantities.

We can represent the bulk composition of the Chukotat Sill
parent magma as far as is possible, by combining iron and
magnesium as magnesium and anorthite and albite as anorthite,
by point A on all three diagrams.

In Fig. 16 (i), the only ternary system of the three,
forsterite begins to crystallize until the liquid reaches the
forsterite pyroxene field boundary at point C. It should be
noted that at point B, the liquid contained normative enstatite
and diopside in a ratio of about 6:4, similar to that of the
parent magma, in equilibrium with forsterite crystals in
quantity equal to the normative olivine content of the parent
magma. Fractional crystallization will result in excess
crystallization of olivine until the composition at point C is
reached, but this excess involves only about 4 percent by
weight, sufficient only to increase the modal olivine content
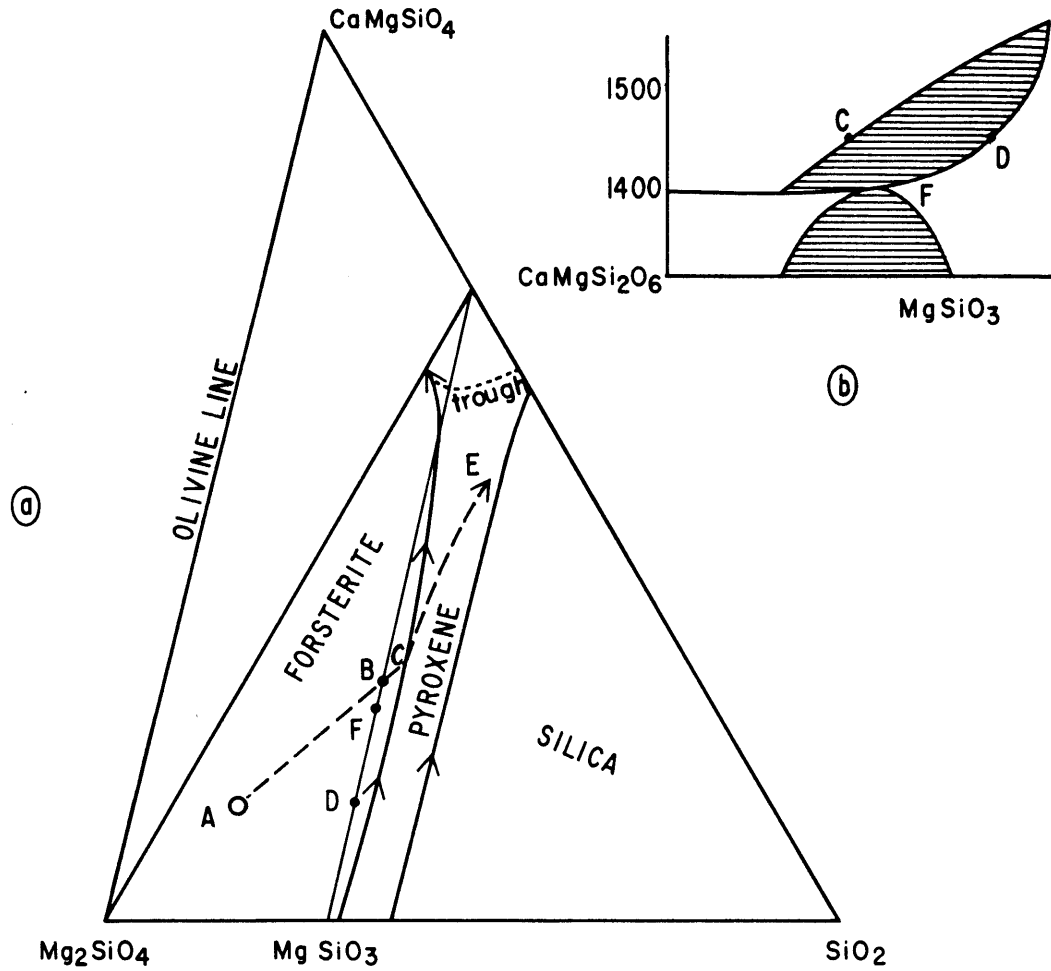
Fig. 16 (i) a.   Liquidus Diagram for the System Mg_2SiO_4-$CaMgSi_2O_6$-SiO_2
(after Bowen, 1914)

Fig. 16 (i) b.   Pseudobinary $CaMgSi_2O_6$-$MgSiO_3$ (liquids saturated with
forsterite are projected through SiO_2) (after Bowen, 1914;
Boyd and Schairer, 1957)

FIG. 16   LIQUIDUS RELATIONS IN THE SYSTEM Mg_2SiO_4-$CaMgSi_2O_6$-
SiO_2 AND THE EFFECTS OF ADDITION OF $CaAl_2Si_2O_8$
AND H_2O.
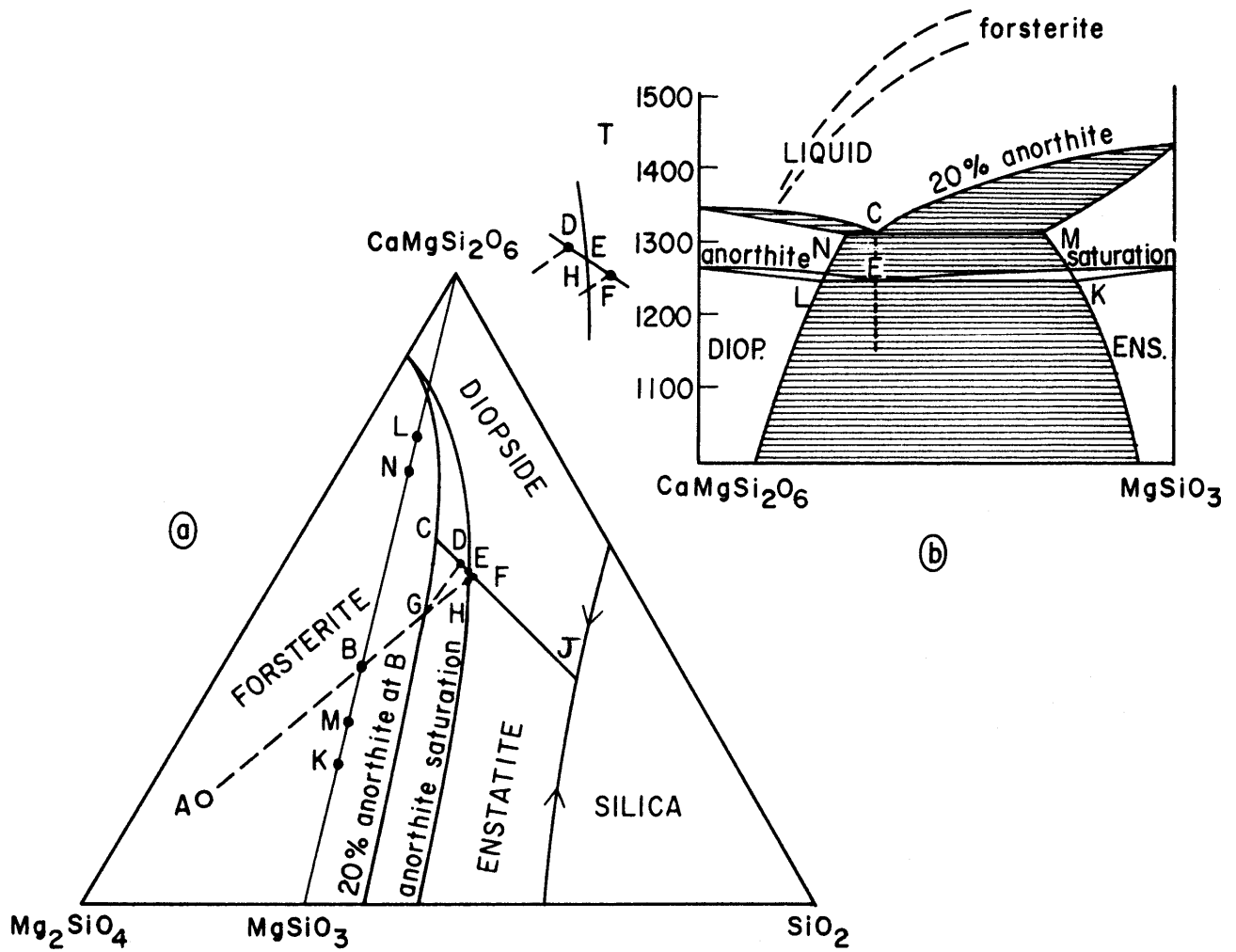
Fig. 16 (ii) a. Schematic liquidus relations for the system Mg_2SiO_4-$CaMgSi_2O_6$-SiO_2-$CaAl_2Si_2O_8$ with 20 % dissolved anorthite and saturated with anorthite (liquid compositions projected through $CaAl_2Si_2O_8$ onto the plane Mg_2SiO_4-$CaMgSi_2O_6$-SiO_2) - data after Andersen (1915), Bowen (1914), and Hytonen and Schairer (1960)

Fig. 16(ii) b. Pyroxene temperature-composition section, liquids projected through SiO_2.

FIG. 16   LIQUIDUS RELATIONS IN THE SYSTEM Mg_2SiO_4-$CaMgSi_2O_6$-
(con'd) SiO_2 AND THE EFFECTS OF ADDITION OF $CaAl_2Si_2O_8$ AND
           H_2O.

Fig. 16 (iii) a. 20% dissolved $CaAl_2Si_2O_8$ in melt at B, saturated with steam at P = ~5 kilobars (schematic)

Fig. 16 (iii) b. Pyroxene temperature-composition section, liquids projected through SiO_2 onto the join $CaMgSi_2O_6$-SiO_2.MgO.

FIG. 16 (con'd)   LIQUIDUS RELATIONS IN THE SYSTEM Mg_2SiO_4-$CaMgSi_2O_6$-SiO_2 AND THE EFFECTS OF ADDITION OF $CaAl_2Si_2O_8$ AND H_2O.

from the normative value of, say 36 percent, to about 40
percent. Furthermore, according to this diagram, a pyroxene
of composition D would be the first mineral to crystallize
after forsterite. As the composition of the liquid then moved
along the path CE, the pyroxenes crystallizing would move along
the line DF. Eventually a diopsidic pyroxene would form but
only after a series of subcalcic pyroxenes had crystallized.
Clearly, the crystallization path indicated is incompatible
with the observed mineralogical trend of the Chukotat magma.

In Fig. 16 (ii), the effect of adding anorthite to the
system is shown. Small quantities of this component cause the
solid solution minimum trough shown on the pyroxene liquidus of
Fig. 16 (i) to move away from diopside and form a cotectic
field boundary between the two pyroxenes enstatite and diopside
as the liquidus temperatures are lowered. This field boundary
reaches a point at an $MgSiO_3/CaMgSi_2O_6$ ratio of 5:8 with about
15 percent of the bulk composition anorthite. If anorthite is
added until saturation occurs, the field boundary remains
essentially at the same position (Figs. 11, 12, 16 (ii)).

The path followed by a liquid crystallizing at A, with an
anorthite content such that the melt will contain 20 percent
anorthite when it reaches the composition B, is AGC under
conditions of equilibrium crystallization and AGDJ under condi-
tions of fractional crystallization. With equilibrium crystal-
lization, forsterite precipitates until the melt composition
reaches G. At G the forsterite reacts with the melt to produce

enstatite of composition K. The melt then moves in composition along GC, and the enstatite along KM. Then, cotectic precipitation of diopside N and enstatite M takes place until the liquid disappears.

With fractional crystallization, the forsterite has been removed from the melt at G. The liquid then follows the curved path GD as enstatite precipitates. At D, largely diopside with a little enstatite coprecipitate, and the melt then moves along the path DJ, becoming richer in silica.

Under conditions of anorthite saturation, the liquid paths from A are, similarly, for equilibrium crystallization, AHE, and for fractional crystallization, AHFJ. It is interesting to note that in both the cases of limited anorthite in solution and of anorthite saturation, enstatite is the first pyroxene to form with diopside separating in abundance later. This is precisely the opposite to what is observed in the Chukotat Sills, where diopside crystallizes first and the liquid becomes richer in normative enstatite.

Fig. 16 (iii) represents the hypothetical conditions of iron free olivine and pyroxene crystallization under conditions of considerable melt volatile content. Forsterite precipitates from the initial liquid at A until the liquid reaches the forsterite-pyroxene boundary at L. At this point, forsterite will be resorbed under equilibrium conditions as the liquid moves in composition from L to P. Diopsidic pyroxenes, in this case, will precipitate as the first pyroxenes, their composition

trending along MN as the liquid moves along LP. At the liquid composition P, enstatite will coprecipitate along with diopside. Forsterite resorption will continue until the liquid disappears.

With fractional crystallization, the liquid, after crossing the forsterite-diopside field boundary, will follow the path LQ, and eventually will arrive at the cotectic field boundary diopside-enstatite, which, as we have seen (pp. 64-68), shifts towards diopside with the introduction of volatiles into the melt. Cotectic precipitation of approximately equal quantities of the two pyroxenes will follow.

Fig. 16 (iii) not only explains the pyroxene crystallization trend in the Chukotat Sills, but also accounts for their very high modal olivine content. It has been estimated (p. 41) that dissolved steam sufficient to lower the olivine liquidus by about 100 degrees will cause the forsterite-enstatite field boundary to move towards a more siliceous composition by about 5 weight percent in the binary system Mg_2SiO_4-SiO_2. Large increases in the extent of the forsterite liquidus region due to volatiles in addition to these due to feldspar would be adequate to explain the high 50 percent modal olivine content of the sills.

The lower settled differentiated sill at Vaillant Lake undoubtedly crystallized at pressures great enough to have caused appreciable quantities of volatiles to dissolve in the melt. It was intruded at a depth of at least three miles and

most likely over five miles. The thickness of the Chukotat
Series exposed in the Cross Lake and Laflamme Lake areas is
15,000 feet, but over 30,000 feet have been reported from the
Bilson Lake section on the western side of the Cape Smith belt
(Bergeron, 1957), and since the lower sill at Vaillant Lake
lies at the base of the Chukotat Series, it likely solidified
at pressures in the two to five kilobar range. Under such
pressures, steam, if present in excess, would dissolve in the
melt in quantities great enough to lower the olivine and
pyroxene liquidi by about 50 to 100 degrees, according to the
data of Yoder and Tilley (1956). The major olivine crystalli-
zation certainly took place at greater depths and pressures
than the sill emplacement, and hence the volatile content of
the magma during the separation of the olivine may have been
very great. Primary amphibole in the gabbros, plus the wide-
spread serpentinization of most of the ultrabasics, believed
to be an autometasomatic process by Shepherd (1959), suggest
that ample volatiles were present in the Chukotat Sill magmas.

Nothing has yet been said concerning the effects of
albite, iron bearing components, or aluminum substitution in
the pyroxenes on the course of crystallization of the Chukotat
Sills. Albite acts very similarly to anorthite in affecting
olivine-pyroxene equilibria (Fig. 11, p. 70), and aluminum
substitution in diopside and enstatite is very small in the
case of precipitation from liquids more siliceous than the
$MgSiO_3$-$CaMgSi_2O_6$ join. The effect of iron, however, is not

negligible. The parent magma of the Chukotat Sills contains about 8.5 weight percent of ferrous oxide, for an FeO/ (FeO + MgO) ratio of approximately 0.35. Furthermore, by the time the olivine-pyroxene-liquid equilibrium was reached after the precipitation of all the olivine, this ratio was much greater, probably about 0.50, since the FeO/FeO + MgO ratio in the analyzed ultrabasics is 0.27, and the ratio of ultrabasic rock to gabbro estimated and used to determine the composition of the parent magma is 6:4.

Adding iron to the systems considered causes the olivine-orthopyroxene field boundary to change from odd to even at a melt FeO/(FeO + MgO) ratio of about 0.22 (Bowen and Schairer, 1935: Fig. 3, p. 39). At a ratio of 0.50, the field boundary has moved about 2.2 percent from the orthopyroxene composition line directly away from the SiO_2 composition towards the olivine composition line, measured in terms of the ternary system $Mg_2 SiO_4 - Fe_2 SiO_4 - SiO_2$. Considering that in the iron free system the forsterite-enstatite field boundary is located 1.6 percent from enstatite towards silica, measured in terms of the binary system $Mg_2SiO_4 - SiO_2$, a net shift of about 3.8 percent away from silica is produced in the orthopyroxene-silica field boundary by adding iron to the melt to equal oxide proportions with magnesium.

It is not known if iron has the same effect in shrinking the olivine field in the analogous calcium bearing system, which is more complex because it is not ternary. It is

expected, however, because of the rapid decrease in the crystallization temperature of olivine with increasing iron, relative to that of both the orthopyroxene and clinopyroxene systems (pp. 38-40), that the addition of iron to the system Mg_2SiO_4-$CaMgSi_2O_6$ will shrink the olivine field moving the olivine-clinopyroxene-liquid equilibrium closer to olivine as well as the olivine-orthopyroxene-liquid equilibrium. Therefore we might expect a shift in the pyroxene-olivine field boundary of about 4 percent away from silica (measured along a silica-olivine line) caused by the iron content of the Chukotat magma. This would reduce, to a considerable extent, the projected shift towards silica caused by the feldspathic content of the magma, which, for anorthite saturation, is from 10 to 15 percent towards silica in the magnesian portion of the triangle Mg_2SiO_4-$CaMgSi_2O_6$-SiO_2 and essentially zero as the diopsidic corner is approached (Fig. 16 (ii)).

We may summarize by emphasizing that only dissolved volatiles seem capable of explaining the trend of pyroxene crystallization in the Chukotat Sills, that is, initial diopside separation in reaction with forsterite from a liquid richer in normative hypersthene than normative diopside. Furthermore, such volatiles would have the effect of expanding the liquidus of olivine, allowing olivine precipitation in greater excess of its normative content than would be expected in a dry melt.

5.3 Serpentinization

The process of serpentinization of ultrabasic rocks is a contraversial one. Many of the peridotites of the Chukotat Sills have been almost completely serpentinized, but this has not been the case at Vaillant Lake, where only the lowest 100 feet of the 900 feet peridotite member studied has been strongly serpentinized. Since no relation has been observed between sill thickness and degree of serpentinization, although great variations in serpentinization exist, it is expected that this process has acted in a volume for volume manner. If so, considerable MgO and SiO_2 must have been removed, some of which may have acted as an agent of metasomatism. Siliceous slates in contact with serpentinite frequently show the effects of such metasomatism, with extensive development of actinolite and/or green hornblende, but such alteration is not generally visible more than ten or twenty feet from the contact.

The process of serpentinization may be autometasomatic, residual water-rich magmatic solutions being the agent of alteration, or it may be a reaction of regional metamorphism produced during the major period of deformation. The upper and lower settled sills at Vaillant Lake, closely separated stratigraphic horizons, show extreme contrast in degree of serpentinization. The ultrabasic portion of the upper sill is almost completely serpentinized, while that of the lower sill, as we have seen, is only slightly serpentinized. This and

other examples of rapidly varying degrees of serpentinization
over short distances suggest that the water of serpentinization
was derived from the original magmas, and that loci of
serpentinization were defined by migration of late magmatic
aqueous phases.

6. Comparison of the Crystallization Trends of the Chukotat
   Sills and the Mafic Complex at Stillwater, Montana

We have just seen how the original very mafic Chukotat
Sill magma, through excess precipitation of olivine such as
would be expected under low temperature conditions of crystal-
lization, produced a common tholeiitic magma. A subsiliceous
magnesian magma, then, after olivine separation, may follow a
differentiation path very similar to that of a tholeiitic magma
crystallizing under similar physical conditions. It is there-
fore desirable to compare the mineralogy of the Chukotat Sills
which formed in a 'wet' environment with that of a typical
layered magnesian tholeiitic intrusive such as the mafic
complex at Stillwater, Montana.

The Stillwater Complex is a well known layered and differ-
entiated intrusive, the petrology and mineralogy of which have
been extensively studied (Hess, 1960; Jones, Peoples, and
Howland, 1960). The section at East Boulder Plateau, where the
most complete exposures occur, is over 16,000 feet in thickness,
and from the floor to the upper limit of exposure it consists,
according to Hess, of five main zones: the ultramafic zone, the
norite zone, the lower gabbro zone, the anorthosite zone, and
the upper gabbro zone. . The basal border zone, which is found
below the ultramafic zone, is a doleritic chill zone whose
bulk composition is believed to approximate that of the original
magma.

The ultramafic zone, 2500 feet in thickness, is composed
of a lower harzburgite layer and an upper bronzitite layer.
The harzburgite represents the result of olivine accumulation
on the floor of the intrusive. Poikilitic bronzite was formed
by an extensive olivine liquid reaction after the settling of
the olivine, and typically makes up about one half of the rock.
Small finer grained patches of bronzite, augite, and plagioclase
represent the final crystallization of the remnant interstitial
liquid. The bronzitite layer above the harzburgite represents
a similar accumulation, this time of bronzite. A molecular
norm of the ultramafic zone calculated from a composite of the
rocks of this sequence is presented in Table 5.

In the norite zone, which is about 2740 feet in thickness,
both plagioclase and orthopyroxene predominate as perieuhedral
crystals. They represent the original crystal mush from which
the bulk of the norite was formed. Interstitial anhedral
augite, orthopyroxene, and plagioclase have crystallized from
the pore liquid.

The lower gabbro zone, 2210 feet in thickness, is similar
to the norite zone except that augite is present as an essen-
tial constituent forming distinct crystals comparable in size
to the orthopyroxene. The ratio of clinopyroxene to
orthopyroxene is about 1:1, the former slightly in excess.

The anorthosite zone, 6210 feet in thickness, and the
upper gabbro zone, 2130 feet in thickness, make up the upper
portion of the complex. The hidden zone, estimated by Hess to

Table 5:   Bulk Composition of Stillwater Complex (Hess, 1960)

	Composite Ultramafic Zone Composite 1	Composite Exposed Complex above Ultramafic Zone Composite 2	Bulk Comp. of Exposed Complex Composite 1 and 2	Border Facies "Parent Magma"
SiO_2	47.73	49.70	49.33	50.68
Al_2O_3	4.82	22.04	19.28	17.64
Fe_2O_3	2.94	0.66	1.02	0.26
FeO	6.54	4.02	4.41	9.88
MgO	28.98	7.03	10.48	7.71
CaO	2.44	13.59	11.80	10.47
Na_2O	0.19	1.79	1.53	1.87
K_2O	0.02	0.07	0.06	0.24
H_2O	5.40	0.91	1.60	0.48
CO_2	0.11	0.07	0.08	0.04
TiO_2	0.12	0.16	0.15	0.45
P_2O_5	0.01	0.02	0.02	0.09
S	0.04	0.04	0.04	--
Cr_2O_3	0.48	0.03	0.10	--
MnO	0.17	0.09	0.10	0.15
	99.99	100.22	100.00	99.96

Table 5:   Bulk Composition of Stillwater Complex (cont.)

	Composite Ultramafic Zone Composite 1	Composite Exposed Complex above Ultramafic Zone Composite 2	Bulk Comp of Exposed Complex Composite 1 and 2	Border Facies "Parent Magma"
Molecular Norm				
An	10.42	51.78	45.59	39.06
Ab	1.62	15.14	12.94	15.72
Or	0.11	0.39	0.33	1.39
Di	--	12.30	9.98	9.95
Hy	62.40	17.35	21.89	31.82
Ol	13.71	0.76	5.39	--
Mt	4.18	0.93	1.49	0.46
Il	0.23	0.30	0.30	0.91
Cm	0.70	--	0.21	--
Cc	0.31	0.16	0.20	--
H_2O	5.40	0.91	1.60	0.48
Cor	0.66	--	--	--
Py	0.07	--	--	--
Ap	--	0.05	--	0.20
Qz	--	--	--	--

be 10,650 feet in thickness, is believed to be mainly quartz ferronorite based on the bulk composition of the exposed complex and the composition of the parent magma.

In Table 5, with the composite analysis of the ultramafic zone, are listed a composite analysis of the exposed complex above the ultramafic zone, an estimated bulk analysis of the complete exposed complex, and an analysis of the border facies, believed equivalent in composition to the parent magma. It can be seen that this parent magma was saturated with respect to silica, there being neither normative olivine nor quartz. However, the composite norm of the exposed section shows 5.4 percent of olivine, which is likely too small a figure for the complex as a whole, since the East Boulder Plateau ultramafic zone is only 4000 feet in thickness as compared to over 6000 feet in the central and western portions of the complex (Jones, Peoples, and Howland, 1960). Furthermore, this figure only represents that portion of the original olivine which failed to react with the melt to form bronzite.

While the olivine liquid reaction was not carried very far in the ultrabasics of the Chukotat Sills where the rocks contain about 80 or 85 percent olivine and serpentine and only 15 or 20 percent poikilitic clinopyroxene, it evidently was very important in the Stillwater ultramafic zone, where typical harzburgites contain about 50 percent poikilitic orthopyroxene. Orthopyroxene was the first pyroxene to crystallize from the Stillwater magma because the bulk composition, as shown by the

norm, was very rich in hypersthene (Fig. 17, Table 5).

Conditions favouring fractional crystallization of olivine were better developed in the Chukotat Sills than in the Stillwater Complex. The interstitial liquid content of the Stillwater mush must have been greater than that of the Chukotat olivine layer judging from the development of fine grained interstitial gabbro in the harzburgite masses and the great extent of the olivine to bronzite reaction. This difference may be due to the fact that the olivine in the Chukotat Sills was largely crystalline before injection, and hence had more chance to settle in a uniform mass before nucleiation of gabbroic crystals began, or it may be due to a viscosity difference caused by higher temperatures of crystallization in the Chukotat magma, a distinct probability judging from the compositions of the pyroxenes of the two intrusives (see below). In any event, this tendency towards a more equilibrium type crystallization in the Stillwater ultramafic zone in comparison to the strong fractionation in the Chukotat Sills would be expected to greatly reduce the amount of olivine to survive complete solidification.

In a dry magnesian melt saturated with anorthite, the forsterite field overlaps the orthopyroxene composition at the projected En 75 Di 25 composition by about 14 percent measured along a line silica-olivine (Fig. 12; also pp. 38-40). If the iron content of the melt is increased to an FeO/MgO + FeO ratio of about 0.57, similar to the Stillwater magma after the
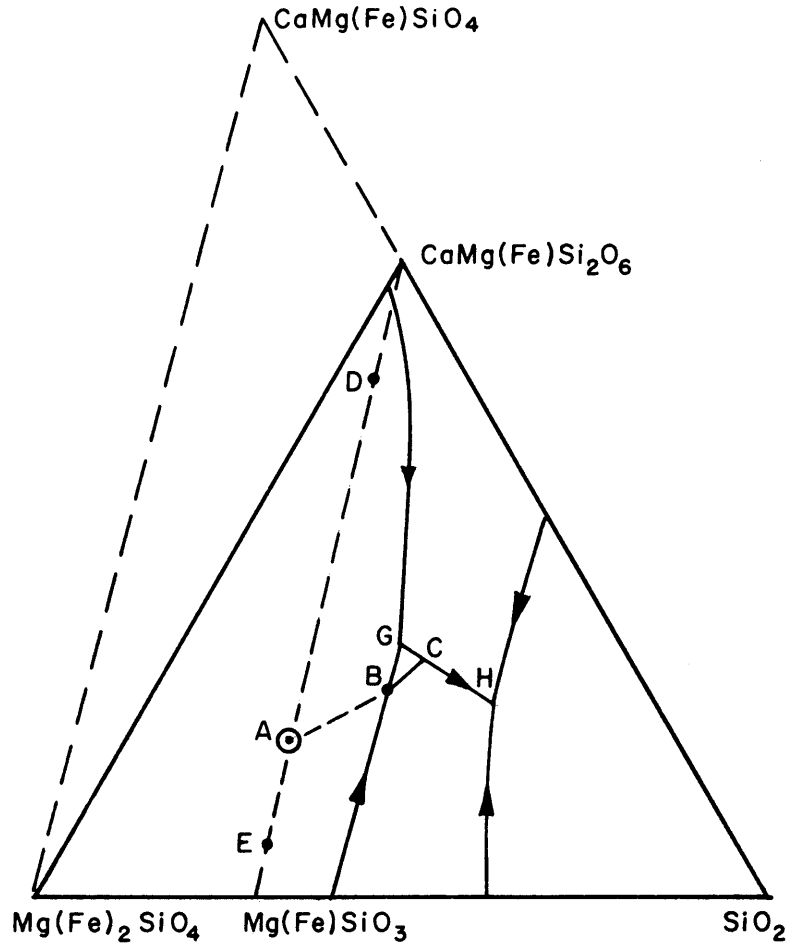
FIG. 17 SCHEMATIC LIQUIDUS DIAGRAM $Mg\,(Fe)_2SiO_4$-$Ca(Mg, Fe)$
Si_2O_6-SiO_2 SATURATED WITH $CaAl_2Si_2O_8$ AND STEAM AT
P = $\sim$5 KILOBARS REPRESENTING CRYSTALLIZATION
PATH OF THE STILLWATER MAGMA.

ABCH represents fractional crystallization path.

ABG represents equilibrium crystallization path.

D and E represent approximate solid solution limits at C.

Liquid compositions are projected from anorthite on plane
of diagram. Point A represents Stillwater parent magma.

Fe, Mg grouped, Al_2O_3 in pyroxene not considered.

main period of olivine precipitation, the field shrinks back
about 5 percent to about a 9 percent overlap. Under these
conditions a maximum of about 13 percent of forsterite can pre-
cipitate under perfect fractional crystallization from a melt
of bulk composition En 75 Di 25. In the natural Stillwater
magma, with over 60 percent feldspar in solution after olivine
separation (Table 5), the percent of olivine that can be pre-
cipitated as a result of the same overlap is less than half as
much, since over half of the melt is feldspar, through which
the olivine pyroxene field boundary is projected (Fig. 17).
This means we could expect about 5 percent of modal olivine in
the Stillwater Complex under conditions of perfect fractiona-
tion. Assuming that there is no olivine in the hidden portion
of the intrusive, the actual modal olivine content of the
whole complex at the East Boulder Plateau section is roughly
60 percent of that of the exposed zone, or about 3.2 percent.
This figure is certainly too small for the entire complex,
since the ultramafic zone at East Boulder Plateau is unusually
thin (Jones, Peoples, and Howland, 1960; Peoples, 1962). More-
over, this probably represents only a fraction of all the
olivine that could have formed if reaction with the melt was
prohibited, i.e. perfect fractional crystallization, because
about half of the original olivine layer, now represented by
harzburgite, has been transformed to bronzite. Then too, some
reaction of olivine and liquid during the slow accumulation of
the ultrabasic layer probably occurred. Despite these reactions,

the quantity of surviving olivine appears to almost equal the predicted maximum amount that could form. It seems, therefore, that the original quantity of olivine which crystallized from the melt was probably considerably greater than 5 percent, the excess being caused by an enhancement of the olivine field due to volatiles dissolved in the melt.

The trend of pyroxene crystallization presents more direct evidence for the presence of large quantities of dissolved volatiles during differentiation. The clinopyroxene orthopyroxene cotectic equilibrium was reached just before the accumulation of the lower gabbro zone. The composition of the melt at this stage as far as normative hypersthene and diopside are concerned, was approximately half way between the compositions of the two pyroxenes that were precipitating (Fig. 17). This is inferred from the modal ratio of augite to hypersthene, just over 1:1. This fractional cotectic crystallization of approximately equal proportions of orthopyroxene and clinopyroxene following large scale single pyroxene precipitation, is, as we have discussed (pp. 64-68), only possible with high melt volatile content.

It is interesting to examine the compositions of the clinopyroxene which coprecipitated with hypersthene. Pyroxene, olivine, and plagioclase compositions at various levels of the complex are shown in Figs. 18 and 19. The composition of the augite of the lower gabbro zone, Ca 41 Mg 48-45 Fe 11-14, represents the limit of solid solution of hypersthene in augite
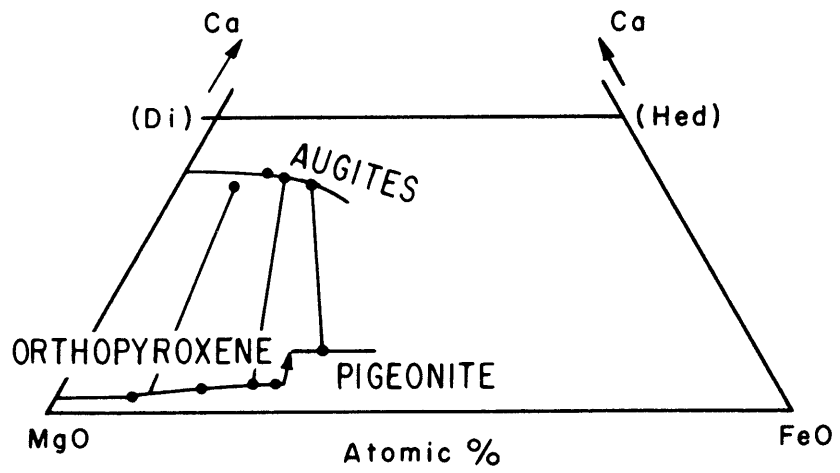
FIG. 18   COURSE OF CRYSTALLIZATION OF STILLWATER
ORTHO- AND CLINOPYROXENES

(after Hess, 1960)
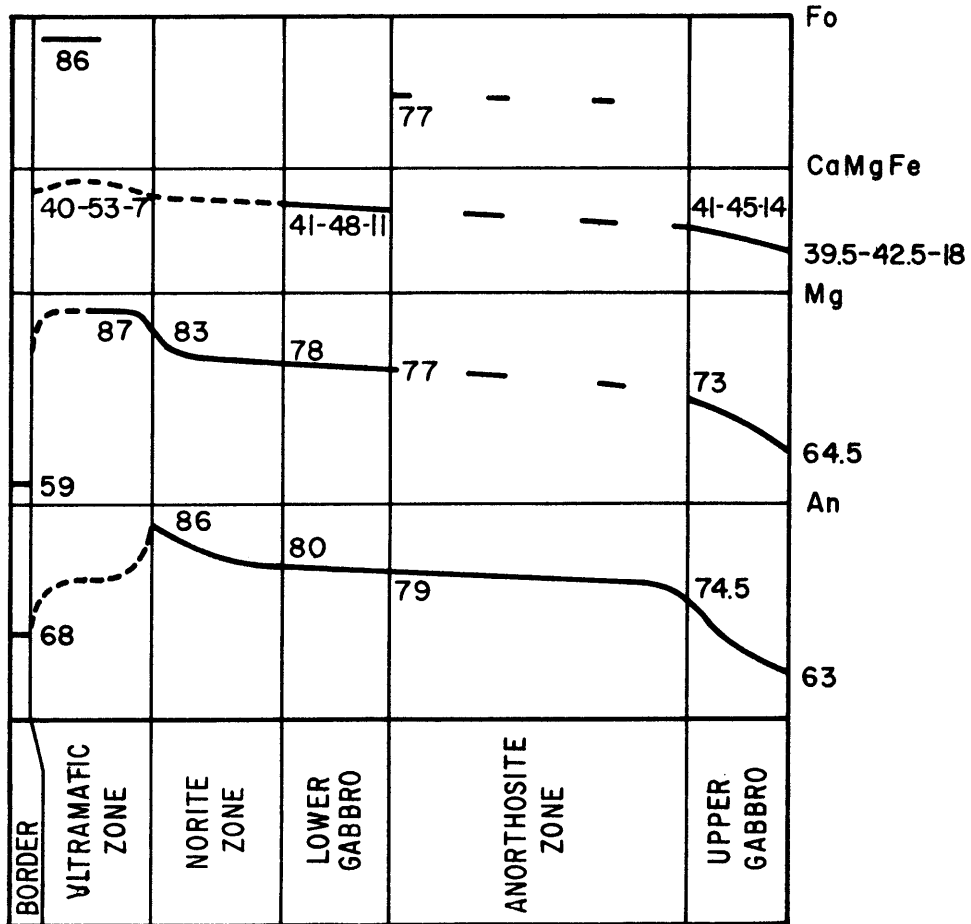
FIG. 19 MINERALOGICAL CHANGES IN STILLWATER COMPLEX
(After Hess, 1960)

at the temperature of crystallization. In the Chukotat gabbros, this composition does not represent the solid solution limit in the augites; a single clinopyroxene as magnesian as Ca 36 Mg 53 Fe 11 is found in the hornblende pyroxenite zone, representing the highest stratigraphic and presumably lowest temperature pyroxene in the sill. This greater pyroxene solid solution limit indicates a greater temperature of crystallization for the gabbros of the Chukotat Sills compared to that of the lower gabbro of the Stillwater Complex.

An estimate of the lowering of the temperature of crystallization of the Stillwater lower gabbro due to the presence of volatiles can, in fact, be made through an extrapolation of the compositions of the clino- and orthopyroxenes in equilibrium to the iron free pyroxene section (Fig. 18). This extrapolation shows a diopside of composition En 16 Di 84 by weight in equilibrium with enstatite En 91 Di 9. Such a miscibility gap, according to Fig. 5 (p. 45), can only occur at a temperature slightly below $1100^{\circ}C$. Since dissolved anorthite, even at saturation, only lowers the temperature of two pyroxene crystallization in an iron free system to $1260^{\circ}C$ (Fig. 11, p. 70), enough volatiles must have been present in the Stillwater magmas to cause an added 150° lowering of the liquidus temperatures and to enlargen the miscibility gap to that inferred from the pyroxene analyses.

The alumina contents of the Chukotat augites, 5.6 and 6.2 percent in the two specimens analyzed, are greater than those

of the Stillwater complex, which average 3.0 percent (Hess, 1960). There seems to be at least in some intrusives a direct relation between the alumina contents of augites and their temperatures of formation. This will be seen in the study of the pyroxenes of the Monteregian Hills (pp.   ), but it is also displayed in the two pyroxenes analyzed from the Chukotat gabbros, the lower level augite which crystallized first being richer in alumina and poorer, as expected, in iron than the upper augite, which crystallized later and at a lower temperature. No relation of this sort has been observed in the Stillwater Complex, however, there being no variations greater than the limits of accuracy in the chemical analyses (Hess, 1960). The more aluminous nature of the Chukotat pyroxenes as compared to those from the Stillwater Complex may be partly due to the effect of a higher temperature of crystallization, since at the time of gabbro crystallization, both Chukotat and Stillwater melts were typical tholeiites and probably were quite similar in bulk composition.

This temperature difference, as inferred both from the clinopyroxene saturation limits and the aluminum contents of similar augites, was likely caused by differing melt volatile contents, greater in the Stillwater and smaller in the Chukotat melts. Both magmas, on producing augites of similar compositions were saturated or almost saturated with plagioclase of labradorite composition, and both melts were at or were very close to the clinopyroxene-orthopyroxene field boundary, and so

no other chemical causes seem possible. If the Stillwater melt contained more dissolved volatiles than the Chukotat, it must have crystallized at great depths, probably greater than five miles.

Direct evidence of high water content is lacking in the exposed Stillwater Complex, but this may be due to a concentration of volatiles near the roof of the crystallizing intrusive. Such volatiles would be expected to either escape upward from the roof or hydrothermally alter the upper zone of the intrusive, now hidden. In either case no visible ramifications would be expected in the lower exposed zone of the thick complex, as long as the dissolved volatile content of the melt was not sufficiently great to cause the crystallization of amphibole before plagioclase, and as long as the volatiles escaped upwards before the temperature was reduced to the point where the lower pyroxenes could be altered to amphiboles.

Summarizing, we can say that the Stillwater Complex generally followed the same trends of crystallization as the Chukotat Sills, namely, the trend followed by melts of high volatile content, i.e. abundant olivine precipitation considerably in excess of the normative content of the liquid, pyroxene crystallization trending towards a stable coprecipitation of roughly equal quantities of augite and hypersthene, and development of oversaturated residual liquids. In the Chukotat Sills, strong fractional crystallization allowed almost maximum olivine accumulation; in the Stillwater Complex, olivine

accumulation was restricted by considerable resorption of
olivine in reaction with the interstitial liquid. In the
Stillwater Complex, a stable augite-hypersthene cotectic
equilibrium was reached through initial bronzite crystalliza-
tion; in the Chukotat Sills, richer in normative diopside than
the Stillwater magma, endiopside and augite formed as the first
pyroxenes, but before cotectic conditions could be reached,
amphibole replaced pyroxene as the major mafic precipitant.

Chapter IV: PETROLOGY OF THE GABBROS OF THE MONTEREGIAN HILLS

1. Introduction: Location and General Geology

Trending slightly south of east from Montreal, Quebec, is an arcuate line of eight conspicuous hills spaced at intervals of about ten miles for a total distance of about 50 miles. These hills represent a suite of Cretaceous[*] intrusives of a strongly subsiliceous character. They are the Monteregian Hills, from west to east: Mt. Royal, Mt. St. Bruno, Mt. St. Hilaire, Mt. Johnson, Rougemont, Mt. Yamaska, Brome Mt., and Shefford Mt. Other intrusive bodies belonging to the Monteregian Hills petrographic province occur at Oka Mt., 20 miles west of Montreal, and at Mt. Megantic, 70 miles east of Shefford Mt. Dikes and sills are numerous in the vicinity of some of the hills, particularly Mt. Royal. Two such minor intrusives, a dike 50 feet in thickness at St. Pie, about two miles north of Mt. Yamaska, and a small stock at Notre Dame de Bon Conseil, 20 miles north of Mt. Yamaska, will be referred to in this study.

Geological mapping and petrographic studies of the rocks of the Monteregian Hills were originally carried out by Dresser (1910), Adams (1913), O'Neill (1914), and Bancroft and Howard (1923). This early work has been summarized by Dresser and Denis (1944).

[*] Fairbairn et al, in press.

The hills range in size from Brome Mt., the largest, about five miles in diameter, to Mt. Johnson, the smallest, about three quarters of a mile in diameter. They are composed of a series of silica-poor igneous rocks ranging in composition from peridotite to nepheline syenite. The five westernmost plutons intrude undisturbed Ordovician strata of the St. Lawrence Lowland area, the easternmost three intrude schistose strata deformed along the western edge of the Appalachian thrust zone. The line of hills is perpendicular to the Appalachian front at the point where the Appalachian trend changes from north to northeast, at the junction of the New England and Gaspe mountain arcs (Wilson, 1954).

The physical conditions of intrusion can be inferred from the field evidence. All the hills, except Shefford and Brome, are circular pipes with vertical contacts. Vertical flow structure parallel to the walls is well displayed on Mt. Royal, Mt. St. Hilaire, Rougemont, and Mt. Johnson (Dresser and Denis, 1944). This structure has been attributed to rapid upwelling of crystallizing magma. Strongly brecciated contacts and the presence of xenoliths of strata of lower stratigraphic horizons than the host intrusive support a theory of explosive injection.

Brome Mt. and Shefford Mt. are believed to be either separate unroofed laccoliths or parts of one large unroofed laccolith (Dresser and Denis, 1944). Sedimentary rocks dip away from the igneous outcrops along the border of both intrusives suggesting a laccolithic shape. Moreover, at one of

the highest points near the centre of Brome Mt., horizontal
sedimentary rocks have been observed overlying plutonic rock.
Upwelling of strata by concordant intrusions is indicative of
shallow intrusion.

Outward dipping ring dikes, shallow structures believed to
result from subsidence along shear cracks radiating from a
magma chamber to the surface, have recently been reported from
the intrusive complex at Oka (Gold, 1962). Diatreme breccia
pipes have also been seen at various points in the St. Lawrence
Lowland in the vicinity of the Monteregian Hills. Perhaps the
most spectacular is exposed at Ste. Helen's Island, opposite
the Montreal harbour. Here a breccia zone almost a mile in
diameter includes chunks of Devonian limestone which is now
completely eroded from the lowlands and is estimated to have
originally lain 3000 feet above the present level of erosion
(Dresser and Denis, 1944). No igneous matrix occurs in this
or in the other breccia pipes, and it seems certain that these
pipes originated from large gas explosions. In one diatreme
breccia pipe northeast of Covey Hill in Chateauguay County,
Quebec, fragments of mixed Ordovician strata have been par-
tially rounded and cemented by water deposited sand, indicating
the pipe was filled with a mixture of large fragments strewn
upwards by a diatreme explosion and abraded during reentry and
fine material deposited from meteoric water.

These structural observations all indicate a very shallow
depth of intrusion for the igneous rocks of the Monteregian

Hills, probably less than a mile, but not likely less than one half mile. Under such conditions, it is safe to say that the quantity of dissolved volatiles in the magma during intrusion was small. The temperature of crystallization might therefore be expected to be relatively high. Extensive contact aureoles have been observed in the strata close to the intrusives, hornfels and marble being developed from shale and limestone, respectively. Grossularite, vesuvianite, diopside, almandite, and cordierite are among the high temperature metamorphic minerals developed. The presence of abundant microperthite and soda orthoclase in the syenites of the hills also indicates a high temperature of crystallization.

There is some evidence that the Monteregian magmas had begun to crystallize prior to or at least during intrusion. Vertical flow banding of dark and light coloured constituents is common. Where two or more igneous rock types are present in considerable quantity within one hill, which is almost always the case, they may grade into one another suggesting differentiation in situ with or without some fractional crystallization before injection, or they may show crosscutting relationships, suggesting two periods of injection. The pyroxene gabbro-essexite-syenite sequence displayed at Mt. Yamaska is an example of a gradational sequence, the crosscutting pyroxenite-nepheline syenite association at Mt. Royal is an example of dual injection.

In the case of multiple injection, the later phases are

generally syenitic, the early phases gabbroic, suggesting
considerable differentiation at depth. Shrinkage of the conduit
during crystallization and cooling might be expected to cause
tension fracture along the frequently brecciated wall zone,
possibly explaining the tendency for the later phases to occur
around the borders of the intrusives.

A mineralogical and petrographic study of selected spec-
imens from the mafic phases of most of the major Monteregian
intrusives and two of the minor intrusives has been carried out
by the writer. 26 thin sections have been examined: 8 from
Mt. Royal, 5 each from Rougemont and Mt. Yamaska, 2 each from
Mt. St. Bruno, Mt. Johnson, and Mt. St. Hilaire, and one each
from the dike at St. Pie and the small stock at N. D, de Bon
Conseil. In addition, 22 pyroxene concentrates have been
analyzed by the rapid silicate techniques, 14 for the 9 major
oxides, and the rest for FeO, MgO, and CaO.

2. Igneous Rocks of the Monteregian Hills

The igneous rocks of the Monteregian Hills can be divided into three groups: (1) calcic gabbros and pyroxenites, (2) essexites and syenodiorites, and (3) soda syenites. The first and second groups have frequently been generally referred to together as essexites (Dresser and Denis, 1944), but in this study, conforming with the general definition of this term, only those mafic rocks containing nepheline or soda orthoclase are termed essexites.

The mafic phases, groups (1) and (2), comprise about 70 percent of the Monteregian igneous rocks now exposed, the syenites making up the remainder. The approximate ratios of mafic rocks to syenite in the hills studied to the nearest ten percent are: Mt. Royal, 80:20, Mt. St. Bruno, 100:0, Mt. St. Hilaire, 60:40, Mt. Johnson, 50:50, Rougemont, 100:0, and Mt. Yamaska, 90:10. According to the breakdown of these mafic phases given by Dresser and Denis (1944), over one half are essexites, only the feldspar lacking or anorthite containing rocks being referred to separately under the terms rougemontite (anorthite gabbro), yamaskite (hornblende pyroxenite), and montrealite (peridotite). If essexites are restricted to actual sodic gabbros containing modal nepheline or soda orthoclase, only a small proportion of the Monteregian gabbros are essexites. It is unfortunate that this term has been misapplied, because actual essexites are characteristically

higher in sodium content than average gabbros, whereas most of the gabbros of the Monteregian Hills are in fact lower in sodium than average gabbros, and are only distinctive by their low silica and high calcium contents (Table 6). The low silica content, of course, will lead to a normative calculation where soda will be represented as nepheline, and this is presumably the reason the term essexite has been invoked. This low silica content, however, is not caused by any alkaline phases, but is due to the low silica nature of the aluminous pyroxenes and amphiboles.

Of 26 thin sections studied by the writer from the mafic rocks of the Monteregian Hills, many of them collected from areas reportedly underlain by essexite (Dresser and Denis, 1944), only two are essexites, the rest being calcic gabbros and related pyroxenites and peridotites. The two essexites came from Mt. Johnson and Mt. St. Bruno, but modal nepheline has also been reported from Mt. Yamaska and Mt. St. Hilaire. It seems unlikely that essexites comprise more than 20 percent of the Monteregian Hills, and probably comprise less, the calcic gabbro group forming the great majority of the Monteregian mafic zones. Judging from the plagioclase composition of the essexites, which is more sodic than that of the gabbros, and the general field relations of gradation from calcic gabbro through essexite to syenite such as is observed on Mt. Yamaska, the essexites likely represent transition phases between the calcic gabbros and the syenites.

Table 6:   Rock Analyses from the Monteregian Hills

	Gabbro[a] Mt. Royal	Gabbro[b] Rougemont	Olivine Gabbro[c] Mt. Yamaska	Essexite[d] Mt. Yamaska
SiO_2	41.55	40.68	39.97	43.91
TiO_2	3.92	2.04	4.05	3.80
Al_2O_3	14.84	19.83	8.68	19.63
Fe_2O_3	6.62	4.68	8.63	4.16
FeO	8.24	6.49	7.99	5.55
MgO	7.83	7.67	10.32	5.20
CaO	14.64	17.64	15.18	9.49
Na_2O	1.93	1.10	1.19	4.49
K_2O	0.25	0.27	0.74	1.51
H_2O	0.19	0.39	1.01	0.64

	Essexite[e] Mt.St.Hilaire	Nepheline[f] Syenite Mt.Royal	Nordmarkite[g] Shefford Mountain	Average[h] Gabbro Daly
SiO_2	49.96	55.90	65.43	48.24
TiO_2	2.40	0.70	0.16	0.97
Al_2O_3	18.83	19.75	16.96	17.88
Fe_2O_3	2.52	1.00	1.55	3.16
FeO	6.64	2.05	1.53	5.95
MgO	3.52	0.59	0.22	7.51
CaO	7.42	3.10	1.36	10.99
Na_2O	5.26	7.25	5.95	2.55
K_2O	2.58	5.61	5.36	0.89
H_2O	0.60	2.00	0.82	1.45

a   Bancroft and Howard, 1923   f   Adams, 1913
b,c O'Neill, 1914   g   Dresser, 1903
c,d Young, 1906   h   Barth, 1952

2.1 Calcic Gabbros and Pyroxenites

This group of plutonic rocks, which comprises over one
half of the Monteregian Hill outcrop, varies in composition from
gabbro through anorthite gabbro to pyroxenite and peridotite.
The major minerals are pyroxene (augite or endiopside),
plagioclase (generally very calcic), titaniferous oxyhornblende,
and olivine; the common accessory minerals are biotite,
titaniferous magnetite, sphene, and apatite. Out of 24 of this
gabbro suite examined in thin section, the approximate average
mineralogical composition is pyroxene, 55 percent, bytownite,
25 percent, oxyhornblende, 10 percent, olivine, 5-10 percent,
and magnetite and sphene, 0-5 percent. The rocks are charac-
teristically coarse grained with very little alteration, and
aside from the occasional rimming of augite or olivine by
oxyhornblende (Plates 8 and 9), no reaction relations can be
seen.

Highly feldspathic gabbros, rare in the Monteregian Hills,
are found only in the laccolith at Brome Mt. and Shefford Mt.
In one zone at Brome Mt., anorthositic gabbro containing 90
percent bytownite occurs (Dresser and Denis, 1944).

Another unusual rock, a hornblende peridotite, occurs in
the small stock at N. D. de Bon Conseil. It is composed of
oxyhornblende, serpentinized olivine, biotite, and pyroxene in
order of abundance. No plagioclase is present. The
oxyhornblende forms large poikilitic crystals enveloping both
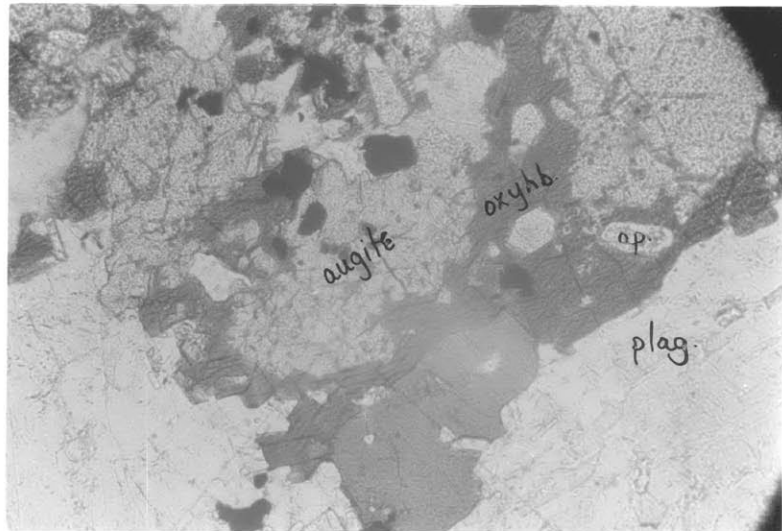
Plate 8: Brown oxyhornblende formed at the expense of
augite
(gabbro, Mt. Johnson, Quebec)
photo length = 4 mm.
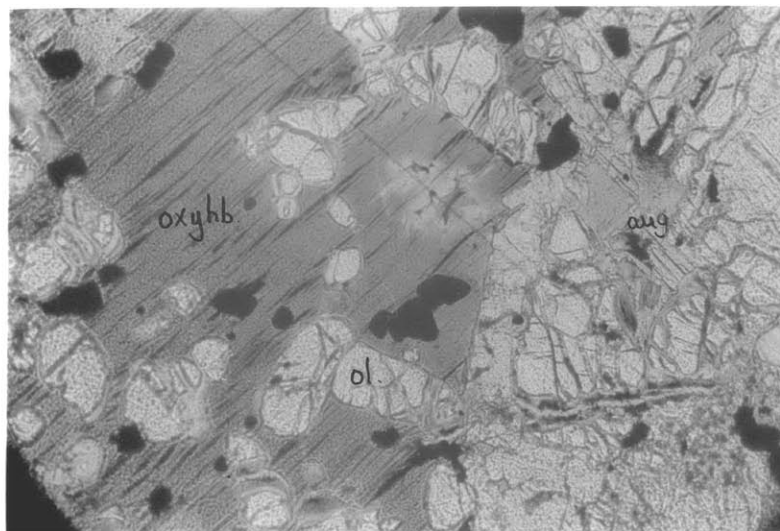
Plate 9: Olivine enclosed in poikilitic oxyhornblende
(hornblende peridotite, Notre Dame de Bon
Conseil, Quebec)
photo length = 4 mm.

olivine and pyroxene, indicating its later formation (Plate 9).
Serpentinization of olivine, rare elsewhere in the Monteregian
peridotites, has occurred here.

An unusual feature of the chemistry of the calcic gabbros
of the Monteregian Hills is their low alkali content. Table 6
shows chemical analyses of three typical calcic gabbros of the
Monteregian Hills, and these can be compared with the average
gabbro composition given by Daly (Barth, 1951, p. 70), and an
analysis of two typical essexites from the Monteregian Hills.
It can be seen that the Monteregian gabbros are lower in
alkalis and in silica than the average gabbro, although the
essexites are, as expected, richer in alkalis. According to
the definition of alkaline rocks given by Shand (Barth, 1951,
p. 203), i.e. alkaline rocks contain minerals in which the
molecular ratio of alkali to silica is not less than 1:4, these
calcic gabbros are not alkaline.

The pyroxenes of these gabbros are augites or endiopsides,
higher in titanium, ferric iron, and aluminum than usual, and
frequently zoned, but otherwise quite normal (pp.   ).
The oxyhornblende, according to the three available analyses
(Table 7) does not qualify as a soda amphibole (Winchell, 1951,
pp. 431-443), but is a titaniferous oxyhornblende intermediate
in composition between the end members hastingsite,
$NaCa_2Mg_4Al_3Si_6O_{22}(OH)_2$, ferrohastingsite, $NaCa_2Fe_4''FeAl_2'''Si_6O_{22}(OH)_2$,
and ferrihastingsite, $NaCa_2Fe_2''(Al,Fe''')_3O_2Si_6Al_2O_{22}$, with
titanium substituting for aluminum and ferric iron. Winchell

Table 7:   Composition of Monteregian Amphiboles

	from Hornblende Gabbro Mt. Royal[a]	from Olivine Gabbro Mt. Royal[a]	from Essexite Mount Johnson[b]
SiO_2	35.65	39.23	38.63
TiO_2	7.99	4.53	5.04
Al_2O_3	11.94	14.38	11.97
Fe_2O_3	5.93	2.92	3.90
FeO	12.04	8.56	11.52
MgO	11.01	13.01	10.20
MnO	0.10	0.65	0.73
CaO	11.21	11.70	12.81
Na_2O	2.33	3.05	3.14
K_2O	0.99	0.98	1.49
H_2O	0.36	0.36	0.33

a   After Bancroft and Howard (1923)

b   After Adams (1913)

classifies such an amphibole as a common and not a soda hornblende, and similarly, the Shand criterion does not qualify this titaniferous mineral as alkaline. This brown oxyhornblende is easily mistaken for the titaniferous soda amphibole barkevikite, because of its yellow-brown pleochroism and relatively high (about 18 degrees) extinction angle. It is higher in extinction angle than pure oxyhornblende because it lies in composition between oxyhornblende and the hastingsite-ferrohastingsite series. In any event, its sodium content is far too low for barkevikite. The low silica content of this mineral, however, is instrumental in giving normative nepheline values to some of the calcic gabbros.

There is therefore no reason to refer to the calcic gabbro suite in the Monteregian Hills as alkaline, and since these rocks make up at least one half of the rocks in the province, references to the Monteregian Hills as a region containing only alkaline rocks are incorrect. Such references are common (see, for example, Dresser and Denis, 1944, p. 457).

Considerable variation occurs in the compositions of the other major gabbro minerals, i.e. olivine and plagioclase. The compositions of olivines determined optically, and those analyses reported in the literature show a variation of from Fo 76 Fa 24 to Fo 62 Fa 38. Plagioclases varied in the sections examined from An 50 to An 93. Some are extensively zoned, with up to 15 percent increases in anorthite content from the borders of grains to their cores.

2.2 Essexites and Syenodiorites

True essexites and nepheline syenodiorites occur on Mt.
Johnson, Mt. Yamaska, Mt. St. Hilaire, and in minor quantity,
on Mt. St. Bruno. The essexites typically contain plagioclase,
soda orthoclase, and pyroxene as the major minerals, with
oxyhornblende, nepheline, biotite, titaniferous magnetite,
sphene, sodalite, and apatite often occurring in small amounts.
The plagioclase was fairly sodic, andesine or soda labradorite,
in the two thin sections of this rock studied by the writer.

On a mineralogical basis, the essexites and syenodiorites
would appear to be transitional between the gabbros and
syenites, and are the most mafic truly alkaline rocks in the
Monteregian Hills. The plagioclase is more sodic than that of
the gabbros, and the single pyroxene analyzed from an essexite
showed a higher sodium content than usual in the gabbro
pyroxenes. More field work is required to determine if the
essexites are transition phases as appears to be the case at
Mt. Yamaska.

Typical essexites from Mt. St. Hilaire and Mt. Yamaska
have been analyzed (Dresser and Denis, 1944), and these analyses
appear in Table 6.

2.3 Soda Syenites

A great variety of soda syenites occur as late

differentiates in the Monteregian Hill province. These can be
divided into two groups: nepheline syenites and nordmarkites.
The nepheline syenites predominate and are present to some
extent in all the Monteregian Hills except Rougemont, which
contains no late differentiate phase, Shefford Mt. and Brome Mt.
Soda orthoclase, nepheline, aegerine augite, soda hornblende,
and sodalite are common major minerals; rutile, garnet, zircon,
and apatite are common accessory minerals.

The syenites of Shefford Mt. and Brome Mt., the eastern of
the eight Monteregian Hills, are nordmarkites. Microperthite is
the only major mineral, but small quantities of hornblende,
augite, biotite, apatite, and rutile are often present. Either
quartz or nepheline may be present (Dresser and Denis, 1944).

Analyses of a typical nepheline syenite and a typical
quartz bearing nordmarkite are listed in Table 6.

3. Differentiation Sequence in the Monteregian Hills

The differentiation displayed in the Monteregian Hills is both highly developed and unusual. The trend of chemical and mineralogical differentiation is illustrated in a simple flow diagram (Fig. 20). Although all the Monteregian plutonic rocks are very low in silica content, all undersaturated with silica except most of the nordmarkites, the behavior of the lime and alkalis is unusual. While the early gabbros are very calcic and very low in alkalis, the late derivatives are very high in alkalis, in particular sodium, and very low in calcium. In other words a differentiation from calcium rich to sodium rich phases is indicated, a differentiation far more pronounced than that found normally in gabbro-granite sequences.

The Monteregian province displays a weakness in the criterion for an alkaline province given by Peacock (1931). This criterion states that a sequence of differentiated igneous rocks is alkaline if the total alkali content is equal to the lime content (weight percent $K_2O + Na_2O = CaO$) in a rock which has a silica content of less than 51 percent. Moreover, if this equality occurs in a rock which has a silica content of less than 45 percent, the province is termed strongly alkaline. Thus the Monteregian province, which is very poor in silica, will qualify as strongly alkaline. This description is valid for the essexites, syenodiorites, and syenites, but the gabbros, which make up over one half the igneous rocks of the province,

Figure 20: <u>Trend of Differentiation of Rocks and Minerals of the Monteregian Hills</u>

CALCIC
GABBRO →ESSEXITE→ SYENO- → SODA
DIORITE SYENITE
(Peridotite, pyroxenite, (Nepheline syenite,
and gabbro) and nordmarkite)

OLIVINE   Chrysolite→Hyalosiderite

PYROXENE   Endiopside → Augite ─────────────────→Aegerine Augite ─────

PLAGIOCLASE   An 90-An 60 ──────→ An 60-An 50 →An 50-An 20──→ An 20-An 0

AMPHIBOLE   ─────── Titaniferous oxyhornblende ────────→ Soda hornblende

IRON ORE   ───────────── Titanomagnetite ───────────────────

TITANIFEROUS   ─── Sphene ──────────   ──────── Rutile ──────
    ACCESSORIES

ALKALI FELDSPAR   ──────────────────────Orthoclase ──────

FELDSPATHOIDS   ────────────────── Nepheline ─────
                          ──────────── Sodalite ─────

are not alkaline; in fact, as we have seen, they contain less
alkalis than the average gabbro.

4. The Pyroxenes of the Monteregian Hills

Clinopyroxene is the most abundant mineral in the gabbros of the Monteregian Hills. Since pyroxenes in general are capable of considerable compositional variation, it is necessary to study in detail the major element concentration in the Monteregian clinopyroxenes before speculating upon the differentiation paths of the Monteregian magmas.

4.1 Chemical Composition in Terms of Hypothetical
Molecules and of Metal Atoms per 6 Oxygens

The chemical and structural formula for clinopyroxenes of the diopside-hedenbergite type can be given as $XY(ZO_3)$, where X represents Ca, Mg, Na, and K, Y represents Mg, Fe^{+2}, Al, Fe^{+3}, and Ti, and Z represents Si and Al.

In the diopside structure, the X position has eight-fold coordination with a metal-oxygen atomic distance of $2.54 \overset{O}{A}$, while the Y position has six-fold coordination with a metal-oxygen atomic distance of $2.10 \overset{O}{A}$ (Warren and Bragg, 1928). The Z position is the standard tetrahedrally coordinated silicon position.

For the purpose of the study of pyroxene phase equilibria, it will prove useful to present the chemical compositions of pyroxenes in terms of various hypothetical molecules or end members of pyroxene solid solution series. To do this,

pyroxene chemical analyses have been subjected to the following treatment:

(1) Oxide weight percents are transformed to mole percents.

(2) Ferric oxide is combined with soda and silica to form acmite, $NaFeSi_2O_6$.

(3) If there is insufficient soda to combine with all the ferric iron to form acmite, the remaining ferric iron is combined provisionally with calcium oxide, alumina, and silica to form calcium ferritschermak's molecule, $CaFeAlSiO_6$.

(4) The remaining sodium oxide, if any, from step 2, is combined with alumina and silica to form jadeite, $NaAlSi_2O_6$.

(5) The remaining alumina from steps 3 and 4 is combined provisionally with calcium oxide and silica to form calcium Tschermak's molecule, $CaAl_2SiO_6$.

(6) The remaining calcium oxide from steps 3 and 5 is combined with silica to form wollastonite, $CaSiO_3$.

(7) Magnesium is combined provisionally with silica to form enstatite, $MgSiO_3$.

(8) Ferrous oxide is combined with silica to form ferrosilite, $FeSiO_3$.

(9) The molecular proportions of Tschermak's molecule, ferritschermak's molecule, wollastonite, and enstatite are now adjusted so that the ratios of magnesium Tschermak's molecule, $MgAl_2SiO_6$, to calcium Tschermak's molecule, and magnesium ferritschermak's molecule, $MgFeAlSiO_6$, to calcium ferritschermak's molecule, are the same as the ratio of the difference of

enstatite and wollastonite to the sum of enstatite and wollastonite.

(10) The molecular proportions of these hypothetical molecules are converted to weight percent of these molecules.

Step 9 allows the molecular ratio of calcium to magnesium, both of which occur in the X-position of the Tschermak's molecules, to be similar to the molecular ratio of calcium to magnesium in the X-position of the actual pyroxene. Iron is not considered because aluminum substitution in pyroxenes, at least in the Monteregian Hills, apparently decreases fairly uniformly as magnesium is replaced by iron in such a way that extrapolation predicts that aluminum substitution would vanish as magnesium disappears in favour of iron (Table 8).

Table 8 shows the results of the chemical analyses of clinopyroxenes from the Monteregian Hills, determined by the rapid silicate method of Shapiro and Brannock (1956), and the results of processing of these analyses according to the above scheme. It is interesting to note, as a possible test of the accuracy of the analyses, that the total of the mole proportions of the hypothetical molecules, which is based on normalization of the oxide moles to mole percents (step 1, p. 169), predicts a value for the total theoretical mole percent of silica. If the analyses are good, the actual mole percent of silica should agree with this theoretical value. In 12 out of 16 of the pyroxenes analyzed by the writer, the agreement is within one percent, in two of the others the discrepancy can

Table 8 - <u>Composition of Monteregian Pyroxenes</u>

Wt. %	Chemical Analyses	MOUNT ROYAL				
		MR 7	MR 8	MR 9	MR 11W	MRT
SiO_2		50.73		49.64		
TiO_2		1.32		1.41		
Al_2O_3		6.91		7.25		
Fe_2O_3		2.23	2.62	2.04	2.07	2.49
FeO		4.57	4.37	5.11	4.83	4.56
FeO^*	total iron as FeO	6.58	6.73	6.95	6.69	6.80
MgO		14.60	13.66	13.58	13.65	13.29
CaO		19.91	20.37	20.93	20.88	20.26
Na_2O		1.10		0.88		
K_2O		0.16		0.17		
	Total	101.53		101.03		

Mole %	sum normalized to	MR 7	MR 9
SiO_2	100 percent	48.45	47.90
TiO_2		0.95	1.02
Al_2O_3		3.89	4.12
Fe_2O_3		0.80	0.74
FeO		3.65	4.12
MgO		20.79	19.54
CaO		20.37	21.64
Na_2O		1.02	0.82
K_2O		0.09	0.09

Table 8 - <u>Composition of Monteregian Pyroxenes</u> (Continued)

Mole %	from chemical analyses	MOUNT ROYAL	
		MR 7	MR 9
SiO_2		48.45	47.90
TiO_2		0.95	1.02
Total		49.40	48.92
Mole %	predicted from		
$SiO_2 + TiO_2$	molecular analyses	49.25	48.94
Wt. %	Molecular Analyses		
$(Na,K)FeSi_2O_6$	Acmite	6.4	5.9
$CaFeAlSiO_6$	Ca-Ferritschermak's mol.	0.0	
$MgFeAlSiO_6$	Mg-Ferritschermak's mol.	0.0	
$(Na,K)AlSi_2O_6$	Jadeite	2.0	1.2
$CaAl_2SiO_6$	Ca-Tschermak's mol.	11.5	13.2
$MgAl_2SiO_6$	Mg-Tschermak's mol.	1.9	1.5
$CaSiO_3$	Wollastonite	34.8	36.6
$MgSiO_3$	Enstatite	34.9	32.3
$FeSiO_3$	Ferrosilite	8.3	9.3
Mole prop.	Wo-En-Fs	42.0-49.1-8.9	43.8-46.2-10.0

Table 8 - Composition of Monteregian Pyroxenes (Continued)

Wt. %	Chemical Analyses	MOUNT ST. BRUNO			STE. PIE	
		BA	BB	BY	St P 1	St P 2
SiO_2			53.06	50.69	48.68	49.69
TiO_2			0.99	1.23	0.90	1.79
Al_2O_3			6.32	4.54	10.09	7.47
Fe_2O_3		1.04	1.38	1.13	1.15	1.95
FeO		4.50	3.57	4.24	3.56	4.60
FeO^*	total iron as FeO	5.44	4.81	5.26	4.60	6.36
MgO		14.65	14.85	15.27	14.22	13.85
CaO		19.52	20.13	21.80	19.47	20.82
Na_2O			0.95	0.49	1.91	0.75
K_2O			0.20	0.06	0.30	0.15
	Total		101.45	99.45	100.28	101.08
Mole %	sum normalized to		BB	BY	St P 1	St P 2
SiO_2	100 percent		50.17	48.33	47.36	47.87
TiO_2			0.70	0.88	0.55	0.58
Al_2O_3			3.52	2.55	5.78	4.24
Fe_2O_3			0.49	0.41	0.42	0.71
FeO			2.82	3.38	2.89	3.71
MgO			20.94	21.71	20.63	19.90
CaO			20.39	22.27	20.29	21.41
Na_2O			1.02	0.82		
K_2O			0.09	0.09		

Table 8 - Composition of Monteregian Pyroxenes (Continued)

		MOUNT ST. BRUNO		STE. PIE	
Mole %	from chemical analyses	BB	BY	St P 1	St P 2
SiO_2		50.17	48.33	47.36	47.87
TiO_2		0.70	0.88	0.65	0.58
Total		50.87	49.21	48.01	48.45
Mole %	predicted from				
$SiO_2 + TiO_2$	molecular analyses	48.03	49.28	51.65	48.22
Wt. %	Molecular Analyses				
$(Na,K)FeSi_2O_6$ Acmite		4.1	3.3	3.2	5.7
$CaFeAlSiO_6$ Ca-Ferritschermak's mol					
$MgFeAlSiO_6$ Mg-Ferritschermak's mol					
$(Na,K)AlSi_2O_6$ Jadeite		3.5	0.5	10.4	0.5
$CaAl_2SiO_6$ Ca-Tschermak's mol.		10.4	8.6	13.1	13.9
$MgAl_2SiO_6$ Mg-Tschermak's mol.		1.4	0.9	2.0	1.8
$CaSiO_3$ Wollastonite		36.9	40.9	31.9	35.8
$MgSiO_3$ Enstatite		37.0	37.9	33.1	33.8
$FeSiO_3$ Ferrosilite		6.7	7.9	6.3	8.5
Mole prop.	Wo-En-Fs	43.2- 49.9- 6.9	44.6- 47.9- 7.5	42.1- 50.6- 7.3	43.5- 47.4- 9.1

Table 8 - Composition of Monteregian Pyroxenes (Continued)

| Wt. % | Chemical Analyses | MT. ST. HILAIRE | | | MOUNT JOHNSON |
		H-1	H-4	H-E	J-A
SiO_2			51.25	50.96	48.97
TiO_2			0.88	1.72	1.63
Al_2O_3			3.29	3.97	5.96
Fe_2O_3		1.66	1.87	1.69	2.26
FeO		9.22	9.02	7.50	5.78
FeO*	total iron as FeO	10.71	10.70	9.02	7.81
MgO		19.27	13.15	12.43	12.41
CaO		19.39	19.81	20.18	20.38
Na_2O			0.78	1.17	1.49
K_2O			0.15	0.28	0.43
	Total		100.20	99.90	99.31
Mole %	sum normalized to				
SiO_2	100 percent		49.39	49.50	48.29
TiO_2			0.64	1.26	1.21
Al_2O_3			1.87	2.27	3.46
Fe_2O_3			0.68	0.62	0.84
FeO			7.27	6.09	4.77
MgO			18.90	18.00	18.25
CaO			20.45	21.00	21.53
Na_2O			0.73	1.10	1.42
K_2O			0.08	0.15	0.23

Table 8 - Composition of Monteregian Pyroxenes (Continued)

Mole %	from chemical analyses	MT. ST. HILAIRE		MOUNT JOHNSON
		H-4	H-E	J-A
SiO_2		49.39	49.50	48.29
TiO_2		0.64	1.26	1.21
Total		50.03	50.76	49.50
Mole %	predicted from			
$SiO_2 + TiO_2$	molecular analyses	49.86	50.09	49.91
Wt. %	Molecular Analyses			
$(Na,K)FeSi_2O_6$	Acmite	5.5	5.0	6.7
$CaFeAlSiO_6$	Ca-Ferritschermak's mol.			
$MgFeAlSiO_6$	Mg-Ferritschermak's mol.			
$(Na,K)AlSi_2O_6$	Jadeite	0.9	4.5	5.7
$CaAl_2SiO_6$	Ca-Tschermak's mol.	5.8	5.7	8.8
$MgAl_2SiO_6$	Mg-Tschermak's mol.	0.7	0.5	1.2
$CaSiO_3$	Wollastonite	38.0	39.3	35.8
$MgSiO_3$	Enstatite	32.5	31.1	31.0
$FeSiO_3$	Ferrosilite	16.6	13.9	10.8
Mole prop.	Wo-En-Fs	42.2- 41.6- 16.2	44.9- 41.1- 14.0	44.1- 44.2- 11.7

Table 8 - Composition of Monteregian Pyroxenes (Continued)

| Wt. % | Chemical Analyses | ROUGEMONT | | | |
		R-1	R-S	R 10	R-U
SiO_2		51.20	46.93	51.05	
TiO_2		1.33	2.29	1.33	
Al_2O_3		4.39	8.12	3.71	
Fe_2O_3		1.36	3.00	1.22	1.74
FeO		6.99	4.17	6.50	5.50
FeO*	total iron as FeO	8.21	6.87	7.60	6.62
MgO		14.24	13.44	14.59	14.77
CaO		20.46	21.78	20.88	21.15
Na_2O		0.51	0.53	0.51	
K_2O		0.09	0.04	0.09	
	Total	100.57	100.30	99.88	
Mole %	sum normalized to				
SiO_2	100 percent	48.84	46.03	48.71	
TiO_2		0.95	1.69	0.95	
Al_2O_3		2.47	4.69	2.09	
Fe_2O_3		0.49	1.11	0.44	
FeO		5.57	3.42	5.18	
MgO		20.25	19.66	20.76	
CaO		20.91	22.88	21.35	
Na_2O		0.47	0.50	0.47	
K_2O		0.05	0.02	0.05	

Table 8 - Composition of Monteregian Pyroxenes (Continued)

Mole %	from chemical analyses	ROUGEMONT		
		R-1	R-S	R 10
SiO_2		48.84	46.03	48.71
TiO_2		0.95	1.69	0.95
Total		49.79	48.92	49.66
Mole %	predicted from			
$SiO_2 + TiO_2$	molecular analyses	48.81	49.22	49.37
Wt. %	Molecular Analyses			
$(Na,K)FeSi_2O_6$	Acmite	4.0	3.9	3.6
$CaFeAlSiO_6$	Ca-Ferritschermak's mol.		4.3	
$MgFeAlSiO_6$	Mg-Ferritschermak's mol.		0.4	
$(Na,K)AlSi_2O_6$	Jadeite	0.2		0.6
$CaAl_2SiO_6$	Ca-Tschermak's mol.	8.1	16.9	6.8
$MgAl_2SiO_6$	Mg-Tschermak's mol.	1.2	1.8	1.2
$CaSiO_3$	Wollastonite	38.4	34.2	39.8
$MgSiO_3$	Enstatite	35.2	31.2	36.0
$FeSiO_3$	Ferrosilite	12.9	7.3	12.0
Mole prop.	Wo-En-Fs	42.4- 45.0- 12.6	44.5- 47.1- 8.4	43.3- 45.2- 11.5

Table 8 - Composition of Monteregian Pyroxenes (Continued)

Wt. %	Chemical Analyses	MT. YAMASKA			BON CONSEIL NDP
		Y-7	Y-D	Y-S	
SiO_2			50.84	50.38	
TiO_2			1.76	1.61	1.94
Al_2O_3		high	4.17	7.25	
Fe_2O_3		4.13	2.30	2.10	2.51
FeO		4.18	7.04	5.00	2.99
FeO[*]	total iron as FeO	7.90	9.11	6.89	5.25
MgO		10.51	12.66	13.50	13.97
CaO		20.45	20.52	20.75	21.20
Na_2O			0.75	0.86	0.79
K_2O			0.15	0.12	0.03
	Total		100.15	101.57	
Mole %	sum normalized to				
SiO_2	100 percent		49.34	48.40	
TiO_2			1.28	1.17	
Al_2O_3			2.39	4.10	
Fe_2O_3			0.84	0.76	
FeO			5.71	4.02	
MgO			18.32	19.34	
CaO			21.34	21.35	
Na_2O			0.71	0.81	
K_2O			0.08	0.06	

Table 8 - Composition of Monteregian Pyroxenes (Continued)

		MT. YAMASKA	
Mole %	from chemical analyses	Y-D	Y-S
SiO_2		49.34	48.40
TiO_2		1.28	1.17
Total		50.62	49.57
Mole %	predicted from		
$SiO_2 + TiO_2$	molecular analyses	48.53	48.19
Wt. %	Molecular Analyses		
$(Na,K)FeSi_2O_6$ Acmite		6.5	6.2
$CaFeAlSiO_6$	Ca-Ferritschermak's mol.	0.4	
$MgFeAlSiO_6$	Mg-Ferritschermak's mol.	0.0	
$(Na,K)AlSi_2O_6$ Jadeite			0.8
$CaAl_2SiO_6$	Ca-Tschermak's mol.	8.5	13.5
$MgAl_2SiO_6$	Mg-Tschermak's mol.	0.8	1.5
$CaSiO_3$	Wollastonite	38.8	35.9
$MgSiO_3$	Enstatite	31.8	32.9
$FeSiO_3$	Ferrosilite	13.2	9.2
Mole prop.	Wo-En-Fs	44.4-42.3-13.3	43.7-46.4-9.9

be accounted for by high silica analyses which are suggested by the high total oxide weight percents (specimens B-B, Y-S, Table 8).

It is noted that titanium oxide is grouped with silica in all these pyroxene calculations, although titanium probably substitutes in the Y-position in the pyroxene structure. This grouping is permissible, as long as chemical considerations are primary, because titanium substitution in the Y-position must be accompanied by equal aluminum substitution in the Z-position in order to maintain electrical neutrality. For example, let us consider titanium substitution in diopside. Such substitution can be represented as introduction of a hypothetical molecule $CaTi(AlAlO_6)$ in solution with $CaMg(SiSiO_6)$. The structural formula $CaTi(AlAlO_6)$, which probably represents the actual titanium and aluminum positions, can be rewritten chemically as $CaAl_2TiO_6$, which is just the Tschermak's molecule with titanium replacing silica. Hence, because of the identical valences, titanium oxide can be grouped for chemical purposes with silica, even though it likely occurs mainly in the Y- and not the Z-position of the diopside structure.

Table 9 shows cation proportions in terms of 6 oxygens (cation numbers) for the analyzed clinopyroxenes, calculated according to the method of Kushiro (1960) and LeBas (1962). The cation number of silicon is subtracted from 2.000 to determine the cation number for the aluminum which substitutes for silicon in the tetrahedral Z position, denoted Al^{iv}. This

assumes that aluminum is the only cation other than silicon in
the Z position. Small quantities of ferric iron and titanium
may also substitute, but these ions are considerably larger
than both silicon and aluminum, and their occurrence in the Z
position is not likely significant in the present discussion
(ionic radii: Si = .39 A, Al = .57 A, Fe^{+3} = .67 A, Ti = .64 A).

The aluminum in the Z position, Al^{iv}, can be subtracted
from the total aluminum to determine the amount of aluminum in
the octahedrally coordinated Y position, denoted by Al^{vi}. The
total of the cation numbers for Al^{vi} and the other metals in
the pyroxene X and Y positions should be equal to the theoret-
ical value, 4.000. All but two of the analyses total within
one percent of this value (Table 9).

The percent of the Z position which is filled by aluminum
determined in this cation analysis, Al^{iv} x 100/ Al^{iv} + Si,
denoted by LeBas as Al_Z, is also listed in Table 9, as is the
percent of total aluminum which is in the Z position. It is
interesting to note that about 60 percent of the aluminum is
in the Z position on the average.

4.2 Significance of Aluminum, Titanium, Ferric Iron, and Sodium

There is a greater concentration of the elements titanium,
ferric iron, sodium, and aluminum in the augites of the
Monteregian Hills than in similar augites from the tholeiitic

Table 9 - Pyroxene Metal Atoms in Terms of 6 Oxygens

		Mt. Royal		Mt. St. Bruno		Ste. Pie		Mt. Johnson
		MR-7	MR-9	B-B	B-Y	St P-1	St P-2	J-A
Z	Si	1.831	1.812	1.873	1.869	1.772	1.806	1.832
	Al^{iv}	0.169	0.188	0.127	0.131	0.228	0.194	0.168
Total Z		2.000	2.000	2.000	2.000	2.000	2.000	2.000
Y	Al^{vi}	0.125	0.124	0.144	0.067	0.204	0.126	0.095
	Ti	0.036	0.039	0.027	0.034	0.024	0.049	0.046
	Fe^{+++}	0.061	0.056	0.038	0.032	0.031	0.054	0.064
	Fe^{++}	0.138	0.156	0.209	0.131	0.108	0.140	0.181
	Mg	0.786	0.739	0.806	0.840	0.772	0.751	0.693
X	Ca	0.770	0.819	0.785	0.861	0.759	0.811	0.817
	Na	0.077	0.062	0.067	0.035	0.135	0.053	0.108
	K	0.007	0.007	0.008	0.002	0.012	0.006	0.017
Total X & Y		2.000	2.002	1.984	2.001	2.045	1.990	2.021
Al_z		8.46	9.41	6.34	6.54	11.42	9.72	8.38
$Al^{iv} - Al^{vi}$		0.044	0.064	-0.017	0.014	0.024	0.068	0.073
$\dfrac{Al^{iv} \times 100}{Al^{iv} + Al^{vi}}$		57.3	57.2	46.8	66.3	52.8	60.8	63.8

Table 9 - Pyroxene Metal Atoms in Terms of 6 Oxygens (Continued)

	Mt. St. Hilaire		Rougemont			Mt. Yamaska	
	H-E	H-4	R-1	R-5	R-10	Y-D	Y-S
Z { Si	1.897	1.910	1.882	1.734	1.889	1.885	1.823
Al^{iv}	0.103	0.090	0.118	0.267	0.111	0.115	0.177
Total Z	2.000	2.000	2.000	2.000	2.000	2.000	2.000
Al^{vi}	0.071	0.055	0.072	0.087	0.051	0.067	0.132
Ti	0.048	0.025	0.037	0.064	0.037	0.049	0.044
Y { Fe^{+++}	0.048	0.053	0.038	0.084	0.034	0.064	0.057
Fe^{++}	0.233	0.281	0.215	0.129	0.201	0.218	0.151
Mg	0.690	0.731	0.780	0.740	0.805	0.700	0.728
Ca	0.805	0.791	0.806	0.862	0.828	0.815	0.804
X { Na	0.084	0.056	0.036	0.038	0.036	0.054	0.061
K	0.011	0.006	0.004	0.002	0.004	0.006	0.004
Total X & Y	1.990	1.998	1.988	2.006	1.996	1.974	1.981
Al_z	5.13	4.49	5.90	13.33	5.55	5.77	8.85
$Al^{iv} - Al^{vi}$	0.032	0.035	0.046	0.180	0.060	0.048	0.045
$\dfrac{Al^{iv} \times 100}{Al^{iv} + Al^{vi}}$	59.0	62.1	62.0	75.4	68.5	63.2	57.3

Stillwater Complex and the Chukotat Sills. The average TiO_2 concentration in the analyzed Monteregian pyroxenes (Table 8) is 1.5 percent which can be compared with 0.3 and 0.4 percents from the tholeiitic Chukotat Sills and Stillwater Complex, (Hess, 1960) respectively. This is not surprising since the Monteregian petrographic province is rich in titanium, sphene or rutile almost always occurring in any rock. The surprising fact is that there is not more titanium in the Monteregian pyroxenes. LeBas (1962) presents analyses on over twenty clinopyroxenes from scattered igneous areas of the peralkaline type. The average TiO_2 content of these pyroxenes is about 4.0 percent, much greater than that of the Monteregian pyroxenes, which were all collected from nepheline normative gabbros of an igneous province which is among the most strongly alkaline according to the alkali-lime index, although the majority of the mafic rocks are merely subsiliceous and not alkaline.

The average ferric oxide concentration of the Monteregian pyroxenes is also considerably greater than that of the Chukotat and Stillwater pyroxenes, 2.0 percent, as opposed to 0.6 and 1.4 percent, respectively. The Monteregian amphiboles, as we have seen (Table 7), display similar high concentrations of ferric oxide. The shallow depths of crystallization of the Monteregian intrusives, probably less than one mile, were perhaps amenable to the development of higher oxygen fugacities in the melt than would normally occur if the melt crystallized

at greater depths. This is not to say that a melt crystal-lizing, say 4000 feet below the surface, is ever in contact with oxidizing solutions of meteoric origin, but rather that the oxygen fugacity could increase through outgassing of a rising magma. If a melt saturated with volatiles under high pressure rises through the crust to shallow depths, outgassing of large quantities of dissolved volatiles occurs. These volatiles, present as a vapour phase, rise through the magma chamber concentrating near the roof. Dissociated hydrogen is the element most likely to escape from the chamber, because of its high mobility. If this occurs, the oxygen fugacity will increase, creating conditions suitable for iron oxidation.

It is also likely that the high temperatures of crystal-lization that characterize shallow intrusives allow freer cation substitution of ferric iron than is usual. The fact that higher temperatures require a greater partial pressure of oxygen to maintain a specific oxidation state than do lower temperatures may cancel this effect, however.

The sodium contents of the analyzed Monteregian clino-pyroxenes is also higher than usual for normal augites, averag-ing 0.9 percent Na_2O in comparison with 0.5 and 0.3 percent in the analyzed clinopyroxenes of the Chukotat Sills and Stillwater Complex. There are two probable reasons for this. Firstly, the oxidized trivalent state of iron in the Y-position of clinopyroxene demands either the introduction of a univalent cation in the X-position (e.g. acmite molecule), or a trivalent

cation in the Z-position (e.g. ferritschermak's molecule) to maintain electrical neutrality. Therefore, considerable quantities of alkalis such as sodium would be expected to accompany ferric iron substitution in pyroxenes as a rule. Secondly, some of the analyzed pyroxene concentrates from the Monteregian Hills have been separated from advanced sodic differentiates approaching syenodiorite in composition. An example is the pyroxene from specimen J-A, a nepheline syenodiorite from Mt. Johnson, which presumably crystallized from a much more sodic melt than the early formed pyroxenes of the alkali-poor calcic gabbros. Such sodic augites, while they do not approach aegerine-augite in alkali content, nevertheless are rich enough in soda (about 1.5 percent) to raise the average significantly.

The average aluminum oxide content of the analyzed Monteregian pyroxenes is 6.0 percent, but the deviation from this mean is great, values ranging from 3.3 percent in a St. Hilaire gabbro to 10.1 percent in a gabbro dike at St. Pie. The average Al_2O_3 content of clinopyroxenes analyzed from the Stillwater Complex is 2.8 percent (Hess, 1960), while that of the two Chukotat pyroxenes analyzed for aluminum is 5.9 percent. Obviously, the extent of aluminum substitution in clinopyroxene is a function of the bulk composition of the melt from which the pyroxene separates. Thus, from highly aluminous melts such as those which precipitate almost pure anorthite, aluminous pyroxenes are expected. Specimen R-5, a calcic gabbro from Rougemont, shows the most calcic (and therefore aluminous)

plagioclase observed by the writer in rocks from the Monteregian province, an anorthite of composition An 93. The coexisting pyroxene shows the greatest Tschermak's molecule content of all the Monteregian pyroxenes, 23.4 percent by weight (Table 8), which can be compared with the value of 27.5 percent found in diopside coexisting with anorthite in the lowest silica two phase equilibrium assemblage of these minerals occurring at $1125^{\circ}C$ (Schairer and Hytonen, 1961).

From a study of the analyses, the extent of aluminum substitution can be seen to be a function of stage of magmatic differentiation, which may reflect a dependence upon temperature. In every case where the Al_2O_3 concentration varies within the pyroxenes of a single intrusive by more than five percent from the mean, the highest aluminum pyroxenes are found to have the lowest ferrous iron to magnesium oxide ratios (Table 8). Since the $FeO/(FeO + MgO)$ ratio is one of the most reliable indicators of the position of a pyroxene in a sequence of differentiation, and always increases with decreasing temperature and progressive crystallization for pyroxenes separating from an igneous body of fixed bulk composition, it appears that aluminum substitution at least in the Monteregian pyroxenes has decreased in extent with differentiation. Whether this decrease was mainly due to the increase in silica which accompanied differentiation, or whether it was primarily due to decreasing temperature is not known.

Aluminum enters into both the Y and Z positions in the

Monteregian pyroxenes, about 40 percent entering the former, on the average, and 60 percent entering the latter position. The Y position is generally occupied by magnesium, which is a larger ion than aluminum, while silicon, the major Z position cation, is smaller than aluminum (ionic radii: Mg = .78 A, Al = .57 A, Si = .39 A). The amount of aluminum substituting for silicon is largely determined by the bulk composition of the melt at crystallization, low silica and high alumina obviously favouring the substitution. As long as the quantity of aluminum entering is relatively small, substitution into both Y and Z positions would be expected to be favoured by high temperatures, since the entropy of mixing will increase with limited substitution.

The data of Table 9 show that the quantity of aluminum substituting for silicon in the Z position decreases with progressive differentiation. Al_Z, the percent of the tetrahedral Z positions filled by aluminum, is seen to decrease with increasing $Fe^{2+}/(Fe^{2+} + Mg)$, an index of differentiation and decreasing temperature, in every intrusive where the aluminum contents of the analyzed pyroxenes show a variation of over five percent.

With aluminum substituting for silicon, trivalent or quadrivalent cations must enter into the Y position to maintain electrical neutrality. LeBas (1962) has shown that an average of over 90 percent of the aluminum in pyroxenes from mafic rocks of peralkaline provinces enters the Z position. Titanium

appears to be the cation which generally contributes the required additional charge in the Y position. Verhoogan (1962) has recognized the importance of titanium as a balance for aluminum preference of the Z position, but also pointed out that titanium would not be available for large scale substitution in pyroxenes under conditions of low partial pressures of oxygen, where it would combine with ferrous iron to form the oxide ilmenite. As we have seen, the oxygen pressure in the Monteregian magmas was likely high, allowing titanium to enter silicate phases. We have also noted, however, that the TiO_2 contents of the Monteregian pyroxenes average only 1.5 percent, very small in comparison to those of the pyroxene of other subsiliceous provinces classified as peralkaline by LeBas, which average about 4.0 percent. The reason for the lack of titanium concentration in the Monteregian pyroxenes is that two other phases, sphene and oxyhornblende, are frequently found coexisting with clinopyroxene. Sphene, $CaTiSiO_5$, is extremely widespread in the Monteregian gabbros, and is often present in quantities exceeding five percent of the rock. Oxyhornblende, the ubiquitous amphibole of the Monteregian gabbros, often contains over five percent of TiO_2. Perhaps the high CaO content of the gabbro magmas aided in the development of sphene, which, along with oxyhornblende, have acted as sinks for titanium. These sinks have prevented titanium from entering the pyroxene phase in large amounts, despite the high average TiO_2 content of the Monteregian gabbros, over three percent

(Table 6).

The tendency for titanium to enter sphene and amphibole
in preference to pyroxene requires the entrance of another high
valence metal ion as the major substitute for magnesium to
balance the substitution of aluminum for silicon. From the
cation proportions of Table 9, it is seen that this metal ion
is aluminum itself. Indeed, the cation numbers of aluminum in
the Y position, Al^{vi}, are almost equal to those in the Z
position, Al^{iv}, the ratio $Al^{iv}/(Al^{iv} + Al^{vi})$ averaging about
0.6. It is not surprising that aluminum will enter the Y
position to balance that in the Z position if the better fitting
ion titanium is not available. This is obviously what happens
in the laboratory where diopside coexisting with anorthite at
liquidus temperatures in the pseudobinary system diopside-
anorthite contains considerable Tschermak's molecule, $CaAl_2SiO_6$.

The about equal substitution of aluminum in both the Y and
Z positions in the Monteregian pyroxenes contrasts sharply with
the general tendancy in the pyroxenes of critically undersat-
urated rocks for aluminum to enter only the Z position with
$Al^{iv}/(Al^{iv} + Al^{vi})$ values greater than 0.9 (LeBas, 1962). This
difference is likely entirely due to the tendency in the
Monteregian Hills for titanium to occur in sphene and amphibole
in favour of the pyroxene Y position. Caution must therefore
be exercised in attempting to use the ratio $Al^{iv}/(Al^{iv} + Al^{vi})$
in pyroxenes as an index of petrologic parentage. Whereas
LeBas states that the pyroxenes of normal, ordinary alkaline,

and peralkaline igneous provinces average a ratio of 0.7, 0.9, and over 0.95, respectively, the Monteregian ratio is smaller than all of these, even though the Monteregian petrographic province, under the classification used by LeBas, would be considered peralkaline.

The index, Al_Z, the percent of the pyroxene Z position filled by aluminum, is also susceptible to anomalous behavior in pyroxenes from undersaturated rocks where titanium is entering predominately into phases other than pyroxene, and hence its use as an indicator of petrological parentage is subject to some doubt. LeBas gives an average value of about 15 for Al_Z in pyroxenes from mafic peralkaline rocks, with a variation of from 10 to 20. In the Monteregian pyroxenes, the average Al_Z value is only 7.8, even though their total Al_2O_3 contents are similar to those of the pyroxenes of other critically under-saturated provinces, averaging 6.0 percent as compared with the average of 6.7 given by LeBas for his survey of the pyroxenes of peralkaline provinces.

There is considerable titanium substitution in the Monteregian pyroxenes, even though much less than in the pyroxenes of similar rocks from other areas, and therefore, a linear relation should exist between titanium content of pyroxenes and excess aluminum in the Z over the Y position. Considerable scatter would be expected because of the presence of varying amounts of other non-divalent cations such as ferric iron, sodium, and potassium, as well as minor ferric iron
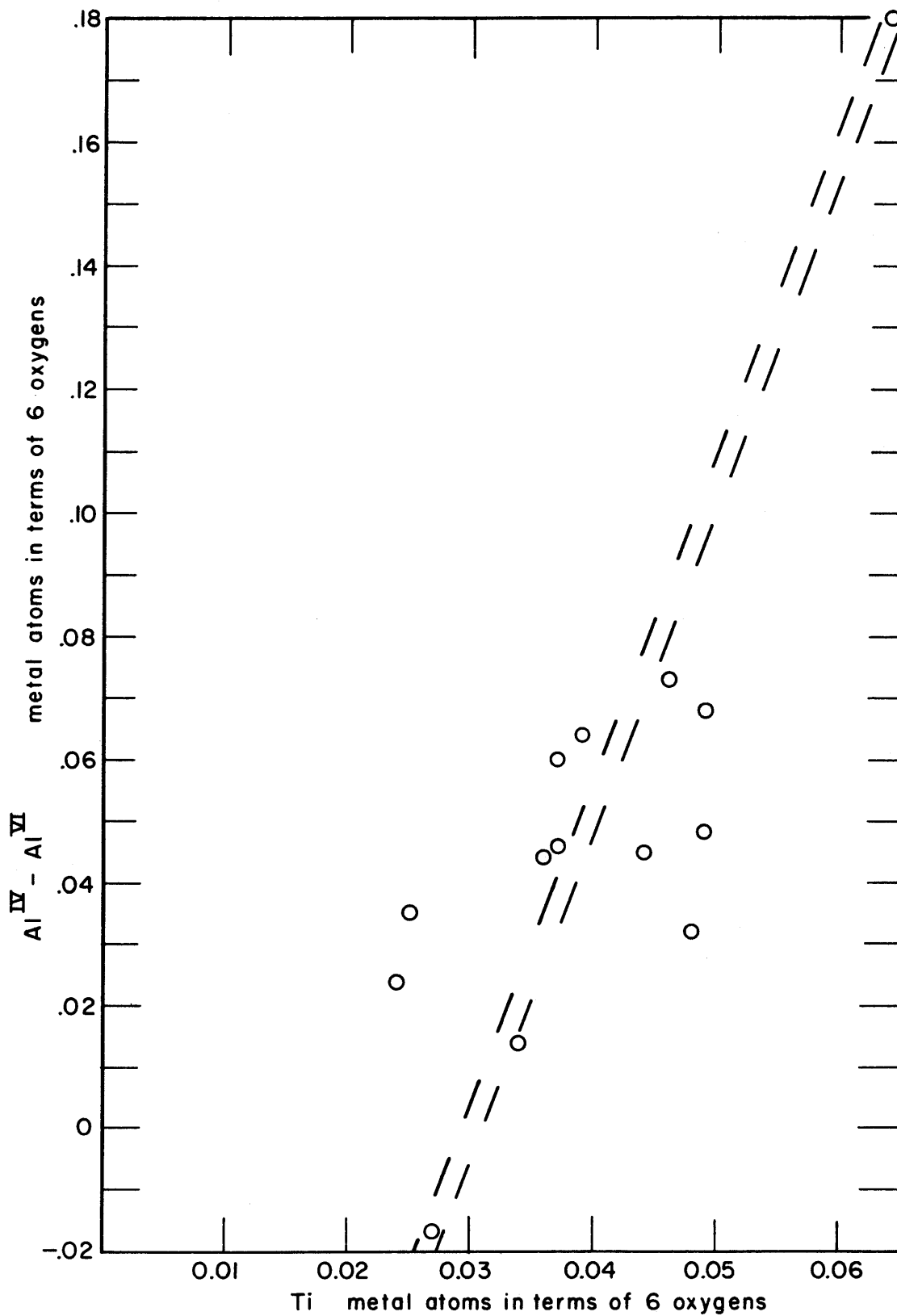
FIG. 21   RELATION BETWEEN TITANIUM AND EXCESS TETRA-
HEDRAL OVER OCTAHEDRAL ALUMINUM IN MONTER-
EGIAN CLINOPYROXENES.

substitution for silicon. Fig. 21 shows such a relationship among the 14 Monteregian pyroxenes on which complete analyses were performed.

4.3 Chemical Trend of Crystallization

The compositions of the Monteregian clinopyroxenes are plotted in Fig. 22, in terms of their molar proportions of calcium oxide, magnesium oxide, and ferrous oxide. This plot can be compared with Fig. 23, where the proportions of the hypothetical molecules wollastonite, enstatite, and ferrosilite calculated according to the steps outlined on p. 169 are used as coordinates. A reduction of the calcium-magnesium scatter in the hypothetical molecule plot is due to the fact that this diagram takes into consideration the large scale substitution of aluminum for magnesium in some of the pyroxenes, and makes allowance for the increase in the ratio of calcium to magnesium caused by this substitution. By removing calcium as Tschermak's molecule in accordance with this substitution, the proportions of wollastonite, enstatite, and ferrosilite components in pyroxenes of varying alumina content can be effectively compared.

The range of composition of the Monteregian clinopyroxenes shown in Fig. 23 is from endiopside to augite. Pyroxenes from rocks of the same intrusion can be seen to generally parallel in composition the trend of scatter of the pyroxenes of the whole province. The trend of crystallization from iron poor
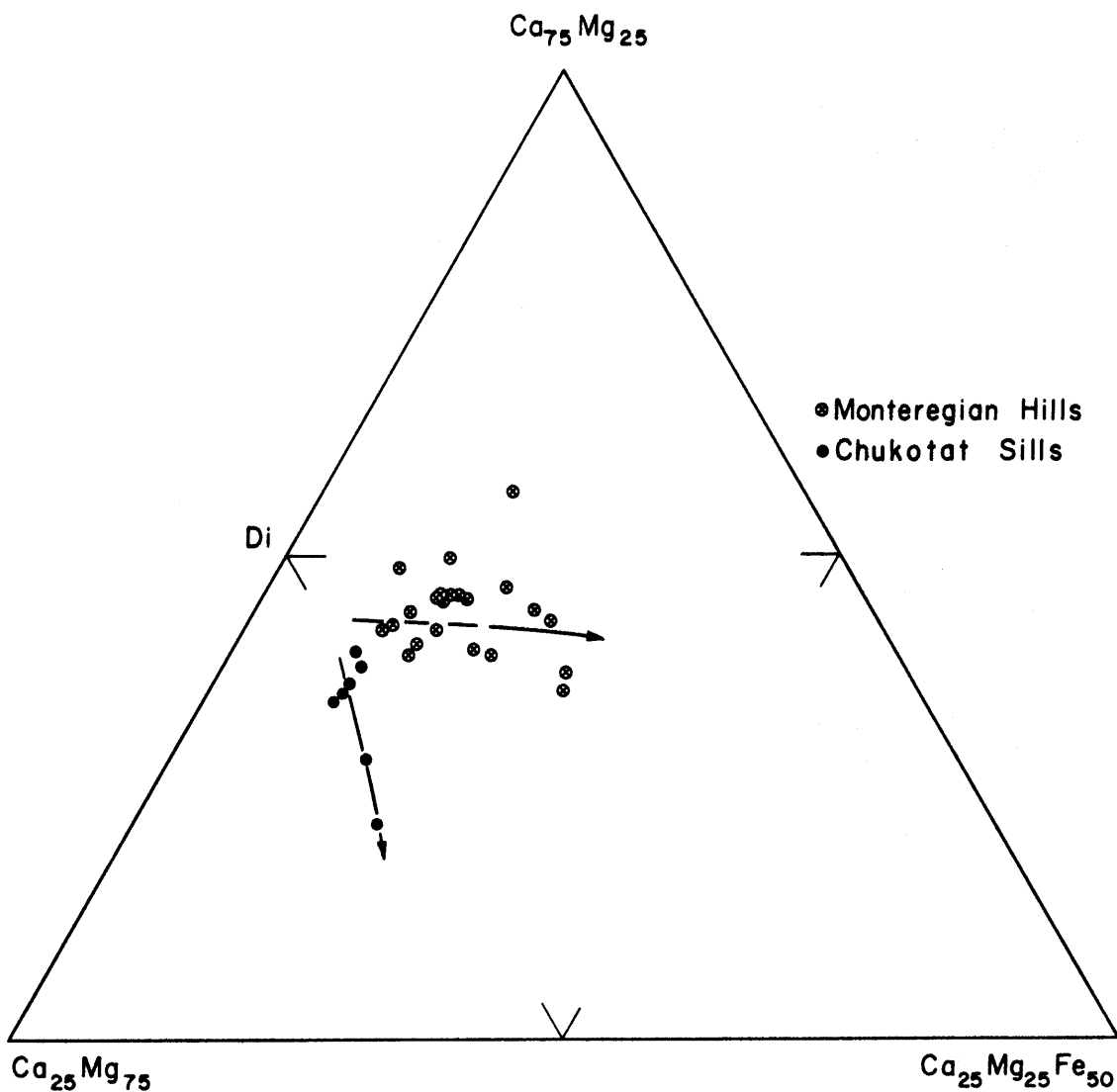
FIG. 22   COMPOSITION OF CLINOPYROXENES OF THE MONTEREGIAN
HILLS AND CHUKOTAT SILLS IN TERMS OF MOLE PROPORTIONS
OF CaO, MgO, AND FeO.
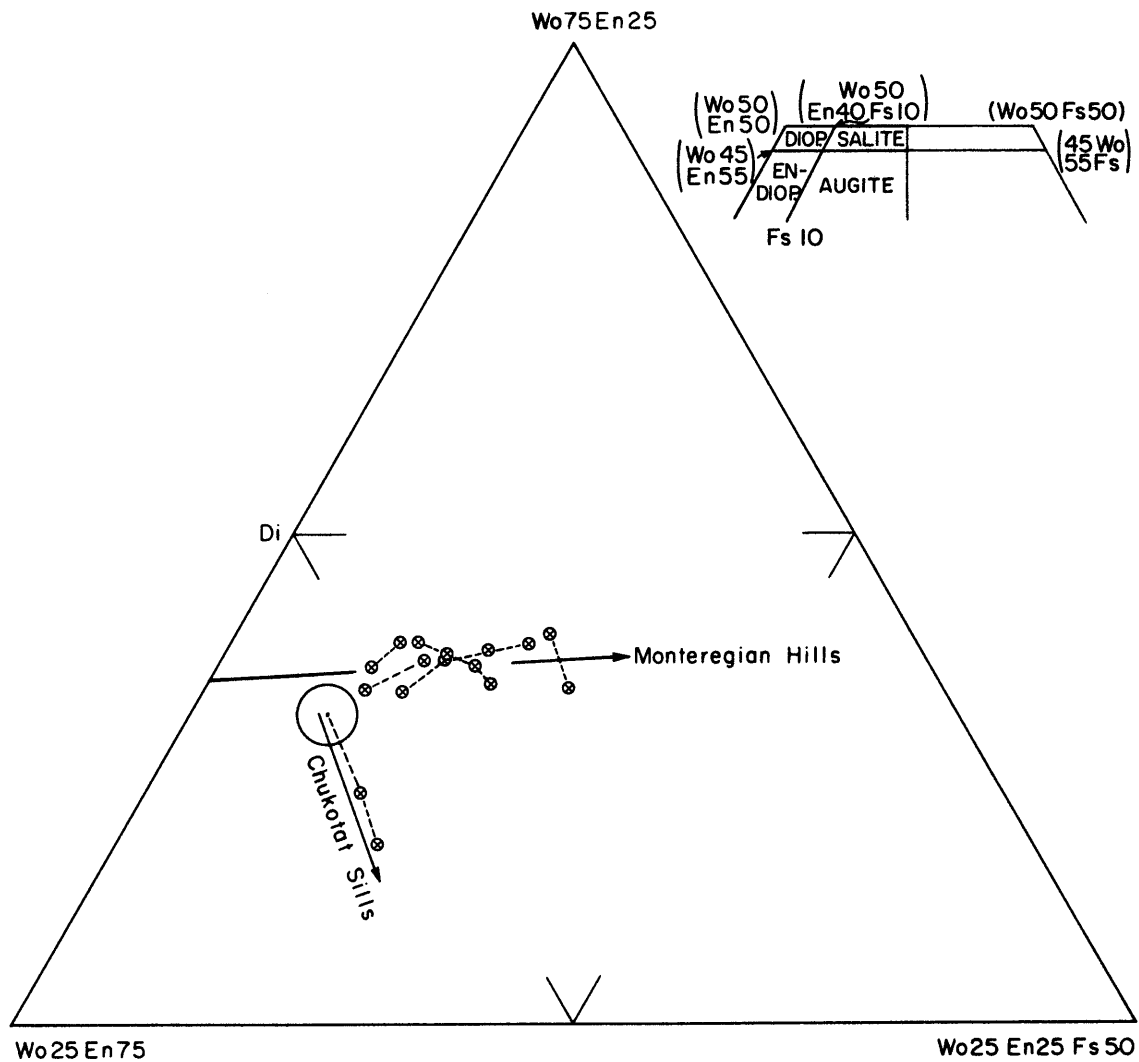
FIG. 23 COMPOSITION AND TREND OF CRYSTALLIZATION OF
PYROXENES OF MONTEREGIAN HILLS AND CHUKOTAT
SILLS IN TERMS OF MOLE PROPORTIONS OF $CaSiO_3$,
$MgSiO_3$, AND $FeSiO_3$.

Mole percents of $CaSiO_3$, $MgSiO_3$, and $FeSiO_3$ are calculated
according to outlined procedure (p. 169).

Dotted lines join pyroxenes of the same intrusive.

Large circle represents probable composition of pyroxenes
of Chukotat peridotites which were not analyzed completely.

species to species richer in iron is seen to involve no appreciable change in the ratio of wollastonite to enstatite components. This differs considerably from the type of pyroxene differentiation displayed in the Chukotat Sills, where increasing iron concentrations are accompanied by decreases in calcium content (see Fig. 23 for comparison of crystallization trends).

An interesting opportunity for studying the changing clinopyroxene composition with differentiation in the Monteregian Hill magmas is presented in a dike at St. Pie. Large phenocrysts of endiopside averaging just less than a centimeter in diameter are rimmed in optical continuity with endiopside of a different composition (Plate 10). Furthermore, endiopside found in the ground mass is similar optically to the rim zone of the phenocrysts. The main phenocryst pyroxene and associated olivine phenocrysts presumably crystallized at depth and were intruded with a later liquid differentiate from which the second pyroxene crystallized. The second pyroxene is richer in ferrous iron than the phenocryst pyroxene indicating its later position in the differentiated sequence. It is also brown in hand specimen in sharp contrast to the green phenocrysts. Chemical analyses on separated concentrates of these pyroxenes indicate the later pyroxene is richer in ferric as well as ferrous iron, richer in calcium and titanium, but poorer in magnesium, aluminum, sodium, and potassium than the original pyroxene. The higher ferrous iron and lower aluminum contents are expected with temperature lowering and progressive
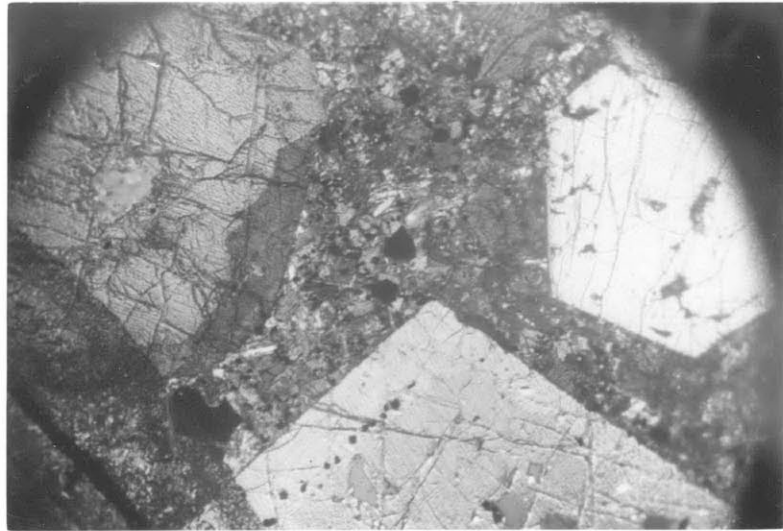
Plate 10: Phenocrysts of green endiopside rimmed by
         brown pyroxene of a slightly different
         composition

    (gabbro dike, St. Pie, Quebec; phenocryst
     rims and groundmass pyroxene are similar)

    cross nicols, photo length = 8 mm.

differentiation, and the higher ferric iron content of the
second pyroxene could be due to its crystallization at much
shallower depths than the phenocryst pyroxene. The increase
in calcium to magnesium ratio with differentiation is not
large, and is not observed in any of the other intrusives.
The decrease in sodium content shown by the later phase is
puzzling, particularly since there is evidence that the sodium
contents of the Monteregian pyroxenes generally increase with
differentiation. If one examines the breakdown of the ground-
mass pyroxene into its hypothetical molecule components, however,
it is seen that the sodium is present with aluminum as jadeite
in solid solution and not with ferric iron as acmite, which is
usually the case with the high sodic Monteregian pyroxenes
(Table 8). The reason for the phenocryst pyroxene being so
rich in jadeitic component, 10.4 percent, is not known, but
there presumably was more sodium in the gabbroic magma from
which the phenocrysts separated than in the typical parent
magmas of most of the Monteregian intrusions.

The behavior of aluminum and titanium in these two
pyroxenes is revealing. The total aluminum content decreases
from the phenocryst to the groundmass, and this is largely due
to a sharp drop, almost 40 percent, in the octahedral aluminum,
Al^{vi} (Table 9). Perhaps aluminum in the Y position is more
sensitive to temperature changes than that in the Z position,
which only decreases by 15 percent from phenocryst to ground-
mass. In any event, the excess aluminum in the Z over the Y

position, $Al^{iv} - Al^{vi}$, is much larger in the groundmass
pyroxene than in the phenocryst, 0.068 atoms per 6 oxygens
compared to 0.024. The titanium content, as expected from
this aluminum behavior, is greater in the groundmass pyroxene,
0.049 atoms per 6 oxygens, than in the phenocrysts, 0.024. In
fact, this titanium increase from phenocryst to groundmass
almost exactly balances, as far as charge is concerned, the
added loss of aluminum in the Y position over that in the Z
position.

4.4 Olivine-Pyroxene Relations

Although olivines are not critical in affecting the course
of differentiation in the Monteregian Hills, it is interesting
to compare their compositional variation with that of coexist-
ing pyroxenes. The compositions of three olivines from
Rougemont, Mt. Royal and Mt. St. Bruno, with the composition of
coexisting clinopyroxenes are shown in Table 10 in comparison
with the compositions of olivines associated with clinopyroxenes
of quite similar composition from the Stillwater Complex.

The variation in the Monteregian olivines is greater than
that in the Stillwater olivines, for a given composition range
of associated clinopyroxenes, 14 percent fayalite variation in
the former group and only 9 percent in the latter.

The more magnesian nature of the Stillwater olivines over
those of the Monteregian Hills, with respect to their coexisting

Table 10:   Compositions of Coexisting Olivines and Clinopyroxenes from the
Monteregian Hills Compared with those of the Stillwater Complex

	Stillwater Complex			Monteregian Hills		
Clinopyroxene[a]	40-53-7	41-51-8	41-48-11	46-47-7	47-48-8	45-44-11
Olivine[b]	86-14	82-18	77-23	76-24	72-28	62-38

a- clinopyroxene compositions in terms of mole proportions of CaO, MgO, and FeO

b- olivine compositions in terms of mole proportions of forsterite and fayalite

(Stillwater analyses after Hess, 1960)

clinopyroxenes, might be explained, at least in part, by the
fact that the Stillwater olivines separated from the melt
earlier than the clinopyroxenes, and were not in equilibrium
with the more iron rich melt at the time of clinopyroxene
crystallization. Evidence for this disequilibrium is textural.
Reaction rims or poikilitic crystals of orthopyroxene are
found surrounding olivine in both the ultramafic and anorthosite
zones, the only zones in which olivine occurs. The clino-
pyroxenes of these olivine bearing rocks have separated after
the initial orthopyroxene crystallization, and are either found
in fine grained clots unassociated with olivine (ultramafic
zone), or as separate grains removed from olivine by serpentine
or orthopyroxene rims (anorthosite zone) (Hess, 1960).

In the olivine bearing rocks of the Monteregian Hills, on
the other hand, olivine and endiopside or augite grains occur
side by side, and appear to have coprecipitated in cotectic
fashion from a single liquid.

5. Course of Crystallization of the Monteregian Magmas

5.1 The Calcic Basalt System

The major aim of this study is to describe the effect of
the crystallization of the early minerals, mainly pyroxenes
and plagioclase, on the course of differentiation of the
Monteregian magmas. The main minerals of the calcic gabbro
suite, can, to a large degree, be represented within the iron
free compositional tetrahedron $CaAl_2SiO_6$-Mg_2SiO_4-$CaMgSiO_4$-SiO_2.
(Fig. 24). In fact, except for the effects of iron and sodium,
which are only of secondary importance in the early mineral
phases of the Monteregian Hills, crystallization trends pre-
dicted from the phase equilibria in this pseudoquaternary
system (monticellite melts incongruently) would apply directly
to the natural magmas of the Monteregian Hills. Even
oxyhornblende, probably the latest major phase to crystallize
in the gabbros, can be crudely represented in the tetrahedron
by ignoring the 'molecules' $NaAlSiO_4$ and H_2O in the 'molecular'
breakdown of the hastingsite formula $NaCa_2Mg_4Al_3Si_6O_{22}(OH)_2$ to
$NaAlSiO_4 \cdot H_2O \cdot 3MgSiO_3 \cdot CaMgSiO_4 \cdot CaAl_2SiO_6$.

It is convenient to project the liquidus phase relations
in the tetrahedron from $CaAl_2Si_2O_8$ onto the face Mg_2SiO_4-
$CaMgSiO_4$-SiO_2 to reduce the graphical representation to two
dimensions. Fig. 25 represents this projection under the
conditions (i) no anorthite in liquid, and (ii) melt saturated
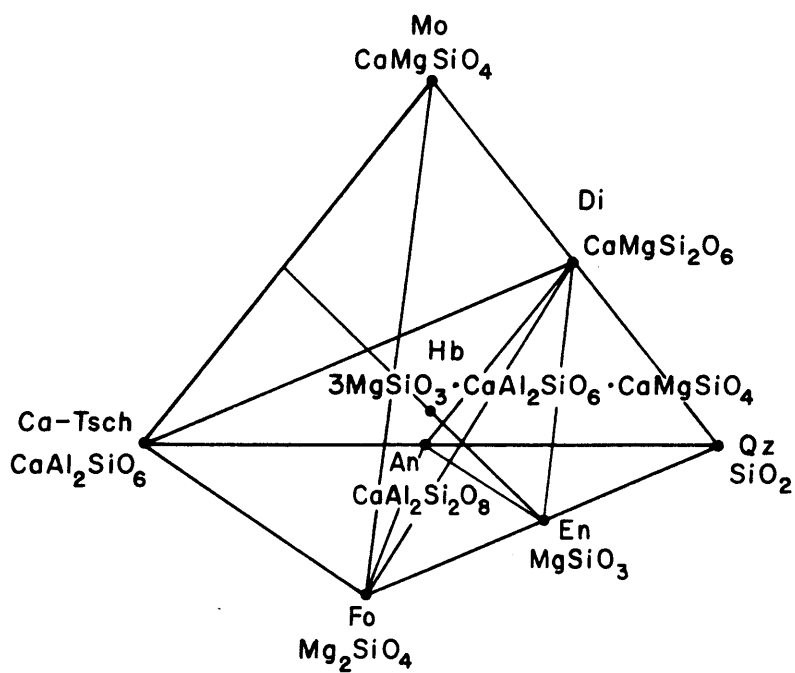
FIG. 24   THE CALCIC BASALT SYSTEM

with anorthite. Since anorthite is essentially stochiometric
if there is no sodium in the system, it is permissible to
project liquidus relations under conditions of melt saturation
with anorthite onto the surface Mg_2SiO_4-$CaMgSiO_4$-SiO_2.

In Fig. 25 (i), that of Bowen (1914), it can be seen that
under conditions of ideal fractional crystallization, any melt
whose composition lies within the area ABCD will yield a
siliceous residua. On the other hand, any melt whose composi-
tion lies within the area ABCJ will yield a melt which is
critically unsaturated with respect to silica, i.e. a melt
which will precipitate undersaturated minerals aside from
olivine, for example, melilite. The lines AB and BC, from
forsterite to the intersection of the forsterite field boundary
and the pyroxene composition line at B, and from B to diopside,
therefore represent a thermal barrier which separates melts
which will differentiate towards silica from those which will
differentiate away from silica. Yoder and Tilley (1961) have
recognized the general thermal barrier forsterite-albite-
anorthite-clinopyroxene, and in their simple basalt system,
$NaAlSiO_4$-Mg_2SiO_4-$CaMgSi_2O_6$-SiO_2, the join forsterite-albite-
diopsidic pyroxene represents this barrier, analogous to the
join forsterite-endiopside B-diopside of Fig. 25 (i).

The effect of anorthite saturation on this thermal barrier
is shown in Fig. 25 (ii). Firstly, as we have seen (pp. 70-72),
anorthite saturation produces a small cotectic valley on the
diopside side of the central portion of the pyroxene liquidus

K - point of change from odd field boundary to even cotectic

L - intersection of cotectic and pyroxene trough
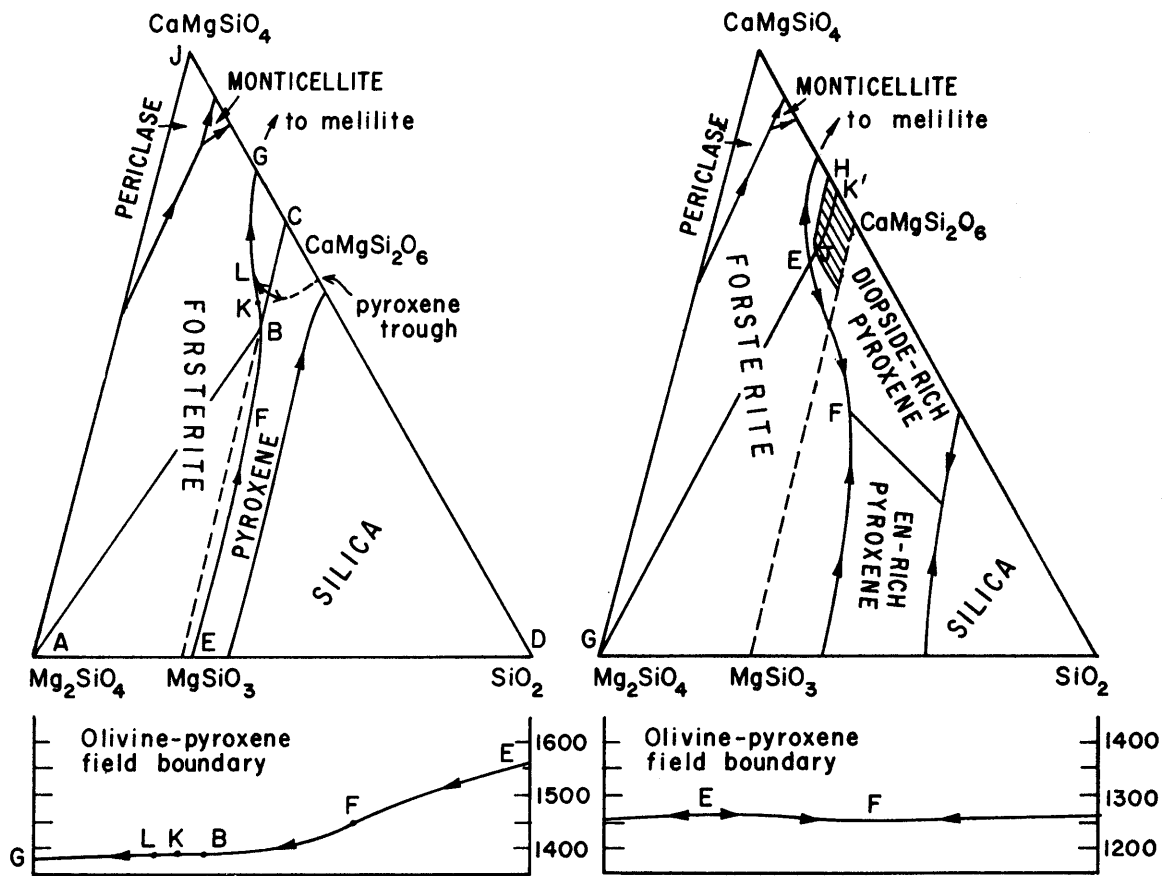
FIG. 25 (i) SYSTEM $CaMgSiO_4$-Mg_2SiO_4-SiO_2

Liquidus relations after Bowen (1914) and Ricker and Osborn (1954).

(ii) SYSTEM $CaMgSiO_4$-Mg_2SiO_4-SiO_2-$CaAl_2Si_2O_8$

Liquidus relations saturated with anorthite and projected through anorthite.

Data after Andersen, 1915, Schairer and Hytonen, 1961, Osborn and Tait, 1952.
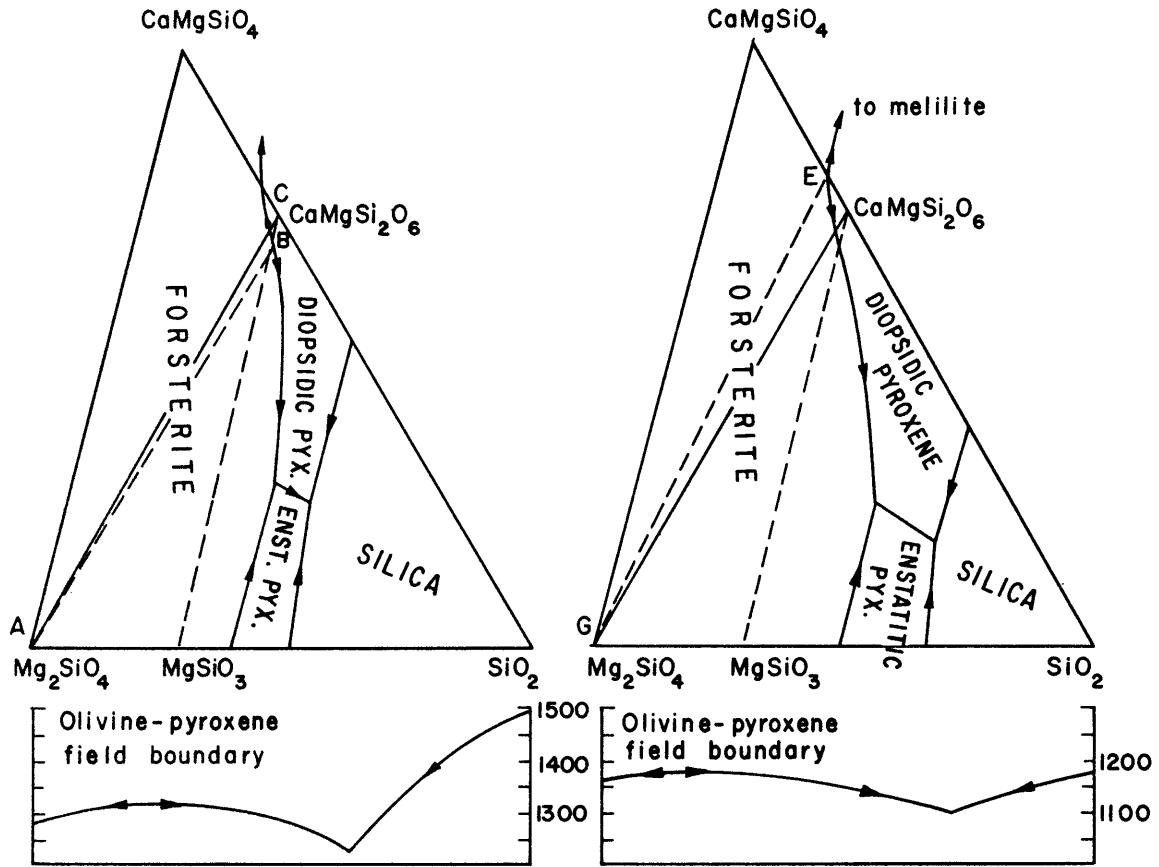
FIG. 26 (i)   SYSTEM $CaMgSiO_4$-SiO_2-H_2O-Mg_2SiO_4

Schematic liquidus relations under conditions of steam
saturation at P = about 5 kilobars, projected through H_2O .

(ii)   SYSTEM $CaMgSiO_4$-SiO_2-$CaAl_2Si_2O_8$-H_2O-Mg_2SiO_4

Schematic liquidus relations under conditions of anorthite and
steam saturation at P = about 5 kbars, projected through H_2O
and anorthite.

surface. This reverses the slope of the olivine-pyroxene field boundary from the ternary univariant point F at the intersection of the pyroxene and olivine-pyroxene field boundaries, to the thermal barrier on the olivine-pyroxene field boundary at some composition E. E thus represents the intersection of the olivine-pyroxene field boundary and the coplanar equilibrium pyroxene J - liquid E - forsterite-anorthite. The clinopyroxene H, represents diopside with 28 percent of dissolved Ca-Tschermak's molecule, $CaAl_2SiO_6$, the maximum Tschermak's concentration observed by Hytonen and Schairer (1961) in diopside in equilibrium with anorthite at $1135^{\circ}C$. The actual maximum concentration may be slightly higher at the liquidus temperatures in this portion of olivine-pyroxene field boundary, in which case the thermal barrier will be slightly farther from silica than is shown. In any event, the shift in the thermal barrier due to anorthite in the magma is considerable, and the region of compositions capable of differentiating to a quartz rich residua is increased by extensive aluminum substitution in clinopyroxenes.

Fig. 26 represents the effect of the addition of dissolved volatile material to the melts of Fig. 25. Though necessarily schematic, the general changes brought about would be expected under conditions of, say, steam saturation at pressures of about five kilobars. Fig. 26 (i), the feldspar free system, shows a thermal barrier ABC which has been shifted away from silica by the expansion of the olivine liquidus area. Fig. 26

(11), the anorthite saturated system, shows a thermal barrier GE from forsterite to the intersection of the olivine-pyroxene field boundary and the diopside-Tschermak's molecule solid solution line. The exact composition of this intersection point is not known for any amount of lowering of liquidus temperatures due to volatiles, of course, because the amount and type of expansion of the forsterite field, particularly in the calcium rich areas of the diagram, is not known.

In any event, the effect of addition of volatiles under high pressures on the calcic basalt system is to restrict the region of compositions which will differentiate away from silica towards critically unsaturated residua. In this respect, the addition of volatiles to mafic magmas produces similar results to the addition of anorthite.

In Fig. 27, the thermal barriers of Figs. 25 and 26 are plotted on a single diagram. The area ABCEHA, bounded by the most extreme thermal barrier segments, represents mafic compositions in which fractional crystallization may produce either oversaturated or critically undersaturated residua, depending on the amounts of dissolved anorthite and volatiles in the melt. Though necessarily only an approximation in size and shape because of incomplete experimental data, this area is obviously of some petrological importance, and can be termed the "zone of residual uncertainty."

The addition of the elements iron and sodium to the calcic basalt system will not affect the importance of the zone of
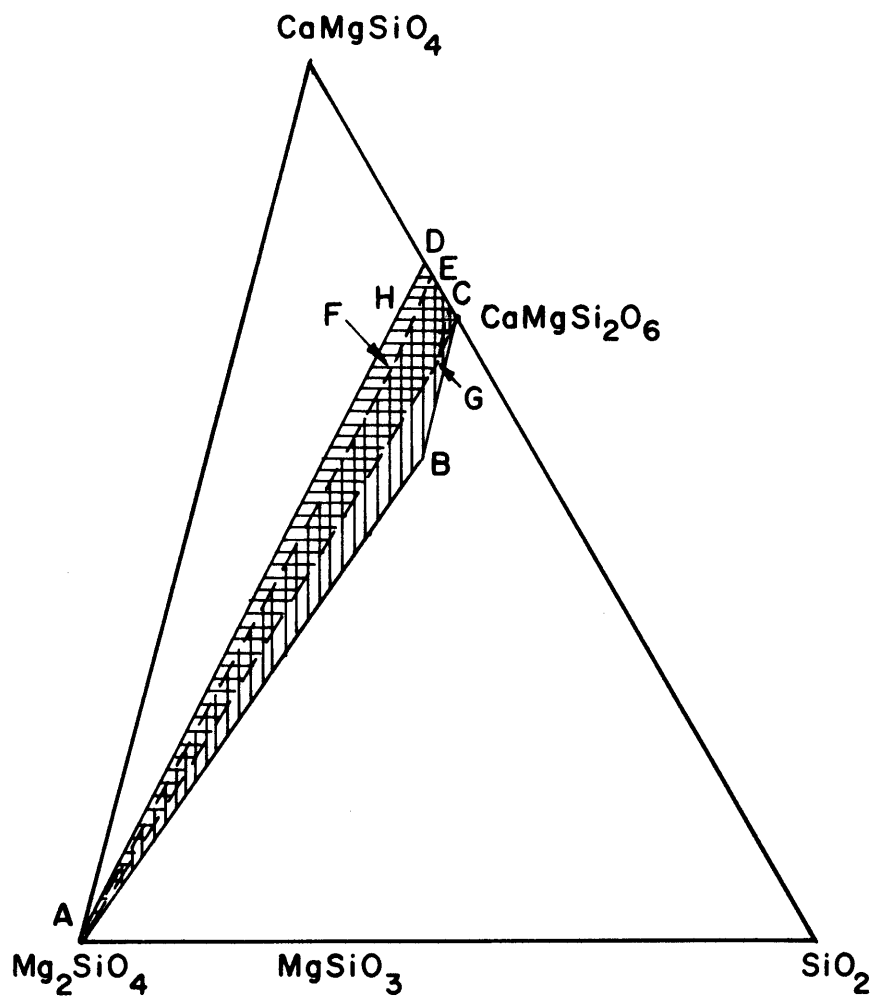
FIG. 27 THE ZONE OF RESIDUAL UNCERTAINTY

Schematic diagram showing composition range from which melts may differentiate towards or away from silica.

ABC-position of thermal barrier in dry system with no anorthite.

AFE-position of thermal barrier in dry system saturated with anorthite (projected through anorthite)

AGC-position of thermal barrier in wet non-feldpathic system.

AHD-position of thermal barrier in wet system saturated with anorthite (projected through anorthite).

residual uncertainty, although late critically undersaturated
residual phases will contain sodium minerals such as nepheline
and sodalite instead of or along with undersaturated calcium
phases such as melilite, hauyne, etc.

It is possible that the zone of residual uncertainty is to
some extent responsible for the common association of saturated
and undersaturated residua from a single basaltic magma or from
basaltic magmas differing only in content of feldspar. There is
little doubt that expansion of the olivine liquidus region with
dissolved melt volatile content will result in higher residual
melt silica contents than would occur under 'dry' conditions.
Moreover, it is certain that high Tschermak's molecule contents
in pyroxenes separating from high alumina melts such as those
saturated with calcic plagioclase will cause higher residual
melt silica contents than would occur if most of the pyroxene
separated from melts poorer in alumina prior to plagioclase
saturation.

The calcic basalt system, and in particular, the zone of
residual uncertainty, will be referred to in the following
study of differentiation in the Monteregian Hill gabbros.

5.2 Parent Magma of the Monteregian Hills

It is impossible to determine accurately the composition
of the parent magma or magmas of the Monteregian Hill intrusives.
The average composition of the early gabbroic phases, however,

would not be expected to differ greatly from a parent magma capable of producing a typical Monteregian igneous suite, except that such a parent would doubtless be more alkaline to be able to produce strongly sodic residua. The average Monteregian gabbro contains about 55 percent augite, 25 percent bytownite, 10 percent oxyhornblende, 5-10 percent olivine, and 0-5 percent titanomagnetite. The norm of such a rock would contain about 55 percent diopside (and hedenbergite), 25 percent anorthite, 5 percent albite, 15 percent olivine, 5 percent magnetite-ilmenite, and 5 percent negative quartz. The negative quartz is due to the low silica amphibole and aluminum substitution in the pyroxene. This estimate of an average gabbro norm can be compared with the molecular norms of three Monteregian gabbros given in Table 11.

A parent magma capable of producing alkaline residua would presumably contain more normative albite and less anorthite, diopside, and olivine than this average gabbro, but on a schematic tetrahedral diagram $(Mg,Fe)_2SiO_4$ - $CaAl_2Si_2O_8$ - $Ca(Mg,Fe)Si_2O_6$ - SiO_2, with liquid compositions projected through anorthite onto the triangle olivine-clinopyroxene-silica, both would be plotted at the same point (Point A, Fig. 28), since the albite component is not considered in this diagram.

5.3 Effect of Pyroxenes and Amphiboles: the Control of Silica in Differentiation

Table 11: Molecular Norms of Monteregian Gabbros

	Mafic[a] Gabbro Rougemont	Feldspathic[b] Gabbro Rougemont	Gabbro[c] Mt. Royal
SiO_2	45.44	40.68	41.55
TiO_2	1.50	2.04	3.92
Al_2O_3	5.85	19.83	14.84
Fe_2O_3	2.84	4.68	6.62
FeO	6.49	6.49	8.24
MgO	16.24	7.67	7.83
CaO	18.16	17.64	14.64
Na_2O	1.03	1.10	1.93
K_2O	0.38	0.27	0.25
Il	2.0	3.0	5.6
Or	1.5	1.5	1.5
Ab	9.0	10.0	17.5
An	11.5	48.5	32.0
Mt	3.0	4.8	7.1
Di	63.6	31.6	34.0
Ol	14.6	7.1	6.0
Qz	- 5.2	-6.5	- 3.7

a   typical Monteregian gabbro
    after O'Neill (1914)

b   after O'Neill (1914)

c   after Bancroft and Howard (1923)

The trend of fractional crystallization of a melt of the Monteregian parent type can qualitatively be described with reference to Fig. 28, as far as the mafic minerals are concerned.

Olivine is the first mineral to crystallize, and the liquid changes in composition from the point A to point B, on the olivine clinopyroxene field boundary. At this point a typical Monteregian augite of projected composition D' precipitates along with olivine, and the liquid follows the cotectic line BC away from silica towards melilite. At some point the melt becomes saturated with anorthite and it begins to precipitate along with olivine and pyroxene. If sodium is considered, the plagioclase will not be pure anorthite, and if the melt contains enough sodium, feldspathoids will eventually precipitate if fractional crystallization is carried out. Melilite, on the other hand, will result if the melt remains very calcic. The significant fact, however, is that the melt differentiates away from silica instead of towards it, which would have been the case if the bulk composition was on the silica side of the thermal barrier DEF.

Had the melt been saturated with anorthite at the time the olivine pyroxene field boundary was reached, the thermal barrier would have been farther from silica at the position DH. As a result, very large Tschermak's molecule substitution in the clinopyroxene (represented by composition H) at this temperature would cause the melt to differentiate towards
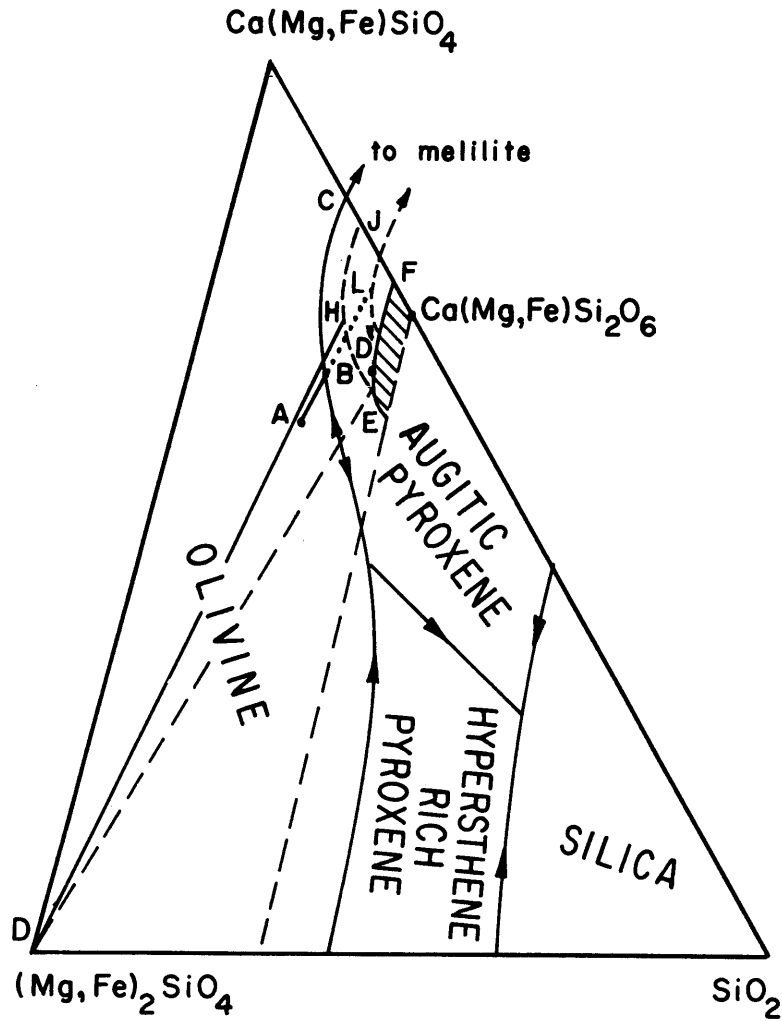
FIG. 28   SCHEMATIC LIQUIDUS DIAGRAM OF SYSTEM $(Mg, Fe)_2SiO_4$-$Ca(Mg, Fe)SiO_4$-$SiO_2CaAl_2SiO_8$ SHOWING TREND OF DIFFERENTIATION OF MONTEREGIAN MAGMAS.

Liquidus relations are projected through anorthite. Iron and magnesium are treated together. Exact position of field boundaries is dependent upon quantity of anorthite and FeO/MgO ratio in the melt.

◄── olivine pyroxene field boundary under high pressure of H_2O

...... magma trend at high pressure of H_2O

diopside solid solution with slight melt anorthite content ($\sim 15\%$)

diopside solid solution at anorthite saturation

silica. Similarly, under conditions of high pressure of
steam saturation, say about 5 kilobars, the olivine field would
expand forcing the melt to the more siliceous position L on the
olivine pyroxene boundary, from which point it would differen-
tiate towards silica without calcic plagioclase saturation, as
long as the melt contained enough anorthite component to pre-
cipitate pyroxenes more aluminous than the line BL.

Of course, all these crystallization paths are dependent
upon the bulk composition of the original melt. If this compo-
sition was poor enough in silica, no amount of anorthite or
volatiles dissolved in the melt could force the residua towards
silica, unless hydrous phases were developed in great quantities.
Similarly, if this original composition contained normative
hypersthene sufficient to bring it to the silica side of the
dry thermal barrier in the case of a non-feldspathic melt, it
could never differentiate away from silica. Since neither the
exact bulk composition of the Monteregian parent magmas nor the
actual composition range of the zone of residual uncertainty in
the complex natural basalt system are known, only this qualita-
tive and hypothetical discussion is presented. The zone of
residual uncertainty, however, must exist, and for bulk compo-
sitions falling into this region, 'dry' and weakly feldspathic
melts might be expected to differentiate away from silica,
while 'wet' feldspathic melts would be expected to differentiate
towards silica.

The Monteregian magmas, crystallizing for the most part at

shallow depths, could not have contained much volatile material in the dissolved state, and so the 'dry' conditions can be said to have prevailed. Similarly, judging from the average feldspar content of the mafic phases, about 25 percent or less, according to the random suite of specimens collected, it can be said that the melt was quite poor in feldspar, and, generally, much pyroxene probably crystallized before plagioclase began to form. It is therefore not surprising that the Monteregian magmas, all close in composition to the olivine-clinopyroxene-plagioclase join, differentiated to critically undersaturated residua. It is perhaps significant that the only oversaturated syenites in the Monteregian Hills, the quartz-nordmarkites of Shefford Mt. and Brome Mt., are found associated with the only highly feldspathic gabbros of the Monteregian province, bytownite gabbros composed of up to 90 percent plagioclase (Dresser and Denis, 1944).

The effect of amphibole crystallization on these fractionation trends is interesting. The approximate position of the Monteregian oxyhornblendes in the calcic basalt system ignoring its sodium, titanium, and hydrous portions, and combining iron with magnesium, is shown in Fig. 24 (p. 204). It is seen to fall on the subsiliceous side of the thermal barrier anorthite-clinopyroxene-forsterite.

Although hornblende is subordinate to pyroxene in the mafic rocks of the Monteregian Hills forming largely as a late mineral often seen mantling pyroxene or forming large poikilitic

laths, it may have been more extensively developed had the
intrusives crystallized at greater depths with a greater pro-
portion of the volatiles dissolved in the melt. If this type
of hornblende, or other low-silica amphiboles, were the major
minerals of the early gabbroic phases, the melt might well have
differentiated towards silica even if its original bulk compo-
sition was critically undersaturated. The role of amphibole
in producing undersaturated rocks was emphasized by Bowen
(1928, p. 271), who noted that fusion of hornblende rich mate-
rial might well cause silica impoverishment. Similarly, the
precipitation of hornblende from undersaturated magma could
produce oversaturated residua. Such large scale separation of
hornblende would be expected under conditions of high dissolved
melt volatile content such as might be expected in magmas
crystallizing at great depths. Thus we see a second example
of the effect of 'wet' conditions in favouring differentiation
towards silica.

The trend of composition of the Monteregian pyroxenes,
approximately parallel to the diopside-hedengergite line from
a composition of about Wo 42 En 51 Fs 7 to about Wo 43 En 41
Fs 16 (Fig. 23) is easily explained with reference to an
isothermal isobaric section of a portion of the system CaO-MgO-
SiO_2 (Fig. 29).

It can be seen that the liquid differentiating away from
silica at A is in equilibrium with a diopsidic pyroxene at B
and forsterite. The join forsterite diopsidic pyroxene prevents
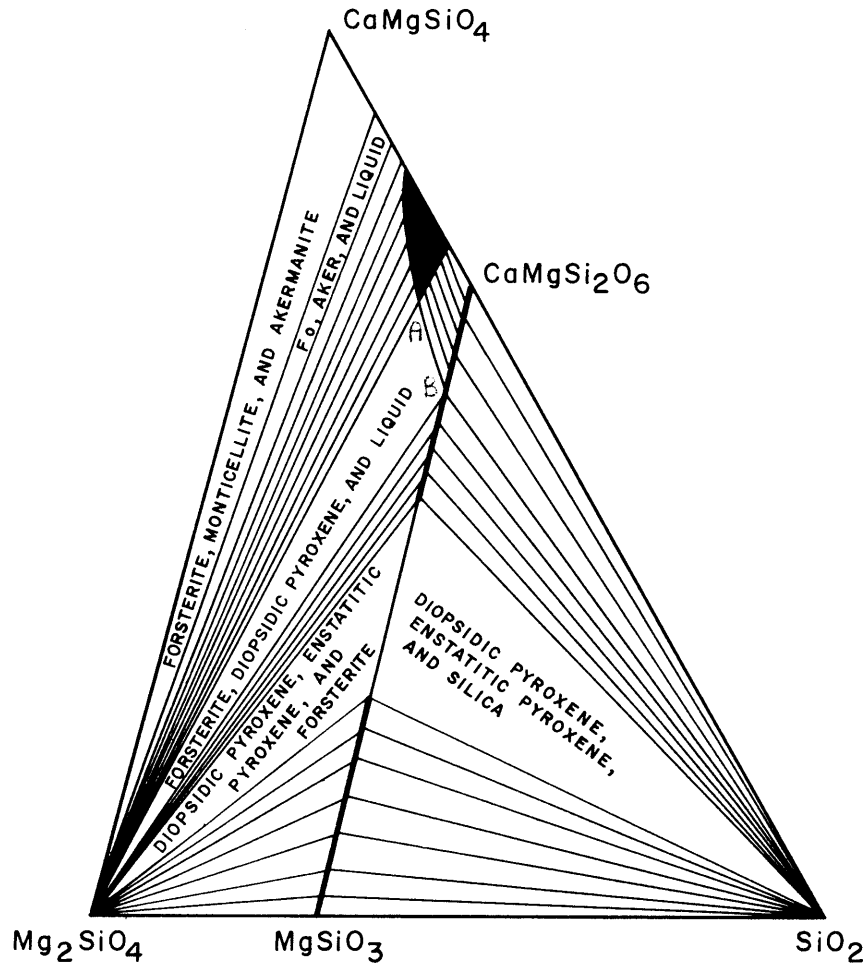
FIG. 29 APPROXIMATE ISOTHERMAL ISOBARIC SECTION FOR PART
OF THE SYSTEM $CaO-MgO-SiO_2$ AT T = ABOUT $1170^{o}C$,
P = 1 ATMOSPHERE.

(Note the two phase equilibrium barrier olivine-diopsidic
pyroxene which prevents subsiliceous diopsidic liquid from
precipitating enstatitic pyroxene.)

pyroxenes more magnesian than B from crystallizing. Hence, as differentiation proceeds in a natural melt of analogous composition, its iron content increases, and clinopyroxenes differentiate towards hedenbergite but not towards subcalcic compositions. Yoder and Tilley (1961) have recognized the incompatibility of hypersthene and pigeonite with critically undersaturated liquids, citing as field evidence the nonoccurrence of nepheline with such pyroxenes.

5.4 Effect of Plagioclase: Derivation of Highly Sodic Residua from Subsiliceous Gabbro Melts

There is almost a complete spectrum of plagioclase compositions in the rocks of the Monteregian Hills, from anorthite in some of the calcic gabbros, to almost pure albite in the perthites of most of the syenites. This illustrates the important fact that the Monteregian gabbros are highly calcic but are poorer in soda than the average gabbro, whereas the residual syenites are characteristically highly sodic. Since hypotheses of two parent magmas are incompatible with the gradational contacts of differentiation seen in the field, we must consider possible reasons for this extreme plagioclase differentiation.

This involves answering the question: why does almost pure anorthite initially crystallize from a magma sodic enough to produce nepheline and sodalite syenite residua? The answer to

this question could have great bearing on the origin of sodic alkaline rocks, since, if anorthite or calcic bytownite instead of soda bytownite or labradorite initially separates from a basaltic melt with a normal sodium to calcium ratio, the residual melt will be greatly enriched in sodium.

Although the liquidus relations in the ternary system nepheline-anorthite-silica have not been studied experimentally, it is possible to predict the form of this phase diagram from the binary systems which have been investigated: albite-anorthite (Bowen, 1912), nepheline-silica (Schairer and Bowen, 1947a; Grieg and Barth, 1938), anorthite-silica (Schairer and Bowen, 1947b), and anorthite-nepheline (Gummer, 1943). The ternary system so derived is shown in Fig. 30. The plagioclase liquidus and saturation curve is contoured, the form of its metastable extension is determined by extrapolation of the albite liquidus in the binary nepheline-albite (Grieg and Barth, 1938), and of the plagioclase liquidus in the pseudobinary section nepheline-anorthite (Gummer, 1943).

It is interesting to study two sections across this system, a low silica section, the section nepheline-anorthite, all compositions on which contain about 43 percent SiO_2, and a high silica section at about 77 percent SiO_2, where plagioclase is the only phase occurring on the liquidus. Fig. 31 shows the form of the liquidus and solidus curves across these sections in a plot of temperature vs. composition. For purposes of comparison, the two sections are shown projected through silica
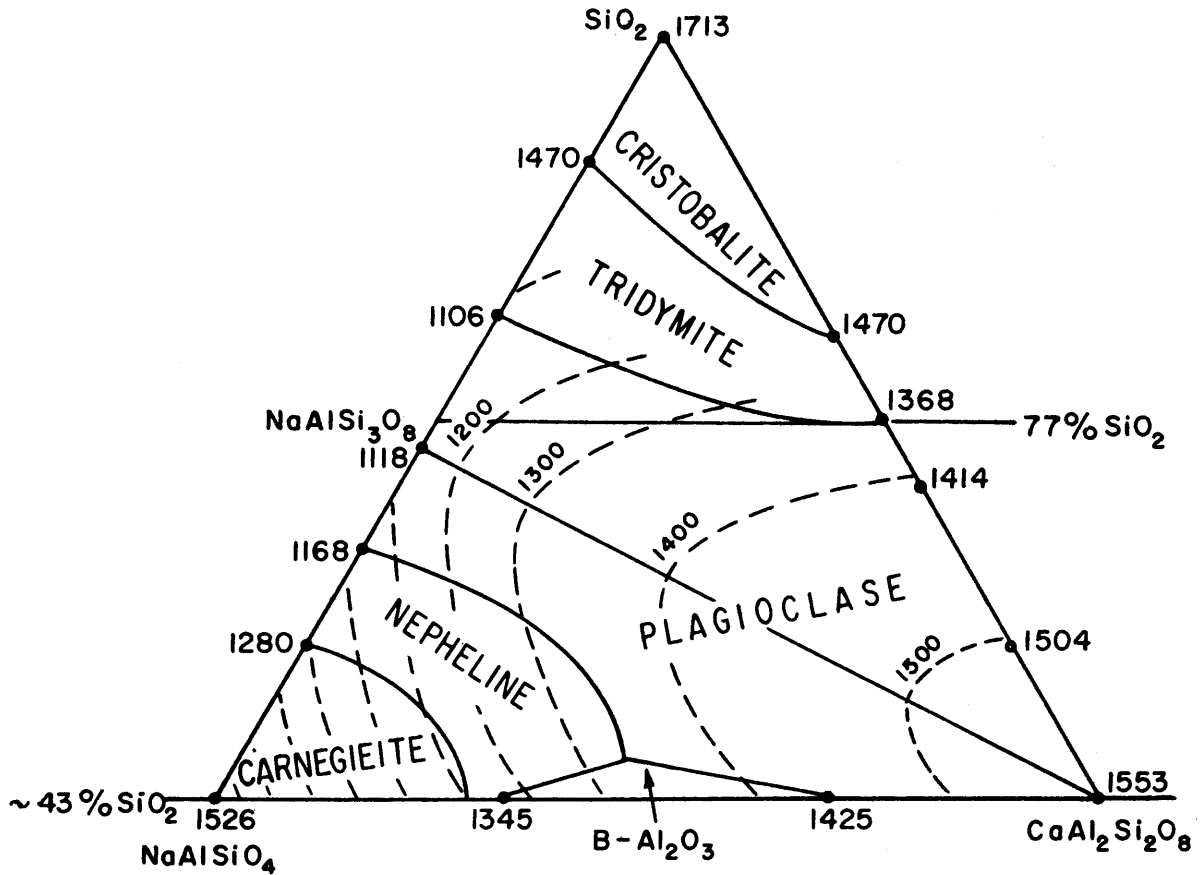
FIG. 30   APPROXIMATE LIQUIDUS RELATIONS IN THE SYSTEM
ANORTHITE-NEPHELINE-SILICA INFERRED FROM
EXPERIMENTAL DATA ON THE BINARY SECTIONS
ANORTHITE-SILICA, NEPHELINE-SILICA, ALBITE-
ANORTHITE AND THE PSEUDOBINARY SECTION NEPHELINE-
ANORTHITE.

(Contours refer to surface of plagioclase saturation, stable
and metastable.)   Data after Schairer and Bowen, 1947a;
Grieg and Barth, 1938; Bowen, 1912; Schairer and Bowen,
1947b; Gummer, 1943.
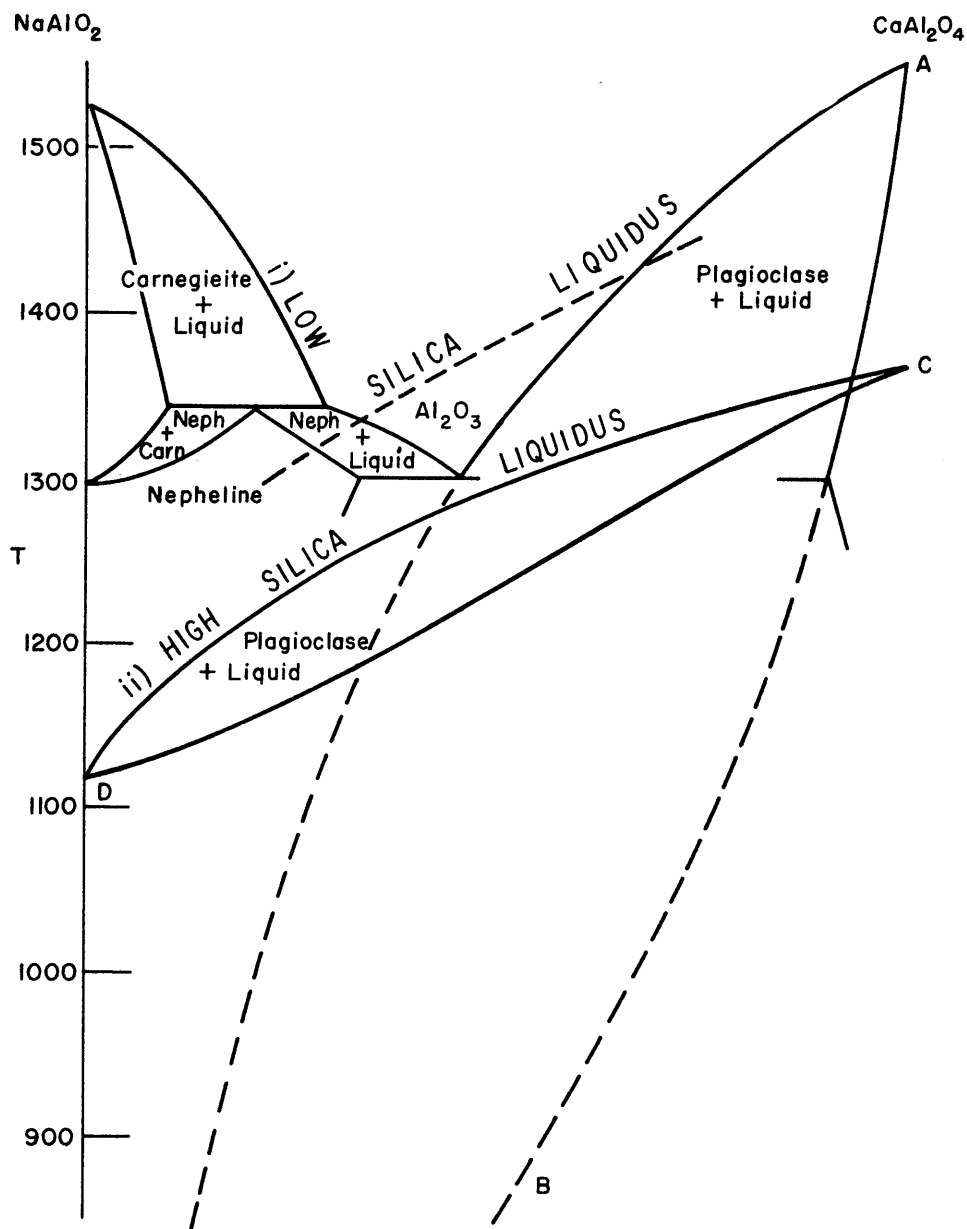
FIG. 31:   TEMPERATURE-COMPOSITION SECTIONS ACROSS THE
SYSTEM NEPHELINE-ANORTHITE-SILICA AT EQUAL
LIQUID PERCENTAGES OF SILICA.

   i)   Low Silica $\sim 43\%$ SiO_2: pseudobinary section nepheline-
        anorthite.

   ii) High Silica $\sim 77\%$ SiO_2: Pseudobinary section projected
        from silica onto nepheline-anorthite section.

Low silica section after Gummer (1943) with plagioclase

compositions inferred from data of Goldsmith (1947),

Grieg and Barth (1938).

onto the section $NaAlO_2$-$CaAl_2O_4$.

The plagioclase liquidus curves are taken from Fig. 30, but the solidus curves were more difficult to obtain. Goldsmith (1947) studied the system nepheline-anorthite-gehlenite ($Ca_2Al_2SiO_7$) and found that the most sodic plagioclase occurring on the liquidus is An 95 at about 40 percent nepheline. The composition of plagioclase which first precipitates at 40 percent nepheline on the section anorthite-nepheline was not determined since corundum occurs on the liquidus at this point, but it would not be expected to differ significantly from the plagioclase on the liquidus at nepheline 40-anorthite 40-gehlenite 20, which is An 95. Using this information, plus the temperature of the metastable albite saturation curve at the nepheline composition, the low silica plagioclase solidus can be drawn (AB, Fig. 31). The high silica solidus was drawn with reference to the liquidus by assuming ideality across the section, and by assuming a partial molar entropy of melting of anorthite across the section as 16.0 e. u., equal to the molar entropy of melting of anorthite. This curve is an approximation to the actual solidus, and if in error, it is likely too far from the liquidus, since a similar calculation for the low-silica solidus predicts a fatter solid-liquid field than that observed.

The important fact which emerges from a comparison of the high and low silica plagioclase-liquid fields is that, for a given ratio of $NaAlO_2$ to $CaAl_2O_4$ in the melt, the low silica

section first precipitates a plagioclase which is far more
calcic than the comparable plagioclase of the high silica sec-
tion. For a ratio $NaAlO_2/CaAl_2O_4$ of unity, the first
plagioclase to precipitate at 43 percent SiO_2 is An 92,
anorthite, whereas from the 77 percent SiO_2 melt, the first
plagioclase is An 71, soda bytownite. The difference in
$NaAlO_2-CaAl_2O_4$ composition between crystal and melt at 77 per-
cent SiO_2 is only one half that at 43 percent.

We can therefore expect, as a general rule, low silica
basaltic melts to favour initial precipitation of very calcic
plagioclase while high silica mafic magmas favour initial pre-
cipitation of more sodic plagioclase. This is not very sur-
prising, since anorthite contains only 43 percent SiO_2 while
albite contains 69 percent SiO_2. If there is very little
silica available, sodium will not enter plagioclase, but will
remain in the melt until another sodium phase like nepheline
can separate. The Monteregian igneous rocks are characteris-
tically poor in silica, and it is therefore not surprising that
the plagioclases of the gabbros are highly anorthitic. The
inability of sodium to enter the early plagioclases caused a
concentration of this element in the residual magmas, which, as
we have seen, crystallized as alkaline rocks: essexites,
syenodiorites, and nepheline and sodalite syenites.

The strongly zoned nature of many of the plagioclases of
the Monteregian gabbros may also be explained by the low silica
nature of the gabbros. Because the $NaAlO_2/CaAl_2O_4$ ratio of the

early formed anorthite crystals in a low silica melt is so much lower than that of the melt itself, modest crystallization of plagioclase will cause a large increase in the sodium content of the melt, and a corresponding increase in the sodium content of the plagioclase in equilibrium with the melt. The spread of plagioclase compositions in equilibrium with the melt during crystallization is so great that the crystals will encounter unusual difficulty in remaining in equilibrium. Since solid diffusion is normally very sluggish, zoning will result unless the cooling is unusually slow and continuous and complete crystal-liquid reaction is allowed, or unless the crystals are removed from the melt immediately or very soon after they begin to form. Contamination of early anorthitic plagioclase and pyroxene accumulates by later sodic residua may also cause zoning. Such contamination is inferred from gradational gabbro-syenite sequences observed in some of the Monteregian outcrops.

5.5 Summary

Composed of normative diopside, plagioclase, olivine, negative quartz, and ilmenite-magnetite, the Monteregian magmas originally lay within or close, on the low silica side, to the zone of residual uncertainty, from which fractional crystalliza-tion can either produce oversaturated or undersaturated residua, depending upon the quantity of feldspar and volatiles dissolved in the melt at the early stages of crystallization.

The conditions of intrusion of these magmas, at shallow depths
and with little dissolved volatile material, favoured a differ-
entiation towards critically undersaturated residua, in this
case largely nepheline syenite. Extreme calcium to sodium
differentiation from anorthite gabbros to soda syenites was
effected by the subsiliceous character of the parent magma.

Chapter V: DEPTH OF ORIGIN OF THE MAGMAS OF THE MONTEREGIAN

HILLS AND CHUKOTAT SILLS

It is interesting to attempt to predict the possible com-
positions of liquids which could form from fusion of a
peridotite composed of normative forsterite, diopside, and
enstatite under both low and high pressure conditions.

The phase relations in the system Mg_2SiO_4-$CaMgSi_2O_6$-SiO_2
at atmospheric pressure was investigated by Bowen (1914).
Fractional fusion of a peridotite falling into this system
would produce a melt whose composition must lie on the path
followed by a magma of the same composition as the peridotite
undergoing equilibrium crystallization. For example, a melt of
composition A (Fig. 32 (1)) would follow the path AFG at atmos-
pheric pressure. Forsterite crystallizes as the liquid changes
in composition along AF. This mineral then reacts with the
liquid to form pyroxenes which change in composition from E to
B as the liquid composition continues to change from F to G.
The liquid disappears at G with the net result a mixture of
forsterite and pyroxene B in such proportion to maintain the
bulk composition at A. Under fractional fusion of a peridotite
of composition A a melt of composition G would first fuse, but
depending upon the temperature, which governs the proportion of
the peridotite which will fuse, any composition along the path
GFA could result.

At a pressure of about 7000 bars, where, as we have seen
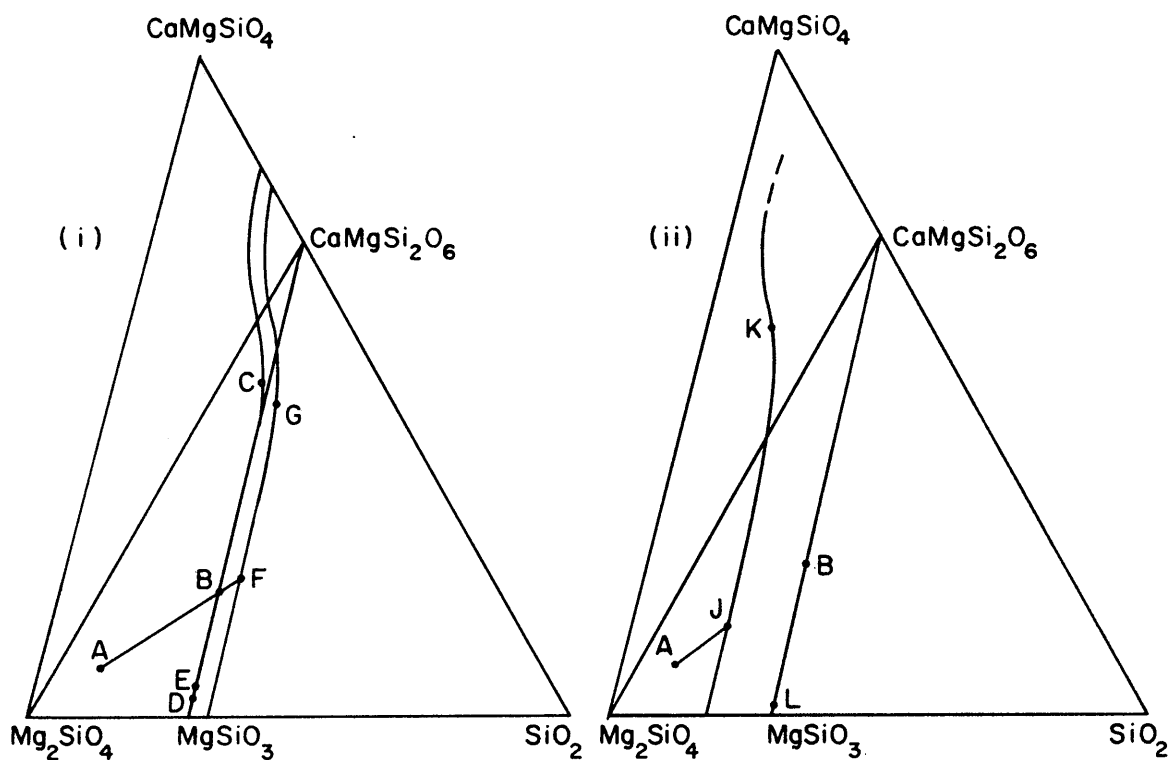
FIG. 32: SCHEMATIC LIQUIDUS DIAGRAMS ILLUSTRATING THE
CHANGE IN POSITION OF THE OLIVINE - PYROXENE FIELD
BOUNDARY WITH TOTAL PRESSURE IN THE SYSTEM
$CaMgSiO_4$-Mg_2SiO_4-SiO_2 AND THE CONPOSITIONS OF
MAGMAS RESULTING FROM SIMPLE PARTIAL FUSION
OF A PERIDOTITE.

Diagram (i) shows its position at atmospheric pressure
and at P = about 7 kilobars. Diagram (ii) shows its
position under high pressures of about 50 kilobars.

ABC, AFG, and AJK represent the compositions of magmas
which can develop by fractional fusion of a peridotite of
composition A under pressures of 1 atm., 7 kilobars, and
50 kilobars, respectively. EB, DB, and LB represent the
ranges of pyroxene compositions in equilibrium with these
liquids.

(pp. 34-38), enstatite melts congruently, the compositions of possible melts fusing from the peridotite at A lie on the path ABC, and are slightly less siliceous than the atmospheric pressure melts (Fig. 32 (i)).

If the pressure is increased to about 50 kilobars, corresponding to depths of about 150 kilometers, the olivine liquidus field continues to shrink, and the compositions of possible melts fusing from the peridotite at A now lie along the path AJK (Fig. 32 (ii)), which is much lower in silica than the low pressure composition paths. The composition K of the first melt to fuse from A at high pressure is not known, but as a first approximation, it is plotted here using the assumption that liquids in equilibrium with pyroxene B are not affected in MgO/CaO ratio, but only in SiO_2 content, by increasing pressure.

In any case, the significant conclusion is that under high pressure conditions, at least in the simple system $CaMgSiO_4$-Mg_2SiO_4-SiO_2, simple partial fusion of a peridotite produces subsiliceous magmas, while under low pressure conditions, melts of normal silica content result.

It is now useful to consider a second more complex mechanism of partial fusion of a peridotite, namely, repetitive partial fusion. Assume that a peridotite partially fuses, and that the resulting melt is carried away from the remaining solid where it crystallizes to a new solid mass. If this solid mass then undergoes another partial fusion, a magma may result which could never form during a simple partial fusion of the

original rock. Such a magma, developing through repetitive partial fusion from a peridotite of given composition, is limited in composition to the paths of residual liquids which could result from complete or partial fractional crystallization of a liquid of the same composition as the peridotite.

In Fig. 33 (i), the paths followed by a liquid undergoing fractional crystallization from a composition A, AFG and ABC, are shown for pressures of 1 atmosphere and 7 kilobars, respectively. These paths also represent liquids which may develop through repetitive fractional fusion from a peridotite at A, and extend into regions substantially more siliceous than those involved in simple fusion. Similarly, in Fig. 33 (ii), the path representing compositions of liquids which may develop through repetitive partial fusion from the same peridotite at high pressures of about 50 kilobars, AJH, extends into highly calcic and low silica compositions.

Repetition of the partial fusion process is an effective means of forming liquids whose compositions differ greatly from the rock from which they developed. It would be expected to be very important in nature, because solids which have resulted from complete crystallization of liquids which previously had fused fractionally from a host rock always will have lower solidus temperatures than the host rock, and hence are very susceptible to refusion.

If we now allow the parent peridotites to contain some aluminum and iron, aluminum in the form of $CaAl_2Si_2O_8$, and iron
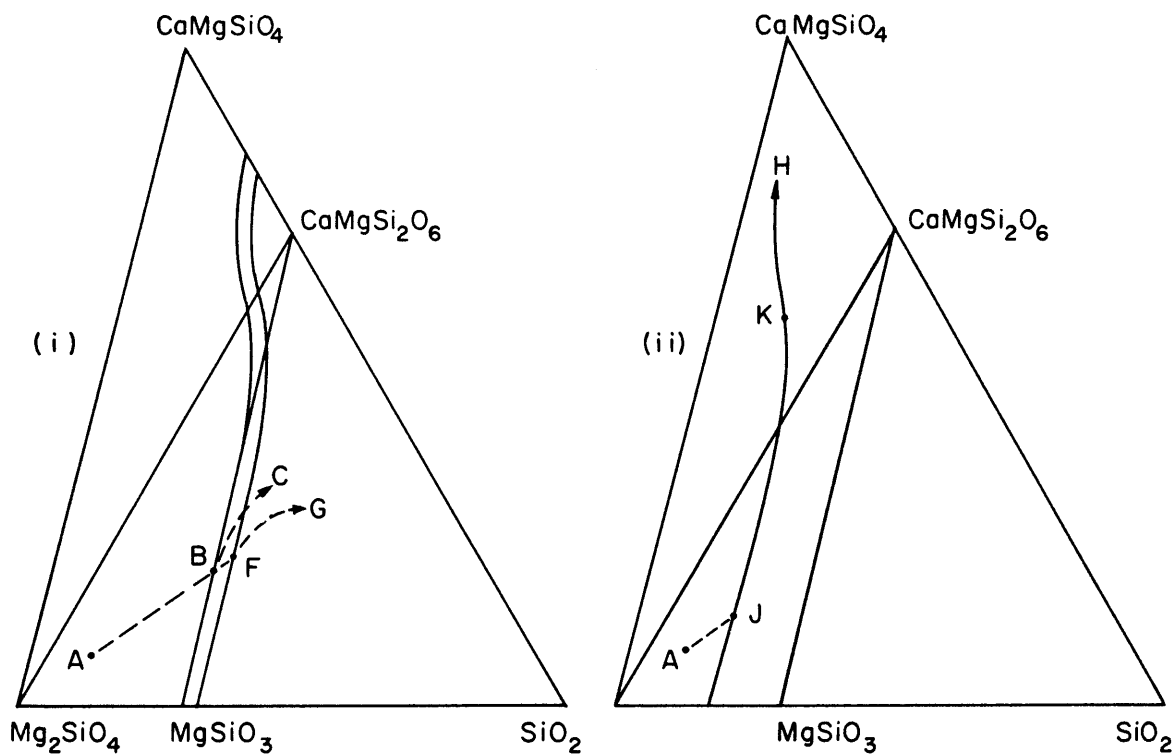
FIG. 33   SCHEMATIC LIQUIDUS DIAGRAMS FOR THE SYSTEM $CaMgSiO_4$-
Mg_2SiO_4-SiO_2 AT LOW AND HIGH PRESSURE INDICATING
COMPOSITIONS OF LIQUIDS WHICH MAY DEVELOP FROM
REPETITIVE PARTIAL FUSION OF A PERIDOTITE.

AFG represents such a series of possible liquids at atmos-
pheric pressure, ABC such a series at 7 kilobars, and AJH,
the series of possible liquids at about 50 kilobars.

A represents the composition of the host peridotite.

combined as Fe_2SiO_4, $FeSiO_3$, and $CaFeSi_2O_6$, the phase relations derived by projection of liquid compositions through $CaAl_2Si_2O_8$ on the triangle $(Mg,Fe)_2SiO_4$-$Ca(Mg,Fe)SiO_4$-SiO_2 would not differ greatly from Figs. 32 and 33, at least in the cases of atmospheric and 7000 bars pressure. The effect of anorthite saturation and of replacement of about one half the magnesium by iron would cause the olivine liquidus to expand slightly from orthopyroxene towards silica and contract slightly from clinopyroxene towards olivine, but these changes would be minor (pp. 38-40).

The liquids resulting from partial fusion of a peridotite in this case would differ from those predicted by Fig. 32, however, because considerable anorthite and iron bearing components would be present. In proportion of normative olivine, clinopyroxene, and orthopyroxene, though, they would not be greatly different, except that highly diopsidic liquids might be prevented by the minimum developed in the olivine-pyroxene field boundary at anorthite saturation (Fig. 12, p. 72).

The effect of the addition of the anorthite component at the high pressures of about 50 kilobars is more difficult to predict. The olivine liquidus will shrink in the triangular section Mg_2SiO_4-$CaMgSiO_4$-SiO_2, as is shown in Fig. 32. In addition, this liquidus field would be expected to shrink even more rapidly with increasing pressure within the tetrahedron Mg_2SiO_4-$CaMgSiO_4$-SiO_2-$CaAl_2Si_2O_8$, because pyroxene would be favoured over olivine by the addition of the anorthite component at high pressures. This is because at high pressures

complete solid solution exists between diopside and lime

Tschermak's molecule (Clark and DeNeufville, 1962), and con-

siderable, if not complete solid solution, would also occur

between enstatite and magnesian Tschermak's molecule,

There is a complication, however, which results from the

appearance of garnet on the liquidus in the system Mg_2SiO_4-

$CaMgSiO_4$-$CaAl_2Si_2O_8$-SiO_2 at high pressures. This mineral will

first appear on the plane Mg_2SiO_4-$CaMgSiO_4$-$CaAl_2Si_2O_8$, since

its composition along the join pyrope-grossularite ($Mg_3Al_2Si_3O_{12}$-

$Ca_3Al_2Si_3O_{12}$) lies in this plane. With increasing pressure,

this liquidus field will expand so that pyroxene, garnet, and

some forsterite are the only plases occurring on the liquidus

in the low silica, low aluminum regions of the tetrahedron

(Fig. 34).

Since pyroxene remains very stable at high pressures, there

is almost certainly an even field boundary between garnet and

pyroxene, which is shown hypothetically as the surface ABCDE

in Fig. 34. Such an even cotectic relation has been confirmed

by Yoder and Tilley (1961) in their studies of the melting of

eclogites.

The surfaces of two-fold saturation, forsterite-pyroxene

and forsterite-garnet (ACG and ACF in Fig. 34, respectively),

and the line of three-fold saturation forsterite-pyroxene-

garnet (AC in Fig. 34), represent the compositions of liquids

which would result from partial fusion of magnesian rocks

whose compositions lie within the forsterite liquidus volume,
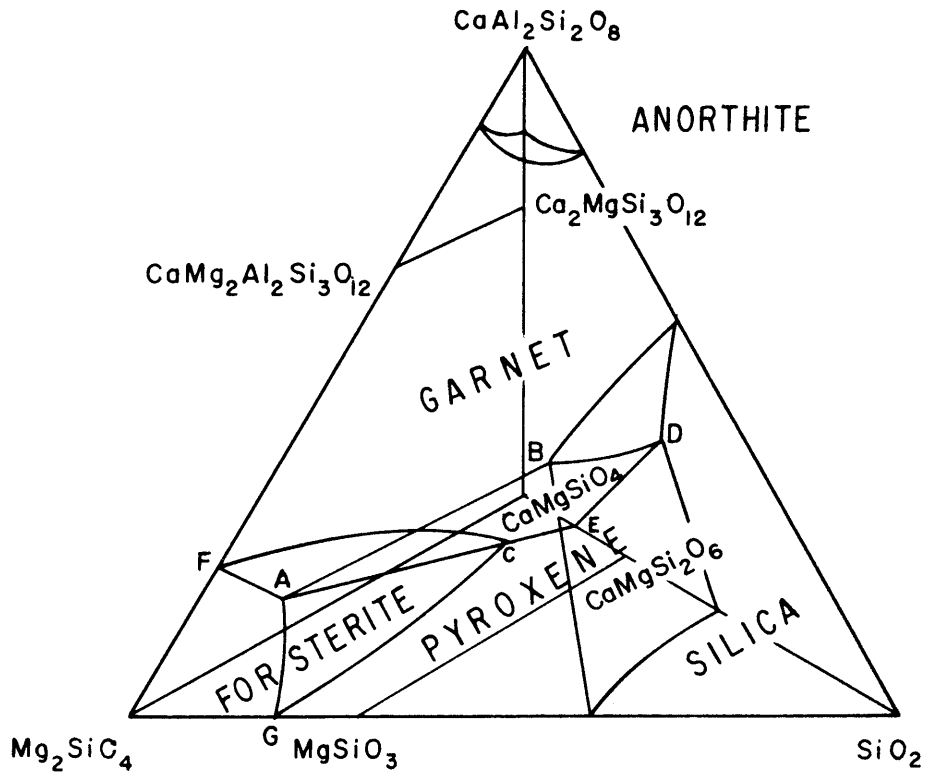
FIG. 34   HYPOTHETICAL LIQUIDUS DIAGRAM AT HIGH PRESSURES
($\sim$ 50 KILOBARS) FOR THE SYSTEM Mg_2SiO_4-$CaMgSiO_4$-
$CaAl_2Si_2O_8$-SiO_2.

(Points A and B are on plane Mg_2SiO_4-$CaAl_2Si_2O_8$-SiO_2,
point C is on plane Mg_2SiO_4-$CaMgSiO_4$-SiO_2, and point D
is on plane $CaMgSiO_4$-$CaAl_2Si_2O_8$-SiO_2).

according to the hypothetical liquidus relations shown in Fig.
34. These liquids show the same subsiliceous character as the
liquids which first fuse from a peridotite in the simple sec-
tion Mg_2SiO_4-$CaMgSiO_4$-SiO_2. Even if the forsterite field is
larger or smaller in the anorthite direction than shown, this
subsiliceous character of partial fusion products of solids
of peridotite composition will still be maintained. Hence, the
introduction of the anorthite component will not affect the
major conclusion, namely, that subsiliceous basaltic magmas
fuse from peridotite at high pressure.

It is now interesting to examine the bulk composition of
the parent magmas of the Stillwater Complex, a typical
tholeiite, the Chukotat Sill Complex, a typical olivine
tholeiite, and the Monteregian Hill gabbro, a typical basanite,
in the light of expected products of fusion of peridotite at
various pressures.

Melt B of Figs. 32 and 33 is very close in composition to
the parent magmas of the Stillwater Complex if plagioclase is
added and about half the magnesium is replaced by iron. This
suggests that the Stillwater magma may have been formed by
simple or repetitive partial fusion from a peridotite at modest
pressures such as occur near the top of the mantle. It is also
possible, of course, that the Stillwater magma fused from
basaltic material of approximately its own composition near the
base of the crust.

Melts J and K of Figs. 32 and 33, if plagioclase is added

and some magnesium is replaced by iron, are similar in composition to the parent magmas of the Chukotat Sills and the Monteregian Hills, respectively, suggesting that these magmas have been formed by simple or repetitive partial fusion of peridotite or material of similar composition at considerable depths in the mantle.

It can be stated as a reasonable hypothesis, on this basis, that low silica magmas originate deep in the mantle while normal tholeiitic basalts fuse near the top of the mantle. Yoder and Tilley (1961) have suggested a similar hypothesis from a different line of reasoning. They envisage a mafic parent magma of fixed composition originating in the mantle. If this magma originates and begins to crystallize at great depths, pyroxenes along the join hypersthene-jadeite-clinopyroxene may form, whereas if a similar magma begins to crystallize at shallow depths, such pyroxenes are prevented from forming by the stable join albite-forsterite-clinopyroxene. The residual melt in the former case will be poorer in silica than in the latter case. Hence, tholeiitic magmas may develop near the top of the mantle and alkaline olivine basalts at greater depths.

It is difficult to imagine that the process of crystallization is more important than the process of fusion in shaping the composition of magmas in the mantle, however. It is also very doubtful that the mineralogical positioning of sodium, a relatively minor element in mafic magmas and one which is

usually concentrated in late crystal phases, is of prime impor-
tance in affecting basalt differentiation. Moreover, it is
expected that jadeitic pyroxene would be frequently transported
into the crust with subsiliceous magmas, had it indeed crystal-
lized in abundance at depth. Such pyroxenes are unknown in the
early phases of subsiliceous petrographic provinces such as the
Monteregian Hills.

In any event, mantle crystallization may not be necessary
in the production of undersaturated magmas capable of producing
critically undersaturated residua. Fractional fusion of
peridotite or similar material at high pressures can be expected
to produce subsiliceous melts. Under high temperature conditions,
where the degree of fusion is considerable, highly magnesian
olivine tholeiites such as the Chukotat Sill parent magma would
be expected. Less complete fusion under lower temperature con-
ditions would be expected to produce more calcic magmas, such
as those of the Monteregian Hills, which, as we have seen, are
capable of differentiation towards critically undersaturated
and alkaline residua.

Independent evidence that the Monteregian Hill magmas did
fuse at great depths in the mantle as this discussion suggests
is derived from a study of the strontium isotope ratios in the
rocks of the Monteregian Hills (Fairbairn et al, 1962). The
initial Sr 87/Sr 86 ratio in the Monteregian gabbros and
syenites average 0.705 compared to that of the average basalt,
0.708. This lower ratio is held significant, and is attributed

to a low ratio of rubidium to strontium in the source material. Since this ratio is believed to decrease in the mantle (Faure, 1961, p. 248), fusion at considerable depths in the mantle is indicated.

SUMMARY AND CONCLUSIONS

There is little doubt that the position of the forsterite-enstatite liquidus boundary in the simple system $MgO-SiO_2$ exerts a major influence in the course of differentiation of magnesium-rich silicate melts. It was recently discovered in the laboratory that the effect of total pressure is to shift this boundary to a less siliceous composition, a conclusion which can also be reached through theoretical considerations.

If the raising of melting temperatures due to increasing pressure causes the forsterite-enstatite cosaturation point to move away from silica, changing it from a peritectic to a eutectic point, the lowering of melting temperatures due to the addition to the system of volatiles under pressure should perform an opposite function, that is, to shift the peritectic towards silica. Quantitative estimates of this shift amount to about 5 percent per 100 degrees lowering of the forsterite melting temperature.

The effect of addition of plagioclase and iron bearing components to the forsterite-silica system also plays an important role in changing the position of the olivine-pyroxene liquidus boundary with respect to olivine and silica components. Albite and anorthite shift the boundary 6 and 8 percent towards silica while replacement of magnesium by iron shifts it about 5 percent away from silica, measured along an olivine-pyroxene line per 100 degrees lowering of the olivine liquidus.

For a given composition, fractional crystallization taking place in a 'wet' environment, under high pressures of steam saturation, for example, will result in the separation of more olivine than would form under 'dry' conditions such as those prevailing at the low pressure regions near the surface of the earth, where volatiles are largely present as a vapour phase separated from the melt. Consequently, the residual magmas of deep and 'wet' crystallization are likely to be more enriched in silica than those which form close to the surface. However, a magnesium-rich melt crystallizing 'dry' at very great pressures far below the crust would not precipitate much olivine due to the shrinkage of this phase on the liquidus with increasing total pressure, and hence would produce low silica residual magmas. Conversely, and more important, fractional fusion of peridotite at such pressures might be expected to form silica-poor melts.

An unusual feature of the simple pyroxene system diopside-enstatite which would be expected to greatly affect pyroxene crystallization in natural rocks is the occurrence of a very shallow liquidus minimum near diopside. It has recently been shown in the laboratory that the addition of albite or anorthite to the system diopside-enstatite, while it lowers the liquidus temperatures producing a cotectic field boundary between diopsidic and enstatitic pyroxene, does not shift this liquidus trough towards enstatite nearly enough to explain

cotectic precipitation of orthopyroxene and clinopyroxene in
approximately equal amounts, such as is commonly observed to
have occurred during the fractional crystallization of layered
gabbros. This observation demands a shift in the pyroxene
trough at least to 50 percent orthopyroxene.

A possible key to this paradox lies in a thermodynamic
analysis of the melting relations in the diopside-enstatite
system. The form of the free energy function for the solid
solution $CaMgSi_2O_6-2MgSiO_3$, can be determined from subsolidus
relations in the diopside-enstatite system. A similar function
for the liquid can be derived from the melting relations in the
same system. It is found that there is an endothermic heat of
mixing in the liquid solution, roughly 850 calories per gram
formula weight, over one third that in the solid solution.
This indicates that the repulsive tendency in this solution,
while not sufficient to produce immiscibility, is nevertheless
great, and suggests that liquids along the diopside-enstatite
composition line contain an incipient pyroxene structure,
perhaps due to the existence of unbroken tetrahedral chain
segments.

It is concluded from theoretical considerations that
dissolved steam, if present in sufficient quantities, will
break up the incipient structure of liquids rich in pyroxene
components producing greater free energies of mixing between
calcium and magnesium and iron. This will cause the minimum
melting composition in the simple diopside-enstatite system to

shift to a position midway between diopside and enstatite and
will also produce a eutectic trough of some 50 degrees at this
point.

An effect of plagioclase, in adding aluminum to a diopside-
enstatite melt, and an effect of dissolved volatiles, in enhanc-
ing the olivine liquidus, and an effect common to both, in pro-
ducing a field boundary in the pyroxene liquidus, all cause the
thermal barrier in the system forsterite-diopside-silica to
shift with respect to the components of this system away from
silica, largely as a result of aluminum substitution in diopside.
Thus, for gabbroic magmas falling close to the normative compo-
sition plagioclase-olivine-clinopyroxene, i.e. magmas without
appreciable normative nepheline or hypersthene, slight differ-
ences in volatile content or plagioclase content can profoundly
affect the chemistry of the residual melt. Abundant plagioclase
and volatiles favour normal differentiation towards a siliceous
residua, dry conditions with a minimum feldspar content favour
differentiation towards alkaline residua.

Two igneous complexes have been studied in detail in an
attempt to test the conclusions reached from this theoretical
and experimental evidence. They are the Chukotat Sills of the
Cape Smith-Wakeham Bay belt of New Quebec, and the Monteregian
Hills of the Montreal area.

The Chukotat Sills are differentiated Precambrian bodies
whose average composition show that they originated from a very

basic, almost an ultrabasic magma, which can be classified as an olivine tholeiite. This subsiliceous hypersthene-normative magma crystallized at considerable depths according to structural evidence, and judging from an abundance of primary hydrous minerals, under conditions of considerable volatiles dissolved in the melt.

Three types of Chukotat Sills occur: ultrabasic, gabbro, and settled differentiated. Field evidence indicates that the ultrabasic sills formed through injection of a largely crystalline olivine mass, lubricated by a small quantity of gabbroic magma and a volatile fluid phase. The gabbro sills formed through injection and differentiation of a tholeiitic gabbro liquid. The settled differentiated sills, twin sills up to 2000 feet in thickness, are composed of an ultrabasic base and a gabbro cap, with an average ratio of ultramafic to gabbro material of 6:4. The sills were injected as a mixture of gabbroic magma and olivine crystals. The latter sank forming a homogeneous mass and the gabbro cap then differentiated. A constancy in chemical composition of the olivines and surrounding poikilitic pyroxene in the peridotite member and chemical differentiation of pyroxenes from the base upward in the gabbro member support this genesis. Widespread serpentinization of the ultramafic members of the settled sills as well as the single ultramafic sills, followed by intense folding in two directions, has produced a refolded complex of serpentinite, gabbro, and host rocks, dominantly lava and slate. Similar

associations in many areas where geological information is difficult to obtain may be the result of an identical process, namely, separation of olivine from an olivine tholeiitic magma at depth, followed by injection of olivine-rich largely crystalline masses lubricated by gabbroic liquid in small or large quantities and by volatile fluids, largely steam.

The mineralogy of the Chukotat Sills shows olivine accumulation far in excess of its normative content in the parent magma. Furthermore, although normative hypersthene outweighs normative diopside, endiopside was the first pyroxene to form, crystallizing with minor resorption of olivine. These facts illustrate the two major effects predicted for basaltic crystallization under high water pressure, namely, the expansion of the olivine liquidus field, and the shift in the pyroxene liquidus trough towards orthopyroxene.

The separation of a great excess of olivine allowed differentiation to produce in the roof zone of the Chukotat gabbros oversaturated rocks such as quartz diorite, despite the fact that the bulk silica composition of the sills ranges around 45 percent. Thus, we may emphasize a probable role for dissolved volatiles as an agent to facilitate the crossing of the 'plane of oversaturation' hypersthene-plagioclase-clinopyroxene in the simple basalt system of Yoder and Tilley from the olivine tholeiite zone to the tholeiite or quartz bearing zone. More generally, dissolved volatiles favour differentiation towards granitic rather than syenitic magmas.

The Monteregian Hills intrusives are a series of differ-
entiated Cretaceous stocks ranging in composition from olivine
gabbros, pyroxenites, and calcic gabbros through essexites and
syenodiorites to highly sodic nepheline and sodalite syenites.
They were formed through shallow emplacement of largely
basaltic magma of a subsiliceous but not necessarily alkaline
character. The parent Monteregian magmas are believed to have
been composed mainly of normative clinopyroxene, olivine,
plagioclase, and some nepheline, and hence are termed basanite.
Nepheline appears in the norm of most of the analyzed gabbros
because of their subsiliceous nature, but very rarely occurs
as a phase in these rocks, which are notably rich in calcium
and poor in sodium.

Because the typical Monteregian parent magma was very
close to the normative olivine-clinopyroxene-plagioclase compo-
sition, or 'plane of critical undersaturation' in the simple
basalt system, it likely fell very close to or within a zone
of residual uncertainty, simply represented as the volume
anorthite-diopside solid solution-forsterite in the tetrahedron
forsterite-monticellite-Tschermak's molecule-silica. From this
zone, depending upon bulk feldspar content and quantity of
dissolved volatiles in the melt, differentiation may either
proceed towards critically undersaturated residua or towards
saturated or even oversaturated residua. Since the Monteregian
intrusions are of the shallow, high temperature, and 'dry' type,
the steam content of the original melts is believed to have

been small. This favours differentiation away from free silica, largely because low-silica primary hydrous minerals are not favoured. The general pattern of differentiation was indeed in this direction, nepheline syenites being the predominant late magmatic rock type instead of ordinary syenite. The only quartz bearing residua present in the Monteregian province occur in association with nordmarkites and bytownite-rich anorthositic gabbros, indicating aluminum substitution in the pyroxenes may have been sufficient to shift the basalt thermal barrier far enough from silica to allow differentiation to proceed towards free silica.

The pyroxenes analyzed from the Monteregian gabbros are rich in ferric iron, aluminum, and titanium, but are not nearly as rich in titanium as similar pyroxenes from the gabbros of other subsiliceous provinces which contain strongly alkaline derivatives. This is due to the entrance of titanium into the phases oxyhornblende and sphene, and this fact beclouds the use of titanium for magnesium and iron and corresponding aluminum for silicon substitutions in clinopyroxenes as an indicator of petrologic parentage, as has been suggested. The aluminum contents are quite variable and appear to decrease with increasing differentiation. This element is distributed roughly evenly in the pyroxene Y and Z positions, with Z substitution predominating slightly.

The general Monteregian pyroxene crystallization trend is from endiopside through augite, that is, a gradual ferrous iron

increase. Orthopyroxenes are prevented by the stable join olivine-clinopyroxene which separates the orthopyroxene composition from that of the subsiliceous liquid.

The production of highly sodic residua from undersaturated but not necessarily alkaline gabbro magma is believed due to the early separation of highly anorthitic plagioclase. Anorthite was favoured over more albitic plagioclases in the Monteregian Hills because of the subsiliceous nature of the parent magmas; the residua therefore became highly sodic, eventually precipitating such feldspathoids as nepheline and sodalite.

The average Chukotat and Monteregian mafic phases have a common subsiliceous character which distinguishes them from normal basaltic rocks. The Chukotat magma produced normal tholeiitic magmas by olivine separation, but the Monteregian magmas, lacking normative hypersthene, could not. Whereas normal basalts of the tholeiitic type are readily produced by fusion of basalt at the base of the crust or by fractional fusion of peridotite near the top of the mantle, subsiliceous mafic magmas would be expected from simple or repetitive partial fusion of material of peridotitic composition at great depths in the mantle. Under extreme pressures the olivine liquidus field is small, and fusion products of compositions along the pyroxene-garnet and pyroxene-olivine field boundaries, very subsiliceous, would form. Under high temperature conditions,

where the percent of fusion is considerable, highly magnesian melts such as the Chukotat parent magma may form. Less complete fusion under lower temperature conditions would likely result in more calcic magmas such as those which formed the Monteregian intrusives.

The magnesian subsiliceous magmas, on crustal emplacement, can differentiate towards siliceous and granitic residua particularly if the crystallization conditions are of the deep and 'wet' type; the calcic subsiliceous magmas, on crustal emplacement, can differentiate towards critically undersaturated residua, particularly if the conditions of crystallization are of the shallow or 'dry' type.

APPENDIX

Mineral Separation

Pyroxene concentrates were separated from a variety of rocks containing one or more of the following additional minerals: olivine, plagioclase, hornblende, serpentine, chlorite, biotite, and magnetite.

The rocks were crushed and seived, and powder within Nos. 100 and 200 mesh sizes was collected. The Frantz Isodynamic Separator was used to remove feldspar, olivine, biotite, and hornblende, magnetite having been first expelled with a hand magnet. In one case, two coexisting pyroxenes were readily separated by the magnetic separator.

Olivine, serpentine, and some chlorite were removed by treatment of the powders with large quantities of concentrated hydrochloric acid.

Under the binocular and petrographic microscopes, the final powders all appeared to have total impurity concentrations of less than three percent by volume. Many showed no visible impurities.

Rapid Silicate Analyses

The chemical analyses of the pyroxene powders were performed according to the methods of rapid analyses of

Table 12: Duplicate Pyroxene Analyses

Vaillant Lake

	A 5	A 7	A 8	A 9	A 10	A 14	A 16	A 17
SiO_2								
TiO_2			0.24				0.26	
Al_2O_3								
CaO	19.35	19.47	19.94	19.37	19.26	19.83	19.71	19.48
MgO	16.17	16.65	15.71	16.88	15.44	15.65	16.38	16.69
FeO	} 4.57*	} 3.89*	3.19	3.44	3.49	} 4.17*	3.56	3.59
Fe_2O_3			0.65	0.46	0.46		0.61	0.68
Na_2O			0.31				0.76	
K_2O			0.07				0.10	

* Total iron as FeO

Table 12: Duplicate Pyroxene Analyses

Vaillant Lake (cont.)

	A 18B			A 21			
	1	2	Mean	1	2	3	Mean
SiO_2	50.80	52.23	51.52	52.23	52.59		52.41
TiO_2	0.32	0.34	0.33	0.43	0.46	0.47	0.45
Al_2O_3	6.18		6.18	5.39	5.71		5.55
CaO	18.42	18.64	18.53	16.94	16.65	16.96	16.85
MgO	17.45	17.36	17.41	17.53	17.40	18.09	17.67
FeO*	6.08	6.08	6.08	6.86	6.79	6.81	6.82
FeO	5.16	5.44	5.30	6.53	6.73		6.63
Fe_2O_3	0.87		0.87	0.21			0.21
Na_2O	0.41		0.41	0.59			0.59
K_2O	0.10		0.10	0.09			0.09
Total			100.65				100.45

* Total iron as FeO

Table 12: Duplicate Pyroxene Analyses

Rougemont

	R 1			R 5		
	1	2	Mean	1	2	Mean
SiO_2	51.59	50.80	51.20	46.85	47.00	46.93
TiO_2	1.32	1.34	1.33	2.23	2.34	2.29
Al_2O_3	4.12	4.66	4.39	8.15	8.08	8.12
CaO	20.37	20.55	20.46	21.85	21.71	21.78
MgO	14.36	14.12	14.24	13.88	13.01	13.44
FeO*	8.28	8.15	8.21	6.86	6.87	6.87
FeO	6.99		6.99	4.12	4.21	4.17
Fe_2O_3	1.36		1.36	3.00		3.00
Na_2O	0.51		0.51	0.53		0.53
K_2O	0.09		0.09	0.04		0.04
Total			100.57			100.30

* Total iron as FeO

Table 12: Duplicate Pyroxene Analyses

Rougemont (cont.)

	R 10			R U		
	1	2	Mean	1	2	Mean
SiO_2	49.29	52.81	51.05			
TiO_2	1.36	1.29	1.33			
Al_2O_3	3.90	3.52	3.71			
CaO	20.84	20.91	20.88	20.92	21.37	21.15
MgO	14.52	14.75	14.59	14.75	14.79	14.77
FeO*	7.70	7.50	7.60	6.51	6.73	6.62
FeO	6.70	6.30	6.50	5.00	5.09	5.05
Fe_2O_3	1.22		1.22	1.74		1.74
Na_2O	0.51		0.51			
K_2O	0.09		0.09			
Total			99.88			

* Total iron as FeO

Table 12: Duplicate Pyroxene Analyses

St. Bruno

	B A			B B			B Y		
	1	2	Mean	1	2	Mean	1	2	Mean
SiO_2				53.10	53.02	53.06	51.37	50.01	50.69
TiO_2				0.99	0.98	0.99	1.22	1.24	1.23
Al_2O_3				6.35	6.28	6.32	4.72	4.35	4.54
CaO	19.56	19.47	19.52	19.97	20.28	20.13	21.95	21.65	21.80
MgO	14.53	14.76	14.65	14.59	15.10	14.85	14.86	15.68	15.27
FeO*	5.47	5.40	5.44	4.77	4.84	4.81	5.23	5.28	5.26
FeO	4.50		4.50	3.65	3.49	3.57	4.24		4.24
Fe_2O_3	1.04		1.04	1.38		1.38	1.13		1.13
Na_2O				0.95		0.95	0.48	0.50	0.49
K_2O				0.20		0.20	0.06		0.06
Total						101.45			99.45

* Total iron as FeO

Table 12: Duplicate Pyroxene Analyses

	Bon Conseil NDP			Mt. Johnson J A			
	1	2	Mean	1	2	3	Mean
SiO_2				48.72	49.22		48.97
TiO_2	1.91	1.97	1.94	1.64	1.62		1.63
Al_2O_3				6.01	5.90		5.96
CaO	21.15	21.24	21.20	20.26	20.46	20.42	20.38
MgO	14.18	13.76	13.97	12.47	12.18	12.57	12.41
FeO*	5.23	5.27	5.25	7.85	7.77		7.81
FeO	2.87	3.12	2.99	5.73	5.83		5.78
Fe_2O_3	2.51		2.51	2.26			2.26
Na_2O	0.79		0.79	1.48	1.49		1.49
K_2O	0.03		0.03	0.48	0.39		0.43
Total							99.31

* Total iron as FeO

Table 12: Duplicate Pyroxene Analyses

Yamaska

	Y 7			Y D			Y S		
	1	2	Mean	1	2	Mean	1	2	Mean
SiO_2				51.59	50.08	50.84	50.66	49.90	50.38
TiO_2				1.79	1.73	1.76	1.62	1.59	1.61
Al_2O_3				4.31	4.02	4.17	7.25		7.25
CaO	20.43	20.47	20.45	20.62	20.41	20.52	20.84	20.66	20.75
MgO	10.31	10.70	10.51	12.96	12.36	12.66	13.02	13.98	13.50
$FeO*$	7.89	7.90	7.90	9.15	9.08	9.11	6.96	6.82	6.89
FeO	4.17	4.18	4.18	7.04		7.04	5.00		5.00
Fe_2O_3	4.13		4.13	2.30		2.30	2.10		2.10
Na_2O				0.75		0.75	0.86		0.86
K_2O				0.15		0.15	0.12		0.12
Total						100.15			101.57

* Total iron as FeO

Table 12: Duplicate Pyroxene Analyses

	MR 7			Mt. Royal MR 8			MR 9		
	1	2	Mean	1	2	Mean	1	2	Mean
SiO_2	50.44	51.01	50.73				50.00	49.29	49.64
TiO_2	1.31	1.32	1.32				1.32	1.49	1.41
Al_2O_3	6.91		6.91				7.28	7.21	7.25
CaO	19.93	19.88	19.91	20.36	20.38	20.37	20.92	20.94	20.93
MgO	14.39	14.80	14.60	13.92	13.40	13.66	13.63	13.53	13.58
$FeO*$	6.61	6.54	6.58	6.82	6.63	6.73	7.09	6.81	6.95
FeO	4.70	4.43	4.57	4.37		4.37	5.11		5.11
Fe_2O_3	2.23		2.23	2.62		2.62	2.04		2.04
Na_2O	1.10		1.10				0.88		0.88
K_2O	0.16		0.16				0.17		0.17
Total			101.53						101.01

* Total iron as FeO

Table 12: Duplicate Pyroxene Analyses

Mt. Royal (cont.)

	MR 11W			MR T		
	1	2	Mean	1	2	Mean
SiO_2						
TiO_2						
Al_2O_3						
CaO	20.83	20.93	20.88	20.37	20.15	20.26
MgO	13.54	13.76	13.65	13.13	13.44	13.29
FeO*	6.62	6.76	6.69	6.90	6.70	6.80
FeO	4.83		4.83	4.56		4.56
Fe_2O_3	2.07		2.07	2.49		2.49
Na_2O						
K_2O						

* Total iron as FeO

Table 12: Duplicate Pyroxene Analyses

ST. Hilaire

| | H 1 | | | H 4 | | | H E | | |
	1	2	Mean	1	2	Mean	1	2	Mean
SiO_2				51.49	51.01	51.25	50.80	51.01	50.96
TiO_2				0.87	0.89	0.88	1.70	1.73	1.72
Al_2O_3				3.43	3.15	3.29	4.02	3.92	3.97
CaO	19.26	19.52	19.39	19.96	19.56	19.81	20.20	20.15	20.18
MgO	13.48	13.25	13.27	13.45	12.85	13.15	12.30	12.55	12.43
FeO*	10.61	10.82	10.71	10.71	10.69	10.70	9.07	8.97	9.02
FeO	9.22		9.22	8.76	9.28	9.02	7.50		7.50
Fe_2O_3	1.66		1.66	1.87		1.87	1.69		1.69
Na_2O				0.77	0.79	0.78	1.15	1.18	1.17
K_2O				0.16	0.14	0.15	0.31	0.25	0.28
Total						100.20			99.90

* Total iron as FeO

-260-

Table 12: Duplicate Pyroxene Analyses

St. Pie

| | St P 1 | | | St P 2 | | |
	1	2	Mean	1	2	Mean
SiO$_2$	48.86	48.50	48.68	49.94	49.44	49.69
TiO$_2$	0.89	0.90	0.90	1.78	1.79	1.79
Al$_2$O$_3$	10.17	10.01	10.09	7.52	7.42	7.47
CaO	19.41	19.52	19.47	20.80	20.84	20.82
MgO	14.04	14.39	14.22	13.80	13.90	13.85
FeO*	4.50	4.70	4.60	6.41	6.30	6.36
FeO	3.51	3.61	3.56	4.43	4.77	4.60
Fe$_2$O$_3$	1.15		1.15	1.96		1.96
Na$_2$O	1.91		1.91	0.75		0.75
K$_2$O	0.30		0.30	0.15		0.15
Total			100.28			101.08

* Total iron as FeO

Table 12: Duplicate Pyroxene Analyses (cont.)

Standard Diabase

	W 1			W 1 accepted		
	1	2	Mean	1	2	Mean
SiO_2	52.88	52.70	52.79	52.6		52.6
TiO_2	1.11	1.09	1.10	1.1		1.1
Al_2O_3	15.47	15.31	15.39	15.2		15.2
CaO	10.75		10.75	10.9		10.9
MgO	6.76		6.76	6.6		6.6
FeO*	9.77	9.78	9.78	10.0		10.0
FeO						
Fe_2O_3						
Na_2O	2.24	2.20	2.22	2.1		2.1
K_2O	0.68	0.62	0.65	0.66		0.66

* Total iron as FeO

silicate rocks proposed by Shapiro and Brannock (1956), with supplementary procedures and modifications developed by graduate students during the last several years at the Massachusetts Institute of Technology. The recent photometric technique for ferrous oxide determination developed by Shapiro (1960) was substituted for the conventional titrimetric method.

The analyses were generally performed in duplicate, that is, duplicate weighings for each sample giving duplicate solutions, and duplicate elemental analyses for each solution. The results of the analyses are shown in Table 12. The analysis performed on the standard diabase, W-1 (Shapiro and Brannock, 1956, p. 56), which was run along with the pyroxenes, can be compared with accepted values.

Optical Analyses

Four olivine powders were analyzed optically by standard refractive index techniques. The results are shown in Table 13 below.

Table 13: Optical Analysis of Olivine Powders

Specimen	n_x	n_y	n_z	Fo	Fa
Vaillant Lake					
A 7	1.669	1.683	1.704	83	17
A 9	1.668	1.682	1.704	83	17
A 14	1.669	1.682	1.704	83	17
Rougemont					
R 10	1.707	1.729	1.748	63	37

The anorthite content of plagioclases were determined by the flat stage statistical method of Michel Levy, and more frequently by the extinction angle method on combined carlsbad and albite twins.

BIBLIOGRAPHY

Adams, F. D. (1913), Geology of Mount Johnson: Geol. Survey of Canada, Int. Geol. Congress Guide Book no. 3, p. 29.

Andersen, Olaf (1915), The system anorthite-forsterite-silica: Amer. Jour. Science, vol. 189, p. 407.

Bancroft, J. A., and Howard, W. V. (1923), The essexites of Mount Royal, Montreal, P. Q.: Royal Soc. Canada Transactions, vol. 17, sect. iv, p. 13.

Barth, Tom F. W. (1951), Theoretical petrology: John Wiley and Sons, Inc., New York.

Beall, G. H. (1959), Preliminary report on the Cross Lake Area, New Quebec: P. R. no. 396, Que. Dept. Mines.

_____ (1960), Preliminary report on the Laflamme Lake Area, New Quebec: P. R. no. 435, Que. Dept. Mines.

_____, Hurley, P. M., Fairbairn, H. W., and Pinson, W. H. Jr., A comparison of K-Ar and whole rock Rb-Sr age dating in New Quebec and Labrador; M. I. T. Age Studies, in press.

Bergeron, Robert (1957), Preliminary report on the Cape Smith - Wakeham Bay belt, New Quebec: P. R. no. 355, Que. Dept. Mines.

Bowen, N. L. (1913), The melting phenomena of the plagioclase feldspars: Amer. Jour. Science, vol. 185, p. 577.

_____ (1914), The ternary system: diopside-forsterite-silica: Amer. Jour. Science, vol. 188, p. 207.

_____ (1928), The evolution of the igneous rocks: Princeton Univ. Press.

_____, and Schairer, J. F. (1935), System $FeO-MgO-SiO_2$: Amer. Jour. Science, 5th Ser., vol. 29, p. 159.

_____, and Tuttle, O. F. (1949), The system $MgO-SiO_2-H_2O$: Bull. Geol. Soc. Amer., vol. 60, p. 439.

Birch, Francis, ed. (1942), Handbook of physical constants: Geol. Soc. Amer. Sp. Paper no. 36.

Boyd, F. R., Jr., and Schairer, J. F. (1957), The join $MgSiO_3$-$CaMgSi_2O_6$: Ann. Rept. Dir. Geophys. Lab., Carnegie Inst. of Wash. Yrbk. 1956-57.

____, and England, J. L. (1961), Melting of silicates at high pressures: Ann. Rept. Dir. Geophys. Lab., Carnegie Inst. of Wash. Yrbk. 1960-61.

Clark, S. P., and DeNeufville, John (1962), Crystalline phases in the system diopside-$CaAl_2SiO_6$-silica at high pressures: Abstract, 43rd Ann. Meeting, Amer. Geophys. Union, Apr. 25-28.

Dresser, J. A. (1903), The geology and petrography of Shefford Mountain, Quebec: Geol. Surv. Can., Ann. Rept., 1900, vol. 13, pt. L.

_____ (1906), The geology of Brome Mountain, Quebec: Geol. Surv. Can., Ann. Rept., 1904, vol. 16, pt. G.

_____ (1910), Geology of St. Bruno Mountain, P. Q.: Geol. Surv. Can. Mem. 7.

_____, and Denis, T. C. (1944), Geology of Quebec, Vol. II, Descriptive geology: Que. Dept. Mines.

Faure, Gunter (1961), The Sr^{87}/Sr^{86} ratio in oceanic and continental basalts and the origin of igneous rocks: Ph. D. Thesis, Mass. Inst. of Technology.

Fairbairn, H. W., Hurley, P. M., Pinson, W. H., Jr., and Faure, G. (1962), The age of the Monteregian Hills, Quebec: M. I. T. Age Studies, in press.

Gold, D. P. (1962), oral communication.

Goldsmith, J. R. (1947), The system $CaAl_2Si_2O_8$-$Ca_2Al_2SiO_7$-$NaAlSiO_4$: Jour. Geol., vol. 55, p. 381.

Grieg, J. W., and Barth, Tom F. W. (1938), the system $Na_2O.Al_2O_3.2SiO_2$ (Nepheline, carnegieite)- $Na_2O.Al_2O_3.6SiO_2$ (albite): Amer. Jour. Science, vol. 235, p. 93.

Gummer, W. K., The system $CaSiO_3$-$CaAl_2Si_2O_8$-$NaAlSiO_4$: Jour. Geol., vol. 51, p. 503.

Hess, H. H., (1941), Pyroxenes of common mafic magmas: Amer. Mineralogist, vol. 26, p. 515.

_____(1960), Stillwater igneous complex, Montana: Geol. Soc. Amer. Mem. 80.

Hytonen, Kai, and Schairer, J. F. (1961), The plane enstatite-anorthite-diopside and its relation to basalts: Ann. Rept. Dir. Geophys. Lab., Carnegie Inst. of Wash. Yrbk. 1960-61.

Jones, W. R., Peoples, J. W., and Howland, A. L. (1960), Igneous and Tectonic Structures of the Stillwater Complex, Montana: U. S. Geol. Surv. B ull. 1071-H.

Kushiro, I. (1960), Si-Al relations in clinopyroxenes from igneous rocks: Amer. Jour. Science, vol. 258, p. 548.

LeBas, M. J. (1962), The role of aluminum in igneous clinopyroxenes with relation to their parentage: Amer, Jour. Science, vol. 260, p. 267.

O'Neill, J. J. (1914), St. Hilaire and Rougemont mountains, Quebec: Geol. Surv. Can., Mem. 43.

Osborn, E. F., and Tait, D. B. (1952), The system diopside-forsterite-anorthite: Amer. Jour. Science, Bowen Volume, p. 413.

Peacock, M. A. (1931), Classification of igneous rock series: Jour. Geol., vol. 39, p. 54.

Peoples, J. W. (1962), oral communication.

Ricker, R. W., and Osborn, E. F. (1954), System CaO-MgO-SiO_2: Jour. Amer. Ceram. Soc., vol. 37, p. 134.

Sahama, Th. G., and Torgeson, D. R. (1959), Some examples of the application of thermochemistry to petrology: Jour. Geol., vol. 57, p. 255.

Schairer, J. F., and Bowen, N. L. (1947a), Melting relations in the systems $Na_2O-Al_2O_3-SiO_2$ and $K_2O-Al_2O_2-SiO_2$: Amer. Jour, of Science, vol. 245, p. 193.

_____, and Bowen, N. L. (1947b), System $CaAl_2Si_2O_8-SiO_2$: Bull. Geol. Soc. Finlande, vol. 20, p. 71.

Schairer, J. F., and Morimoto, N. (1959), The system forsterite-diopside-silica-albite: Ann. Rept. Dir. Geophys Lab., Carnegie Inst. of Wash. Yrbk. 1958-1959.

_____, and Yoder, H. S., Jr. (1959), The system albite-forsterite-silica: Ann. Rept. Dir. Geophys. Lab., Carnegie Inst. of Wash. Yrbk. 1959-60.

Shapiro, Leonard (1960), A spectrophotometric method for the determination of FeO in rocks: U. S. Geol. Surv. Research 1960, Short Paper no. 226.

_____, and Brannock, W. W. (1956), Rapid analysis of silicate rocks: U. S. Geol. Surv. Bull 1036-C.

Shepherd, Norman (1959), Geology and mineralogy of the Cross Lake area, New Quebec: Ph. D. Thesis, Univ. of Toronto.

Turner, F. J., and Verhoogan, Jean (1951), Igneous and metamorphic petrology: 1st ed., McGraw-Hill Book Co. Inc.

Verhoogan, Jean (1962), Distribution of titanium between silicates and oxides in igneous rocks: Amer. Jour. Science, vol. 260, p. 211.

Warren, B. E., and Bragg, W. L. (1928), The structure of diopside $CaMg(SiO_3)_2$: Zeit. Kristallogr., vol. 69, p. 168.

Wasserburg, G. J. (1957), The effects of H_2O in silicate systems: Jour. Geol., vol. 65, p. 15.

Wilson, J. T. (1954), The development and structure of the crust: The Earth as a Planet, The Solar System - vol. ii, ed. by G. Kuiper; Univ. Chicago Press, p. 138.

Winchell, A. N. (1951), Elements of optical mineralogy, part ii, descriptions of minerals: 4th ed., John Wiley and Sons, New York.

Yoder, H. S., Jr. (1952), Change of the melting point of diopside with pressure: Jour. Geol., vol. 60, p. 364.

_____, (1955), Diopside-water system: Ann. Rept. Dir. Geophys Lab., Carnegie Inst. of Wash. Yrbk. 1954-55.

Yoder, H. S., Jr., and Tilley, C. E. (1956), Natural tholeiite basalt - H_2O system: Ann. Rept. Dir. Geophys. Lab., Carnegie Inst. of Wash. Yrbk., 1955-56.

_____, and Tilley, C. E. (1957), Basalt magmas: Ann. Rept. Dir. Geophys. Lab., Carnegie Inst. of Wash. Yrbk., 1956-57.

_____, and Tilley, C. E. (1960), Simple basalt systems: Ann. Rept. Dir. Geophys. Lab., Carnegie Inst. of Wash. Yrbk., 1959-60.

_____, and Tilley, C. E. (1961), Simple basalt systems: Ann. Rept. Dir. Geophys. Lab., Carnegie Inst. of Wash. Yrbk., 1960-61.

Young, G. A. (1906), The geology and petrography of Mount Yamaska: Geol. Surv. Can., Ann. Rept., 1904, vol. 16, pt. H.

BIOGRAPHY

The author was born in Montreal, Quebec, on October 14, 1935. He received his schooling in the Westmount public school system, attending King's School, Westmount Junior High School, and Westmount Senior High School.

The author studied at McGill University in Montreal from September 1952 to May 1958. He received the Bachelor of Science degree with Honours in Physics and Geology in 1956 and was awarded the Logan Gold Medal in Geology. He received the Master of Science degree in Geology in 1958. During his years at McGill University the author held the following scholarships and fellowships: the Arthur Campbell University Entrance Scholarship, 1952-53, the California Standard Scholarship, 1954-55, the Mobil Oil Scholarship, 1955-56, the Leroy Memorial Fellowship, 1956-57, and the Quebec Department of Mines Scholarship, 1956-58.

At the Massachusetts Institute of Technology, which he entered as a candidate for the Doctor of Philosophy degree in September, 1958, the author was awarded the Quebec Department of Mines Scholarship in 1958-59. He was research assistant in the M. I. T. Geochronology Laboratory for the academic years 1958-59 and 1959-60. He was appointed Instructor of Geology during the fall terms of 1960 and 1961 and taught the undergraduate course in structural geology.
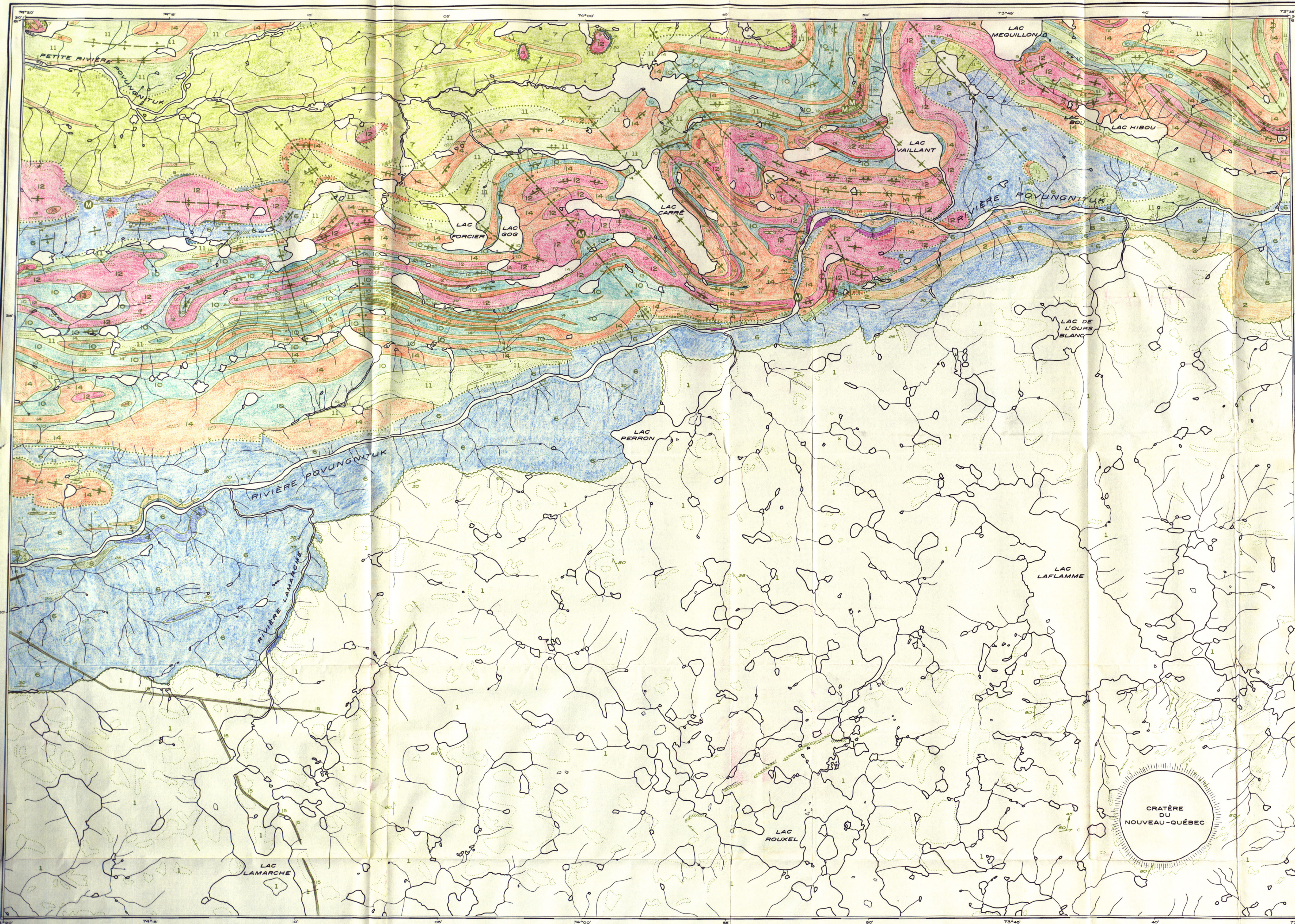
In the summers, the author has primarily been engaged in

geological and geophysical field work in Canada. He spent two summers in the Rocky Mountains doing seismic and stratigraphic surveying with the Shell Oil Company and five summers with the Quebec Department of Mines doing geological mapping in northern Quebec. In addition, he spent one summer as a research assistant at McGill University constructing an argon purification system. This summer, he was employed as a Science Counselor at the Wesleyan Science Center, Wesleyan University, Middletown, Connecticut.

In addition to several preliminary geological reports for the Quebec Department of Mines, the author has two recent publications:

"The Age of Authigenic Biotite in the Utica Shale", American Mineralogist, in press, and

"A Comparison of K-Ar and Whole Rock Rb-Sr Age Dating in New Quebec and Labrador", G. H. Beall, P. M. Hurley, H. W. Fairbairn, and W. H. Pinson, in press.
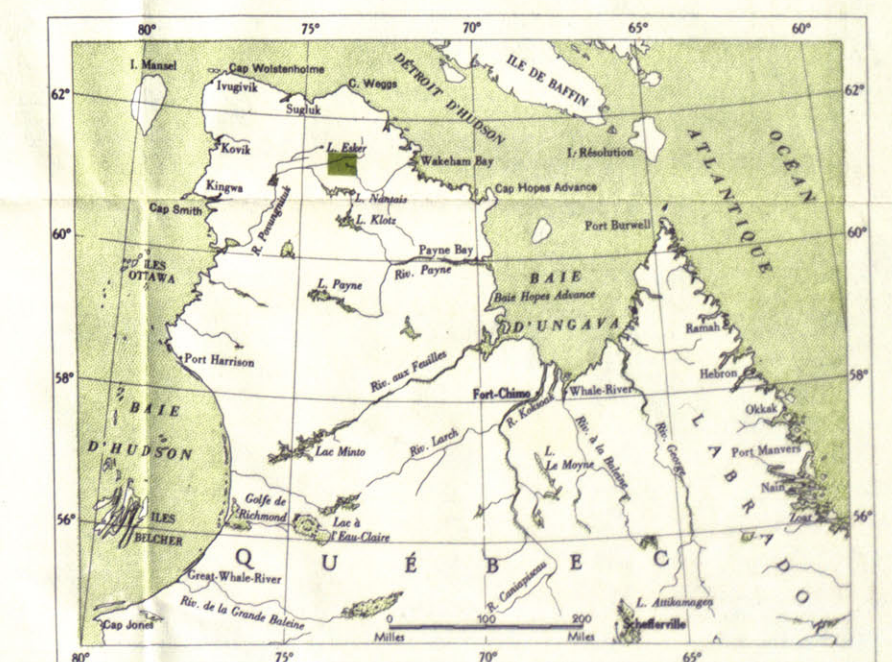
In September, the author plans to be married to Miss Janet M. Overton of Forestdale, Rhode Island. He will then join the Research and Development Division of Corning Glass Works, Corning, New York, where he will continue research in the field of synthetic geology.

PROVINCE DE QUÉBEC, CANADA
MINISTÈRE DES RICHESSES NATURELLES
L'honorable RENÉ LÉVESQUE, ministre
PAUL E. AUGER, sous-ministre

1961

PROVINCE OF QUEBEC, CANADA
DEPARTMENT OF NATURAL RESOURCES
Honourable RENÉ LÉVESQUE, Minister
PAUL E. AUGER, Deputy Minister

LÉGENDE / LEGEND

PRÉCAMBRIEN / PRECAMBRIAN

POST-POVUNGNITUK

Diabase

GROUPE DE CHUKOTAT / CHUKOTAT GROUP

14 — Gabbro, gabbro feldspathique, épidiorite / Gabbro, feldspathic gabbro, epidiorite
13 — Pyroxénite ouralitisée, amphibolite / Pyroxenite, uralitite, amphibolite
12 — Serpentinite, serpentinite à augite, péridotite serpentinisée / Serpentinite, augite serpentinite, serpentinized peridotite
11 — Basalte coussiné, fracturé et massif, et leucobasalte / Pillowed, sheared, and massive basalt and leucobasalt
10 — Schiste ardoisier, argilite et phyllite / Slate, argillite, and phyllite
9 — Quartzite et chert / Quartzite and chert

GROUPE DE POVUNGNITUK / POVUNGNITUK GROUP

8 — Métabasalte, surtout du schiste à chlorite / Metabasalt, mainly chlorite schist
7 — Basalte massif / Massive basalt
6 — Phyllite, schiste à séricite chloritique, schiste quartzifère à mica / Phyllite, chloritic sericite schist, quartz-mica schist
5 — Formation ferrifère silicatée / Silicate iron formation
4 — Quartzite / Quartzite
3 — Dolomie, microgrès dolomitique / Dolomite, dolomitic siltstone
2 — Gabbro, métagabbro / Gabbro, metagabbro

COMPLEXE DE BASE / BASEMENT COMPLEX

1 — Granite et gneiss granitique / Granite and granite gneiss

SIGNES CONVENTIONNELS / SYMBOLS

(a) affleurement, (b) région d'affleurements / (a) outcrop, (b) outcrop area
Esker / Esker
Anticlinal: (a) normal, (b) renversé / Anticline: (a) normal, (b) overturned
Synclinal: (a) normal, (b) renversé / Syncline: (a) normal, (b) overturned
Contour géologique: (a) relevé, (b) présumé / Geological contact: (a) observed, (b) assumed
Gneissosité, schistosité, clivage: (a) inclinés, (b) verticaux / Gneissosity, schistosity, cleavage: (a) inclined, (b) vertical
Stratification, structure ellipsoïdale en coussinet: (a) sommet non déterminé, (b) sommet déterminée, (c) renversé (sommet au nord-ouest) / Stratification, pillow structure: (a) top not indicated, (b) top indicated, (c) overturned (top to northwest)
Discordance: (a) à la base du groupe de Chukotat, (b) à la base du groupe de Povungnituk / Unconformity: (a) at base of Chukotat group, (b) at base of Povungnituk group
M — Minéralisation de sulfure / Sulphide mineralization
Linéation / Lineation

Déclinaison magnétique approximative: 40° 45' W. / Approximate magnetic declination: 40° 45' W.

Géologie par: / Geology by: G. H. BEALL, 1959
SERVICE DE LA CARTE GÉOLOGIQUE / GEOLOGICAL SURVEYS BRANCH

PETITE RIVIÈRE POVUNGNITUK
LAC MEQUILLON
LAC HIBOU
LAC BOU
LAC VAILLANT
LAC CARRÉ
LAC SORCIER
LAC GOG
RIVIÈRE POVUNGNITUK
LAC DE L'OURS BLANC
LAC PERRON
RIVIÈRE POVUNGNITUK
RIVIÈRE LAMARCHE
LAC LAFLAMME
LAC ROUXEL
LAC LAMARCHE
CRATÈRE DU NOUVEAU-QUÉBEC

Échelle 1 mille au pouce ou 1:63,360
Scale 1 mile to inch or 1:63,360
Miles

DIFFERENTIATION CONTROLS IN SUBSILICIOUS GABBROS - G. H. Beall
M. I. T. Thesis

RÉGION DU LAC LAFLAMME
NOUVEAU-QUÉBEC

LAFLAMME LAKE AREA
NEW-QUEBEC

No. 1351

CARTE PRÉLIMINAIRE   No. 1351   PRELIMINARY MAP

LEGEND — LÉGENDE

PRECAMBRIAN — PRÉCAMBRIEN
CHUKOTAT GROUP — GROUPE DE CHUKOTAT

18 — Gabbro, feldspathic gabbro, epidiorite
Gabbro, gabbro feldspathique, épidiorite

17 — Pyroxene gabbro, serpentinized pyroxene gabbro
Gabbro à pyroxène, gabbro à pyroxène serpentinisé

16 — Serpentinite, augite serpentinite, pyroxenite, uralitite
Serpentinite, serpentinite à augite pyroxénite, ouralitite

15 — Pillow lava: (a) leucobasalt, (b) basalt, (c) andesite
Lave coussinée: (a) leucobasalte, (b) basalte, (c) andésite

14 — Massive lava: (a) leucobasalt, (b) basalt, (c) andesite
Lave massive: (a) leucobasalte, (b) basalte, (c) andésite

13 — Sheared lava
Lave cisaillée

12 — Volcanic breccia
Brèche volcanique

11 — Dolomite, dolomitic slates
Dolomie, schistes ardoisiers dolomitiques

10 — Slate, argillite, some greywacke
Schiste ardoisier, argilite, un peu de grauwacke

9 — Quartzite, chert
Quartzite, chert

8 — Sedimentary breccia, conglomerate
Brèche sédimentaire, conglomérat

POVUNGNITUK GROUP — GROUPE DE POVUNGNITUK

7 — Metabasalt, mainly chlorite schist and chlorite actinolite schist
Métabasalte, principalement schiste à chlorite et schiste à chlorite et actinote

6 — Massive basalt with some andesite
Basalte massif avec un peu d'andésite

5 — Phyllite, chloritic sericite schist, quartz sericite schist, graphitic sericite schist
Phyllite, schiste à séricite chloritique, schiste à séricite quartzifère, schiste à séricite graphitique

4 — Slate, argillite
Schiste ardoisier, argilite

3 — Quartzite
Quartzite

2 — Dolomite, dolomitic siltstone
Dolomie, microgrès dolomitique

1 — Gabbro
Gabbro

(Formations not necessarily in order of succession)
(Formations non nécessairement en ordre chronologique)

SYMBOLS — SYMBOLES

(a) Outcrop, (b) group of outcrops
(a) Affleurement, (b) groupe d'affleurements

Esker
Esker

Geological contact
Contact géologique

Anticline: (a) normal, (b) overturned
Anticlinal: (a) normal, (b) renversé

Syncline: (a) normal, (b) overturned
Synclinal: (a) normal, (b) renversé

Schistosity or cleavage: (a) inclined, (b) vertical
Schistosité ou clivage: (a) incliné, (b) vertical

Bedding: (a) top known, (b) top unknown, (c) overturned, (d) horizontal
Couches: (a) sommet connu, (b) sommet inconnu, (c) renversées, (d) horizontales

Fault: (a) dip unknown, (b) dip known, (R reversed, N normal)
Faille: (a) direction inconnue, (b) direction connue, (R renversée, N normale)

Shear zone
Zone de cisaillement

Angular unconformity
Discordance angulaire

M — Sulphide mineralization
Minéralisation de sulfures

A — Chrysotile asbestos
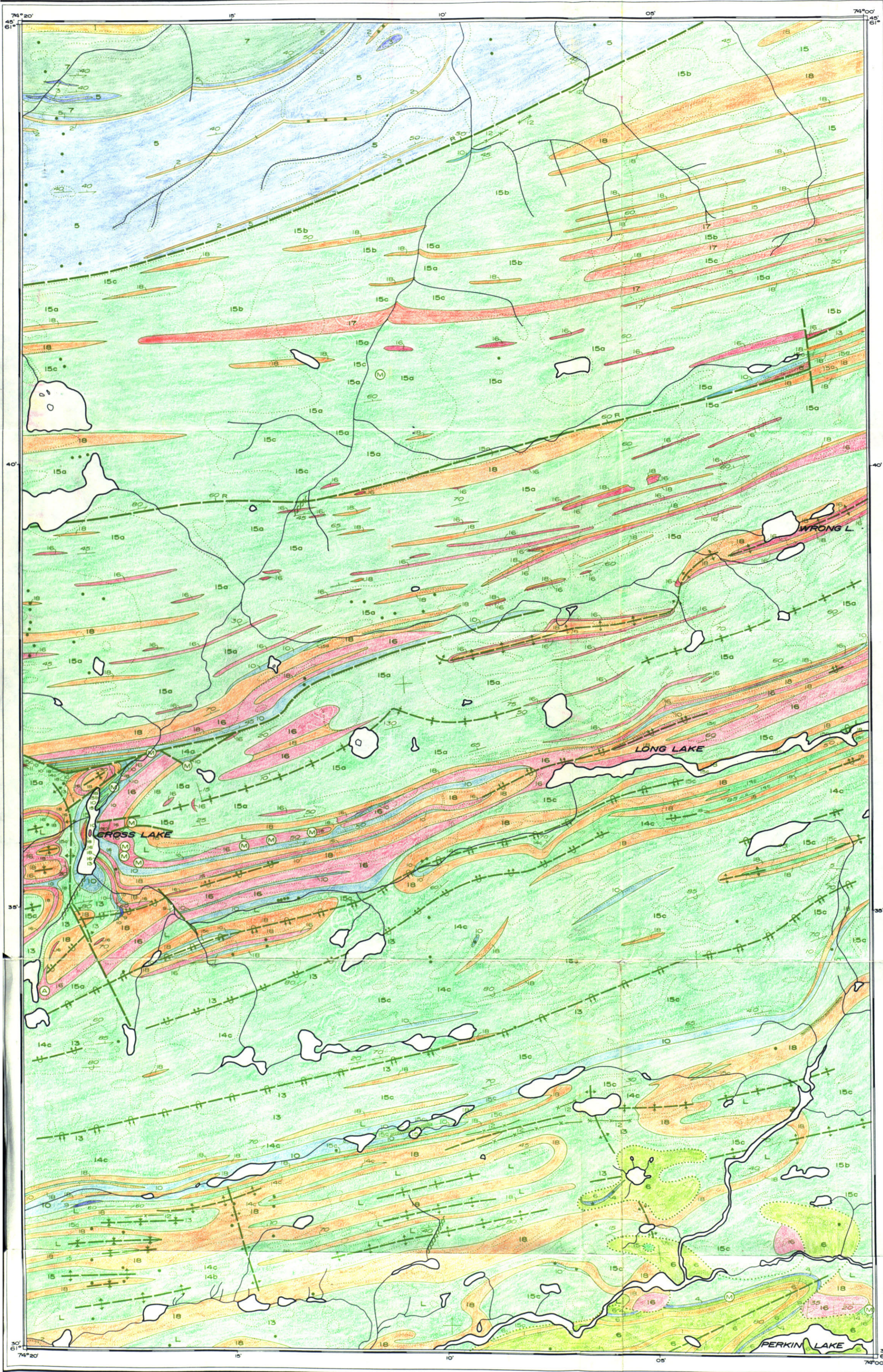*Amiante à chrysotile*

40°W.

INDEX MAP — LIEU DE LA CARTE

WRONG L.
LONG LAKE
CROSS LAKE
PERKIN LAKE
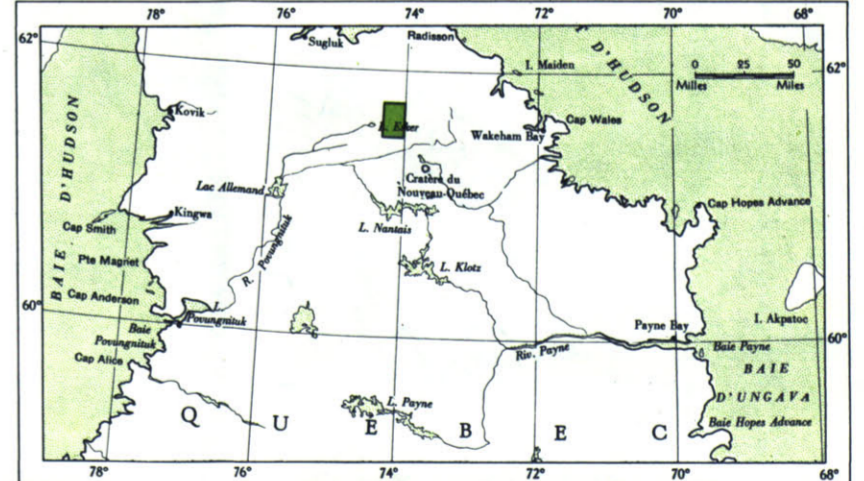
RÉGION DE **CROSS LAKE** AREA

NOUVEAU QUÉBEC — NEW QUEBEC

Geology by: G. H. BEALL, 1958
Géologie par:

0   1   2   3
Milles
Échelle: 1 mille au pouce ou 1:63,360
Scale: 1 mile to inch or 1:63,360
Miles

DIFFERENTIATION CONTROLS IN SUBSILICEOUS GABBROS - G. H. Beall
M. I. T. Thesis

No. 1267